Crosstalk signaling between circadian clock components and iron metabolism

Samuel Peter Schiffhauer

Dissertation submitted to the faculty of the Virginia Polytechnic Institute and State University in partial fulfillment of the requirements for the degree of

Doctor of Philosophy

In

Biological Sciences

Carla V. Finkielstein

Peter J. Kennelly

Shihoko Kojima

Zhaomin Yang

April 18, 2017

Blacksburg VA

Keywords: Circadian rhythm, iron, Period 2, peripheral clocks, liver metabolism, hepatocellular carcinoma

Crosstalk signaling between circadian clock components and iron metabolism

Samuel Peter Schiffhauer

ABSTRACT

Circadian rhythms are daily molecular oscillations within cells ranging from prokaryotes to humans. This rhythm is self sustaining, and receives external cues in order to synchronize an organism's behavior and physiology with the environment. Many metabolites utilized in metabolic processes seem to follow a pattern of circadian oscillation. Iron, an essential component in cellular processes such as respiration and DNA synthesis, is obtained almost exclusively through diet, yet little is known about how the clock governs iron metabolism. The regulation of iron within the cell is very tightly controlled, as iron is highly reactive in the generation of oxidative stress and the excretion of excess iron is very limited. There are limited findings indicating that there are molecular ties between the circadian clock and the regulation of iron metabolism.

The first half of my dissertation focuses on the role of the circadian clock in modulating expression of iron metabolic components. We found that key components of iron import, in *TFRC*, and export, in *SLC40A1*, show altered expression in response to changes in the expression of clock transcription components. Furthermore, in circadian synchronized HepG2 hepatocytes *TFRC* and *SLC40A1* showed rhythms in their mRNA expression, although expression of these genes was highly altered in conditions of high iron availability. We also examined *IREB2*, which expresses a master regulator of iron concentration in IRP2. IRP2 showed rhythms in phase with circadian component PER2, and IRP2's rhythmicity was lost under iron overload conditions. We observed that the ability of these three critical iron metabolic components to respond to sudden increases in available iron was mitigated in cells with clock impairment. Whole cistrome and transcriptome analysis was used to determine that rhythmicity in *TFRC* and *SLC40A1* are not equal in their recruitment of circadian protein binding or in the stage of transcription in which circadian rhythms are generated. The cumulative effect of all of this regulation is that rhythmic variation in intracellular hepatic ferrous iron is clock controlled.

The second half of my dissertation focuses on understanding how iron uptake influences clock resetting. Initially, iron was added to the cells in the form of ferrous sulfate, or chelated out of the cells using 2-2'-dipyridyl and clock gene expression was monitored. Altered rhythmicity of these components was seen at both the mRNA and protein level in cells with disrupted iron homeostasis. Then, we measured changes in period, phase, and amplitude of these rhythms, ultimately using a luciferase reporter cell line to demonstrate that even slight changes in cellular iron produce an effect on rhythmic period. We find that the circadian clock and iron metabolism pathway are intimately related, and that the intracellular iron concentration plays a role in circadian clock behavior.

Overall, our research illustrates the importance of the circadian clock in liver metabolism and physiology. Improper iron metabolism due to genetic or dietary shortcomings is common in humans, and our work builds on the importance of chronotherapy in treatment of these conditions. Conversely, our research into the effect intracellular iron has on the clock contributes to the growing body of research into how circadian clocks, especially the peripheral clock of the liver, receive input from a range of metabolites in conjunction with signals from the master oscillator of the suprachiasmatic nucleus.

Crosstalk signaling between circadian clock components and iron metabolism

Samuel Peter Schiffhauer

GENERAL AUDIENCE ABSTRACT

The circadian clock is the system allowing the body to stay in synchrony with its environment. Clocks are found in organisms ranging from bacteria to humans, and use environmental cues such as light and temperature to coordinate important processes inside the cell. Many of these processes require enzymes which contain iron in order to function. Iron is obtained almost exclusively through feeding, and high iron levels are toxic to the cell. In this work, we looked at how the circadian clock helps maintain the amount of iron within the cell at healthy levels. We showed that the genes which are involved in managing iron are expressed in different amounts depending on the time of day, and that this causes the amount of iron within the cell to vary over time. We also examined how the amount of iron in the cells goes on to alter the circadian clock. The way the circadian rhythm oscillates is altered when either too much or too little iron is available to the cells. These findings have health impacts, especially in the context of the liver where poor management of the circadian clock or iron metabolism have been linked to the development of various forms of liver cancer.

Dedicated to my grandparents for their inspiration, to my parents for their support, and to Maggie for her love.

Table of Contents

Abbreviations

bHLH/PAS: Basic Helix-Loop-Helix Per-Arnt-Sim

BMP6: Bone morphogenic protein 6

BMAL1: Brain and Muscle ARNT-Like 1

CA-AM: Chelator Calcein Acetoxymethyl Ester

CK1δ/ε: Casein Kinase 1ε and 1δ

CLOCK: Circadian Locomoter Output Cycles Kaput

CREB: Cyclic AMP responsive element-binding protein

CRY1/2: Cryptochrome 1 and 2

D-box: DBP/E4BP4 Binding Element

DMT1: Divalent Metal Transporter 1

E-box: Enhancer Box

FBS: Fetal bovine serum

FPN1: Ferroportin 1

FTH1: Ferritin Heavy Polypeptide 1

FTL: Ferritin Light Polypeptide

HAMP: Hepcidin Antimicrobial Peptide

HFE: Hemochromatosis gene

HH: Hereditary Hemochromatosis

HIF: Hypoxia inducible factor

HJV: Hemojuvulin

HMOX1: Heme Oxygenase 1

IRE: Iron Response Element

IRP1/2: Iron Regulatory Protein 1 and 2

LCN2: Lipocalin 2

LIP: Labile Iron Pool

MUTYH: MutY-homolog

NAMPT: Nicotinamide phosphoribosyltranferase

NCOR: Nuclear receptor corepressor 1

NR1D1: Nuclear Receptor Subfamily 1, Group D, Member 1 gene

PARP1: Poly(ADP-ribose) polymerase

PER2: Period Circadian Clock 2

PGC-1α: Peroxisome proliferator-activated receptor gamma coactivator 1-alpha

PHD: Prolyl hydroxylase

PK2: Prokineticin 2

PP1: Protein phosphatase 1

REV-ERBα: Nuclear Receptor Subfamily 1, Group D, Member 1 protein

RLS: Restless leg syndrome

RORα: RAR-related orphan receptor alpha

RORE: Retinoic Acid-Related Orphan Receptor Response Element

ROS: Reactive oxygen species

RPKM: Reads per kilobase measured

RRM: Ribonucleotide reductase M

SCN: Suprachiasmatic Nucleus

SIRT1: Sirtuin 1

SLC40A1: Solute Carrier Family 40 Member 1

STEAP3: Six transmembrane epithelial antigen of the prostate family member 3

TF: Transferrin

TFRC: Transferrin Receptor 1

TGFα: Transforming growth factor-α

UCP2: Uncoupling protein 2

UTR: Untranslated Region

Preface

Parts of this dissertation have been published.

Appendix A was published as **Association of the circadian factor Period 2 to p53 influences p53's function in DNA-damage signaling** [1]**.** Samuel Schiffhauer contributed to figures S5, S7, and statistical analysis for figures S5, S7, and S9. Other author contributions are addressed in the acknowledgements section of Appendix A.

Appendix B was published as **Chronotherapy: Intuitive, Sound, Founded…But Not Broadly Applied.** Samuel Schiffhauer contributed to figure 3 [2]. Other author contributions are addressed in the acknowledgements section of Appendix B.

Appendix C has been submitted for publication as **Interplay between E3 ligases modulate Period 2's accumulation and influences circadian oscillation.** Samuel Schiffhauer contributed to figures 5D and S4. Other author contributions are addressed in the acknowledgements section of Appendix C.

Chapter 1: Introduction

1.1 Circadian rhythms synchronize an organism to its environment

The circadian clock is a widely conserved mechanism by which organisms coordinate their biological functions with the periodicity of their environment [3, 4]. Environmental cues are primarily photic, but non-photic cues such as temperature and food intake are also translated into biochemical regulation of clock rhythmicity [5-7]. By responding to these environmental cues, the allocation of cellular resources can be temporally optimized to coincide with the organisms' interaction with its environment. For example, blood pressure needs to be adjusted in accordance with an organism's active state, and therefore there is circadian regulation of blood pressure, which is why the majority of strokes in humans occur in the early morning [8]. Mice in which the circadian gene circadian locomoter output cycles kaput (*CLOCK*) has been knocked out are hypotensive compared to control animals, animals with a knockout of cryptochrome 1 and 2 (*CRY1*/2) are hypertensive, while mice in which brain and muscle ARNT-like 1 (*BMAL1*) is knocked out lack any rhythm in their blood pressure, highlighting how the role of the clock in physiology is rarely due to interaction with a single circadian component but depends on the health of the clock as a whole [8-10]. In addition to blood pressure, heart rate is linked to circadian regulation in order to raise heart rate during the active period [8]. The circadian clock regulates heart rate by controlling expression of calcium channels in the heart, and BMAL1 knockout mice develop weakened, enlarged hearts with age [11, 12]. Circadian clocks are essential to renal function, with renal blood flow and excretion of potassium and sodium all undergoing circadian rhythms [13]. The Na^+/H^+ exchanger 3 protein aids in sodium reabsorption and is known to be rhythmic, however sodium excretion patterns are lost in CLOCK knockout mice [9, 14].

Circadian clocks may influence metabolism, and this is a clear case where peripheral clocks are receiving entrainment cues directly from the environment, in the form of nutrients from food, as opposed to indirect cues from the suprachiasmatic nucleus (SCN) [15]. This is believed to occur through the NAD-dependent deacetlyase Sirtuin-1 with the CLOCK:BMAL1 heterodimer [16]. Generation of circadian mutant mice quickly revealed the role of the clock in metabolism and obesity. CLOCK (Δ19) mutant mice develop obesity, as do period 3 (PER3) knockout mice, regardless of diet [8, 17]. Studies have looked into restricting the time of feeding as a factor in weight gain, and found that mice fed either exclusively during the active or inactive period gained weight slower, had higher metabolic rate, and increased insulin sensitivity compared to mice with 24 h access to food [18]. Coinciding with metabolic function, clock impairment is linked to development of diabetes through findings such as BMAL1 knockout mice demonstrating reduced glucose-stimulated insulin secretion, theorized to be linked to an upregulation of mitochondrial uncoupling protein 2 (UCP2) in these animals [19]. In addition, the circadian clock impacts other cellular processes such as endocrine function, hormone production, body temperature and immunity [8, 20-24]. Disregulation of the circadian clock has been linked to a number of diseases and disorders including tumorigenesis and this is one of the reasons that solving these molecular unknowns are of significant importance to researchers [25-28].

1.1.1 Core circadian clock mechanism

In mammals, circadian entrainment primarily begins in the suprachiasmatic nucleus (SCN), a region of the hypothalamus approximately 20,000 neurons in size which is able to receive photic signals throughout the retinohypothalamic tract by using the photopigment melanopsin within retinal ganglion cells [29]. This is a distinct sensory mechanism from rod and cone based conscious perception of light. When malanopsin is stimulated in the ganglion cells, they release glutamate and

activate the NMDA and metabotropic receptors of SCN cells [30]. Retinohypothalamic fibers directly translate these signals to the SCN [29]. Light exposure of retinal ganglion cells leads to rapid induction of *PER1* in SCN neurons *via* cyclic AMP responsive element-binding protein (CREB) binding to cAMP-responsive elements in the *PER1* promoter, showing how light can induce phase changes in the master clock [31, 32]. The clock in the SCN is also sensitive to certain nonphotic cues, such as melatonin, GABA, and serotonin [29]. The SCN has the capability to synchronize the circadian rhythm of peripheral tissues throughout the body by direct autonomous neuronal interaction, as well as indirectly through glucocorticoid hormone release and behavioral patterns [32]. For example, the SCN regulates wake/sleep periods, which results in feeding during specific times of the day. This rhythmic influx of nutrients then has a synchronizing effect on the peripheral clock of the liver [15]. SCN afferent neurons are able to govern behavioral activity patterns by rhythmically inducing neuropeptides transforming growth factor-α (TGFα) and prokineticin-2 (PK2) [32].

The core circadian clock is comprised of a feedback loop which generates a rhythmic oscillation that has a period of roughly 24 h (Diagram 1). In the positive arm of the feedback loop, circadian proteins Brain and Muscle ARNT-Like 1 (BMAL1) and Circadian Locomotor Output Cycles Kaput (CLOCK) bind through a basic helix-loop-helix Per-Arnt-Sim (bHLH/PAS) domain to form a heterodimer which positively drives transcription of a number of genes through enhancer box (E-box) *cis* elements within their promoters[33, 34]. The canonical E-box sequence is CACGTG, although several noncanonical sequences have been found to bind the CLOCK:BMAL1 heterodimer [35]. E-box containing genes include other core clock genes such as *PERIOD 2* (*PER1-3*) and *CRYPTOCHROME 1,2*(*CRY1-2*) which are positively regulated [36]. In addition to E-box-mediated transcriptional regulation, there is another *cis* element called the DBP/E4BP4 binding element (D-box), which functions to delay the transcription of certain clock genes such as *CRY1*,

which in turn acts upon E-box elements in other genes[37]. In this way, a further delay in the feedback loop can be generated. At least one D-box is present in *PER1*, *PER2, PER3*, and RAR-related orphan receptor alpha (*RORα*), and by operating antiphase to E-box dependent transcription, higher amplitude transcriptional activity is generated [36].

Among the many target genes transcriptionally activated by BMAL1:CLOCK are *PERIOD* and *CRYPTOCHROME* genes [36]. Upon transcription and translation, PERs and CRYs accumulate in the cytoplasm. Casein Kinase 1ε and 1δ (CK1δ/ε) are critical kinases which function to generate a delay in the circadian feedback loop[38]. CK1δ/ε phosphorylates PER1 and PER2, which enhances their rate of degradation as well as blocking PER1 and PER2 from being able to reenter the nucleus [38, 39]. Degradation occurs when β-TrCP binds phosphorylated PER leading to ubiquitination and degradation by the 26S proteosome [40]. CK1δ/ε phosphorylation of PER however is counteracted by protein phosphatase 1 (PP1), and the rate of cytosolic accumulation is dependent on the balance of these two proteins in modulating the phosphorylation state of PER. Loss of a single phosphorylation site in PER2 (S662G) is sufficient to cause shortened circadian rhythms in humans [4]. Due to this balance of phosphorylation and degradation, it takes longer for PER to accumulate in the cytoplasm to a sufficient concentration where it forms a heterodimer with CRY, and reenters the nucleus [39]. PER2:CRY1 heterodimers then bind and inhibit the transcriptional activity of the CLOCK:BMAL1 complex, downregulating the expression of its transcriptional targets, which include *PER* and *CRY* themselves [41]. Eventually, ubiquitin-dependent pathways degrade PER and CRY in the nucleus, and CLOCK and BMAL1 are able to resume their roles as transcription factors, and the cycle repeats [42]. Generating further robustness in the cycle are the orphan nuclear receptors Nuclear Receptor Subfamily 1, Group D, Member 1 (*NR1D1*, expressing the protein REV-ERBα) and RAR-Related Orphan Receptor Alpha (*RORα),*

which are transcriptionally driven by the CLOCK:BMAL1 heterodimer [43]. Subsequently, RORα can then bind to retinoic acid-related orphan receptor response elements (ROREs) in the promoter of *BMAL1* and drive its transcription [43]. However, when REV-ERBα binds to these same elements, *BMAL1* transcription is repressed [43]. This adds a secondary negative feedback loop to the rhythm generation.

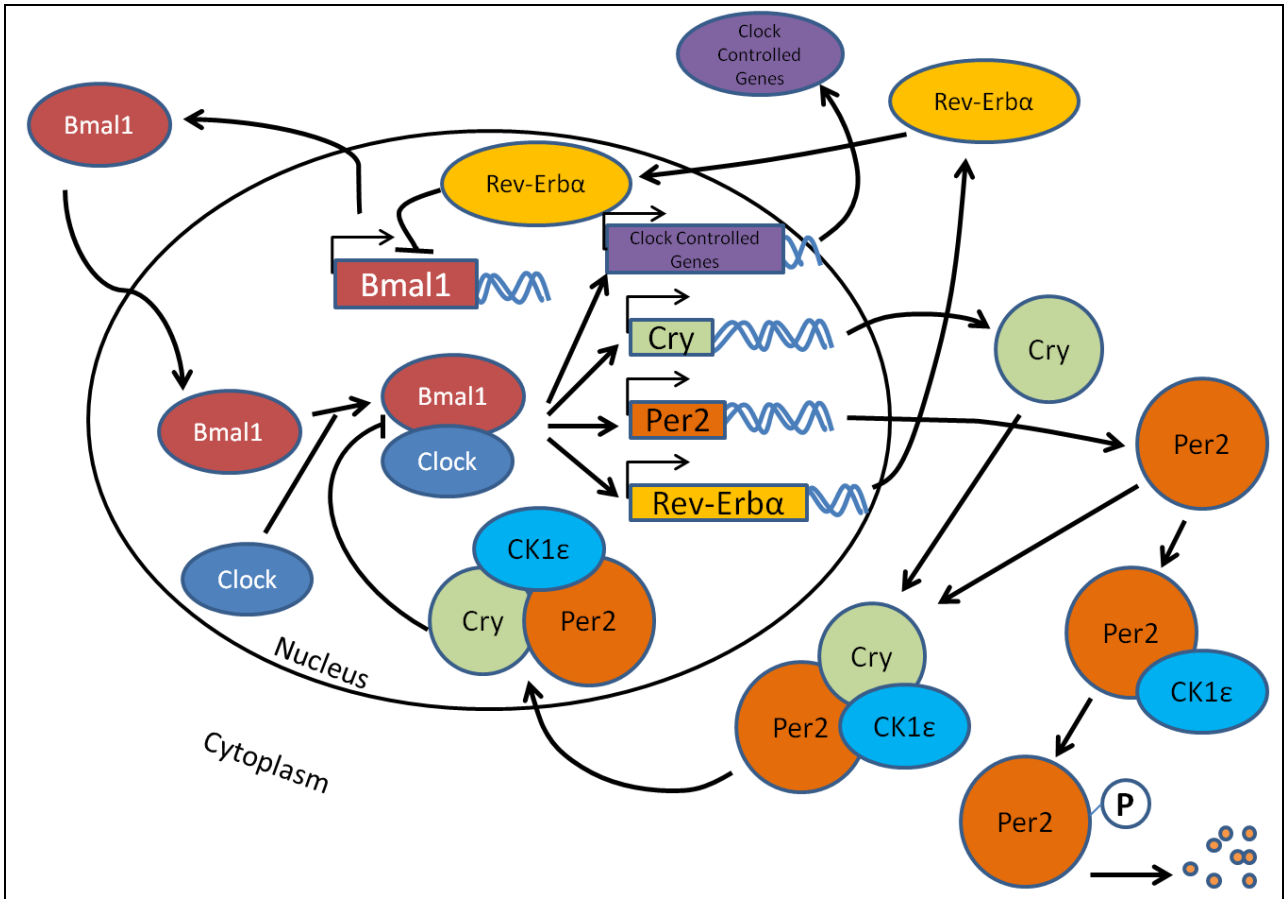

Diagram 1: An overview of the core circadian feedback loop. CLOCK and BMAL1 form a heterodimer to bind specific *cis*-elements and drive circadian gene transcription. Two such gene families, *CRY* and *PER*, comprise a negative feedback arm on this transcriptional loop. CRY and PER2 accumulate in the cytoplasm, with a delay in their accumulation driven by CK1ε-mediated degradation of PER2. When a threshold has been reached, the PER2:CRY complex reenters the nucleus, and inhibits the DNA binding activity of BMAL1:CLOCK, inhibiting their own transcription. Robustness of this cycle is promoted by two other proteins which are transcribed by BMAL1:CLOCK. Rev-Erbα functions to inhibit *BMAL1* transcription, while RORα (not shown) inhibits *BMAL1*

transcription. These components work together to maintain a self-sustained 24h oscillation. Therefore, the large number of genes which are transcriptional targets of BMAL1:CLOCK are transcribed with a 24h rhythmicity.

1.1.2 Circadian clock and cancer

The International Agency for Research on Cancer has stated that "shift work that involves circadian disruption is probably carcinogenic to humans"[44]. Evidence in both humans and other model organisms establish that disruption of circadian rhythms increases the risk of cancer development and progression [45-47]. There is evidence that this correlation between reduced expression of clock genes and cancer may be due in part to the loss of rhythmic signaling by p53, allowing the activation of oncogene *c-MYC* [48]. Importantly, there is direct binding between PER2 and p53 which mediates the activity of p53 in unstressed cells in response to DNA damage [1, 49].

There is evidence that the circadian clock regulates cell cycle components at multiple stages of the cell cycle. Control of G1 phase is regulated by Cyclin D1, and this cyclin has been shown to be rhythmically expressed [50]. Stability of Cyclin D1 is linked to *PER* expression, and deregulation of Cyclin D1 in *PER* mutants leads to heightened proliferation [51]. Often genes associated with enhanced carcinogenesis are linked to breakdowns in G1/S transistion, such as *p21* and *p27* [50, 52]. In this case there is *c-MYC* dependent regulation by the circadian clock, which is one of the primary ways the circadian clock regulates downstream transcription [53]. Similar to the role of *c-MYC* in allowing the clock to regulate the G1/S transition, the circadian clock uses an intermediary to control the G2/M transition. In this instance, clock regulation of *WEE1* and *CDC25A* control the timing of the G2/M checkpoint [50, 54]. Loss of WEE1 is strongly linked to tumorigenesis, it is thought that is due to the lack of cell cycle arrest during the G2/M transition [55, 56]. In addition to unchecked proliferation by degradation of cell cycle checkpoints, a large cause of tumorigenesis is a loss of apoptotic regulation [57]. Genes of the Bcl2 family which make up the intrinsic apoptotic

pathway are frequently found to be expressed rhythmically. This includes both pro-apoptotic genes such as *BID,BIM,* and *BAX*, as well as anti-apoptotic genes such as *BCL2 [50]*. In the extrinsic apoptotic pathway, some of the executioner caspases such as *CASP3* and *CASP8* exhibit circadian rhythms in their expression [50]. Whether intrinsic or extrinsic, maintaining the correct balance of apoptotic signaling is key to cellular homeostasis, and this balance is in part maintained through circadian regulation [58].

Decreased *PER* expression is associated with breast tumor formation, and both *PER1* and *PER2* have been classified as tumor suppressor genes [59]. Not only do these proteins inhibit tumor growth, they also promote apoptosis [60]. Reduced expression levels of *BMAL1* and *CRY1* correlate with development of epithelial ovarian cancer, with expression profiles of these genes being used as prognostic indicators [61]. Downregulation of core circadian genes is also found in myeloid leukemia, *PER1-3*, *CRY1-2*, and *CK1ε* are all expressed below normal levels [62]. This evidence together supports the hypothesis that many circadian genes serve functions inside the cell that are autonomous from their circadian duties and relevant to processes such as DNA damage response and oncogenesis. Also supporting this theory is that circadian mutant mice are more prone to tumor development regardless of light conditions [48].

1.2 Iron metabolism

1.2.1 Iron influx and efflux

Cytosolic concentration of iron is very tightly regulated due to the element's reactive nature and the variety of key pathways in which iron is involved. Iron enables ribonucleotide reductase to catalyze the conversion of ribonucleotides to deoxyribonucleotides, and is critical to the citric acid cycle as a unit of the heme molecule[63]. Mammalian cells derive their required iron primarily

through dietary intake, as well as through recycling of previously ingested iron by macrophages [64, 65]. An overview of the mammalian iron metabolic pathway governing the net transfer of iron in and out of the cell is seen in Diagram 2. In mammals, absorbed dietary iron is bound within transferrin (TF), in its ferric state. This nonreactive iron can then circulate through the bloodstream to peripheral tissues, where it can be uptaken by cells through the surface receptor transferrin receptor 1 (TFRC). Following endocytosis, the acidic environment of the endosome triggers the release of ferric iron from TF[66]. At this point the ferrireductase six transmembrane epithelial antigen of the prostate family member 3 (STEAP3) reduces the ferric iron to its ferrous state, enabling the transport of iron from the endosome to the cytosol by divalent metal transporter 1 (DMT1) [66-68]. Iron that is not being actively incorporated into proteins and transported throughout the cell is stored in ferritin [69]. Ferritin is a spherical storage protein composed of two polypeptides, a heavy chain and a light chain [70]. These polypeptides are expressed by the genes ferritin heavy polypeptide 1 (*FTH1*) and ferritin light polypeptide (*FTL*). While iron stored in ferritin is considered bioavailable, many cell types maintain a labile iron pool (LIP) of ferrous iron in the cytosol loosely bound to weak chelators such as citrate or pyrophosphate[66, 71]. Excess ferrous iron in vertebrates is removed through only a single known exporter protein, ferroportin [63]. Ferroportin 1(FPN1), is a membrane-bound protein encoded by solute carrier family 40 member 1 (*SLC40A1*), post-translationally regulated in part by binding the peptide hormone hepcidin and followed by internalization and subsequent proteasome-mediated degradation [72]. In environments with low circulating iron available, the liver will upregulate transcription of hepcidin antimicrobial peptide (*HAMP*), to reduce the concentration of ferroportin in the surface of the cell, which results in the cell retaining more ferrous iron. The hepcidin feedback mechanism is a general strategy used by cellular systems including hepatic cells to regulate iron recycling as shown in macrophages [65]. Almost immediately after ferrous iron is pumped out of the cell by ferroportin,

the oxidase cerruloplasmin converts Fe^{2+} to Fe^{3+} where it is available for binding once again by transferrin[73].

An additional level of regulation in the iron metabolic pathway is through the mRNA binding activity of iron regulatory proteins (IRPs). These proteins function as posttranscriptional regulators of multiple iron metabolic genes in both a positive and negative manner to regulate the intracellular iron concentration [66, 74]. IRPs bind to iron response elements (IREs) in either the 5' or 3' untranslated region (UTR) of target mRNAs. When the IRE is located in the 5' UTR, translation is blocked, and subsequent protein expression is reduced. This is found in iron storage and export proteins such as ferritin and ferroportin, resulting in higher intracellular concentrations of available ferrous iron[66, 74]. However, IRPs will stabilize the mRNA, promoting protein synthesis, if the IRE is found in the 3' UTR [74]. This is observed with genes involved in iron import, such as *TFR1* and *DMT1*. The overall mRNA binding activity of IRPs is inversely related to the intracellular iron concentration, resulting in a system in which iron regulatory protein expression is constantly modulated to manage intracellular iron. At times of low intracellular iron, IRPs are able to effectively bind IREs resulting in decreased translation of *FTH*, *FTL*, and *SLC40A1* mRNAs, yet simultaneously increasing translation of *TFR1* and *DMT1* mRNAs, resulting in a net increase in intracellular iron concentration [66, 74]. When intracellular iron concentrations are high, IRPs no longer bind to IRE sequences, and the expression of iron storage and export proteins increases once again, while translation of *TFR1* and *DMT1* mRNAs will decrease to limit iron uptake[74]. Accordingly, there is a multilevel system of control over the intracellular concentration of iron, which is dependent both on the extracellular availability of iron, as well as the metabolic demands of the cell. Under pathological conditions, for example when considering the tumor microenvironment, it appears that both an abundance of systemic iron and heightened metabolic

demand are deregulated, and that the breakdown of iron homeostasis can't be attributed to any single component of the regulatory system[63, 75, 76].

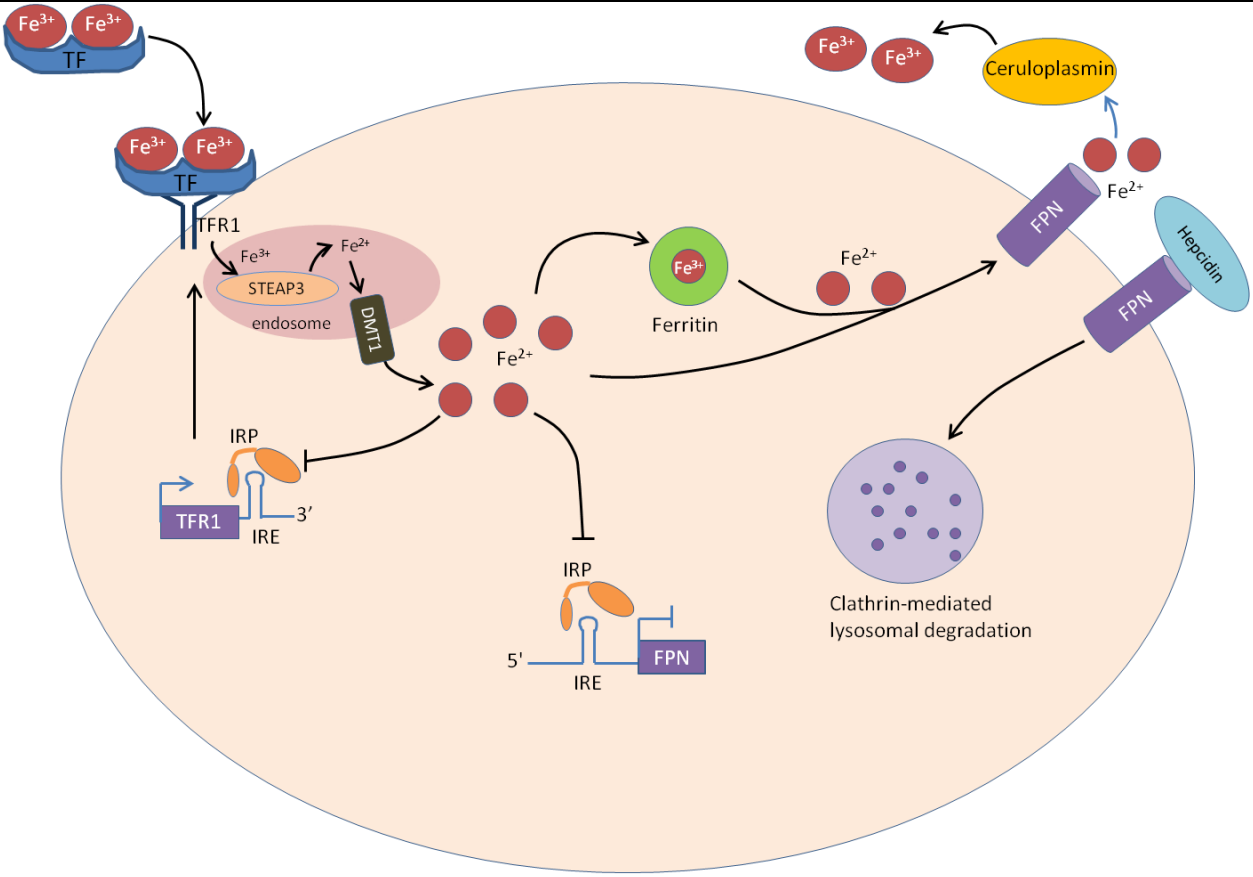

Diagram 2: An overview of iron import, storage, and export in the mammalian cell. Transferrin bound ferric iron is brought into the cell through the TFR1 surface membrane receptor in an endosomal process. Ferric iron is released in the endosome, reduced to ferrous iron by the ferriductase STEAP3, and transported out of the endosome DMT1 to join the metabolically available labile iron pool. Excess iron is stored in ferritin, or exported out of the cell by FPN. In periods of low iron availability, the peptide hormone Hepcidin will bind to FPN and initiate its degradation, conserving intracellular iron. Iron influx and efflux is transcriptionally regulated by IRPs which repress or enhance expression by binding to IREs at the 5' or 3' end of a gene's mRNA, respectively.

1.2.2 Iron in diet and physiology

Because of the low potential for excretion of excess iron, it must be tightly controlled, with efficient processes for recycling iron that is already within the body as well as selectively limiting absorption of new iron. The majority of iron within the body (~2 g) is functioning in hemoglobin

of the red blood cells, while ~1 g is stored in the liver [66, 77]. Reticuloendothelial macrophages are constantly recycling these cells, and they function as a flexible storage site for excess iron along with the liver [77]. The daily iron needs amount to around 25 mg of iron, the majority of which is sourced from recycling of erythroid cells which have a circulatory lifespan of around 120 days, with 1-2 mg of dietary iron in the form of inorganic ferric iron and heme absorbed through the duodenum of the small instestine [77]. To prevent gradual accumulation of iron within the body, 1-2 mg of iron are lost each day through the sloughing of dead epithelial cells [77]. This emphasis on maintaining the correct combination of circulating and stored iron through controlled uptake rather than excretion makes conditions of excess iron very difficult to manage.

In normal physiology, circulating iron is bound by transferrin. The clinical term of transferrin saturation refers to the percent of iron binding sites on serum transferrin which are occupied by ferric iron molecules, which is typically 20%-40% [78]. There is also a smaller pool of circulating transferrin which can be quantified as a measure of iron stores, levels of which can correspond with inflammation or infection [77]. It is possible for the concentration of circulating iron to surpass the circulatory carrying capacity, and this reactive iron will tend to accumulate in the liver, heart and pancreas, often causing damage [79]. The main sensor for the overall balance of stored versus circulating iron is hepcidin secreted by the liver [77]. Conditions such as hypoxia or anemia which stimulate erythropoiesis, or iron deficiency will suppress hepcidin expression in order to increase available circulating iron [77]. When the systemic iron needs to be lowered, either due to excessive circulating iron for normal physiology, or in the case of infective inflammation when an organism is trying to restrict iron available to pathogens, hepcidin will be stimulated [77].

Nearly one eighth of the world's population suffers from iron deficiency, with another eighth having anemia for other reasons [80]. Deficiency can be due to nutritional deficiency, improper gut absorption, pregnancy, or excessive blood loss, and this can lead to health

complications such as child development impairment, cognitive decline, and even mortality [77]. In other cases, the total iron in the body is within normal ranges, but the circulating iron pool is still impaired, functionally limiting processes such as erythropoiesis. This is known as anemia of chronic disease, and is found in patients with cancer or autoimmune diseases [81].

Conditions such as hereditary hemochromatosis or transfusional overload result in excess iron accumulating in the body, and leads to health complications such as cirrhosis, diabetes mellitus, and cardiomyopathy [77]. Hereditary hemochromatosis results in chronically low hepcidin levels and therefore overactive ferroportin, whereas other iron overload conditions such as iron-loading anemias are the result of insufficient red blood cell generation, meaning slower than normal incorporation of circulating iron [77]. Because the liver is the primary organ for iron storage, it is often associated with damage in conditions of iron overload. Resultant oxidative damage is associated with cirrhosis and hepatocarcinoma [82]. Damage to the liver by other measures such as alcoholic fatty liver disease or hepatitis can result in iron overload within the organ, which only serves to progress the damage further [83]. Iron overload is strongly associated with diabetes mellitus, and even high dietary iron in otherwise healthy individuals is associated with this metabolic disorder, for reasons that are not strongly understood [84]. Abnormal iron concentration in the heart is associated with multiple health conditions. Excessive iron can lead to cardiomyopathy and erythmia, while iron deficiency is associated with 30%-50% of patients with chronic heart failure, which is partly why iron supplementation is such a common treatment in this population [85].

Aberrant iron metabolism in the brain is connected to multiple neurological conditions, with both iron deficiency and iron overload connected to diseases. In rats, iron deficiency led to permanent impairment of the striatal dopaminergic-opiate system causing irreversible learning impairments [86]. Iron accumulation has been implicated in the development of Parkinson's and Alzheimer's disease, and it is thought that in patients developing these conditions excessive iron

contributes to oxidative stress and neurotoxicity in the brain [77]. This is even more noteworthy when we consider that non-heme bound iron naturally accumulates in cells of the brain, liver, and heart during aging [87, 88]. While we commonly associate the elderly with anemia and subsequent health complications with strength and cognition, this problem may be more due to iron circulation rather than total body iron stores [87].

1.2.3 Aberrant iron regulation in cancer

Multiple studies have linked abnormal iron levels to cancer development and prognosis[63, 75, 76, 89, 90]. As a vital component of multiple cellular functions, there is a constant need for elemental iron within the cell but its intrinsically reactive nature makes unchecked intracellular iron damaging. Accordingly, saturation of transferrin with iron was shown to be a significant indicator of cancer development later in life in a 14,000 individual population study[91]. This overload of iron can be due to genetic or dietary factors, and it seems that in both cases correlates with an increased risk of cancer development [82, 91-93]. Hereditary hemochromatosis (HH) is a genetic disorder, typically resulting from mutations in the gene *hemochromatosis* (*HFE*) resulting in iron overload, and individuals who suffer from this condition face a much higher risk of developing hepatocellular carcinoma[94]. Loss of HFE function results in abnormal hepcidin regulation in response to changes in intracellular iron, and ultimately to accumulation of iron within the liver [94]. Whether through a hereditary condition or through the accumulation of genetic defects as is typically seen in cancer development, one thing that seems to be consistent is that cancer cells tend to increase the amount of available intracellular iron, enhancing the potential for replication without concern for the inherent increase in oxidative stress potential[63, 95, 96]. Conversely, there is evidence that clinical steps taken to lower iron stores in the body such as phlebotomy can reduce the risk of cancer

development. Indeed, frequent phlebotomy was correlated with decreased risk of liver, lung, colon, and other cancers [97].

One of the connections between increased iron load in cells and cancer cell behavior is the role of iron in generating reactive oxygen species (ROS) [98]. ROS molecules such as superoxide, hydrogen peroxide, and hydroxyl radicals are produced naturally in the cell, however high levels in normal cells will induce apoptosis and necrosis[99]. In cancer cells, proliferation and disease progression are linked to the altered functionality of ROS control pathways[100, 101]. Excess ROS promotes malignant phenotypes by altering Wnt signaling and angiogenesis[102, 103]. Higher rates of ROS accumulation further cause DNA damaging oxidation of deoxyribose, enhancing mutation rates in cells cancer cells which are likely to have impaired repair mechanisms[104].

Increase in intracellular free iron in malignant cells often results from overexpression of genes involved in iron uptake[63, 105]. TFR1 is commonly overexpressed in many types of cancers, and antibodies against this receptor have been used to combat tumor growth directly as well as a target to deliver chemotherapeutics[95, 106]. A complementary method to transferrin mediated iron uptake is through the small iron binding ligand catachol, which will complex in the blood with the protein lipocalin 2 (LCN2)[107]. This iron-catechol-LCN2 complex can then be internalized by recognizing the cell surface receptor SLC22A17, providing a secondary method of iron uptake by the cell [108]. In MCF7 cells, overexpression of LCN2 increases replication, and this may bear out in human patients as upregulated LCN2 was associated with hepatocellular carcinoma and reduced survival in patients [109, 110].

As previously stated, cytosolic iron can be oxidized by the heavy subunit of the ferritin protein, and stored in this form within the ferritin shell to reduce the amount of reactive species generated in the cell[74]. Ferritin contains a ferri-hydrite mineral core that can hold up to 4,500 iron atoms[63]. Unsurprisingly, as the tumor is restructuring its environment to aid in proliferation,

increased levels of available iron are demanded [98]. Through upregulation of the IRPs, ferritin is found to be downregulated in some cancer cells, increasing the available iron pool. As a result, there is a higher level of oxidative damage in the cell. The differential expression of IRP1 and IRP2 is known to have an unusual effect on malignant cells, one that highlights how much is left to learn about the post-transcriptional regulatory power of IRP:IRE binding activity. IRP1 and IRP2 have very similar RNA-binding roles within the cell, however IRP1 also functions as a cytoplasmic aconitase [74]. However, overexpression of IRP1 leads to reduced tumor growth, while overexpression of IRP2 is reported to enhance tumor growth, possibly through additional oncogene related transcriptional roles unrelated to its iron metabolic activity [111, 112].

Mammalian cells which need to export protein from the cell rely on a single mode of export, and as such relatively minor changes to the expression pattern of the responsible protein, ferroportin, can have a large impact on the concentration of iron in the cell. For example, hereditary hemochromatosis highlights how the ferroportin-hepcidin pathway can lead to chronic health issues and greatly increase the risk of cancer development and progression[94]. Although hepcidin is mainly expressed in the liver in response to circulating iron concentrations, it has also been found to express in breast epithelial cells, so perhaps there are tissue specific responses to systemic changes in iron availability [75]. There may also be differing roles between systemic hepcidin secreted by the liver, and local hepcidin expression in the tumor microenvironment. This is likely due to the hypoxic nature of tumors and the role downregulation of hepcidin in hypoxic conditions [113]. However, systemic hepcidin expression in organisms with cancer often increases, although this varies based on cancer type and malignancy stage [113, 114]. Decreased ferroportin is a common trait of breast cancer cell lines and breast tumor tissue samples, and decreased ferroportin has been used as a marker for poorer prognosis in the growth of primary tumors as well as the onset of metastasis [75, 115]. Not only was the ferroportin expression significant in the eventual outcome of

patients, but hepcidin expression was also found to play a role in determining the final intracellular iron balance, and subsequently the prognosis of the patient[75]. This is one example of how the role of local hepcidin expression, in this case in breast tissue, can differ from systemic hepcidin secreted by the liver. High levels of hepcidin expression in mammary epithelial cells contributes to the accumulation of iron [75].

1.3 Initial connections between iron metabolism and the circadian cycle

The feedback loops that govern the circadian cycle as well as the concentration of cellular iron are clearly essential to healthy cell behavior, and both have been strongly linked to the development and progression of cancer [46, 63]. One of the key uses of iron within the body involves the synthesis of heme in erythroid cells, which is rate limited by the heme inhibiting the uptake of transferrin bound ferric iron, creating a negative feedback loop unique to this cell type [116, 117]. Heme is a well categorized molecule that uses iron to sequester several gasses for cellular respiration as well as monitor the overall redox state of the cell. Heme is tightly related to the balance of the labile iron pool, in times of low intracellular iron heme oxygenase 1 (HMOX1), involved in heme degradation, releases iron to be used in metabolism [118]. Heme binds to the circadian transcription factors NPAS2 and REV-ERBα, through a Per-ARNT-Sim (PAS) domain or histidine containing ligand binding domain, respectively [119, 120]. When in the heme-bound state these transcription factors are not able to bind DNA. Additionally, it has been shown that heme functions at the posttranslational level to degrade Per2, altering the negative feedback arm of the circadian clock [121]. This binding between heme and PER2 occurs through a novel heme-regulatory motif, and is dependent on the redox state of the iron contained in heme [121]. Heme was also found to dampen the oscillation of PER2 in the SCN, and that this effect was both reversible and tissue specific [122].

Outside of heme, there is physiological evidence of serum iron levels and transferrin saturation levels exhibiting a circadian pattern [123, 124]. Because the intracellular iron pool is regulated in response to the extracellular iron supply, the circadian oscillation of serum iron is a promising lead for our research. Dietary iron deprivation is sufficient to disrupt circadian behavior in a murine model, once again showing that this is not the case of one pathway regulating the other, but there appears to be crosstalk between the two in order to maintain normal function [125]. This study was using a murine model for restless leg syndrome, in which symptoms of impaired rest present themselves in the late subjective night phase. Another study in rodents used a four week iron-free diet to severely deplete iron reserves in rats, and monitor the effect on dopaminergic neuronal activity [126]. Observed rhythms of body temperature and motor activity were completely antiphasic in anemic animals, suggesting a drastic shift in the clock and dopaminergic neuron function[126]. Intriguingly, this study found that when anemia was relieved through dietary supplementation, physiology quickly returned to normal[126]. There is a limited amount of evidence regarding circadian expression of iron metabolic components. One study shows rhythmicity of *TFR1* is dependent on rhythmic *c-MYC* transcription factor activity [127]. This group also showed a time dependent efficacy of a transferrin conjugated antitumor agent, theorizing that internalization of the agent was dependent on the abundance of TFR1 at the cell surface [127]. In addition to transcriptional regulation by *c-MYC*, the same group later reported that there was posttranscriptional regulation of *TFR1* transcripts by rhythmic expression of *IRP2* [128]. The authors show that *IRP2* transcription is driven by CLOCK:BMAL1 heterodimer activity, and that in their model of tumors implanted in mice, there was variation in the concentration of iron within the tumor tissue [128].

The tumor suppressor gene p53 is well known to be under circadian control, and recently it has been implicated in the expression of multiple iron regulatory proteins [60, 63, 129]. p53 inhibits

IRP binding to IREs, which in turn induces ferritin [130]. Growth arrest initiated by p53 may have to do with a depletion of available iron due to induced ferritin expression[130]. p53 is a known transcriptional activator of *HAMP*, this is thought to be another anticancer defense mechanism by minimizing the export of dietary iron by enterocytes [131]. In mice, iron overload from either a genetic or dietary cause was shown to correlate with a significant downregulation of p53, due to the ability of heme to destabilize p53 protein upon binding [129]. Here we can see evidence of a feedback loop between a circadian protein exerting a regulatory effect across multiple iron metabolism factors, while p53 itself is simultaneously being regulated by the overall state of iron in the cell.

There are an ever increasing number of pathways which have been proposed to operate in a circadian manner, controlling many of the most vital cellular functions [26, 132]. Many of these processes involve enzymes which require iron for their catalytic domains. Logically, the demand for synthesis of these enzymes will result in a corresponding increase in demand for free iron. Table 1 shows a selection of enzymes which utilize iron and are involved in pathways that have been connected to the circadian clock. The enzymatic requirement for iron is found across diverse pathways, which can lead to a host of pathologies when these pathways are disturbed.

We hypothesize that the circadian clock exerts a direct regulatory role on the expression of iron metabolic components, as a further means of coordinating metabolism with the environment. We also hypothesize that there is heme-independent mediation of circadian clock components dependent upon the iron status of the cell.

Process	Iron-dependent Protein	Circadian Connections of Pathway
Circulatory oxygen transport	hemoglobin[133]	Heme synthesis peaks at end of subjective night. [134]
Mitochonidrial Respiration	Respiratory Complex I-III Cytochrome C[133]	Hepatic mitochondrial respiration peaks during subjective light.[135] Oxygen consumption was in phase with PER2 expression in synchronized C2C12 cells.[136]
DNA Synthesis	Ribonucleotide Reductase DNA Primase[133]	S-phase of tongue keratinocytes peaks late in subjective dark phase.[137] Ribonucleotide reductase expression is rhythmic, and helps the mouse liver coordinate nucleotide synthesis.[138]
DNA Damage Response and Repair	mutY-homolog[133] Xeroderma pigmentosum D[139]	Nucleotide excision repair activity peaks at the transition from rest to active period in mouse brain.[140]. Excision repair in mouse liver peaks at the end of inactive period, but is arrhythmic in testis.[141]
Cell Signaling	Guanylate Cyclase[133]	Guanylate cyclase activity and cGMP increase at night in hamster retina.[142] Rhythmic guanylate cyclase in aortic tissue helps modulate blood pressure.[143]

Table 1: A representative selection of circadian cellular processes which utilize iron-dependent proteins. Note, in not all cases are the proteins listed specifically demonstrated to be rhythmic, in some cases information is only available on the rhythmicity of other components of the cellular process. They are mentioned here to illustrate the shared utilization of circadian regulation and iron catalytic activity in many cellular processes.

1.4 Specific Aims

The circadian clock is increasingly implicated in regulation of metabolism, as a key interface between cellular demands and an organism's environment [3, 144]. In mammals, the molecular clock is formed by a transcriptional-translational feedback loop where the expression of its core components drives the different phases of the daily cycle and whose protein products influence the cell's biochemistry. As such, the objective of this research is twofold; first, to expose the cellular mechanisms responsible for synchronizing iron metabolic processes to specific times of the day, and second, to provide a rationale for understanding how time-dependent uptake of iron triggers clock resetting in target tissues. Therefore, we propose to study the following specific aims:

Aim 1: To determine if fluctuations in intracellular iron levels result from the regulation of iron metabolic components by circadian clock components.

Peripheral clocks are especially important for metabolic regulation of liver function, and this tissue is the primary organ for iron metabolism [145, 146]. Our preliminary data show that circadian synchronized human hepatocyte cells previously known to exhibit functional hepatic metabolism, also display a 24-h oscillation in their labile iron pools as determined by using a ferrous specific colorimetric chelator [147, 148]. *Thus, we hypothesize that circadian regulation of iron metabolic components results in fluctuations in the size of the labile iron pool.* We will explore whether circadian regulation is occurring at one or more stages of iron import, storage, and export from the cell. To accomplish this, we will first evaluate how various circadian scenarios impact the steady-state expression of iron metabolic genes and their products. We will then use timecourse experiments to examine rhythms in expression of iron metabolic components. To determine whether these effects are sustained at the mRNA or protein level, we will analyze rhythmicity of both expression stages using qRT-PCR and western blot. Because destabilization of the circadian clock and iron metabolic pathways can

lead to pathological conditions, we will evaluate the impact of clock impairment on the response of iron metabolic genes to sudden increase in intracellular iron. We expect that deregulation of specific circadian genes will impair the ability of the iron metabolic pathway to buffer changes in iron levels. In order to correlate patterns of circadian transcription factor binding and transcriptional activity on iron metabolic genes, we will use genome-wide ChIP-seq and nascent-seq datasets obtained from synchronized mouse liver tissue. By mapping circadian factors' binding to iron metabolic genes in the mouse genome, we will determine to what degree rhythmicity in intracellular iron is due to direct transcriptional regulation by the clock.

Aim 2: To identify points of control at which endogenous labile iron influences clock core regulation and impacts resetting.

Iron overload can be acquired through both genetic and dietary factors, and can lead to widespread health detriments[64, 93, 149]. Proper homeostasis requires an organism to be in sync with its environment and dietary sources, including iron, and therefore *we hypothesize that internalized iron may exert a level of feedback on the circadian clock in order to maintain homeostasis.* Our preliminary data show that core circadian components are expressed rhythmically in synchronized HepG2 cells. We will first investigate how either enriching or depleting the labile iron pool influences the steady state level of expression of core clock components and their capacity to sustain circadian rhythmicity. We will use a combination of molecular tools and a cell knock-in PER2 reporter system to monitor changes in circadian parameters (*i.e.,* phase, period, and amplitude) and establish the relevance of iron levels for maintaining circadian oscillations.

Impact: Our studies will provide insight into how the circadian clock coordinates rhythmic iron uptake through feeding with hepatic homeostasis and thus we aim to provide a means for considering the relevance of circadian factors in individuals who, for genetic or behavioral reasons, are unable to maintain iron homeostasis. In addition, applications of this molecular crosstalk help

guide future translational studies regarding the timing of cancer treatments which use iron metabolism components as conjugates for targeted therapy. Among individuals with clock impairment due to genetic mutations or behavioral obstacles such as shift work, the detriment to iron metabolism homeostasis could place these individuals at increased risk of liver damage and ultimately hepatocellular carcinoma.

Chapter 2: Role of the circadian clock mechanism in balancing the level of the intracellular labile pool of iron.

2.1 Introduction

The body uses several signaling mechanisms to modulate iron concentrations. One of the primary methods is through the hepcidin/ferroportin axis[133]. Hepcidin production in the liver is upregulated in response to excessive iron conditions, subsequently binding to ferroportin and causing internalization and degradation [133]. This results in less iron absorbed by duodenal enterocytes being exported into the circulation, as well as reducing the export of iron stored in hepatocytes and macrophages [133]. Transcriptional induction of hepcidin in high circulatory iron conditions is reliant on HFE sensitivity to transferrin saturation levels [133]. In order for hepcidin production to also be sensitive to intracellular iron conditions, an alternative mechanism composed of bone morphogenic protein 6 (BMP6) is needed [150]. BMP6 acts in conjunction with hemojuvulin (HJV) to stimulate hepcidin production [150]. Loss of function in hepcidin, HFE, and hemojuvulin result in unchecked export of iron by ferroportin, and are common causes of the iron overload disorder hemochromatosis [133].

Another iron sensing mechanism is the hypoxia inducible factor (HIF) pathway, in which the HIF-α/β heterodimer is sensitive to both oxygen and iron levels in the management of hypoxia and anemia [133]. The regulatory subunit of the heterodimer is HIF-α, which is stabilized in hypoxic conditions and leads to transcriptional activity of HIF target genes including *TRF, TFRC*, and *HAMP* [133]. In order for the HIF pathway to respond to systemic iron levels, the enzyme family prolyl hydroxylase 1-3 (PHDs) is required [133]. PHDs require a ferrous iron ion for catalytic function, in which PHDs hydroxylates HIF-α and triggers its degradation [133]. Therefore under low iron conditions PHD activity is low and HIF transcription factor activity increases [133]. HIF

goes on to bind and inhibit *HAMP* transcription while also enhancing *TRF* and *TFRC* transcription, serving to increase the amount of intestinal iron absorption and export of iron stores into the circulation [151-153].

The balance of intracellular iron import, storage, and export is largely regulated by the IRPs binding to iron responsive elements (IREs) in iron metabolic transcripts [66]. During conditions of low iron, IRPs bind to 5' IREs in transcripts for H-ferritin and ferroportin, thereby blocking their translation and inhibiting iron storage and export, while simultaneously enhancing iron intake by binding 3' IREs in *TFRC* mRNA [66]. Because the binding of IRPs to IREs is inhibited by iron, this provides a sensitive method for iron homeostasis to be maintained. Dual knockouts of *IRP1* and *IRP2* are embryonically lethal, illustrating the critical importance of this iron sensing pathway [154].

Because iron is poorly excreted from the body, its absorption in the small intestine and metabolism throughout the body must be tightly regulated. The circadian clock is a regulatory pathway which coordinates physiology with the environment, and is found in organisms ranging from mammals to plants and bacteria [155]. In humans, the main pacemaker of the clock is the suprachiasmatic nucleus in the brain, although peripheral oscillators semi-autonomously maintain rhythms as well [156]. The liver contains an especially robust peripheral clock, in addition to being the primary organ of iron storage. There is a limited amount of evidence which suggests that the circadian clock is involved in regulation of iron metabolic components [127, 128]. In tumor implants in mice, *IRP2* oscillated with a circadian rhythm, in turn generating post-transcriptional oscillation in *TFRC* mRNA [127, 128]. In clinical studies, there is evidence that metrics such as serum iron concentration and transferrin saturation fluctuate with daily rhythms [123, 124]. Slowly, a picture is emerging of how the circadian clock coordinates iron homeostasis in hepatocytes with the rhythmic ingestion of iron by feeding.

2.2 Materials and Methods

Cell cultures

Human hepatocellular carcinoma (HepG2) cells were a gift from Dr. Herbert Bonkovsky (Wake Forest University) and maintained in Dulbecco's Modified Eagle's Medium (DMEM, MT 10-014-CV, Corning) supplemented with 10% (v/v) fetal bovine serum (2916254 MP Biomedicals, 30μM Fe^{+}), 50 units/ml penicillin, and 50 units/ml streptomycin. The use of this fetal bovine serum resulted in a growth media with an iron concentration of 3 μM, which is very low compared to the physiological range of iron in the serum of human blood (10-30 μM). Mouse embryonic fibroblasts expressing a PER2::Luciferase fusion protein (MEF PER2::LUC) cells were a gift from Dr. Shihoko Kojima (Virginia Tech University) and were cultured in Dulbecco's Modified Eagle's Medium (DMEM, MT-10-013-CV, Corning) supplemented with 10% FBS (2916254 MP Biomedicals), 50 units/ml penicillin, and 50 units/ml streptomycin. Alpha mouse liver 12 (AML12) cells were purchased from ATCC and were cultured in a 1:1 mixture of DMEM (MT 10-013-CV, Corning) and Ham's F12 (12-615F Lonza) supplemented with 10% FBS (35-010-CV, Corning), 40 ng/ml dexamethasone, 0.005 mg/ml insulin, 0.005 mg/ml transferrin, and 5 ng/ml selenium (ITS, 25-800-CR, Cellgro). All cells were maintained at 37°C in a cell culture incubator injected with CO_2 to achieve a 5% (v/v) final CO_2 concentration.

Transfection of recombinant DNA and siRNAs

Cells were seeded at $3x10^5$ cells/well in 6-well plates and grown until an estimated 50-80% confluence was reached as judged by microscopy. Transfection was optimized using Lipofectamine LTX (Life Technologies) according to manufacturer's instructions. Transfections were carried out

in HyClone HyQ-RS reduced serum media (SH30565.02, HyClone) for 4 h. Cells were then maintained in appropriate media without antibiotics, at 37°C and 5% CO_2 (v/v) for 24 h to allow transfected proteins to express prior to harvesting or further treatment. Transfections with siRNAs were performed using Dharmafect 4 (T-2004-01, GE Healthcare) and 25 nanomoles of siRNA according to manufacturer's instructions. Cells were incubated in serum-free media with siRNA liposomes for 24 h, then complete growth media for a further 24 h before collection or further experimentation to allow for maximum protein knockdown. Protein extraction was performed in NP-40 lysis buffer containing 10mM Tris-HCL (pH 7.5), 137 mM NaCL, 1mM EDTA, 10% (v/v)glycerol, 0.5% (v/v) NP-40, 80 mM β-glycerophosphate, 1mM Na_3VO_4, 10 mM NaF, 10 uM leupeptin, 1uM aprotinin A, and 0.4 uM pepstatin.

In vitro circadian synchronization of mammalian cells

HepG2 cells were circadian synchronized using a serum shock procedure. At time -2h, regular growth media was replaced with media containing 50% (v/v) FBS (2916254 MP Biomedicals), with the understanding that this results in an increase in the iron concentration of the media to 15uM. At time 0h, this media was replaced with serum free media, and the synchronized cells would be harvested by trypsinization at the various times and stored at -80°C until further use. For all experiments involving synchronization of HepG2 cells, it was necessary to maintain the cells for 2 h in serum free media prior to addition of serum shock media. Therefore, cells cultured in plates which were to be synchronized would be maintained as normal in media with 10% FBS. At time -4h, the media would be replaced with serum free DMEM. At time -2h, the media would be replaced with the serum shock synchronization media containing 50% FBS. At time 0h, the media was replaced with serum free DMEM, and the synchronized cells were harvested at specified timepoints.

Immunoblot assays

Cell lysates (~70μg) were resolved by SDS-PAGE, and proteins analyzed by immunoblotting using primary antibodies directed against PER2 (Sigma-Aldrich), IRP2 (Cell Signaling) and tubulin (Sigma-Aldrich). Chemiluminescence reactions were visualized in a ChemiDoc XRS+ molecular imager (BIO RAD) using SuperSignal West Pico. Quantification of protein bands was performed using Image Lab software (BIO RAD).

Total RNA purification and qRT-PCR

RNA was extracted using Trizol reagent (15596-026, Life Technologies), following manufacturer's instructions. RNA samples were resuspended in DEPC treated water, and their purity and integrity analyzed using Agilent TapeStation by the Genomics Research Laboratory at the Biocomplexity Institute of Virginia Tech. Samples were incubated with DNase using an RQ1 DNase Kit (M6101, Promega), and cDNA was synthesized using the iScript cDNA Synthesis Kit (170-8891, BIO RAD), following manufacturers' instructions. Specific gene mRNA expression was analyzed by qRT-PCR using PerfeCTa SYBR Green FastMix (95072-012 Quanta BioSciences) in 384 well plates (1438-4700, USA Scientific). Plates were thermocycled and scanned to measure fluorescence in a QuantStudio 6 Flex machine (Life Technologies), running QuantStudio Real-Time PCR System software. Primers used are listed in Table 2, FW indicates forward primer and RV indicates reverse primer.

Primer Name	Sequence (5' to 3')
TBP FW	cac gaa cca cgg cac tga tt
TBP RV	ttt tct tgc tgc cag tct gga c
PER2 FW	tga gaa gaa agc tgt ccc tgc cat
PER2 RV	gac gtt tgc tgg gaa ctc gca ttt
CLOCK FW	agt tca gca acc atc tca ggc tca
CLOCK RV	ttg ctg gtg atg tga ctg agg gaa
CRY2 FW	atc att ggt gtg gac tac
CRY2 RV	tct gct tca ttc gtt ca
BMAL1 FW	tca ttc tca ggg cag cag atg gat
BMAL1 RV	gag ctg ctc ctt gac ttt ggc aat
IREB2 FW	tcg atg tat cta aac ttg gca cc
IREB2 RV	gcc atc aca att tcg tac agc ag
SLC40A1 FW	ttg aac atg agc aag agc cta
SLC40A1 RV	agt agg aga ccc atc cat ctc g
HAMP FW	tcc tgc tcc tcc tcc tc
HAMP RV	cag atg ggg aag tgg gtg tc
FTH1 FW	cgc ctc cta cgt tta cct gt
FTH1 RV	cac act cca ttg cat tca gc
TFRC FW	ggc tac ttg ggc tat tgt aaa gg
TFRC RV	cag ttt ctc cga caa ctt tct ct
TRF FW	tga ttg cat cag ggc cat tg
TRF RV	gcc agg taa gca tca tac acc a

Table 2. List of qRT-PCR primer sequences used.

In vitro iron treatment and quantification of the endogenous iron pool.

To induce iron overload, ferrous sulfate ($FeSO_4$, S25326, Fisher Scientific) was added to HepG2 cell media to a final concentration of 100nM-1 mM, and MEF PER2::LUC cell media had $FeSO_4$ added to a final concentration of 1 μM. Ferrous sulfate was added directly to the DMEM complete growth

media (10%FBS) at 37°C to avoid precipitation of the compound. Intracellular iron was depleted from the cells by supplementing the DMEM+10% FBS with up to 15 μM final concentration of 2-2'-dipyridyl (DP, D216305, Sigma), only supplementing the media with the chelator at concentrations which maintained cell viability. Viability was evaluated by using a MTT Cell Viability Assay (KA1606, Abnova). In order to measure intracellular iron levels, ~$5x10^6$ cells were cultured in 100 mm dishes for 24 h before adding aqueous $FeSO_4$ or DP for either 8h or 48h. Cells were harvested and rapidly homogenized at 4°C. Iron content of lysates was measured using a ferrozine based commercially available iron assay kit (MAK025-IKT, Sigma) in a 96 well plate. This colorimetric assay was quantified by measuring absorbance in a spectrophotometer plate reader (Molecular Devices SpectraMAX 190).

Analyses of ChIP-seq and RNA-seq datasets

The ChIP-seq and mRNA-seq datasets utilized in our studies were published by (Koike et. al. 2012) and analysis was performed using the UCSC Genome Browser. Briefly, datasets were generated from mice entrained first in Light/Dark (LD)12:12 condition before being switched over to DD12:12. Liver samples from 3-6 mice were collected every 4 h. For ChIP-seq experiments, antibodies directed against BMAL1, CLOCK, PER1, PER2, CRY1, and CRY2 were incubated with liver homogenate, before crosslinking and sonication. Fragmented chromatin was eluted, purified, and amplified in order to generate a sequencing library as described [157]. Sequencing was performed on an Applied Biosystems SOLid4 or 5500xl instrument and reads were mapped to the NCBI m37/mm9 mouse genome (RefSeq ID 165668). Sequencing depth was adjusted for by down sampling among the time points for each antibody. Liver samples used for whole transcriptome mRNA-seq were collected over a 48 h period, and RNA was extracted using Trizol. Total RNA

from 3 mice was pooled for each time point. Sequencing libraries were constructed and run using SOLid sequencing technology, and reads were mapped to the NCBI m37/mm9 mouse genome. Read mapping was normalized to reads per kilobase measured (RPKM), and visualized on the UCSC Genome Browser (https://genome.ucsc.edu/index.html). All datasets are published in the Gene Expression Omnibus, under accession number GSE39860.

Nascent-seq datasets were from Menet et. al., 2012. Briefly, mice acclimated to LD12:12 were sacrificed every 4 h, and liver tissue was homogenized and nuclei were isolated. Total RNA was isolated by Trizol extraction, before removal of mRNA using beads to target polyadenylated RNA. The remaining nascent RNA was precipitated and prepared into an Illumina sequencing library, and sequenced using an Illumina Genome Analyzer. Reads were mapped to the NCBI mm9 mouse genome (RefSeq ID 165668), and deposited in the Gene Expression Omnibus under accession number GSE36916.

For our analysis in UCSC Genome Browser, the deposited BEDGRAPH file for each collection time within a series was imported as a custom track. Track scaling for all tracks within a series was dictated by the maximum peak height observed within the gene of interest among those tracks. The UCSC Genes track was selected as the visual representation of validated gene sequences for reads to map to. The Mammal Cons track was utilized to look for regions of conservation among placental mammals. For ChIP-seq datasets, any areas of the gene of interest which displayed binding peaks had those regions of the gene sequence searched for E-box motifs [158].

2.3 Results

The intracellular labile iron pool follows an oscillatory circadian rhythm.

Initially, we asked whether the intracellular iron concentration varied in cells maintained in cell culture. Specifically, we were interested in the labile pool of ferrous iron that cells maintain for incorporation into a multitude of critical enzymes. It is known that physiological iron parameters such as serum iron concentration or transferrin saturation vary in patients throughout the day, yet whether this translates in to a change in the intracellular iron remains unclear [123]. Furthermore, rather than working in an animal model in which bioavailablity of iron to hepatocytes varies according to daily feeding rhythms, we asked whether hepatocytes grown in culture and maintained at constant extracellular iron levels would show rhythmic oscillation in intracellular iron simply due to circadian synchronization. HepG2 cells were circadian synchronized, and ferrous iron concentration was analyzed as described in Materials and Methods. Our data show a rhythmic change in the size of the labile iron pool maintained by the cells, despite there being no change in the amount of iron available to the cells (Figure 1A). While the amplitude of the labile oscillation was low, this is to be expected given the tight regulation of iron concentration required to minimize genotoxic effects. This suggests there is rhythmicity of iron metabolism that is independent of the extracellular iron environment. The observed rhythm in labile iron could be generated by oscillations in one or more iron metabolic components responsible or import, storage, or export of iron.

Circadian factors modulate the expression of iron metabolic genes.

After observing temporal variation in the labile iron pool, we asked whether oscillations were due to clock involvement in the expression of iron metabolic genes. Initially, we monitored the expression of *IREB2*, *SLC40A1*, and *TFRC* genes under conditions in which *CLOCK*, *BMAL1*, or *PER2* were overexpressed in HepG2 cells. These iron regulatory genes were chosen because they are involved

in overall iron metabolism, iron export, and iron import respectively. *TRF, HAMP,* and *FTH1* were also measured (Figure S4), however they no change was observed following circadian perturbation as seen with *IREB2, SLC40A1,* and *TFRC*. *IREB2* and *SLC40A1* showed in increase in mRNA quantity in response to *myc-BMAL1* transfection, while TFRC was largely invariant (Figure 1B). Overexpression of PER2 resulted in lowered expression of *IREB2*, while *SLC40A1* and *TFRC* remained unchanged. *PER2* mRNA levels were measured as a control because it is known to be a classically controlled circadian gene through E-box binding. Next, we monitored the expression of iron metabolic genes in a background in which *PER2* expression was downregulated using siRNA (Figure 1C). In both HepG2 cells as well as AML12 mouse hepatocytes there was a significant increase in *IREB2, SLC40A1,* and *TFRC* mRNA quantity. By downregulating *PER2* expression we inhibit the negative arm of the circadian feedback loop, which should have the same net effect on circadian transcriptional regulation as when a positive component such as *BMAL1* is overexpressed. Therefore, the consistent results we see for *IREB2* and *SLC40A1* transcription in response to both types of circadian manipulation are in agreement with the context of the pathway.

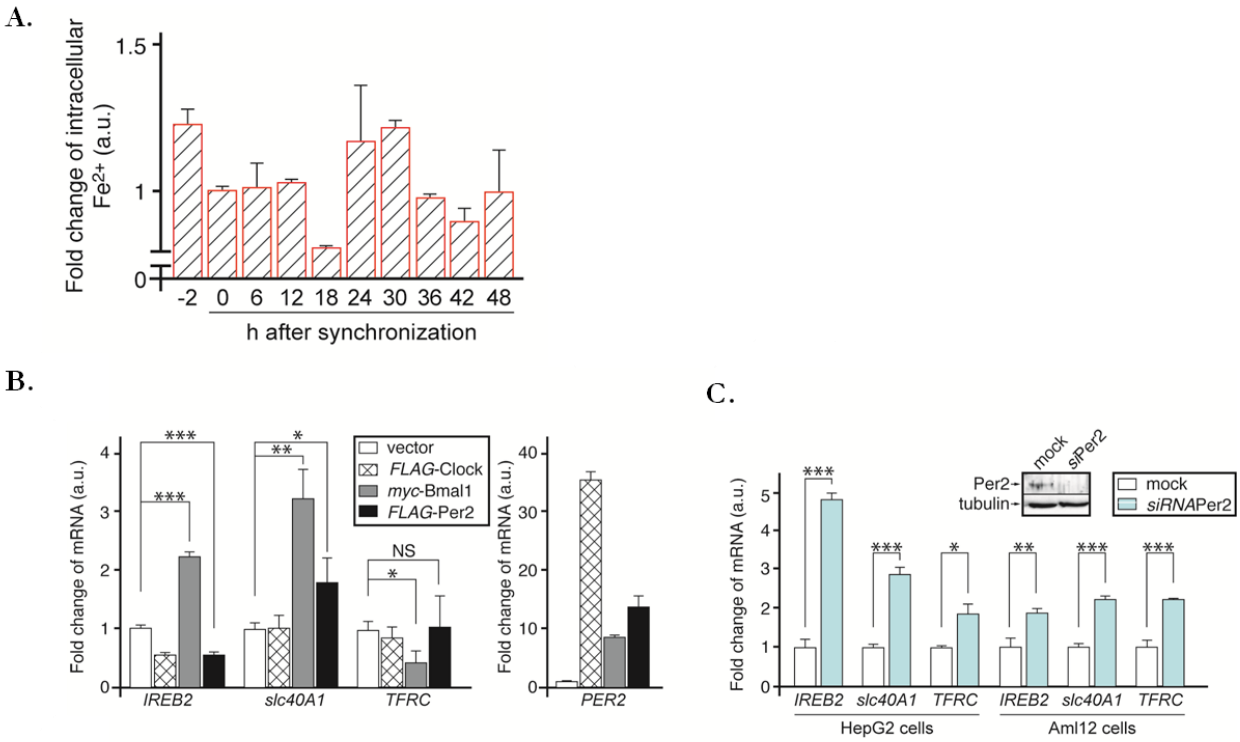

Figure 1. The expression of iron metabolic genes is sensitive to overexpression or repression of core circadian components. A. Endogenous ferrous intracellular iron was quantified by ferrozine assay (Sigma) in HepG2 cells circadian synchronized by a 2h incubation with 50% FBS. Results represent biological triplicates, each replicate comprised of $2x10^6$ cells. The assay was quantified in a plate reader at 593 nm, and results were normalized to the 0h timepoint. **B.** HepG2 cells were transfected with pCS2+FLAG-CLOCK, pCS2+myc-BMAL1, pCS2+FLAG-PER2, or empty vector using Lipofectamine LTX Plus as described in Materials and Methods. Cells were harvested 24h after transfection. Expression of *IREB2, SLC40A1,* and *TFRC* was analyzed by qRT-PCR. *PER2* was used as a control. **C.** HepG2 and AML12 cells were transfected with siRNA targeting *PER2* using Dharmafect. Iron metabolic gene expression was quantified by qRT-PCR for HepG2 cells, and by microarray (Affymatrix) for AML12 cells. Significant changes in expression were determined by t-test. *$p \leq 0.05$; ** $p \leq 0.005$; *** $p \leq 0.001$

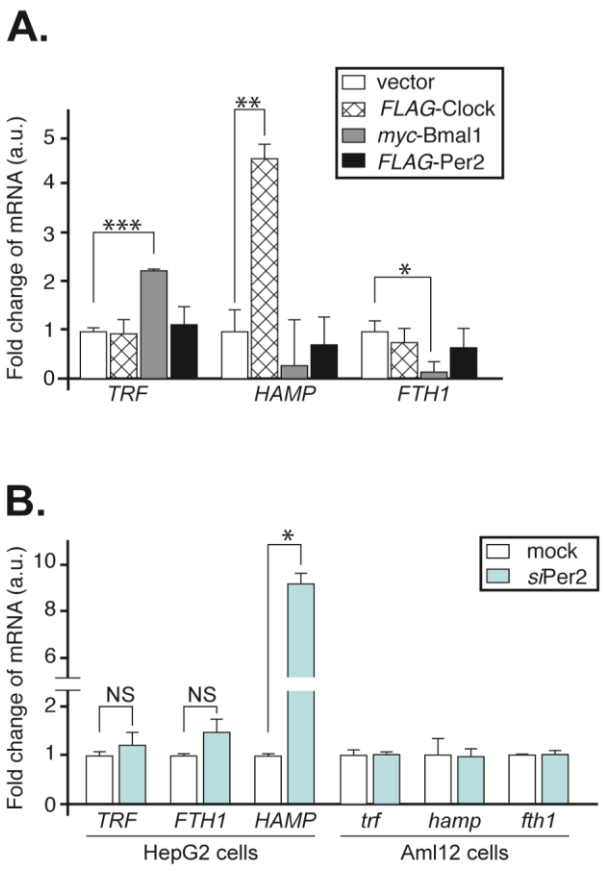

Figure S4. The expression of *TRF, FTH1,* and *HAMP* in HepG2 cells with altered clock gene expression.

A. HepG2 cells were transfected with pCS2+FLAG-CLOCK, pCS2+myc-BMAL1, pCS2+FLAG-PER2, or pCS2+ empty vector using Lipofectamine LTX Plus. Expression of *TRF, HAMP,* and *FTH1* was analyzed by qRT-PCR. **B.** HepG2 and AML12 cells were treated with si*PER2* in order to knockdown PER2 expression. Expression of *TRF, FTH1,* and *HAMP* was analyzed by qRT-PCR in HEPG2 cells and by microarray in AML12 cells. Significance was determined by t-test. *$p \leq 0.05$; ** $p \leq 0.005$; *** $p \leq 0.001$

Rhythmicity of TFRC expression is generated post-transcriptionally and is dependent on the cellular iron status

Because we previously measured changes in *TFRC* expression due to altered levels of BMAL1, we hypothesized that there may be circadian rhythmicity of the transcript, we therefore measured the latter's expression in a 48 h time course experiment using qRT-PCR (Figure 2A). We observed that *TFRC* oscillates with a circadian rhythm in untreated cells. Interestingly, when ferrous sulfate (30uM final concentration) is added to the media the level of transcription in several genes related to the iron metabolic pathway was affected. *TFRC* transcription is strongly repressed in order to limit the influx of extracellular iron. By supplementing the media with ferrous sulfate, we can increase the intracellular iron concentration (Figure S1C); the observed downregulation of *TFRC* confirms that our hepatocytes are able to modulate transferrin internalization in response to environmental surges in available iron.

Next, asked whether the observed rhythm in TFRC expression was mediated by binding of clock components to the gene's regulatory region. We analyzed clock factor binding to *TFRC*, and identified circadian protein binding near the transcription start site by BMAL1, CLOCK, PER2, CRY1, and CRY2 (Figure 2B). This binding showed rhythmicity, with positive clock components BMAL1 and CLOCK binding peaking between CT0 and CT8, while binding by the negative clock components PER2 and CRY2 was maximal from CT16 to CT20. Binding by these circadian clock proteins does not necessarily mean that they are driving rhythmicity of transcription, therefore we turned to the nascent-seq dataset to quantify *de novo TFRC* transcription over time (Figure 2C). Surprisingly, the rhythmic protein binding by CLOCK and BMAL1 observed in Figure 2A did not lead to rhythms in transcription of *TFRC*, suggesting factors other than clock components need to be recruited by the core complex to trigger circadian transcription. Having already observed that our qRT-PCR data suggests a rhythm in *TFRC* mRNA, we sought to verify our findings by

analyzing the mouse liver transcriptome. Here, as in our synchronized HepG2 cells, *TFRC* mRNA displayed an oscillation, peaking ~CT12. This data together indicates that although there is robust binding of circadian clock factors to the *TFRC* gene, rhythms in *TFRC* expression are generated at the post-transcriptional level.

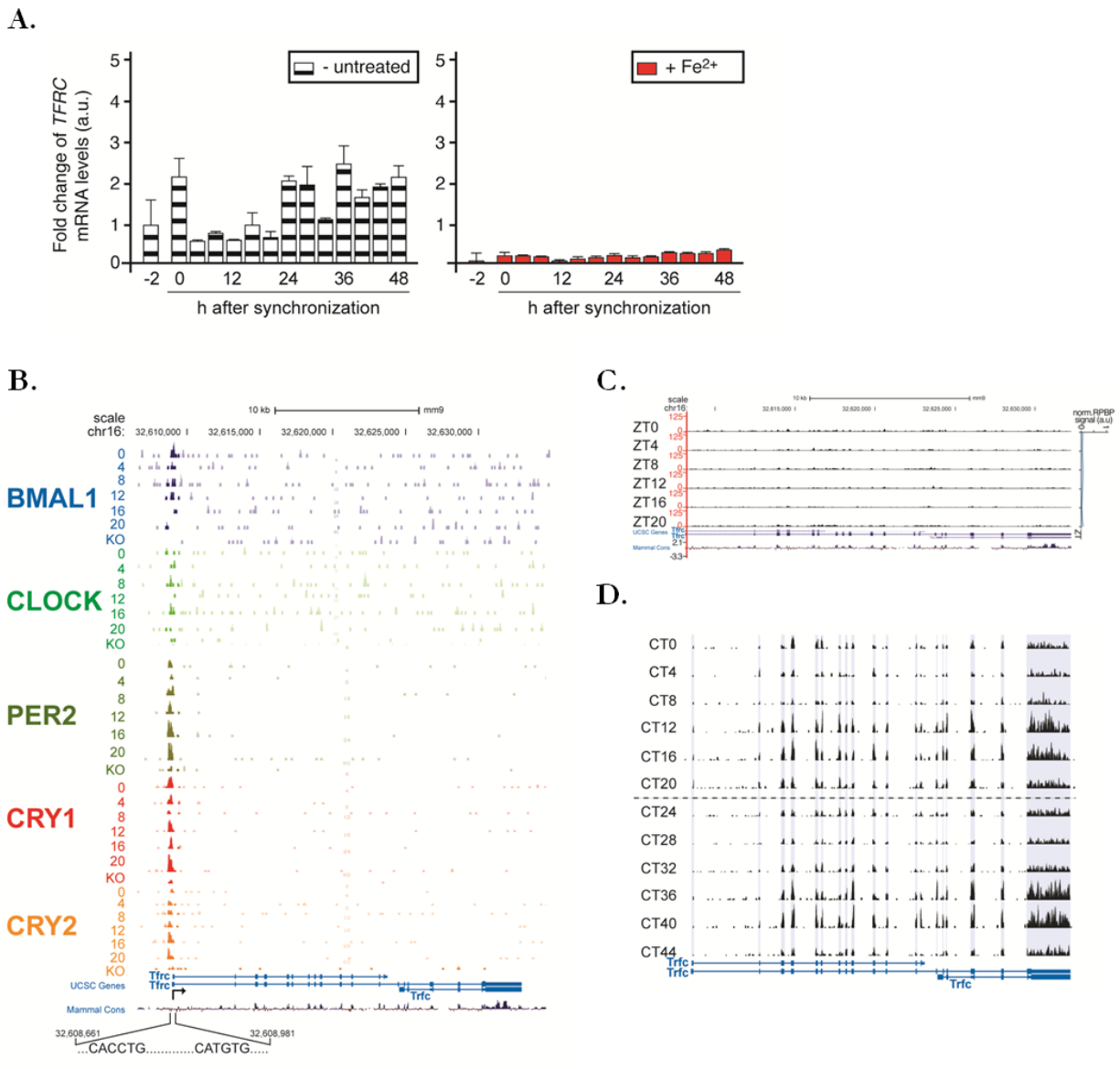

Figure 2. Circadian oscillations in *TFRC* expression are not generated by rhythmic *de novo* transcription.

Figure 2. Circadian oscillations in *TFRC* expression are not generated by rhythmic *de novo* transcription. A. HepG2 cells were treated with $FeSO_4$ for 8h prior to synchronization with dexamethasone (100nM). Cells were then maintained in serum free media that contained $FeSO_4$ in the case of treated cells, and collected at the times indicated. Expression of *TFRC* was quantified by qRT-PCR, normalizing within each treatment group to the -2h timepoint. Between treatment groups, the $+Fe^{2+}$ and +2,2'-DP groups were normalized to the untreated group using the ΔCT values of *TFRC* in each -2h timepoint and using this normalization factor from the unsynchronized cells to properly represent the comparative expression of *TFRC* between the time series. **B-D.** Figures generated from dataset deposited by (Menet et. al., 2012) and (Koike et. al., 2012). **B.** ChIP-seq data was used to analyze circadian protein binding to *TFRC*. Liver samples were taken from entrained mice maintained in D:D 12:12 from CT0 to CT20. Knockout mice which did not express circadian gene of interest were included as a control. Mouse liver homogenate was incubated with antibodies directed against the indicated circadian proteins before crosslinking, and the resulting isolated chromatin was amplified and SOLiD sequenced, before reads were mapped to the mouse genome (NCBI m37/mm9). Circadian protein binding to *TFRC*, occurs predominantly near the transcription start site. **C.** Nascent RNA was isolated from mouse liver, from animals housed in LD 12:12. Purified nascent RNA was used to generate Illumina libraries, sequenced using an Illumina Genome Analyzer. Sequences were aligned to the mouse genome (UCSC mm9), and analyzed using UCSC Genome Browser. Transcription of *TFRC* is nonrhythmic, **D.** mRNA was isolated from the livers of entrained mice maintained in DD 12:12, collected every 4h from CT0 to CT44. Sequencing libraries were constructed using SOLiD Total RNA-seq Kit, and sequencing was run on an ABI SOLiD4 instrument. Sequences were aligned to the mouse genome (UCSC mm9) and analyzed on UCSC Genome Browser. *TFRC* mRNA is rhythmic in contrast to the nascent RNA data.

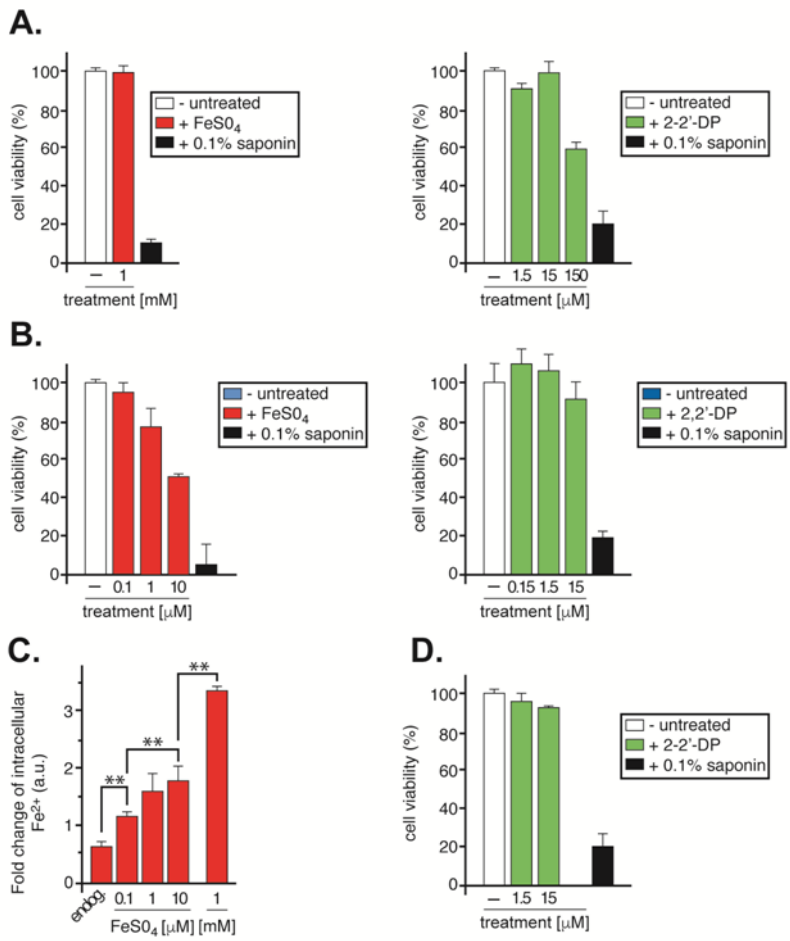

Figure S1. Intracellular iron concentration can be manipulated while maintaining cell viability. **A.** Treatment of HepG2 Cells with $FeSO_4$ (1mM) or 2,2'-DP (1.5uM, 15uM) does not noticeable impact cellular viability, measured by MTT assay (Abnova). Saponin (0.1%) was used as a control. Treatment of HepG2 cells with 2,2'-DP (150uM) did have a detrimental impact on viability, and therefore 15uM was chosen to treat cells in all relevant experiments. Chemicals were added directly to the media for 48h prior to viability assay. **B.** MEF PER2::LUC cells were treated with either $FeSO_4$ (0.1 μM, 1 μM, 10 μM) or 2,2'-DP (0.15 μM, 1.5 μM, 15 μM) for 48h prior to viability analysis by MTT assay. **C.** HepG2 cells were treated with $FeSO_4$ (0.1 μM, 1 μM, 10 μM, 1mM), and increase in intracellular iron relative to untreated controls was measured using a ferrozine based assay (Sigma). Significance was calculated using t-tests. *$p \leq 0.05$; ** $p \leq 0.005$; *** $p \leq 0.001$ **D.** HepG2 cells were treated with 2-2'-DP (1.5 μM, 15μM), and intracellular ferrous iron was measured as described in Materials and Methods.

IRP2 circadian rhythmicity is dampened by iron overload.

We hypothesized that rhythms in *TFRC* transcript levels were being generated post-transcriptionally. Therefore we tested whether the expression of IRP2 exhibits a circadian variation.

By modulating *TFRC* and other iron metabolic post-transcriptional events IRP2 functions as a master regulator of intracellular iron concentration, therefore we chose to examine whether there were oscillations in *IREB2* mRNA and its product IRP2 protein[74]. To determine whether the observed rhythms in IRP2 protein were due to changes in mRNA levels, we analyzed *IREB2* mRNA rhythms by qRT-PCR (Figure 3A). These results indicate that the transcription of the gene varies over time, but not in a manner that conforms to a significant circadian rhythm over the 48h of collection (Figure 3A, Figure S2).

In both control and iron-treated cells there was a strong induction of *IREB2* expression during the last 12 h, that may have obscured any detectable rhythm in the transcript. *IREB2* transcription is upregulated in proliferating cells, and due to the nature of the time course experiment initial seeding density is low, therefore the final 12 h of collection may have taken place when cellular confluence is optimal for proliferation, and therefore *IREB2* is transcribed to enhance intracellular iron concentration [159]. Iron depletion by chelators is known to inhibit proliferation, and therefore may explain why the induction of *IREB2* after t=36 h is not seen in our 2-2'-DP treated cells [160]. Increased *IREB2* mRNA levels in the overloaded cells did not correlate with an increase in IRP2 protein (Figure 3C). Overall levels of *IREB2* mRNA are lower in chelated cells compared to control (Figure 3A), and peak protein levels at t=20h decreased by close to 50% as quantified by Western blot signal intensity (Figure 3C). MetaCycle analysis of *IREB2* mRNA rhythms showed that iron overload has a more noticeable effect on *IREB2* mRNA (Figure 3B). The phase is delayed by over 9 h, and the period of oscillation was shorter by almost 4 h. In cells grown in chelator-treated media, once again phase is the most sensitive rhythmic parameter calculated, with a phase delay in *IREB2* mRNA. This sensitivity of phase to iron status is logical if iron is acting as a secondary entrainment signal for the circadian clock in the liver. In animals, phase of the clock in the liver can be controlled by feeding entirely independently of light patterns or the SCN [5], and

iron is one of many metabolites taken in during feeding which may serve as inputs to the liver clock. Because feeding is a behavior which occurs with 24 h patterns, using nutritional inputs to orient the phase of the clock in the liver to times when metabolic demand are highest while keeping the 24 h period in the liver consistent with global circadian behavior best allows for synchrony of liver physiology with an organism's behavior.

IRP2 protein showed circadian rhythmicity (p-value: 1.8E-10, Figure S3) in synchronized HepG2 cells which did not receive any treatment relating to iron availability (Figure 3C). This result alone could be sufficient to explain the observed rhythms in intracellular iron concentration. Like the observed downregulation of PER2 protein in cells treated with ferrous sulfate, IRP2 also showed decreased expression in iron overloaded cells, and ablation of detectable rhythmicity (Figure 3C, Figure S3). This is consistent with the literature on proteosome mediated degradation of IRP2 in cells cultured with 400ug/ml ferric ammonium citrate, an iron additive [161]. In aqueous media, iron is primarily present to the ferric state regardless of the oxidative state it is added as, so the use of ferric ammonium citrate is not functionally different from our use of ferrous sulfate [162]. In iron depleted cells treated with 2-2'-DP, there was a shortening of the period and phase advance of IRP2 rhythms according to MetaCycle analysis (Figure 3D). MetaCycle indicated a shortening of the period by over 4 h in overloaded cells, however such rhythmic parameters are very difficult to quantify due to IRP2 protein levels being downregulated 4-fold, with an amplitude 31 times lower than untreated cells (Figure 3C, Figure S3). Downregulation of IRP2 during iron overload is expected because IRP2 functions to synergistically regulate other iron metabolic mRNAs and raise the intracellular iron concentration. Under conditions of extreme iron overload, the repression of IRP2 would be more important than maintaining typical daily fluctuations in expression. We speculate this is an attempt to restore homeostasis to the cell, which is what we see in Figure 3C.

If IRP2 were causing rhythmicity of *TFRC* mRNA by positively regulating transcript stability, we would expect for peaks of IRP2 protein to coincide of *TFRC* mRNA, and indeed this is exactly what we observe. The oscillations are in phase with peaks ~0 h and 24 h, strongly suggesting that post-transcriptional rhythm generation in *TFRC* is due to rhythmic binding by IRP2.

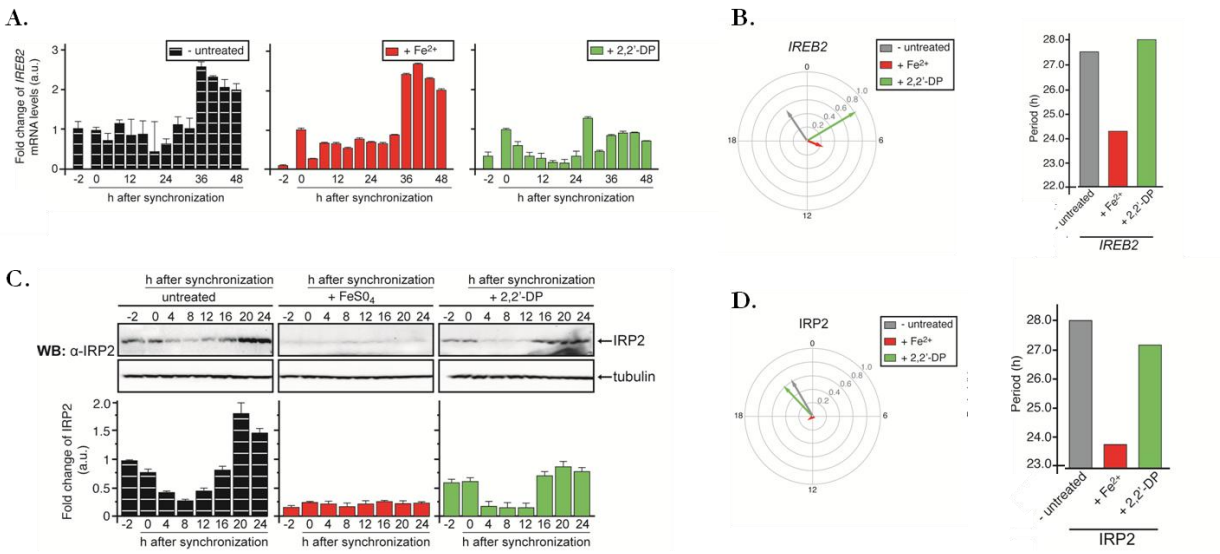

Figure 3. Expression of iron metabolism regulator IRP2 in circadian synchronized HepG2 cells which have compromised iron status. A. HepG2 cells were treated with $FeSO_4$ (1mM) or 2,2'-DP (15uM) for 8h before synchronization with dexamethasone (100nM, t=-2). Cells were then collected every 4h for 48h, and mRNA expression of *IREB2* was quantified by qRT-PCR. The -2h timepoint was used to normalize relative expression levels between treated groups and the untreated cells. **B.** Analysis of period, phase, and amplitude of mRNA rhythms was performed using MetaCycle. Phase is indicated by the direction of the arrow, and normalized amplitude by the length of the arrow as indicated on the graph's scale. **C.** Following 48h incubation with either $FeSO_4$ or 2,2'-DP, HepG2 cells were synchronized by 2h serum shock (FBS, 50%). Cells were collected every 4h for 24h, and lysates were resolved by SDS-PAGE and analyzed by immunoblotting using α-IREB2 antibody. α-tubulin was used as a loading control. Protein levels were quantified by densitometry using ImageJ software. Quantification of IRP2 was normalized to tubulin, and the -2h timepoint was used to calculate relative protein amounts between $FeSO_4$ or 2,2'-DP treated groups and untreated. Multiple exposures of each blot were used to calculate standard deviation of the densitometry signal. **D.** Analysis of the period, phase and amplitude of the protein rhythms observed in (**C.**) was performed using MetaCycle, by integrating the ARSER, JTK-Cycle, and Lomb-Scargle methods with Fisher's method for integration of p-values. Phase is indicated by the direction of the arrow, and amplitude corresponds to the length of the arrow. Untreated is shown in grey, $+Fe^{2+}$ in red, and +2-2'-DP in green.

mRNA	treatment	Benjamini-Hochberq q-values (BH.Q)	Permutation-based p-values	Period	Phase	Amplitude
Per2	none	9.07E-05	3.02E-05	27.51	15.51	0.692
	+ Fe^{2+}	0.076	0.038	22.61	11.81	0.724
	+ 2,2'-DP	1.86E-06	3.11E-07	28	16.12	1.203
IREB2	none	0.753	0.753	28	21.71	0.517
	+ Fe^{2+}	0.246	0.164	24.3	7.41	0.244
	+ 2,2'-DP	0.642	0.535	28	15.97	0.818

Figure S2. MetaCycle analysis of *PER2* and *IREB2* mRNA levels in synchronized HepG2 cells. MetaCycle is a freely available statistics package run in R. language which enables analysis of circadian rhythms. The MetaCycle2D algorithm was applied to qRT-PCR quantification of *PER2* and *IREB2* mRNA in synchronized HepG2 cells. Cells were treated with either $FeSO_4$ (1mM) or 2,2'-DP (15uM), and compared to untreated control. MetaCycle calculates circadian properties by integrating the ARSER, JTK-Cycle, and Lomb-Scargle methods with Fisher's method for integration of p-values.

protein	treatment	Benjamini-Hochberq q-values (BH.Q)	Permutation-based p-values	Period	Phase	Amplitude
PER2	none	0.0166	0.0107	26	24.14	0.2801
	+ $FeS0_4$	0.3423	0.2852	28	4.78	0.0189
	+ 2,2'-DP	1.22E-8	4.05E-9	25.35	24.07	0.3337
IRP2	none	1.08E-9	1.80E-10	28	22	0.6142
	+ $FeS0_4$	0.9997	0.9997	23.74	14.92	0.0194
	+ 2,2'-DP	1.27E-7	6.37E-8	27.15	21.11	0.6170

Figure S3. MetaCycle analysis of PER2 and IREB2 protein levels in synchronized HepG2 cells. MetaCycle is a freely available statistics package run in R. language which enables analysis of circadian rhythms. The MetaCycle2D algorithm was applied to densitometry quantification of immunoblotting by α-PER2 and α-IREB2 antibodies for a 24h timecourse in HepG2 cells. Cells were treated with either $FeSO_4$ (1mM) or 2,2'-DP (15uM), and compared to untreated control. MetaCycle calculates circadian properties by integrating the ARSER, JTK-Cycle, and Lomb-Scargle methods with Fisher's method for integration of p-values.

The iron exporter *SLC40A1* is transcriptionally regulated by circadian factors.

In addition to the observed effect of *TFRC,* rhythms in intracellular labile iron can be generated by varying the rate of iron export throughout the day. Because iron is exported from the mammalian cell by a single known protein, ferroportin, we decided to study the expression of *SLC40A1,* the gene encoding ferroportin. In untreated synchronized HepG2 cells, *SLC40A1*

mRNA was oscillatory, and this oscillation was also observed in cells which were under iron overload (Figure 4A). Unlike *TFRC,* which was downregulated under iron overload, the expression of *SLC40A1* increased over 5 fold in response to iron treatment, highlighting the importance of this factor in maintaining iron homeostasis (Figure 4A). The fact that apparent circadian variation persists in iron overloaded cells suggests that the circadian clock and iron metabolic pathways can work in parallel to regulate gene expression (Figure 4A).

As with *TFRC*, we analyzed patterns of circadian protein binding to the *SLC40A1* regulatory region (Figure 4B). Unlike the robust patterns of circadian protein binding to *TFRC* observed in Figure 2B, only CRY1 and CRY2 were detected bound to *SLC40A1*, suggesting a lack of CLOCK:BMAL1 driven transcription, however it does not rule out circadian involvement entirely. In fact, when we observe nascent RNA levels in mouse liver, we see a robust rhythm peaking sharply at CT8 (Figure 4C). This is in phase with the nascent RNA oscillation of DBP, a classical example of circadian transcriptional targets (Figure S5). This finding prompted us to evaluate whether the oscillation of *SLC40A1* mRNA expression was maintained. Surprisingly, we found that rhythmicity was largely lost in the mature transcript compared to the immature transcript, with a slight peak ~CT12-CT16 dampened compared to the sharp peak of expression at ZT8h observed in the nascent RNA (Figure 4D). As with *TFRC,* IRP2 acts upon *SLC40A1* mRNAs, however rather than enhancing mRNA stability IRP2 acts to block *SLC40A1* translation therefore it is likely that a different mechanism is responsible for obscuring rhythmicity in *SLC40A1*. Figure 4E is a schematic summarizing the differences observed between *TFRC* and *SLC40A1* with regards to transcriptional and post-transcriptional regulation by the clock. The observed patterns in circadian protein binding also seem to contradict the transcriptomics data at first, as *TFRC* was bound by many circadian proteins yet it is *SLC40A1* which shows rhythmic *de novo* transcription. However, if there were direct transcriptional regulation of these iron metabolic genes by the circadian clock, we could

expect there to be E-box *cis*-elements proximal to the transcription start site, yet we do not observe these elements within ~5 kb of the transcription start site in any of the iron metabolic genes analyzed. This does not mean that there is no transcriptional regulation by the circadian clock, it simply means regulation of iron metabolism might occur through the binding of additional transcription factors. Our understanding of global circadian regulation is decreasingly reliant on direct transcriptional activity by CLOCK:BMAL1, and these two iron metabolic genes seem to fall into different categories of circadian regulation, as well as being modulated differently by IRP2 which is itself rhythmic.

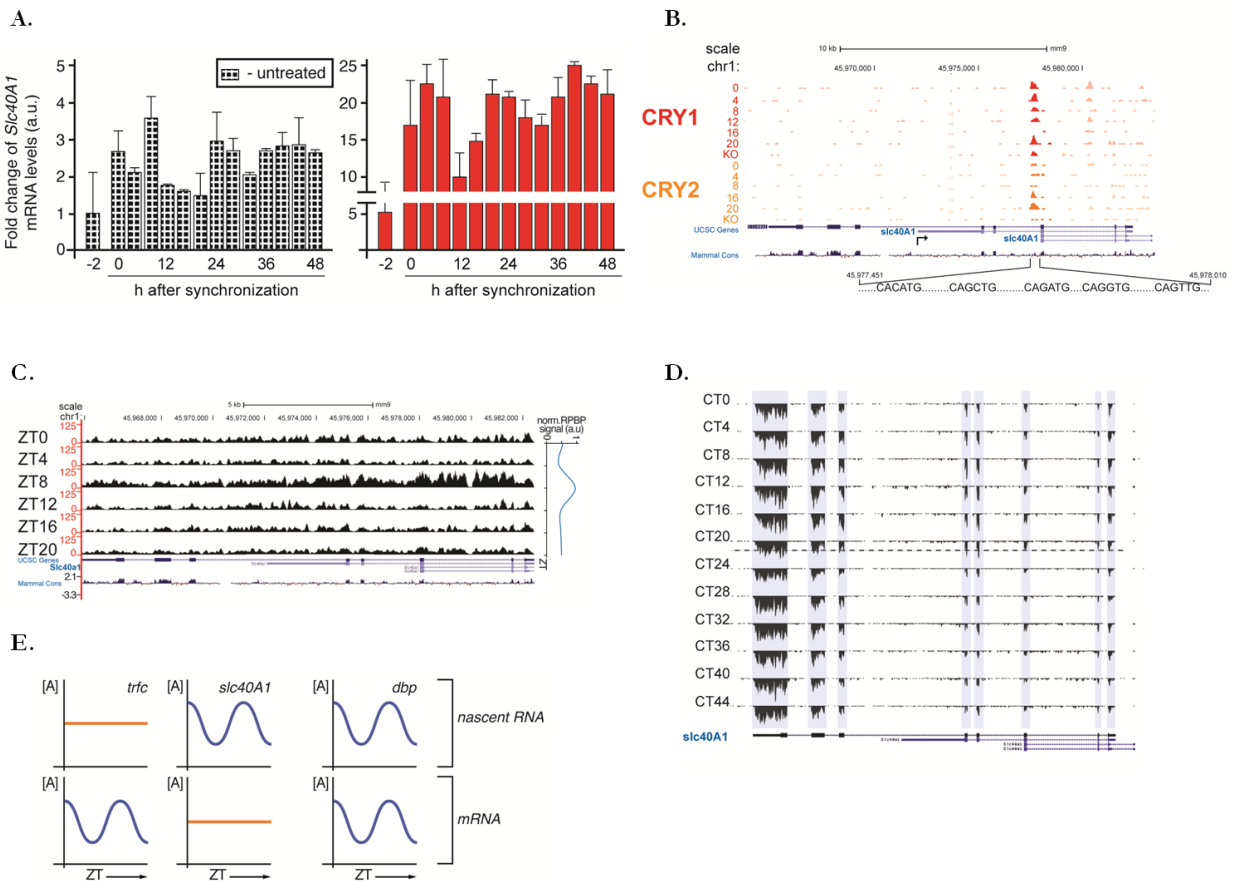

Figure 4. Transcriptional rhythms of *SLC40A1* are minimized by post-transcriptional effects. A. HepG2 cells were treated with $FeSO_4$ for 8h prior to synchronization with dexamethasone (100nM). Cells were then maintained in serum free media that contained $FeSO_4$ in the case of treated cells, and collected at the times indicated. Expression of *SLC40A1* was quantified by qRT-PCR, normalizing within each treatment group to the -2h timepoint. Between treatment groups, the $+Fe^{2+}$ and +2,2'-DP groups were normalized to the untreated group using the ΔCT values of *SLC40A1* in each -2h timepoint and using this normalization factor from the unsynchronized cells to properly represent the comparative expression of *SLC40A1* between the time series. **B-D.** Figures generated from dataset deposited by (Menet et. al., 2012) and (Koike et. al., 2012). **B.** ChIP-seq data was used to analyze circadian protein binding to *SLC40A1*. Liver samples were taken from entrained mice maintained in D:D 12:12 from CT0 to CT20. Knockout mice which did not express circadian gene of interest were included as a control. Mouse liver homogenate was incubated with antibodies directed against the indicated circadian proteins before crosslinking, and the resulting isolated chromatin was amplified and SOLiD sequenced, before reads were mapped to the mouse genome (NCBI m37/mm9). Analysis of *SLC40A1* shows only binding by CRY1/2 in mouse liver. **C.** Nascent RNA was isolated from mouse liver, from animals housed in LD 12:12. Purified nascent RNA was used to generate Illumina libraries, sequenced using an Illumina Genome Analyzer. Sequences were aligned to the mouse genome (UCSC mm9), and analyzed using UCSC Genome Browser. Transcription of *SLC40A1* shows a rhythmic *de novo* transcription, with a peak at ZT8. **D.** mRNA was isolated from the livers of entrained mice maintained in DD 12:12, collected every 4h from CT0 to CT44. Sequencing libraries were constructed using SOLiD Total RNA-seq Kit, and sequencing was run on an ABI SOLiD4 instrument. Sequences were aligned to the mouse genome (UCSC mm9) and analyzed on UCSC Genome Browser. *SLC40A1* mRNA no longer displays the robust oscillation observed in the nascent RNA data. **E.** Schematic showing the different stages at which *TFRC* and *SLC40A1* transcription is regulated by the circadian clock in mouse liver.

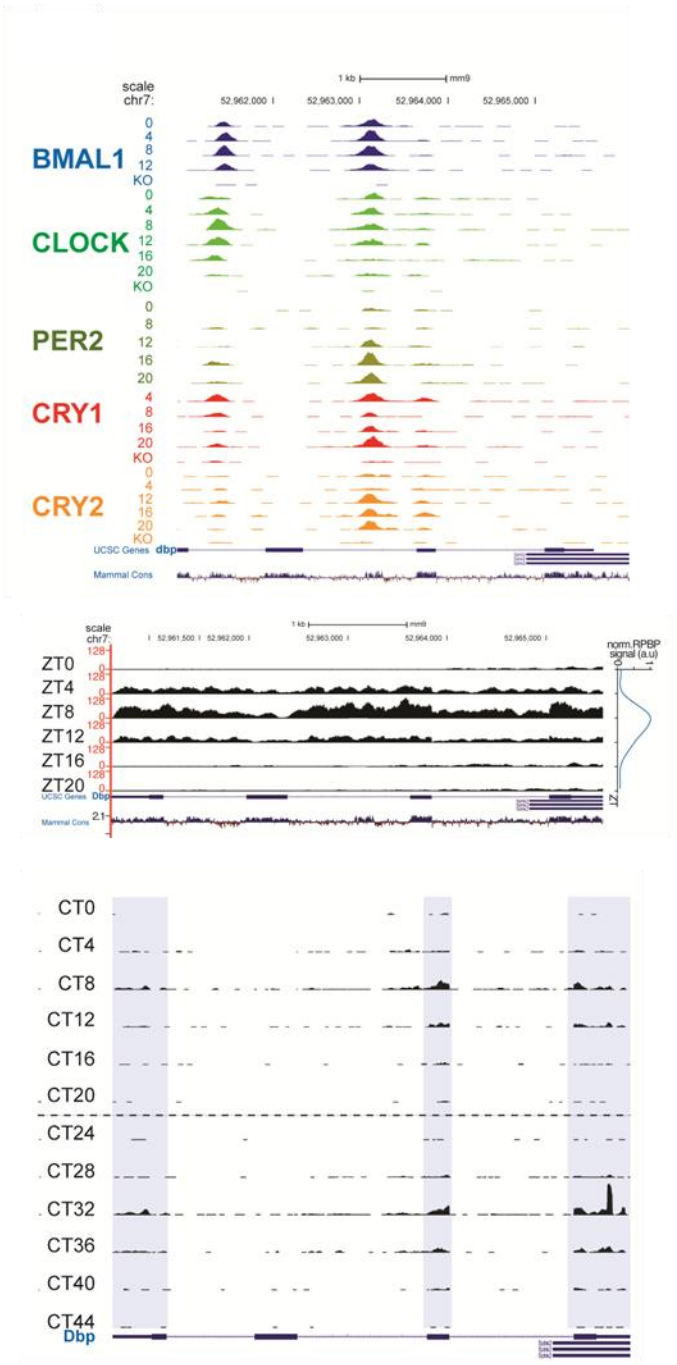

Figure S5. Genome wide cistrome and transcriptome analysis reveals variation in iron metabolic gene transcriptional regulation.

Figure S5. Genome wide cistrome and transcriptome analysis reveals variation in iron metabolic gene transcriptional regulation. Figures generated from dataset deposited by (Menet et. al., 2012) and (Koike et. al., 2012). ChIP-seq data was used to analyze circadian protein binding to *DBP* (**Top**). Liver samples were taken from entrained mice maintained in D:D 12:12 from CT0 to CT20. Knockout mice which did not express circadian gene of interest were included as a control. Mouse liver homogenate was incubated with antibodies directed against the indicated circadian proteins before crosslinking, and the resulting isolated chromatin was amplified and SOLiD sequenced, before reads were mapped to the mouse genome (NCBI m37/mm9). *DBP* is shown as a classical example of circadian transcription factor binding activity. Nascent RNA was isolated from mouse liver, from animals housed in LD 12:12. Purified nascent RNA was used to generate Illumina libraries, sequenced using an Illumina Genome Analyzer. Sequences were aligned to the mouse genome (UCSC mm9), and analyzed using UCSC Genome Browser (**Middle**). *DPB* is shown as an example of a classical clock-controlled gene, with high amplitude rhythmicity in nascent transcription. mRNA was isolated from the livers of entrained mice maintained in DD 12:12, collected every 4h from CT0 to CT44. Sequencing libraries were constructed using SOLiD Total RNA-seq Kit, and sequencing was run on an ABI SOLiD4 instrument. Sequences were aligned to the mouse genome (UCSC mm9) and analyzed on UCSC Genome Browser (**Bottom**). *DBP* is shown as an example of a classical clock-controlled gene, showing high amplitude rhythmicity in mRNA quantity within mouse liver.

siRNA knockout of PER2 *diminishes the ability of HepG2 to respond to acute iron influx.*

We next investigated the role of the circadian clock in the acute response to iron overload, as this reflects the physiological response to feeding. We devised an experiment where a sudden influx of iron was used to challenge HepG2 cells in which PER2's expression was downregulated by siRNA transfection (Figure 5). Cells were treated with 1mM ferrous sulfate at t=0h, and cells in this iron rich media were harvested every hour for the first 6 h in order to observe an immediate transcriptional response of the key iron metabolic genes *TFRC, IREB2,* and *SLC40A1*. Further collections at later time-points allowed us to see if the immediate transcriptional response was maintained for multiple days in a high iron media.

Our findings show a response in iron metabolic gene expression within 1 h to of increased iron availability, with an increase in *TFRC* mRNA levels. However, within 2 h the intracellular iron concentration had reached a plateau with a concentration 4-fold the initial value (Figure 5 inset), and by this point the expression of *TFRC* had begun to decrease. By 6 h after iron addition the transcript was barely detectable. *IREB2* expression showed an acute response of 2 fold increase in mRNA levels 1 h after iron addition; however by 24h after iron addition expression had increased 4 fold.

Interestingly, we saw transcriptional upregulation of *IREB2* more than 24 h after iron treatment in Figure 3A as well, where *IREB2* expression increased almost 3 fold after 36 h. In that time course we did not observe a corresponding increase in IRP2 protein, so it is unclear if the delayed increase in *IREB2* transcription is specifically involved in regulation of cellular response to acute iron influx. Alternatively, the expression of *SLC40A1* steadily increased over the first 6 h, in what we speculate is the result of an attempt by the cell to export the massive excess of iron.

HepG2 cells in which PER2 was downregulated by siRNA did not follow the same pattern of transcriptional response to iron influx, indicating that PER2 plays a role in the ability of hepatocytes to form an acute response to iron challenge. There was still a gradual increase in *SLC40A1* expression, but the initial immediate response by the transferrin receptor was not present, nor was the eventual upregulation of *IREB2*. We have already seen the clock play a role in the expression of IRP2, *TFRC,* and *SLC40A1*, and Figure 5 suggests that rapid adjustment to changes in iron is impaired in cells with a deficient clock. Because mammals receive iron almost entirely from dietary consumption, it is paramount that iron metabolism is able to rapidly respond to availability of iron in the duodenum, and eventually the bloodstream. One study showed that serum iron increased almost 13 μg/dl in individuals who ate breakfast versus those who fasted [163]. Our findings here indicate that this ability may be hindered in organisms with clock impairment.

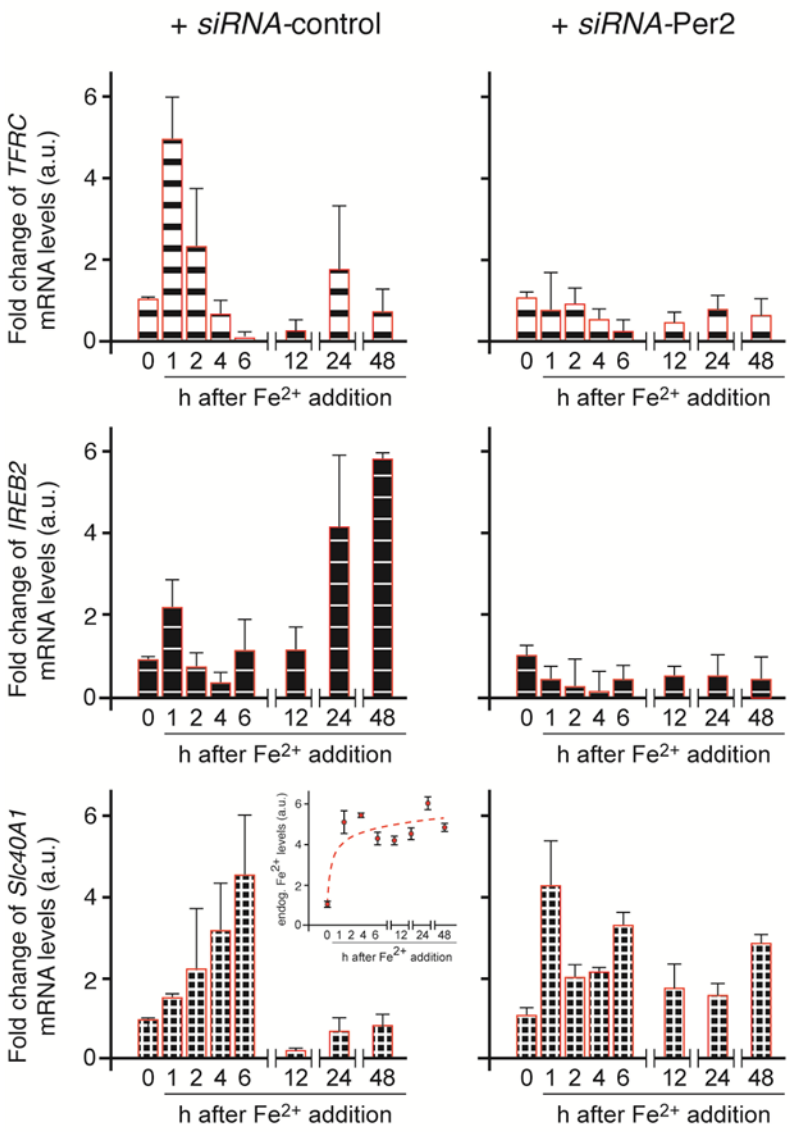

Figure 5. Cellular response to acute iron influx is minimized in cells with downregulated PER2.

A. HepG2 cells were transfected with siRNA to knockdown PER2 expression, as described in materials and methods. 48h after transfection, cells were dosed with $FeSO_4$ (1mM), and collected at timepoints indicated. Ferrous iron concentration was measured as described in Materials and Methods for cells expressing endogenous PER2 (inset). Expression of *SLC40A1*, *TFRC*, and *IREB2* was quantified using qRT-PCR. Within each data series, expression is normalized to the -2h timepoint.

2.4 Discussion

Our study sought to determine molecular mechanisms by which iron metabolism may be regulated by the circadian clock. While there is an increasing body of knowledge on the extent of circadian regulation of physiological processes, very little work has been done on iron metabolism and the clock[164]. First, we demonstrated that outside of any environmental fluctuations, the intracellular labile iron pool oscillates in tune with the circadian rhythm of the cell (Figure 1). While clinical studies have been done on the daily variance in circulating iron metrics such as serum iron concentration and transferrin saturation, only recently has a study demonstrated daily rhythmic changes in intracellular iron in tumors implanted in mice [78, 123, 128]. One of the drawbacks of this approach in mice is that the intracellular iron concentration cannot be disconnected from the cycling of available iron due to the animal's feeding pattern and thus, an accurate representation of the molecular landscape regulated by the clock in response to iron overload cannot be achieved. Our result demonstrates that by providing a stable source of extracellular iron *via* the media, synchronized hepatocytes still demonstrate rhythmic fluctuation in intracellular iron concentration.

We hypothesize that the levels of intracellular iron fluctuate because many of the cellular processes that incorporate iron into key enzymes frequently occur with circadian rhythms, and therefore the availability of iron in the cell is modulated by rhythmic iron metabolic components according to this fluctuation in demand. The most well studied example of this is the rate limiting enzyme of DNA synthesis, ribonucleotide reductase M (RRM) which utilizes a differic iron core [138]. Its abundance oscillates with a peak at the beginning of subjective dark phase. In addition to RRM, iron is critical for additional enzymes controlling DNA synthesis such as DNA primase [165]. During the subjective dark there are also peaks of DNA repair pathways, involving iron-sulfur cluster-dependent enzymes such as mutY-homolog (MUTYH) [133, 140]. One of these pathways which demonstrates rhythmicity is the nucleotide excision repair pathway, which is involved in

oxidative damage such as that caused by excess iron [140]. The overall timing of S-phase is also regulated by the circadian clock, in rodents DNA synthesis occurs primarily in the night during early active phase [137, 156]. This is shortly after the peak of *PER2* expression in mouse peripheral clocks [34]. We observed intracellular iron oscillations to be in phase with *PER2* transcriptional rhythms (Figure 1,6), suggesting that times of peak intracellular iron may coincide with the highest demand for iron to be incorporated into necessary enzymes.

We observed that contributing to this rhythm in intracellular iron there are transcriptional and posttranscriptional regulatory rhythms in key iron metabolic components (Figure 2 and 4). Other studies have posited that rhythmic *TFRC* mRNA results from post-transcriptional regulation by IRP2 [127, 128]. Our analysis of the transcriptome complements these studies, showing rhythmicity only at the level of the mature transcript. IRP2 protein post-transcriptionally regulates multiple iron regulatory gene transcripts, and therefore intracellular iron rhythms may not be solely due to *TFRC* fluctuations [74]. While we observe circadian rhythms in the nascent transcript of *SLC40A1*, the observed rhythms in IRP2 do not seem to derive exclusively from rhythmic transcription of *IREB2*. Because the degradation rate of IRP2 is iron dependent [161], this may be a key node in the interaction between these two pathways, with both iron status and circadian timing playing a role in the accumulation of IRP2 protein [161]. While it was long thought that circadian regulation was modulated by transcription factor activity, there are an increasing number of studies indicating that this is an oversimplification, and in fact rhythmic expression in the genome is due to multiple layers of transcriptional and post-transcriptional effects [166, 167]. Our analysis of the cistrome and transcriptome in regards to circadian regulation of iron metabolism supports this view, with *TFRC* and *SLC40A1* demonstrating rhythmicity at the mRNA and nascent transcript levels, respectively (Figure 4). Genome wide analysis have found that circadian rhythms of transcription

are only responsible for around 22% of cycling mRNAs, and our finding place TFRC in the category of mRNAs whose rhythmicity is generated by post-transcriptional events[166].

We also consider the hierarchical nature of iron metabolic component regulation. While previous studies have solely looked at the role of the circadian clock on iron metabolism gene expression, they neglect to look at how that regulation changes when the iron status of the cell is disrupted [127, 128]. We show that iron status has a pronounced effect on overall expression of iron metabolic genes by upregulating *SLC40A1* mRNA and downregulating *TFRC* mRNA as well as IRP2 protein levels (Figure 2-4). Because the IRE binding activity of IRP2 enhances *TFRC* mRNA stability, the downregulation of observed *TFRC* in iron overloaded cells can be attributed to the loss of IRP2 protein. While MetaCycle analysis of our qRT-PCR data did not find significant rhythmicity of *SLC40A1*, and our UCSC Genome Browser analysis of mouse liver showed rhythmicity in *SLC40A1* to occur primarily at the level of the nascent transcript, in both datasets the mRNA does seem to exhibit variation over the day. In our time course experiment, the timing of these variations was consistent between untreated and iron treated cells, despite the overall *SLC40A1* expression levels being five-fold higher during iron overload. This suggests that these two pathways simultaneously regulate expression of iron metabolic components, but that in conditions of iron overload cellular demand to return to iron homeostasis has a larger effect on iron metabolic gene expression than the clock does. During conditions of iron homeostasis, the regulation of iron metabolic components by the circadian clock still allows for smaller daily fluctuations in iron to accommodate rhythms in iron demand from the cell (Diagram 3).

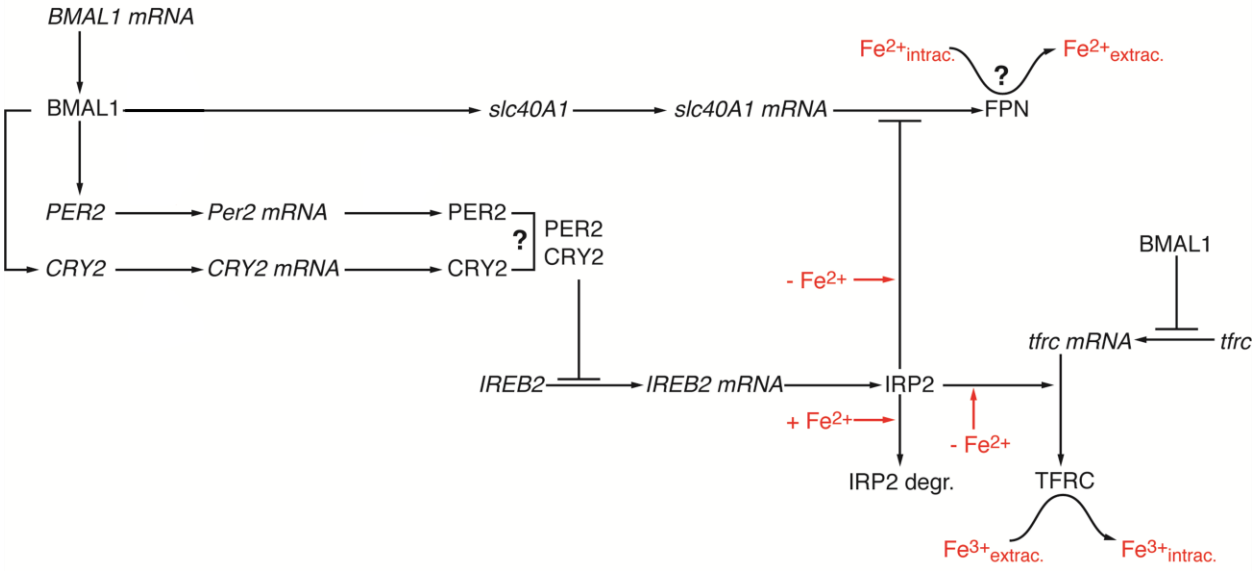

Diagram 3: An overview of modulation of iron metabolic components by the circadian clock. Rhythmic transcriptional regulation by the circadian clock leads to variable transcription of *SLC40A1*, as well as rhythmic post-transcriptional regulation of *IREB2 via* PER2. Rhythmic IRP2 goes on to further regulate the translational rate of *SLC40A1* and the mRNA stability of *TFRC*, leading ultimately to oscillations in the concentration of the labile iron pool. The iron-sensitive nature of IRP2 ensures that this system remains sensitive to overall iron homeostasis.

The concept of the circadian clock priming a metabolic system has been discussed with regards to glucose metabolism, and we found evidence that a functional circadian clock may facilitate the iron metabolic pathway's response to surges in iron supply (Figure 3). Increases in daily glucose uptake by cells occurs simultaneously with daily increases in serum glucose concentration prior to the beginning of the active period, and the clock plays a role in the liver's ability to respond to sudden glucose rises [168]. Insulin response to an oral glucose load in humans as well as rats was dependent on the time of day, and clock deficient animals in the form of SCN lesion lost these functional fluctuations [169-171]. We observed deficient response of the iron metabolic pathway in response to iron challenge in cells which had an impaired clock (Figure 3), it is possible the rate of iron loading in the cells is dependent on circadian phase since we observed that expression of IRP2, the master regulator of iron homeostasis, is in phase with PER2 (Figure 2). Glucose and iron are

both acquired through feeding behavior. As in the case of glucose, it seems reasonable to hypothesize that the circadian clock may prime the iron metabolic pathways to maximize the potential benefit from rhythmic iron availability.

Chapter 3: Relevance of the endogenous labile pool of iron in expression of circadian genes and clock resetting.

3.1 Introduction

While the regulation of metabolism by the circadian clock is being elucidated, researchers are becoming increasingly aware of the ways aspects of metabolism in turn provide feedback to the clock. Shifting the feeding time in mice can induce a phase shift in the clock of the liver after only 2 days, and restricting the time of food intake is sufficient to restore rhythmicity to a large proportion of genes in the liver of clock-deficient mice [15, 172]. Just the single macronutrient of glucose was sufficient to shift the timing of wheel running behavior in rats with lesions of the SCN [173]. Interestingly, this study found that nutrients from the fatty calorie source of vegetable oil were unable to generate the same response, possibly due to their longer absorption time than a simple sugar [173]. Much of the connection between energy levels and the circadian clock revolves around the rhythmic accumulation of NAD^+ and it's modulation of enzyme functionality [174]. One such enzyme is sirtuin 1 (SIRT1), an NAD^+ dependent histone deacetylase which is active during fasting when NAD^+ levels are high [175]. Energy production during glycolysis depletes NAD^+ by converting it to NADH, and therefore SIRT1 is rendered inactive [174]. Interestingly, SIRT1 functions antagonistically to the histone acetyltransferase activity of CLOCK, modulating circadian chromatin remodeling [176]. Therefore, enzymatic activity of SIRT1 on the clock is mediated by a metabolite which is rhythmically present, demonstrating that the interaction between the circadian clock and metabolism is bidirectional. To complete the feedback loop, it was discovered that the rate limiting enzyme in NAD^+ synthesis, nicotinamide phosphoribosyltransferase (NAMPT), is a direct target of CLOCK:BMAL1 heterodimer [177]. This rhythmic oscillation of NAD^+/NADH metabolism results in rhythmic activity of not just SIRT1. Poly(ADP-ribose) polymerase 1 (PARP-

1) activity is circadian despite lacking rhythms in protein abundance, due to its enzymatic dependence on NAD^+ [178]. PARP-1 actually recognizes CLOCK as one of its targets, controlling the DNA binding affinity of CLOCK:BMAL1 [174, 178]. Another connection between metabolic control and the circadian clock is the peroxisome proliferator-activated receptor gamma coactivator 1-alpha (PGC-1α) [174]. PGC-1α regulates gluconeogenesis and glycolysis, however it also functions similar to RORα to enhance *BMAL1* transcription, and PGC-1α knockout mice display impaired circadian rhythms of O_2 consumption [179].

Heme synthesis and activity is another link between metabolism and the circadian clock. Heme is required for complex formation between REV-ERBα and nuclear receptor corepressor 1 (NCOR), which exerts negative feedback on the circadian clock [134]. Additionally, gluconeogenesis in the liver is impacted by heme synthesis due to changes in clock function [134]. In addition to REV-ERBα, heme has been linked to degradation of PER2, and this effect may be tissue specific [121, 122]. The binding of heme to PER2 is through a redox sensitive motif on the C-terminus of PER2, resulting in loss of binding to CRY, and subsequently enhanced rates of degradation [121].

There is some evidence that circadian stability is challenged in conditions where iron homeostasis is impaired. Rats fed an iron free diet displayed antiphasic circadian physiology and behavioral rhythms compared to controls, both body temperature and motor activity were antiphasic to rats fed with a normal dietary iron [126].

Restless leg syndrome (RLS) is a neurological condition in which the symptoms manifest themselves during the resting period, disrupting sleep cycles. Restless leg syndrome has been associated with iron deprivation, and a mouse model of RLS was found to have disrupted circadian periods of activity and rest when undergoing dietary iron deprivation [125]. Because impaired iron homeostasis is so prevalent, especially among the elderly, it is important to learn how these irregularities in iron may be affecting the circadian clock.

3.2 Materials and Methods

Cell culture

Mouse embryonic fibroblasts (MEF) expressing a PER2::Luciferase fusion protein (MEF PER2::LUC) cells were a gift from Dr. Shihoko Kojima (Virginia Tech University) and cultured in Dulbecco's Modified Eagle's Medium (DMEM, MT-10-013-CV, Corning) supplemented with 10% FBS (35-010-CV Corning), 50 units/ml penicillin, and 50 units/ml streptomycin. All cells were maintained at 37°C in an incubator which is injected with CO_2 to a 5% (v/v) final concentration.

Live cell luminescence recording and data analyses

MEF PER2::LUC cells that were used in luminescence recording were grown as described above, to 100% confluence in 35mm dishes (627 160, CellStar). Circadian synchronization was performed by treatment with 100 ng/ml dexamethasone for 2 h at 37°C. Following synchronization media was replaced with DMEM without phenol red (17-205-CV, Corning), supplemented with 2% (v/v) FBS and 0.05 mM luciferin (L-8240, BioSynth). Dishes were then sealed with glass coverslips using a layer of grease on the rim of the dish, and placed in the lumicycle. Luminescence was recorded by Lumicycle data collection software for at least 5 days, and recordings were processed using the Lumicycle software and JMP. The function used for data modeling is as described in [180]:

$$y = l+mt+nt^2+(a+bt+ct^2)\sin[2\pi((t-\phi)/\tau)]$$

In which the following symbols are used: y, raw luciferase data; l, baseline; m, linear baseline trend; t, time; n, parabolic baseline trend; a, amplitude; b, linear dampening; c, parabolic dampening; ϕ, phase; τ, period.

3.3 Results

HepG2 cells can be circadian synchronized in vitro.

In order to study the molecular interplay between the circadian clock and iron metabolism, it was first necessary to find a cell model in which we could manipulate iron concentration, as well as synchronize the circadian clock *in vitro*. Because there were no prior investigations into these two pathways simultaneously, we were required to validate our own cell model. Hepatocyte cell lines were the preferred target, due to the robustness of the liver peripheral clock and to the function of the liver as the primary organ of iron storage[145, 181-183]. HepG2 is a widely used hepatic carcinoma cell line which we proved to be circadian synchronizable by serum shock (Figure 6A-C) as well as dexamethasone [184, 185]. Transcriptome studies found gene expression in ontological groups of "stimulus response" and "immune system process" were lower in HepG2 compared to liver biopsy tissue [186]. Because these processes are involved in normal liver function, the observed downregulation may be due to cultivating HepG2 *in vitro* where the functional demands of the hepatocytes are different than in tissue [186]. However, we feel that HepG2 is an appropriate cell line to work in to model hepatic clock function and iron metabolism. We showed that HepG2 exhibited a rhythmic transcription of *PER2* and *CRY2* (Figure 6A, 6B respectively), components of the negative arm of the circadian feedback loop, which was antiphase to rhythms in *BMAL1* (Figure 6C), the primary oscillating component of the positive arm of the core molecular clock.

Transcription of circadian clock components is dysregulated by iron overload or depletion.

To further investigate whether the intracellular iron status had an impact on expression of core circadian clock genes, we dosed cells with 10μM, 100μM, or 1mM of ferrous sulfate and analyzed gene expression by qRT-PCR (Figure 6D). Our findings demonstrate that *PER2* and

BMAL1 expression is decreased by iron addition, *CRY2* levels followed a dose-dependent increase in expression and *CLOCK* expression remains constant even under conditions of high iron (1mM). Expression of *SLC40A1* was used to verify that cells show a transcriptional response to increasing intracellular iron concentration. Next, we checked the converse experiment in which depletion of endogenous iron pool was achieved by treating cells with 2-2'-DP (Figure 6E). By contrast with the results shown in Figure 5D, *CLOCK* showed significantly increased expression in cells depleted of iron, whereas *CRY2* decreased. *PER2* and *BMAL1* were largely unchanged by treatment with the chelator, demonstrating modest increases in expression. These results taken together suggest that the transcription of core circadian clock genes is sensitive to the concentration of the labile iron pool.

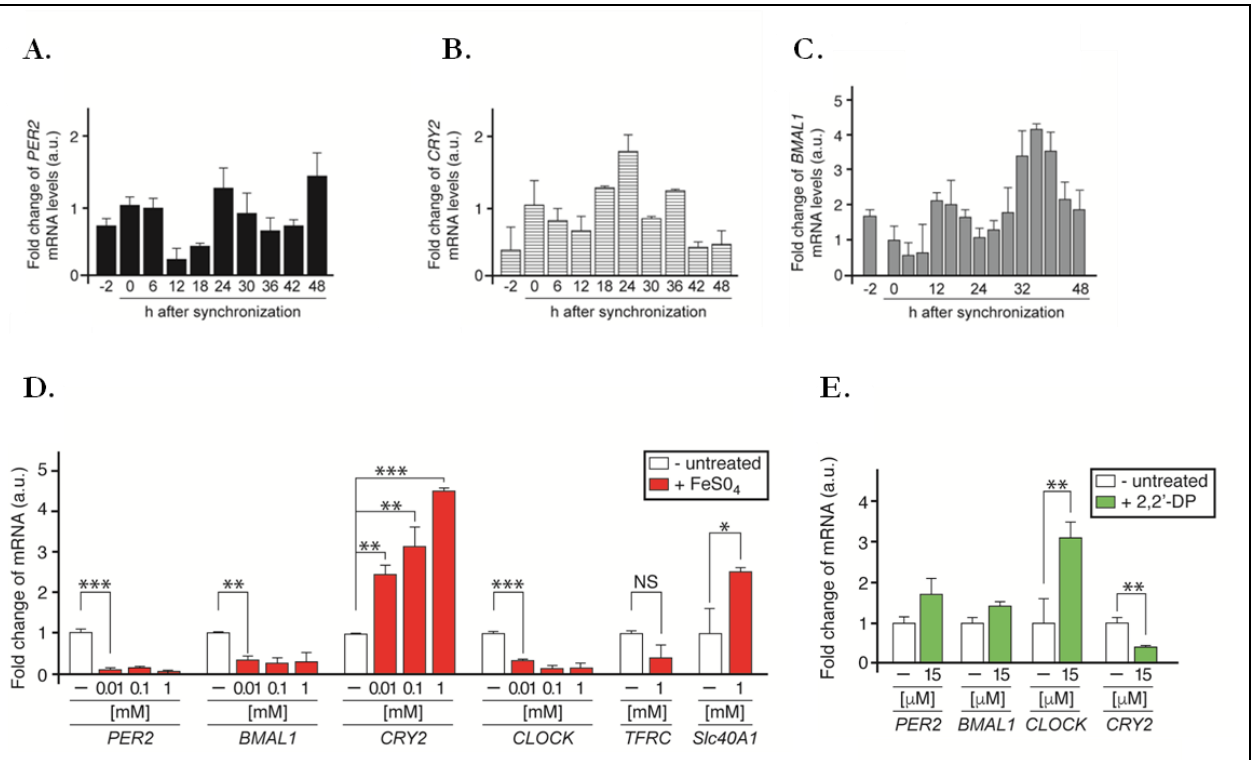

Figure 6. Core circadian components oscillate in synchronized HepG2 cells, and their expression is responsive to changes in intracellular iron level.

A. *PER2* mRNA was quantified by qRT-PCR from HepG2 cells synchronized with serum shock (FBS, 50%) for 2h before being incubated in media containing 0% FBS and collected every 6h. Timepoint -2h is before serum shock, 0h is right after synchronization. Relative expression was quantified using Livak method, and the time series was normalized to the 0h timepoint. **B.** *CRY2* mRNA was quantified by qRT-PCR from HepG2 cells synchronized with serum shock (FBS, 50%) for 2h before being incubated in media containing 0% FBS and collected every 6h. Timepoint -2h is before serum shock,0h is right after synchronization. Relative expression was quantified using Livak method, and the time series was normalized to the 0h timepoint. *PER2* and *CRY2* oscillate roughly in phase with each other, as expected for complementary components of the negative arm of the circadian feedback loop. **C.** *BMAL1* mRNA was quantified by qRT-PCR from HepG2 cells synchronized with serum shock (FBS, 50%) for 2h before being incubated in media containing 0% FBS and collected every 4h. Timepoint -2h is before serum shock, 0h is right after synchronization. Relative expression was quantified using Livak method, and the time series was normalized to the 0h timepoint. *BMAL1* mRNA oscillation is antiphase to *PER2* and *CRY2*. **D.** HepG2 cells were treated with $FeSO_4$ (0.01mM-1mM) directly to the media 48h prior to collection and analysis of mRNA expression by qRT-PCR. Relative expression was quantified using Livak method. **E.** HepG2 cells were treated with 2,2'-DP (15uM) for 48h before collection and analysis of mRNA expression by qRT-PCR. Relative expression was quantified using Livak method. Statistical significance was determined by t-test. *$p \leq 0.05$; ** $p \leq 0.005$; *** $p \leq 0.001$

The oscillation of core clock genes is altered in response to changes in the labile iron pool.

Once we knew that HepG2 cells could be entrained, and circadian clock mRNA expression could be modulated by altering iron levels, we asked whether the rhythm of one of the core transcripts, *BMAL1,* was maintained when the intracellular iron status was manipulated. Ferrous sulfate was added to the media at 30 μM concentration in order to increase the level of available iron outside the cells to a concentration which is near the upper range of plasma iron in healthy individuals (Figure S1) [187]. In other experiments the endogenous iron pool was depleted by adding 2-2'-DP to the media, at a final concentration (15μM) which lowered intracellular iron without adversely affecting cell viability (Figure S1). Circadian oscillations of *BMAL1* mRNA in these cells show that rhythmicity is sensitive to intracellular iron status (Figure 7A). Transcriptional rhythms are not completely abolished, indicating that there is not a total loss of clock function at the tested levels of iron disruption, but high iron loading especially impairs the robustness of *BMAL1* oscillations (Figure 7A).

Analysis of these rhythms shows that manipulating the intracellular iron concentration alters the phase and amplitude of *BMAL1* rhythms (Figure 7B). We see a larger impact on fold change of peak mRNA levels under iron overload than iron depletion (Figure 7A). However the amplitude of oscillation is greater and the period length is increased by over 1 h in iron depleted cells as compared to untreated or iron addition (Figure 7B). This decrease in overall *BMAL1* mRNA due to iron overload in our time-course is in agreement with our previous data showing that iron addition downregulates *BMAL1* in unsynchronized cells (Figure 6D). Our MetaCycle analysis also indicated that both iron overload and depletion cause phase delays in the rhythm, while only depletion has a noticeable effect on period length, increasing the period of *BMAL1* rhythm by about 1 h (Figure 7B). Similarly, *CRY2* expression oscillations were dampened in cells treated with 2-2'-DP (Figure

7C). Alteration of circadian rhythm is not limited just to the positive arm of the circadian clock, such as *BMAL1*, because we ovserved that changes to the concentration of the labile iron pool also affect mRNA expression of the negative arm component *CRY2*. However, *BMAL1* rhythms are more severely impaired under iron overload, while *CRY2* rhythms show greater dampening under iron depletion. This divergence suggests that not all clock components may respond to iron challenge in the same manner, similar to how the different components of the clock are associated with different reactions to the same drug [188]. This is in agreement with our previous expression data, where *BMAL1* and *CRY2* transcription was opposed in cases of iron overload or iron depletion (Figure 6D and 6E, respectively). The strength of rhythmic amplitude appears to be connected to the transcriptional effect of iron on each particular circadian component.

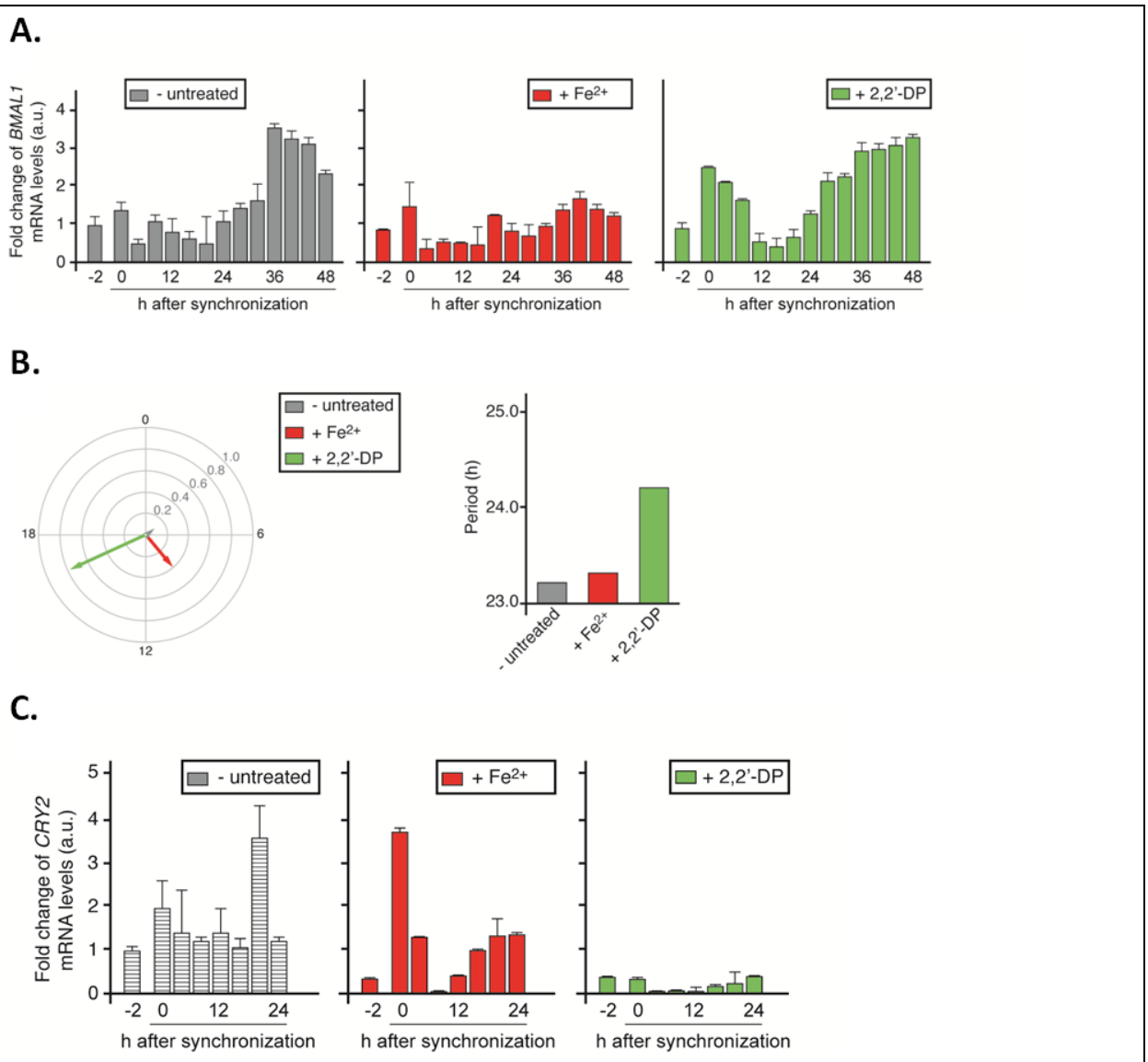

Figure 7. Oscillations of core circadian components are impacted by impaired iron homeostasis.

Figure 7. Oscillations of core circadian components are impacted by impaired iron homeostasis.

A. Intracellular iron concentration in HepG2 cells was manipulated by dosing with $FeSO_4$ (30μM) to increase intracellular iron or 2,2'-DP (15uM) to deplete intracellular iron. Both compounds were added directly into the media. Cells were then synchronized by dexamethasone (100nM) before collection every 4h for 48h, and relative *BMAL1* mRNA levels were quantified by qRT-PCR. Within each treatment group, time series are normalized to the -2h timepoint. Between treatment groups, the $+Fe^{2+}$ and +2,2'-DP groups were normalized to the untreated group using the ΔCT values of *BMAL1* in each -2h timepoint and using this normalization factor from the unsynchronized cells to properly represent the comparative expression of *BMAL1* between the time series. **B.** HepG2 cells were treated exactly as in (**A**) *BMAL1* mRNA rhythms was analyzed using MetaCycle. Amplitude corresponds to the length of the arrow, and phase corresponds to the arrow's direction. . **C.** HepG2 cells were treated with $FeSO_4$ or 2,2'-DP for 48h prior to synchronization with dexamethasone (100nM) for 2h (t=-2h). Cells were then incubated in serum free media in the presence of $FeSO_4$ or 2-2'-DP and harvested at different times for 24h. Relative expression of *CRY2* mRNA was analyzed by qRT-PCR and quantified using Livak method, normalizing within each treatment group to the 0h timepoint. Between treatment groups, the $+Fe^{2+}$ and +2,2'-DP groups were normalized to the untreated group using the ΔCT values of *CRY1* in each -2h timepoint and using this normalization factor from the unsynchronized cells to properly represent the comparative expression of *CRY1* between the time series.

Circadian rhythms of PER2 *mRNA and protein are downregulated by iron overload.*

Transcriptional response to iron addition by *TFRC, IREB2,* and *SLC40A1* was blunted in cells that lacked PER2 due to siRNA knockdown (Figure 5). Additionally, we saw increased steady state level of expression of these three iron components in unsynchronized HepG2 and AML12 cell lines in response to PER2 knockdown (Figure 1B). This knowledge, combined with the known heme-sensing role for PER2 [121] led us to ask whether PER2 was in turn sensitive to the intracellular ferrous iron concentration. To determine this, we synchronized HepG2 cells treated with either ferrous sulfate (30μM) or 2-2'-DP (15μM) as described previously, and extracted both mRNA for analysis by qRT-PCR as well as protein for immunoblotting. Targeting PER2 in both cases, we were able to compare rhythms of mRNA and protein in growth conditions of abnormal iron availability. Both iron overload as well as iron depletion showed noticeably dampened rhythms in *PER2* mRNA expression (Figure 8A) suggesting that there is a homeostatic range of intracellular iron which is necessary for robust circadian transcription to be maintained. Our previously observed increase in *PER2* transcription under iron chelation (Figure 6E) was not observed in this

time course however the effect of serum shock and synchronizing the cell population could have altered the reaction to iron depletion and this may further indicate that the effect of iron on the cell is influenced by its circadian status. The phase of *PER2* rhythms in iron depleted cells was less than 0.5 h different from untreated cells, and while the period lengthened by less than 1 h, the observed mRNA rhythms appears to still be sufficient to maintain functional oscillations. When these rhythms were analyzed in MetaCycle, we found that iron overload caused phase advance of almost 4 h and shortening of period length by 4.9 h in *PER2* mRNA oscillations (Figure 8B, Figure S2) suggesting that circadian disruption due to iron overload is consistent with period shortening seen in genetic *PER2* knockout animals[20, 189].

Interestingly, we found that these impaired rhythms at the transcript level in ferrous sulfate treated cells were largely mirrored at the protein level. PER2 showed observable rhythms in untreated cells, as well as in 2-2'-DP treated cells with peaks of expression at t=0h and t=24h (Figure 8C). The downregulation of mRNA (Figure 8A) in cells as a result of iron depletion did not lead to an equivalent depletion of PER2 protein (Figure 8C). This could be due to an increase in translational rate of PER2 in chelated cells compared to overloaded cells, in addition to the downregulation of mRNA seen in both treatment groups. Two distinct mechanisms of heme interaction with the circadian clock exist, in the form of transcriptional regulation through REV-ERBα and protein stability with PER2, our data suggests that there are multiple regulatory mechanisms at work here as well [120, 121]. In cells overloaded with iron there was severe decrease in PER2 expression, with almost total ablation of rhythmicity (Figure 8C, Figure S3). This decrease in PER2 protein levels is likely at least partially due to the negative regulation of PER2 by heme [121]. This ablation of rhythmicity was confirmed by the MetaCycle analysis and immunoblot quantification (Figure 8C, Figure 8D). Quantitative analysis shows that iron depleted cells maintained normal rhythmic parameters much better than overloaded cells (Figure S3). This is of

importance when considered in the physiological context of individuals with chronically impaired iron regulation, and the potential impact this can have on the clock and all of the downstream clock controlled pathways.

Next, we were interested in observing the effect that iron concentration had on circadian rhythms over several circadian cycles. To accomplish this, we took advantage of a luciferase reporter cell line and a live cell luminescence imager system [190]. The treatment concentrations utilized were lower for ferrous sulfate in MEF PER2::LUC compared to the previously used HepG2, due to an observed difference in viability of treated fibroblasts as opposed to the hepatocytes (Figure S1). Our results demonstrate a dose dependent shortening of PER2 circadian period in MEF PER2::LUC cells treated with ferrous sulfate, ultimately resulting in an oscillation which was almost 3 h shorter than control cells (Figure 8E). Conversely, cells treated with 2-2'-DP showed lengthening of PER2 luminescence rhythms of about 1 h (Figure 8E). These results fit logically with what is known about the impact of PER2 protein on circadian period length[191]. As a key organ in metabolism, the liver has been shown to respond to metabolites such as glucose as entrainment signals, our data indicates that iron intake through feeding may exert an effect on the liver's circadian clock as well [5, 173]. Whether iron itself is sufficient to entrain a desynchronized clock is unknown. Because PER2 is not an isolated molecule, but works in conjunction with the rest of the core feedback loop to generate a global rhythm in the cell, the knockdown of PER2 during iron overload results in a circadian rhythm which is significantly sped up. This in turn can impact all the other processes the circadian clock interfaces with, and provides insight into how chronic iron overload can lead to a range of disease states [192].

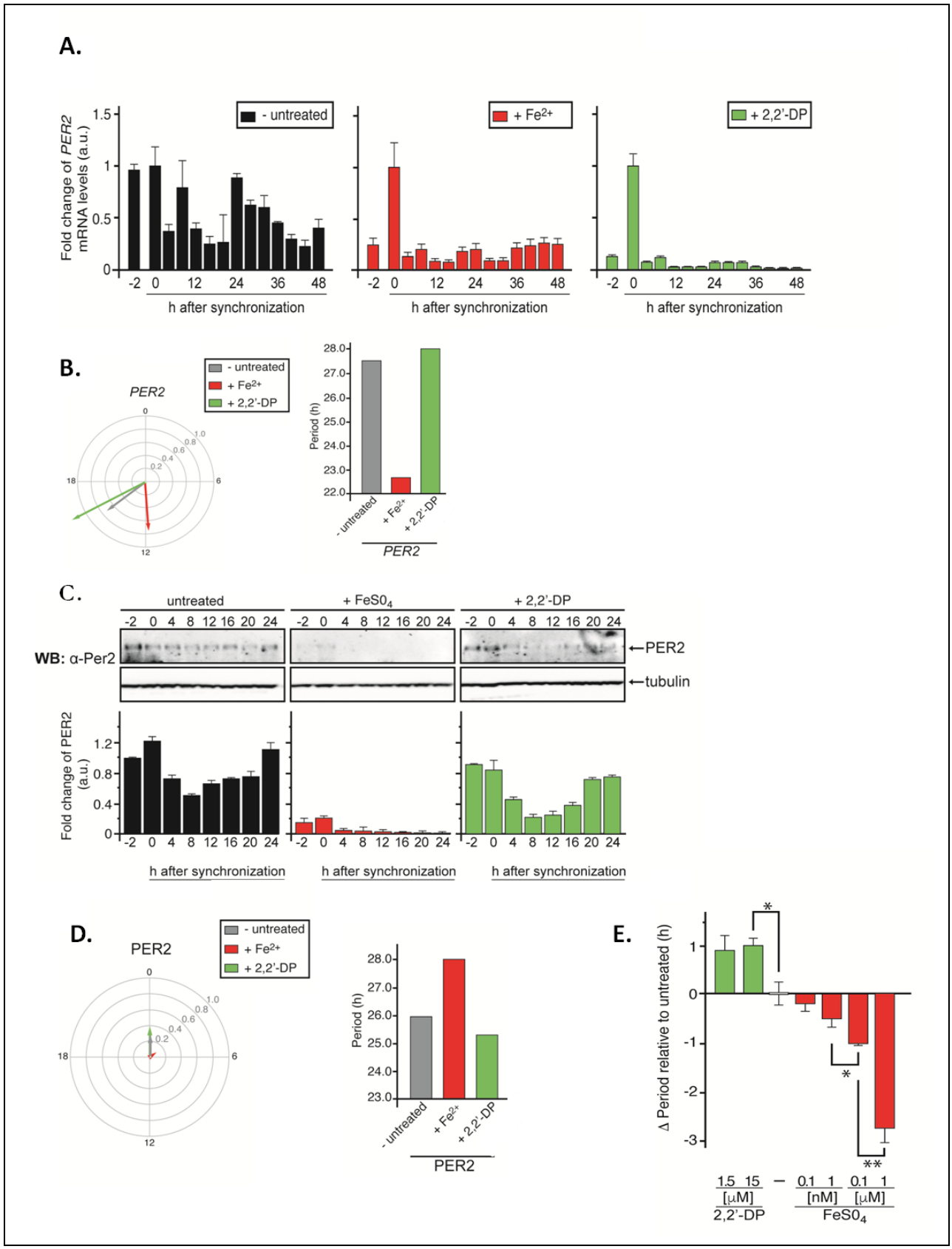
A.
Fold change of PER2 mRNA levels (a.u.)
- untreated
+ Fe2+
+ 2,2'-DP
h after synchronization
B.
PER2
Period (h)
C.
untreated
+ FeSO4
+ 2,2'-DP
WB: α-Per2
←PER2
←tubulin
Fold change of PER2 (a.u.)
D.
E.
Δ Period relative to untreated (h)
1.5 15 [μM] 2,2'-DP
0.1 1 [nM] 0.1 1 [μM] FeSO4

Figure 8. Circadian rhythms in PER2 mRNA and protein are altered in HepG2 cells where intracellular iron homeostasis is compromised.

A. HepG2 cells were treated with $FeSO_4$ (1mM) or 2,2'-DP (15uM) for 8h before synchronization with dexamethasone (100nM, t=-2). Cells were then collected every 4h for 48h, and mRNA expression of *PER2* was quantified by qRT-PCR. The -2h timepoint was used to normalize relative expression levels between treated groups and the untreated cells. *PER2* mRNA was downregulated in cells either overloaded or depleted of iron. **B.** Analysis of period, phase, and amplitude of mRNA rhythm was performed using MetaCycle. Phase is indicated by the direction of the arrow, and normalized amplitude by the length of the arrow as indicated on the graph's scale. **C.** Following 48h incubation with either $FeSO_4$ or 2,2'-DP, HepG2 cells were synchronized by 2h serum shock (FBS, 50%). Cells were collected every 4h for 24h, and lysates were resolved by SDS-PAGE and analyzed by immunoblotting using α-PER2 antibody. α-tubulin was used as a loading control. Protein levels were quantified by densitometry using ImageJ software. Quantification of PER2 was normalized to tubulin, and the -2h timepoint was used to calculate relative protein amounts between $FeSO_4$ or 2,2'-DP treated groups and untreated. Multiple exposures of each blot were used to calculate standard deviation of the densitometry signal. **D.** Analysis of the period, phase and amplitude of the protein rhythms observed in (**C.**) was performed using MetaCycle, by integrating the ARSER, JTK-Cycle, and Lomb-Scargle methods with Fisher's method for integration of p-values. Phase is indicated by the direction of the arrow, and amplitude corresponds to the length of the arrow. Untreated is shown in grey, $+Fe^{2+}$ in red, and +2-2'-DP in green. **E.** MEF PER2::LUC cells were treated with varying concentrations of either $FeSO_4$ or 2,2'-DP and synchronized with dexamethasone treatment as described in Materials and Methods. Period length was quantified using curve fitting in JMP, with biological quadruplicate for each treatment. Statistical significance in period length was determined by t-test. $*p \leq 0.05$; $** p \leq 0.005$; $*** p \leq 0.001$

3.4 Discussion

While relationships between the circadian clock and iron metabolism have been superficially investigated before, there is little known how the intracellular iron status affects, if at all, the expression of circadian clock components and a potential impact on overall clock phase, period, and amplitude. Here we sought to clarify this molecular relationship, to provide insight into how metabolism can impact circadian well-being in hepatocytes. First, we demonstrated that the expression of core circadian *BMAL1* and *PER2* mRNAs is inversely correlated to the concentration of ferrous free iron within the cell, while expression of *CRY2* is directly correlated (Figure 5). Clock components often serve additional functions outside of their roles in the transcriptional feedback loop, therefore it is reasonable that the response to changes in iron varies [20, 193]. Iron availability is linked to functional heme production, and heme in turn degrades PER2 protein [121, 194]. The role of PER2 as a heme-sensing molecule may explain why we see increased *CRY2* expression in

response to iron overload, as compensatory expression between these two clock components has been previously described [195]. CRY is able to function as a negative regulator of CLOCK:BMAL1 independently of PER proteins, therefore our observed increase in *CRY2* expression may be a compensatory mechanism for the loss of PER2 protein [196].

As stated in the case of PER2, we saw that protein expression was severely dampened when cells were overloaded with iron. While it is unknown if iron directly undermines PER2 stability, this is in agreement with studies showing the inverse correlation between heme and PER2 stability; it remains to be seen if the mechanism regulating PER2 degradation resulting from iron overload is independent from heme-dependent degradation [121, 122]. In conjunction with this, circadian rhythmicity of the protein and mRNA was severely dampened in PER2 in cases of iron overload. Unlike previous studies which have suggested that light is the only strong inducer of phase shifting, our PER2 data indicates that iron treatment induces a delay in circadian phase (Figure 7) [197]. The overall robustness of the clock is dependent on stoichiometric relationships between the positive and negative feedback loop components, and therefore the dramatic downregulation of PER2 as one of these components suggests that maintenance of clock function in tissues with dysregulated iron metabolism is likely impaired [34]. The dampening of amplitude in rhythms at the transcript level (Figure 6) and protein level (Figure 7) of core circadian components under iron overload suggest that the clock's ability to drive robust rhythms in clock controlled genes is impaired. Our MEF PER2::LUC reporter cell data shows that the disruption of the clock is dose dependent and within the physiologically relevant range altered the period of PER2 oscillations [71]. Below is a simple schematic image outlining some of the ways iron impacts circadian component function and clock stability (Diagram 4).

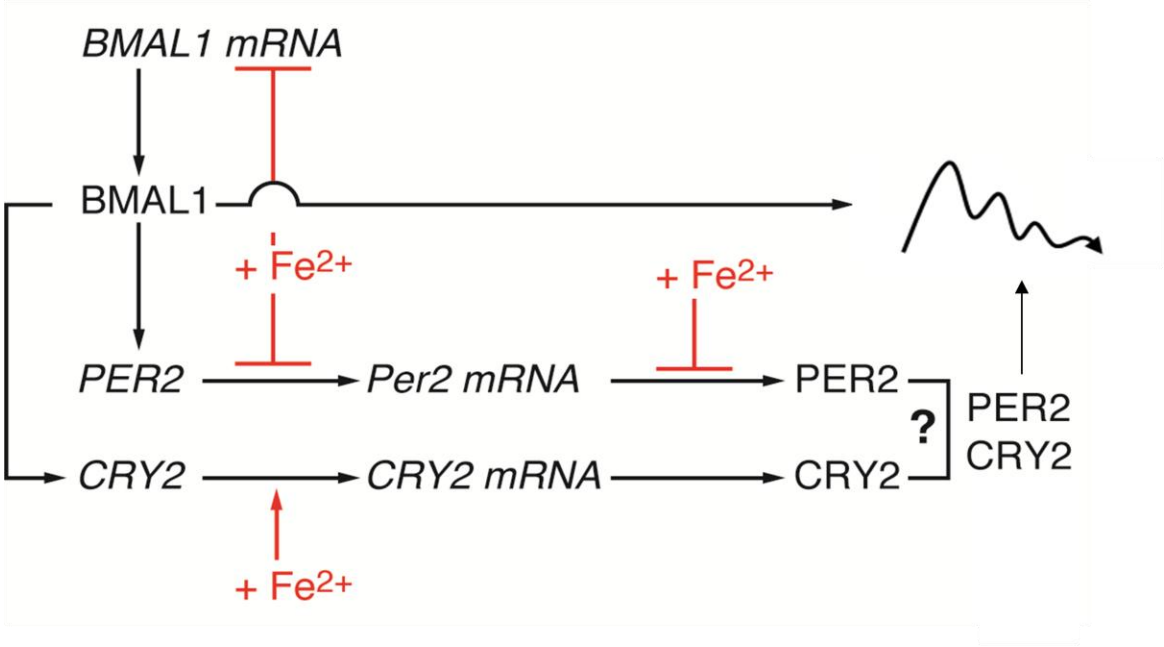

Diagram 4. A representative model of ways iron interacts with the core circadian clock mechanism. The concentration of the labile iron pool impacts the mRNA levels of *BMAL1* and *PER2*, either by limiting transcription or mRNA stability. In addition, excess iron exerts negative feedback on PER2 protein within the cell, either by inhibiting translation or enhancing PER2 degradation. The net effect of this modulation of clock components by excessive intracellular iron is a weakening of circadian rhythms, including phase delay and period shortening.

While our use of chelators to investigate the impact of insufficient labile iron on circadian rhythms showed smaller changes in phase and amplitude of circadian clock components, there was still a noticeable impact on both circadian gene expression as well as resulting circadian period. Iron deficiency is the most common nutritional disorder worldwide, there is certainly justification for further exploration of how circadian clocks in these individuals may be effected[80, 81, 198]. There is already evidence that behavioral patterns are altered in animal models of iron deficiency, with iron deprived mice mimicking the human condition of restless legs syndrome and displaying disrupted sleep patterns [125]. While it doesn't appear that restless leg syndrome itself is a disorder of the circadian clock, the symptoms, namely disruption of the beginning of the inactive period, are presented in a circadian manner [125]. Additionally, rats experiencing induced anemia from four weeks of iron-free diet showed inversions of sleep/wake cycles as well as timing of hypothermic

response to d-amphetamine [126]. These behaviors are linked to reductions in the activity of the dopaminergic pathway in the midbrain, and the expression of dopamine-related genes is altered in cases of iron deficiency [126, 199]. While impaired dopaminergic function and circadian clock disruption are both observed in cases of iron deficiency, it is unknown if they are due to the same molecular mechanism. These studies begin to show the physiological relevance of our investigation into phase and period shifts in hepatocytes with disrupted iron homeostasis. Unlike the rodent models of iron deficiency which focus on effects in the brain, we show that peripheral clocks are also sensitive to iron status. The detrimental effects of circadian disruption range from metabolic syndromes to cancer, and the potential for impaired iron homeostasis to exacerbate these effects needs to be considered [200].

Chapter 4: Conclusions and Future Directions

4.1 Conclusions

Our work seeks to further expand the role of the circadian clock on regulating mammalian iron metabolism, as well as establish the free ferrous iron pool as a modulator of the circadian clock. An overview of our observed nodes of interaction (Diagram 5) demonstrates the complexity of this crosstalk.

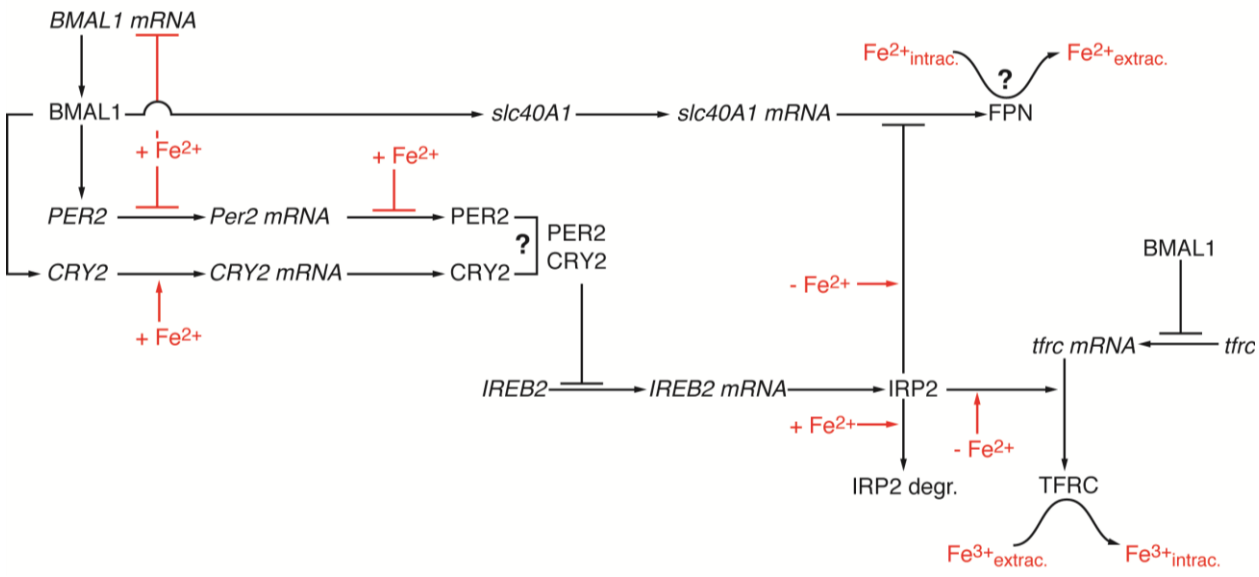

Diagram 5: A model of the molecular interface between the circadian clock and iron metabolism. The generation of rhythmic ferrous free iron in the cytosol is dependent on the transcriptional regulation of *SLC40A1* and post-transcriptional regulation of *IREB2*, with IRP2 subsequently going on to post-transcriptionally generate rhythmic *TFRC* mRNA. These rhythmic changes in the balance between iron import and export result in daily fluctuations in ferrous free iron. Conversely, we see iron feedback onto the circadian clock by downregulating mRNA expression of *PER2* and *BMAL1* as well as repressing PER2 protein levels. These effects were found to induce changes in rhythmic phase and period, which will have repercussions on other cellular processes.

Previous studies have shown that clinicians studying circulatory iron parameters such as transferrin saturation need to be mindful of daily fluctuations, and we now know that the ferrous free iron of the cytosol follows circadian patterns as well. This is achieved through circadian regulation of core iron metabolic components, which raises clinical considerations for the use of iron metabolic components such as TFRC for targeted drug delivery. By taking into account the

circadian phase of the patient, delivery can be optimized to maximize efficacy and minimize toxicity. Furthermore, establishing the role of circadian regulation in iron metabolism provides information on how iron status may be impaired in patients who suffer from clock deficiencies. The homeostatic window for intracellular iron concentration needs to be fairly small in order to minimize redox-related cytotoxicity, and circadian disruption may make homeostasis harder to maintain. Even modest increases in oxidative stress over a long time period can have a compounding negative effect on health and this may present a common thread between the high incidence of cancer in individuals with impaired circadian or iron metabolic function [201].

The feedback that iron exerts on the circadian clock is another instance where molecular interaction can be implicated in broader physiology and health. Iron deficiency is the most common nutritional disorder in the world, and severe deficiency has been shown to drastically alter circadian function [80, 126]. If impairment of the circadian clock during lack of iron homeostasis occurs under less severe conditions of iron metabolism, then there are a large number of people at risk. We see that even modest changes to intracellular iron have measurable changes on period length of circadian driven luminescence oscillations, suggesting that a broad number of people globally may be subjected to hepatic circadian modulation *via* iron which is not in phase with global entrainment signals from the SCN. However, just as oral iron supplementation has been shown to reduce the circadian presentation of symptoms in restless leg syndrome, this opens the door to the study of iron as selective modulator of circadian clocks. Taking an iron pill upon landing will not become a cure for jet-lag, however controlling ferrous free iron may become one of multiple tools in helping a patient's endogenous circadian clock restore function to other impaired biological pathways.

4.2 Future Directions

As of this time we do not know if the cellular response to iron influx is dependent on the circadian phase at the time of treatment, as has been demonstrated for glucose and certain drugs like amphetamines [126, 169]. Measuring the rate of iron absorption immediately after addition to the media at different points in the circadian phase could reinforce the hypothesis that the clock regulates iron metabolic components in anticipation of increases in iron availability due to rhythmic feeding behavior. Conversely, we have shown that circadian rhythms are sensitive to iron load, and therefore it may be revealing to quantify the degree of phase shifting induced in vitro by iron addition depending on when in the circadian phase iron was added.

One area for further exploration will be to see if an animal model of genetic or dietary iron overload demonstrates impaired circadian rhythmicity. Genetic models for conditions such as hereditary hemochromatosis can have their wheel-running activity monitored, and compared to normal mice as well as wild-type mice which have been fed a high iron diet. To examine the specific effect on the peripheral clock of the liver, tissue could be excised and circadian gene expression quantified by qRT-PCR. This could provide insight into individuals with genetic conditions such as hereditary hemochromatosis. There is some evidence that iron deficiency disrupts circadian behavior in rodent models, but this needs to be further explored especially with regards to impact on expression of circadian components. Conversely, in-vivo models of circadian impairment can be used to observe the physiological response to dietary iron overloading. The circadian defects of many of these models is already established, for example a homozygous CLOCK mutant mouse displays a slightly shorter period [202]. Based on our findings in this study, it would be fascinating to see if chelating iron from these mice resulted in a lengthening of circadian period equivalent to the wild-type.

References

1. Gotoh, T., et al., *Association of the circadian factor Period 2 to p53 influences p53's function in DNA-damage signaling.* Mol Biol Cell, 2015. **26**(2): p. 359-72.
2. Selfridge, J.M., et al., *Chronotherapy: Intuitive, Sound, Founded...But Not Broadly Applied.* Drugs, 2016. **76**(16): p. 1507-1521.
3. Rutter, J., M. Reick, and S.L. McKnight, *Metabolism and the control of circadian rhythms.* Annu Rev Biochem, 2002. **71**: p. 307-31.
4. Partch, C.L., C.B. Green, and J.S. Takahashi, *Molecular architecture of the mammalian circadian clock.* Trends Cell Biol, 2014. **24**(2): p. 90-9.
5. Stokkan, K.A., et al., *Entrainment of the circadian clock in the liver by feeding.* Science, 2001. **291**(5503): p. 490-3.
6. Hastings, M.H., et al., *Entrainment of the circadian system of mammals by nonphotic cues.* Chronobiol Int, 1998. **15**(5): p. 425-45.
7. Bodenstein, C., I. Heiland, and S. Schuster, *Temperature compensation and entrainment in circadian rhythms.* Phys Biol, 2012. **9**(3): p. 036011.
8. Richards, J. and M.L. Gumz, *Mechanism of the circadian clock in physiology.* Am J Physiol Regul Integr Comp Physiol, 2013. **304**(12): p. R1053-64.
9. Zuber, A.M., et al., *Molecular clock is involved in predictive circadian adjustment of renal function.* Proc Natl Acad Sci U S A, 2009. **106**(38): p. 16523-8.
10. Nikolaeva, S., et al., *The circadian clock modulates renal sodium handling.* J Am Soc Nephrol, 2012. **23**(6): p. 1019-26.
11. Ko, G.Y., L. Shi, and M.L. Ko, *Circadian regulation of ion channels and their functions.* J Neurochem, 2009. **110**(4): p. 1150-69.
12. Lefta, M., et al., *Development of dilated cardiomyopathy in Bmal1-deficient mice.* Am J Physiol Heart Circ Physiol, 2012. **303**(4): p. H475-85.
13. Stow, L.R. and M.L. Gumz, *The circadian clock in the kidney.* J Am Soc Nephrol, 2011. **22**(4): p. 598-604.
14. Nishinaga, H., et al., *Circadian expression of the Na+/H+ exchanger NHE3 in the mouse renal medulla.* Biomed Res, 2009. **30**(2): p. 87-93.
15. Damiola, F., et al., *Restricted feeding uncouples circadian oscillators in peripheral tissues from the central pacemaker in the suprachiasmatic nucleus.* Genes Dev, 2000. **14**(23): p. 2950-61.
16. Imai, S., *"Clocks" in the NAD World: NAD as a metabolic oscillator for the regulation of metabolism and aging.* Biochim Biophys Acta, 2010. **1804**(8): p. 1584-90.
17. Turek, F.W., et al., *Obesity and metabolic syndrome in circadian Clock mutant mice.* Science, 2005. **308**(5724): p. 1043-5.
18. Sherman, H., et al., *Timed high-fat diet resets circadian metabolism and prevents obesity.* FASEB J, 2012. **26**(8): p. 3493-502.
19. Lee, J., et al., *Loss of Bmal1 leads to uncoupling and impaired glucose-stimulated insulin secretion in beta-cells.* Islets, 2011. **3**(6): p. 381-8.
20. Albrecht, U., et al., *The multiple facets of Per2.* Cold Spring Harb Symp Quant Biol, 2007. **72**: p. 95-104.
21. Schibler, U. and P. Sassone-Corsi, *A web of circadian pacemakers.* Cell, 2002. **111**(7): p. 919-22.
22. Krauchi, K. and A. Wirz-Justice, *Circadian rhythm of heat production, heart rate, and skin and core temperature under unmasking conditions in men.* Am J Physiol, 1994. **267**(3 Pt 2): p. R819-29.
23. Tonsfeldt, K.J. and P.E. Chappell, *Clocks on top: the role of the circadian clock in the hypothalamic and pituitary regulation of endocrine physiology.* Mol Cell Endocrinol, 2012. **349**(1): p. 3-12.

24. Hastings, M., J.S. O'Neill, and E.S. Maywood, *Circadian clocks: regulators of endocrine and metabolic rhythms.* J Endocrinol, 2007. **195**(2): p. 187-98.
25. McClung, C.A., *Circadian genes, rhythms and the biology of mood disorders.* Pharmacol Ther, 2007. **114**(2): p. 222-32.
26. Takahashi, J.S., et al., *The genetics of mammalian circadian order and disorder: implications for physiology and disease.* Nat Rev Genet, 2008. **9**(10): p. 764-75.
27. Takeda, N. and K. Maemura, *Circadian clock and cardiovascular disease.* J Cardiol, 2011. **57**(3): p. 249-56.
28. Maury, E., K.M. Ramsey, and J. Bass, *Circadian rhythms and metabolic syndrome: from experimental genetics to human disease.* Circ Res, 2010. **106**(3): p. 447-62.
29. Challet, E., *Minireview: Entrainment of the suprachiasmatic clockwork in diurnal and nocturnal mammals.* Endocrinology, 2007. **148**(12): p. 5648-55.
30. Ebling, F.J., *The role of glutamate in the photic regulation of the suprachiasmatic nucleus.* Prog Neurobiol, 1996. **50**(2-3): p. 109-32.
31. Shigeyoshi, Y., et al., *Light-induced resetting of a mammalian circadian clock is associated with rapid induction of the mPer1 transcript.* Cell, 1997. **91**(7): p. 1043-53.
32. Reppert, S.M. and D.R. Weaver, *Coordination of circadian timing in mammals.* Nature, 2002. **418**(6901): p. 935-41.
33. Bozek, K., et al., *Regulation of clock-controlled genes in mammals.* PLoS One, 2009. **4**(3): p. e4882.
34. Ko, C.H. and J.S. Takahashi, *Molecular components of the mammalian circadian clock.* Hum Mol Genet, 2006. **15 Spec No 2**: p. R271-7.
35. Kondratov, R.V., et al., *BMAL1-dependent circadian oscillation of nuclear CLOCK: posttranslational events induced by dimerization of transcriptional activators of the mammalian clock system.* Genes Dev, 2003. **17**(15): p. 1921-32.
36. Ueda, H.R., et al., *System-level identification of transcriptional circuits underlying mammalian circadian clocks.* Nat Genet, 2005. **37**(2): p. 187-92.
37. Minami, Y., K.L. Ode, and H.R. Ueda, *Mammalian circadian clock: the roles of transcriptional repression and delay.* Handb Exp Pharmacol, 2013(217): p. 359-77.
38. Camacho, F., et al., *Human casein kinase Idelta phosphorylation of human circadian clock proteins period 1 and 2.* FEBS Lett, 2001. **489**(2-3): p. 159-65.
39. Lee, H., et al., *Essential roles of CKIdelta and CKIepsilon in the mammalian circadian clock.* Proc Natl Acad Sci U S A, 2009. **106**(50): p. 21359-64.
40. Eide, E.J., et al., *Control of mammalian circadian rhythm by CKIepsilon-regulated proteasome-mediated PER2 degradation.* Mol Cell Biol, 2005. **25**(7): p. 2795-807.
41. Reppert, S.M. and D.R. Weaver, *Molecular analysis of mammalian circadian rhythms.* Annu Rev Physiol, 2001. **63**: p. 647-76.
42. Yu, W., M. Nomura, and M. Ikeda, *Interactivating feedback loops within the mammalian clock: BMAL1 is negatively autoregulated and upregulated by CRY1, CRY2, and PER2.* Biochem Biophys Res Commun, 2002. **290**(3): p. 933-41.
43. Guillaumond, F., et al., *Differential control of Bmal1 circadian transcription by REV-ERB and ROR nuclear receptors.* J Biol Rhythms, 2005. **20**(5): p. 391-403.
44. Kantermann, T. and T. Roenneberg, *Is light-at-night a health risk factor or a health risk predictor?* Chronobiol Int, 2009. **26**(6): p. 1069-74.
45. Gery, S. and H.P. Koeffler, *The role of circadian regulation in cancer.* Cold Spring Harb Symp Quant Biol, 2007. **72**: p. 459-64.
46. Gery, S. and H.P. Koeffler, *Circadian rhythms and cancer.* Cell Cycle, 2010. **9**(6): p. 1097-103.
47. Savvidis, C. and M. Koutsilieris, *Circadian rhythm disruption in cancer biology.* Mol Med, 2012. **18**: p. 1249-60.

48. Lee, S., et al., *Disrupting circadian homeostasis of sympathetic signaling promotes tumor development in mice.* PLoS One, 2010. **5**(6): p. e10995.
49. Gotoh, T., et al., *The circadian factor Period 2 modulates p53 stability and transcriptional activity in unstressed cells.* Mol Biol Cell, 2014. **25**(19): p. 3081-93.
50. Sotak, M., A. Sumova, and J. Pacha, *Cross-talk between the circadian clock and the cell cycle in cancer.* Ann Med, 2014. **46**(4): p. 221-32.
51. Fu, L., et al., *The circadian gene Period2 plays an important role in tumor suppression and DNA damage response in vivo.* Cell, 2002. **111**(1): p. 41-50.
52. Massague, J., *G1 cell-cycle control and cancer.* Nature, 2004. **432**(7015): p. 298-306.
53. Zeller, K.I., et al., *An integrated database of genes responsive to the Myc oncogenic transcription factor: identification of direct genomic targets.* Genome Biol, 2003. **4**(10): p. R69.
54. Matsuo, T., et al., *Control mechanism of the circadian clock for timing of cell division in vivo.* Science, 2003. **302**(5643): p. 255-9.
55. Polidarova, L., et al., *Temporal gradient in the clock gene and cell-cycle checkpoint kinase Wee1 expression along the gut.* Chronobiol Int, 2009. **26**(4): p. 607-20.
56. Sotak, M., et al., *An association between clock genes and clock-controlled cell cycle genes in murine colorectal tumors.* Int J Cancer, 2013. **132**(5): p. 1032-41.
57. Cotter, T.G., *Apoptosis and cancer: the genesis of a research field.* Nat Rev Cancer, 2009. **9**(7): p. 501-7.
58. Elmore, S., *Apoptosis: a review of programmed cell death.* Toxicol Pathol, 2007. **35**(4): p. 495-516.
59. Wood, P.A., X. Yang, and W.J. Hrushesky, *Clock genes and cancer.* Integr Cancer Ther, 2009. **8**(4): p. 303-8.
60. Hua, H., et al., *Circadian gene mPer2 overexpression induces cancer cell apoptosis.* Cancer Sci, 2006. **97**(7): p. 589-96.
61. Tokunaga, H., et al., *Clinicopathological significance of circadian rhythm-related gene expression levels in patients with epithelial ovarian cancer.* Acta Obstet Gynecol Scand, 2008. **87**(10): p. 1060-70.
62. Yang, M.Y., et al., *Altered expression of circadian clock genes in human chronic myeloid leukemia.* J Biol Rhythms, 2011. **26**(2): p. 136-48.
63. Torti, S.V. and F.M. Torti, *Iron and cancer: more ore to be mined.* Nat Rev Cancer, 2013. **13**(5): p. 342-55.
64. Siah, C.W., et al., *Normal iron metabolism and the pathophysiology of iron overload disorders.* Clin Biochem Rev, 2006. **27**(1): p. 5-16.
65. Ganz, T., *Hepcidin--a regulator of intestinal iron absorption and iron recycling by macrophages.* Best Pract Res Clin Haematol, 2005. **18**(2): p. 171-82.
66. Wang, J. and K. Pantopoulos, *Regulation of cellular iron metabolism.* Biochem J, 2011. **434**(3): p. 365-81.
67. Kruszewski, M., *Labile iron pool: the main determinant of cellular response to oxidative stress.* Mutat Res, 2003. **531**(1-2): p. 81-92.
68. Ohgami, R.S., et al., *Identification of a ferrireductase required for efficient transferrin-dependent iron uptake in erythroid cells.* Nat Genet, 2005. **37**(11): p. 1264-9.
69. Theil, E.C., *Ferritin: structure, gene regulation, and cellular function in animals, plants, and microorganisms.* Annu Rev Biochem, 1987. **56**: p. 289-315.
70. Cairo, G., et al., *Induction of ferritin synthesis by oxidative stress. Transcriptional and post-transcriptional regulation by expansion of the "free" iron pool.* J Biol Chem, 1995. **270**(2): p. 700-3.
71. Breuer, W., M. Shvartsman, and Z.I. Cabantchik, *Intracellular labile iron.* Int J Biochem Cell Biol, 2008. **40**(3): p. 350-4.
72. Nemeth, E., et al., *Hepcidin regulates cellular iron efflux by binding to ferroportin and inducing its internalization.* Science, 2004. **306**(5704): p. 2090-3.

73. Roeser, H.P., et al., *The role of ceruloplasmin in iron metabolism.* J Clin Invest, 1970. **49**(12): p. 2408-17.
74. Eisenstein, R.S., *Iron regulatory proteins and the molecular control of mammalian iron metabolism.* Annu Rev Nutr, 2000. **20**: p. 627-62.
75. Pinnix, Z.K., et al., *Ferroportin and iron regulation in breast cancer progression and prognosis.* Sci Transl Med, 2010. **2**(43): p. 43ra56.
76. Torti, S.V. and F.M. Torti, *Cellular iron metabolism in prognosis and therapy of breast cancer.* Crit Rev Oncog, 2013. **18**(5): p. 435-48.
77. Dev, S. and J.L. Babitt, *Overview of iron metabolism in health and disease.* Hemodial Int, 2017.
78. Dale, J.C., M.F. Burritt, and A.R. Zinsmeister, *Diurnal variation of serum iron, iron-binding capacity, transferrin saturation, and ferritin levels.* Am J Clin Pathol, 2002. **117**(5): p. 802-8.
79. Wood, J.C., *Guidelines for quantifying iron overload.* Hematology Am Soc Hematol Educ Program, 2014. **2014**(1): p. 210-5.
80. Miller, J.L., *Iron deficiency anemia: a common and curable disease.* Cold Spring Harb Perspect Med, 2013. **3**(7).
81. DeRienzo, D.P. and A. Saleem, *Anemia of chronic disease: a review of pathogenesis.* Tex Med, 1990. **86**(10): p. 80-3.
82. Fracanzani, A.L., et al., *Increased cancer risk in a cohort of 230 patients with hereditary hemochromatosis in comparison to matched control patients with non-iron-related chronic liver disease.* Hepatology, 2001. **33**(3): p. 647-51.
83. Pietrangelo, A., *Iron and the liver.* Liver Int, 2016. **36 Suppl 1**: p. 116-23.
84. Jiang, R., et al., *Dietary iron intake and blood donations in relation to risk of type 2 diabetes in men: a prospective cohort study.* Am J Clin Nutr, 2004. **79**(1): p. 70-5.
85. Comin-Colet, J., et al., *Iron deficiency is a key determinant of health-related quality of life in patients with chronic heart failure regardless of anaemia status.* Eur J Heart Fail, 2013. **15**(10): p. 1164-72.
86. Youdim, M.B., *Brain iron deficiency and excess; cognitive impairment and neurodegeneration with involvement of striatum and hippocampus.* Neurotox Res, 2008. **14**(1): p. 45-56.
87. Xu, J., et al., *Impaired iron status in aging research.* Int J Mol Sci, 2012. **13**(2): p. 2368-86.
88. Sohal, R.S., et al., *Iron induces oxidative stress and may alter the rate of aging in the housefly, Musca domestica.* Mech Ageing Dev, 1985. **32**(1): p. 33-8.
89. Xiong, W., L. Wang, and F. Yu, *Regulation of cellular iron metabolism and its implications in lung cancer progression.* Med Oncol, 2014. **31**(7): p. 28.
90. Wang, Q., et al., *Ferroportin in the progression and prognosis of hepatocellular carcinoma.* Eur J Med Res, 2013. **18**: p. 59.
91. Stevens, R.G., et al., *Body iron stores and the risk of cancer.* N Engl J Med, 1988. **319**(16): p. 1047-52.
92. Kabat, G.C., et al., *Dietary iron and haem iron intake and risk of endometrial cancer: a prospective cohort study.* Br J Cancer, 2008. **98**(1): p. 194-8.
93. Kew, M.C. and G.A. Asare, *Dietary iron overload in the African and hepatocellular carcinoma.* Liver Int, 2007. **27**(6): p. 735-41.
94. Pietrangelo, A., *Hereditary hemochromatosis: pathogenesis, diagnosis, and treatment.* Gastroenterology, 2010. **139**(2): p. 393-408, 408 e1-2.
95. Daniels, T.R., et al., *The transferrin receptor and the targeted delivery of therapeutic agents against cancer.* Biochim Biophys Acta, 2012. **1820**(3): p. 291-317.
96. Steegmann-Olmedillas, J.L., *The role of iron in tumour cell proliferation.* Clin Transl Oncol, 2011. **13**(2): p. 71-6.
97. Edgren, G., et al., *Donation frequency, iron loss, and risk of cancer among blood donors.* J Natl Cancer Inst, 2008. **100**(8): p. 572-9.

98. Bystrom, L.M., M.L. Guzman, and S. Rivella, *Iron and reactive oxygen species: friends or foes of cancer cells?* Antioxid Redox Signal, 2014. **20**(12): p. 1917-24.
99. Snyder, C.M. and N.S. Chandel, *Mitochondrial regulation of cell survival and death during low-oxygen conditions.* Antioxid Redox Signal, 2009. **11**(11): p. 2673-83.
100. Ghaffari, S., *Oxidative stress in the regulation of normal and neoplastic hematopoiesis.* Antioxid Redox Signal, 2008. **10**(11): p. 1923-40.
101. Torti, S.V. and F.M. Torti, *Ironing out cancer.* Cancer Res, 2011. **71**(5): p. 1511-4.
102. Bienz, M. and H. Clevers, *Linking colorectal cancer to Wnt signaling.* Cell, 2000. **103**(2): p. 311-20.
103. Wu, X.N., et al., *Roles of the hepcidin-ferroportin axis and iron in cancer.* Eur J Cancer Prev, 2014. **23**(2): p. 122-33.
104. Dizdaroglu, M., et al., *Free radical-induced damage to DNA: mechanisms and measurement.* Free Radic Biol Med, 2002. **32**(11): p. 1102-15.
105. Kondo, K., et al., *Transferrin receptor expression in adenocarcinoma of the lung as a histopathologic indicator of prognosis.* Chest, 1990. **97**(6): p. 1367-71.
106. Yang, D.C., et al., *Expression of transferrin receptor and ferritin H-chain mRNA are associated with clinical and histopathological prognostic indicators in breast cancer.* Anticancer Res, 2001. **21**(1B): p. 541-9.
107. Yang, J., et al., *An iron delivery pathway mediated by a lipocalin.* Mol Cell, 2002. **10**(5): p. 1045-56.
108. Bao, G., et al., *Iron traffics in circulation bound to a siderocalin (Ngal)-catechol complex.* Nat Chem Biol, 2010. **6**(8): p. 602-9.
109. Fernandez, C.A., et al., *The matrix metalloproteinase-9/neutrophil gelatinase-associated lipocalin complex plays a role in breast tumor growth and is present in the urine of breast cancer patients.* Clin Cancer Res, 2005. **11**(15): p. 5390-5.
110. Zhang, Y., Y. Fan, and Z. Mei, *NGAL and NGALR overexpression in human hepatocellular carcinoma toward a molecular prognostic classification.* Cancer Epidemiol, 2012. **36**(5): p. e294-9.
111. Chen, G., et al., *Overexpression of iron regulatory protein 1 suppresses growth of tumor xenografts.* Carcinogenesis, 2007. **28**(4): p. 785-91.
112. Maffettone, C., et al., *Tumorigenic properties of iron regulatory protein 2 (IRP2) mediated by its specific 73-amino acids insert.* PLoS One, 2010. **5**(4): p. e10163.
113. Kamai, T., et al., *Increased serum hepcidin-25 level and increased tumor expression of hepcidin mRNA are associated with metastasis of renal cell carcinoma.* BMC Cancer, 2009. **9**: p. 270.
114. Ward, D.G., et al., *Increased hepcidin expression in colorectal carcinogenesis.* World J Gastroenterol, 2008. **14**(9): p. 1339-45.
115. Jiang, X.P., R.L. Elliott, and J.F. Head, *Manipulation of iron transporter genes results in the suppression of human and mouse mammary adenocarcinomas.* Anticancer Res, 2010. **30**(3): p. 759-65.
116. Ponka, P., *Tissue-specific regulation of iron metabolism and heme synthesis: distinct control mechanisms in erythroid cells.* Blood, 1997. **89**(1): p. 1-25.
117. Ponka, P., *Cell biology of heme.* Am J Med Sci, 1999. **318**(4): p. 241-56.
118. Khan, A.A. and J.G. Quigley, *Control of intracellular heme levels: heme transporters and heme oxygenases.* Biochim Biophys Acta, 2011. **1813**(5): p. 668-82.
119. Dioum, E.M., et al., *NPAS2: a gas-responsive transcription factor.* Science, 2002. **298**(5602): p. 2385-7.
120. Raghuram, S., et al., *Identification of heme as the ligand for the orphan nuclear receptors REV-ERBalpha and REV-ERBbeta.* Nat Struct Mol Biol, 2007. **14**(12): p. 1207-13.
121. Yang, J., et al., *A novel heme-regulatory motif mediates heme-dependent degradation of the circadian factor period 2.* Mol Cell Biol, 2008. **28**(15): p. 4697-711.
122. Guenthner, C.J., D. Bickar, and M.E. Harrington, *Heme reversibly damps PERIOD2 rhythms in mouse suprachiasmatic nucleus explants.* Neuroscience, 2009. **164**(2): p. 832-41.

123. Cao, G.Y., et al., *Circadian rhythm in serum iron levels.* Biol Trace Elem Res, 2012. **147**(1-3): p. 63-6.
124. Guillygomarc'h, A., et al., *Circadian variations of transferrin saturation levels in iron-overloaded patients: implications for the screening of C282Y-linked haemochromatosis.* Br J Haematol, 2003. **120**(2): p. 359-63.
125. Dean, T., Jr., et al., *The effects of dietary iron deprivation on murine circadian sleep architecture.* Sleep Med, 2006. **7**(8): p. 634-40.
126. Youdim, M.B., S. Yehuda, and Y. Ben-Uriah, *Iron deficiency-induced circadian rhythm reversal of dopaminergic-mediated behaviours and thermoregulation in rats.* Eur J Pharmacol, 1981. **74**(4): p. 295-301.
127. Okazaki, F., et al., *Circadian rhythm of transferrin receptor 1 gene expression controlled by c-Myc in colon cancer-bearing mice.* Cancer Res, 2010. **70**(15): p. 6238-46.
128. Okazaki, F., et al., *Circadian Clock in a Mouse Colon Tumor Regulates Intracellular Iron Levels to Promote Tumor Progression.* J Biol Chem, 2016. **291**(13): p. 7017-28.
129. Shen, J., et al., *Iron Metabolism Regulates p53 Signaling through Direct Heme-p53 Interaction and Modulation of p53 Localization, Stability, and Function.* Cell Rep, 2014. **7**(1): p. 180-93.
130. Zhang, F., et al., *Post-transcriptional modulation of iron homeostasis during p53-dependent growth arrest.* J Biol Chem, 2008. **283**(49): p. 33911-8.
131. Weizer-Stern, O., et al., *Hepcidin, a key regulator of iron metabolism, is transcriptionally activated by p53.* Br J Haematol, 2007. **138**(2): p. 253-62.
132. Zhang, R., et al., *A circadian gene expression atlas in mammals: implications for biology and medicine.* Proc Natl Acad Sci U S A, 2014. **111**(45): p. 16219-24.
133. Evstatiev, R. and C. Gasche, *Iron sensing and signalling.* Gut, 2012. **61**(6): p. 933-52.
134. Simcox, J.A., et al., *Dietary iron controls circadian hepatic glucose metabolism through heme synthesis.* Diabetes, 2015. **64**(4): p. 1108-19.
135. Jacobi, D., et al., *Hepatic Bmal1 Regulates Rhythmic Mitochondrial Dynamics and Promotes Metabolic Fitness.* Cell Metab, 2015. **22**(4): p. 709-20.
136. Peek, C.B., et al., *Circadian clock NAD+ cycle drives mitochondrial oxidative metabolism in mice.* Science, 2013. **342**(6158): p. 1243417.
137. Garcia, M.N., et al., *Circadian rhythm of DNA synthesis and mitotic activity in tongue keratinocytes.* Cell Biol Int, 2001. **25**(2): p. 179-83.
138. Fustin, J.M., et al., *Rhythmic nucleotide synthesis in the liver: temporal segregation of metabolites.* Cell Rep, 2012. **1**(4): p. 341-9.
139. Feltes, B.C. and D. Bonatto, *Overview of xeroderma pigmentosum proteins architecture, mutations and post-translational modifications.* Mutat Res Rev Mutat Res, 2015. **763**: p. 306-20.
140. Kang, T.H., et al., *Circadian oscillation of nucleotide excision repair in mammalian brain.* Proc Natl Acad Sci U S A, 2009. **106**(8): p. 2864-7.
141. Kang, T.H., et al., *Circadian control of XPA and excision repair of cisplatin-DNA damage by cryptochrome and HERC2 ubiquitin ligase.* Proc Natl Acad Sci U S A, 2010. **107**(11): p. 4890-5.
142. Faillace, M.P., M.I. Keller Sarmiento, and R.E. Rosenstein, *Daily variations in cGMP, guanylate cyclase and phosphodiesterase in the golden hamster retina.* Vision Res, 1996. **36**(10): p. 1365-9.
143. Witte, K., et al., *Contribution of the nitric oxide-guanylyl cyclase system to circadian regulation of blood pressure in normotensive Wistar-Kyoto rats.* Cardiovasc Res, 1995. **30**(5): p. 682-8.
144. Johnston, J.D., et al., *Circadian Rhythms, Metabolism, and Chrononutrition in Rodents and Humans.* Adv Nutr, 2016. **7**(2): p. 399-406.
145. Ferrell, J.M. and J.Y. Chiang, *Circadian rhythms in liver metabolism and disease.* Acta Pharm Sin B, 2015. **5**(2): p. 113-22.

146. Sharma, N., et al., *The emerging role of the liver in iron metabolism.* Am J Gastroenterol, 2005. **100**(1): p. 201-6.
147. Hirayama, M., et al., *Regulation of iron metabolism in HepG2 cells: a possible role for cytokines in the hepatic deposition of iron.* Hepatology, 1993. **18**(4): p. 874-80.
148. Huang, X., et al., *Ferrous ion autoxidation and its chelation in iron-loaded human liver HepG2 cells.* Free Radic Biol Med, 2002. **32**(1): p. 84-92.
149. Lunova, M., et al., *Hepcidin knockout mice fed with iron-rich diet develop chronic liver injury and liver fibrosis due to lysosomal iron overload.* J Hepatol, 2014. **61**(3): p. 633-41.
150. Camaschella, C., *BMP6 orchestrates iron metabolism.* Nat Genet, 2009. **41**(4): p. 386-8.
151. Rolfs, A., et al., *Oxygen-regulated transferrin expression is mediated by hypoxia-inducible factor-1.* J Biol Chem, 1997. **272**(32): p. 20055-62.
152. Bianchi, L., L. Tacchini, and G. Cairo, *HIF-1-mediated activation of transferrin receptor gene transcription by iron chelation.* Nucleic Acids Res, 1999. **27**(21): p. 4223-7.
153. Peyssonnaux, C., et al., *Regulation of iron homeostasis by the hypoxia-inducible transcription factors (HIFs).* J Clin Invest, 2007. **117**(7): p. 1926-32.
154. Galy, B., et al., *Iron regulatory proteins are essential for intestinal function and control key iron absorption molecules in the duodenum.* Cell Metab, 2008. **7**(1): p. 79-85.
155. Paranjpe, D.A. and V.K. Sharma, *Evolution of temporal order in living organisms.* J Circadian Rhythms, 2005. **3**(1): p. 7.
156. Hastings, M.H., A.B. Reddy, and E.S. Maywood, *A clockwork web: circadian timing in brain and periphery, in health and disease.* Nat Rev Neurosci, 2003. **4**(8): p. 649-61.
157. Kim, T.K., et al., *Widespread transcription at neuronal activity-regulated enhancers.* Nature, 2010. **465**(7295): p. 182-7.
158. Ripperger, J.A. and U. Schibler, *Rhythmic CLOCK-BMAL1 binding to multiple E-box motifs drives circadian Dbp transcription and chromatin transitions.* Nat Genet, 2006. **38**(3): p. 369-74.
159. Wu, K.J., A. Polack, and R. Dalla-Favera, *Coordinated regulation of iron-controlling genes, H-ferritin and IRP2, by c-MYC.* Science, 1999. **283**(5402): p. 676-9.
160. Buss, J.L., F.M. Torti, and S.V. Torti, *The role of iron chelation in cancer therapy.* Curr Med Chem, 2003. **10**(12): p. 1021-34.
161. Iwai, K., et al., *Iron-dependent oxidation, ubiquitination, and degradation of iron regulatory protein 2: implications for degradation of oxidized proteins.* Proc Natl Acad Sci U S A, 1998. **95**(9): p. 4924-8.
162. Fang, C., et al., *Protein alteration of HepG2.2.15 cells induced by iron overload.* Proteomics, 2012. **12**(9): p. 1378-90.
163. Lazarou, C. and A.L. Matalas, *Breakfast intake is associated with nutritional status, Mediterranean diet adherence, serum iron and fasting glucose: the CYFamilies study.* Public Health Nutr, 2015. **18**(7): p. 1308-16.
164. Turek, F.W., *Circadian clocks: Not your grandfather's clock.* Science, 2016. **354**(6315): p. 992-993.
165. Frick, D.N. and C.C. Richardson, *DNA primases.* Annu Rev Biochem, 2001. **70**: p. 39-80.
166. Koike, N., et al., *Transcriptional architecture and chromatin landscape of the core circadian clock in mammals.* Science, 2012. **338**(6105): p. 349-54.
167. Beckwith, E.J. and M.J. Yanovsky, *Circadian regulation of gene expression: at the crossroads of transcriptional and post-transcriptional regulatory networks.* Curr Opin Genet Dev, 2014. **27**: p. 35-42.
168. La Fleur, S.E., *Daily rhythms in glucose metabolism: suprachiasmatic nucleus output to peripheral tissue.* J Neuroendocrinol, 2003. **15**(3): p. 315-22.
169. Lee, A., et al., *Diurnal variation in glucose tolerance. Cyclic suppression of insulin action and insulin secretion in normal-weight, but not obese, subjects.* Diabetes, 1992. **41**(6): p. 750-9.

170. Strubbe, J.H., et al., *Daily variation of food-induced changes in blood glucose and insulin in the rat and the control by the suprachiasmatic nucleus and the vagus nerve.* J Auton Nerv Syst, 1987. **20**(2): p. 113-9.
171. Kalsbeek, A. and J.H. Strubbe, *Circadian control of insulin secretion is independent of the temporal distribution of feeding.* Physiol Behav, 1998. **63**(4): p. 553-8.
172. Vollmers, C., et al., *Time of feeding and the intrinsic circadian clock drive rhythms in hepatic gene expression.* Proc Natl Acad Sci U S A, 2009. **106**(50): p. 21453-8.
173. Stephan, F.K. and A.J. Davidson, *Glucose, but not fat, phase shifts the feeding-entrained circadian clock.* Physiol Behav, 1998. **65**(2): p. 277-88.
174. Eckel-Mahan, K. and P. Sassone-Corsi, *Metabolism and the circadian clock converge.* Physiol Rev, 2013. **93**(1): p. 107-35.
175. Rodgers, J.T., et al., *Nutrient control of glucose homeostasis through a complex of PGC-1alpha and SIRT1.* Nature, 2005. **434**(7029): p. 113-8.
176. Belden, W.J. and J.C. Dunlap, *SIRT1 is a circadian deacetylase for core clock components.* Cell, 2008. **134**(2): p. 212-4.
177. Ramsey, K.M., et al., *Circadian clock feedback cycle through NAMPT-mediated NAD+ biosynthesis.* Science, 2009. **324**(5927): p. 651-4.
178. Asher, G., et al., *Poly(ADP-ribose) polymerase 1 participates in the phase entrainment of circadian clocks to feeding.* Cell, 2010. **142**(6): p. 943-53.
179. Liu, C., et al., *Transcriptional coactivator PGC-1alpha integrates the mammalian clock and energy metabolism.* Nature, 2007. **447**(7143): p. 477-81.
180. Oklejewicz, M., et al., *Phase resetting of the mammalian circadian clock by DNA damage.* Curr Biol, 2008. **18**(4): p. 286-91.
181. Kornmann, B., et al., *System-driven and oscillator-dependent circadian transcription in mice with a conditionally active liver clock.* PLoS Biol, 2007. **5**(2): p. e34.
182. Tahara, Y. and S. Shibata, *Circadian rhythms of liver physiology and disease: experimental and clinical evidence.* Nat Rev Gastroenterol Hepatol, 2016. **13**(4): p. 217-26.
183. Anderson, E.R. and Y.M. Shah, *Iron homeostasis in the liver.* Compr Physiol, 2013. **3**(1): p. 315-30.
184. Cheng, C.M., et al., *Iron Regulatory Protein 1 Suppresses Hypoxia-Induced Iron Uptake Proteins Expression and Decreases Iron Levels in HepG2 Cells.* J Cell Biochem, 2015. **116**(9): p. 1919-31.
185. Gao, J., et al., *The hereditary hemochromatosis protein, HFE, inhibits iron uptake via down-regulation of Zip14 in HepG2 cells.* J Biol Chem, 2008. **283**(31): p. 21462-8.
186. Tyakht, A.V., et al., *RNA-Seq gene expression profiling of HepG2 cells: the influence of experimental factors and comparison with liver tissue.* BMC Genomics, 2014. **15**: p. 1108.
187. Card, R.T., G.M. Brown, and L.S. Valberg, *Serum Iron and Iron-Binding Capacity in Normal Subjects.* Can Med Assoc J, 1964. **90**: p. 618-22.
188. Gorbacheva, V.Y., et al., *Circadian sensitivity to the chemotherapeutic agent cyclophosphamide depends on the functional status of the CLOCK/BMAL1 transactivation complex.* Proc Natl Acad Sci U S A, 2005. **102**(9): p. 3407-12.
189. Albrecht, U., *Per2 has time on its side.* Nat Chem Biol, 2007. **3**(3): p. 139-40.
190. Yamazaki, S. and J.S. Takahashi, *Real-time luminescence reporting of circadian gene expression in mammals.* Methods Enzymol, 2005. **393**: p. 288-301.
191. Ramanathan, C., et al., *Cell type-specific functions of period genes revealed by novel adipocyte and hepatocyte circadian clock models.* PLoS Genet, 2014. **10**(4): p. e1004244.
192. Sebastiani, G. and K. Pantopoulos, *Disorders associated with systemic or local iron overload: from pathophysiology to clinical practice.* Metallomics, 2011. **3**(10): p. 971-86.

193. Ritz, T., et al., *Cryptochrome: A photoreceptor with the properties of a magnetoreceptor?* Commun Integr Biol, 2010. **3**(1): p. 24-7.
194. Gozzelino, R. and M.P. Soares, *Coupling heme and iron metabolism via ferritin H chain.* Antioxid Redox Signal, 2014. **20**(11): p. 1754-69.
195. Liu, A.C., et al., *Intercellular coupling confers robustness against mutations in the SCN circadian clock network.* Cell, 2007. **129**(3): p. 605-16.
196. Ye, R., et al., *Biochemical analysis of the canonical model for the mammalian circadian clock.* J Biol Chem, 2011. **286**(29): p. 25891-902.
197. Duffy, J.F., R.E. Kronauer, and C.A. Czeisler, *Phase-shifting human circadian rhythms: influence of sleep timing, social contact and light exposure.* J Physiol, 1996. **495 (Pt 1)**: p. 289-97.
198. Caro, J.J., et al., *Anemia as an independent prognostic factor for survival in patients with cancer: a systemic, quantitative review.* Cancer, 2001. **91**(12): p. 2214-21.
199. Jellen, L.C., et al., *Iron deficiency alters expression of dopamine-related genes in the ventral midbrain in mice.* Neuroscience, 2013. **252**: p. 13-23.
200. Potter, G.D., et al., *Circadian Rhythm and Sleep Disruption: Causes, Metabolic Consequences, and Countermeasures.* Endocr Rev, 2016. **37**(6): p. 584-608.
201. Wilking, M., et al., *Circadian rhythm connections to oxidative stress: implications for human health.* Antioxid Redox Signal, 2013. **19**(2): p. 192-208.
202. Debruyne, J.P., et al., *A clock shock: mouse CLOCK is not required for circadian oscillator function.* Neuron, 2006. **50**(3): p. 465-77.

Appendix A:

Association of the circadian factor Period 2 to p53 influences p53's function in DNA-damage signaling

Tetsuya Gotoh*, Marian Vila-Caballer*,†, Jingjing Liu, Samuel Schiffhauer, and Carla V. Finkielstein
Integrated Cellular Responses Laboratory, Department of Biological Sciences, Virginia Polytechnic Institute and State University, Blacksburg, VA 24061

ABSTRACT **Circadian period proteins influence cell division and death by associating with checkpoint components, although their mode of regulation has not been firmly established. hPer2 forms a trimeric complex with hp53 and its negative regulator Mdm2. In unstressed cells, this association leads to increased hp53 stability by blocking Mdm2-dependent ubiquitination and transcription of hp53 target genes. Because of the relevance of hp53 in checkpoint signaling, we hypothesize that hPer2 association with hp53 acts as a regulatory module that influences hp53's downstream response to genotoxic stress. Unlike the trimeric complex, whose distribution was confined to the nuclear compartment, hPer2/hp53 was identified in both cytosol and nucleus. At the transcriptional level, a reporter containing the hp21$^{WAF1/CIP1}$ promoter, a target of hp53, remained inactive in cells expressing a stable form of the hPer2/hp53 complex even when treated with γ-radiation. Finally, we established that hPer2 directly acts on the hp53 node, as checkpoint components upstream of hp53 remained active in response to DNA damage. Quantitative transcriptional analyses of hp53 target genes demonstrated that unbound hp53 was absolutely required for activation of the DNA-damage response. Our results provide evidence of the mode by which the circadian tumor suppressor hPer2 modulates hp53 signaling in response to genotoxic stress.**

Monitoring Editor
Mark J. Solomon
Yale University

Received: May 20, 2014
Revised: Oct 29, 2014
Accepted: Nov 13, 2014

INTRODUCTION

Transcription of *period* genes oscillates in a circadian manner and is essential for maintaining a functional clock that is driven by interacting transcription-translation–based autoregulatory feedback loops (for review, see Takahashi *et al.*, 2008). Three homologues (*period* 1–3) have been identified in mammals, whose levels oscillate in the suprachiasmatic nuclei, where the master clock is located, and in peripheral tissues (Albrecht *et al.*, 2007). Period (Per), cryptochrome (Cry), casein kinase Iε/δ (CKIε/δ), circadian locomoter output cycles kaput (Clock), and brain and muscle Arnt-like protein 1 (Bmal1) are the main players responsible for driving the primary negative-feedback loop of the clock, where transcriptional activation, heterodimerization, and translocation maintain

This article was published online ahead of print in MBoC in Press (http://www.molbiolcell.org/cgi/doi/10.1091/mbc.E14-05-0994) on November 19, 2014.

*These authors contributed equally.

†Present address: Department of Biology, University of Padova, Via U. Bassi, 58/B, 35121, Padova, Italy

T.G. provided data in Figures 1, 2, 4, and 5D and Supplemental Figures S1, S2, S4, S8F, S9, B and C, and S10 and contributed with reagents in Figures 3 and 5 and Supplemental Figures S3, S5, and S8. M.V.-C. performed the experiments shown in Figures 3 and 5, B and C, and Supplemental Figures S3, S8, A–E, and S9A, contributed in the execution of the experiments shown in Figure 5D and Supplemental Figures S1, S8F, and S9C, and performed the statistical analyses except for those mentioned otherwise. J.L. performed the experiments shown in Supplemental Figures S6 and S7 (top and middle) and S9C. S.S. provided Supplemental Figures S5 and S7 (bottom) and the statistical analyses shown in Supplemental Figures S5, S7, and S9. C.V.F., T.G., and M.V.-C. analyzed the overall data, refined the hypothesis, and proposed the model. C.V.F. supervised and coordinated all investigators for the project and wrote the manuscript.

Address correspondence to: Carla V. Finkielstein (finkielc@vt.edu).

Abbreviations used: *BAX*, encodes the Bcl-2-associated X protein (Bax); *CDKN1a*, encodes cyclin-dependent kinase inhibitor p21 (p21$^{CIP1/WAF1}$); *GADD45α*, encodes growth arrest and DNA damage–inducible protein 45α (Gadd45α); H1299, human non–small cell lung carcinoma cells; HCT116, human colorectal carcinoma-116 cells; hp53, human p53 transcription factor; hPer2, human Period 2; Mdm2, murine [human] double minute-2; *SFN*, encodes 14-3-3σ.

Supplemental Material can be found at:
http://www.molbiolcell.org/content/suppl/2014/11/17/mbc.E14-05-0994v1.DC1

the dynamics of the process (for review, see Takahashi *et al.*, 2008).

In recent years, it has been determined that clock component roles have expanded beyond their strict function as modulators of the organism's adaptive response to environmental cues (i.e., light/dark cycles) to include regulating sleep–wake cycles and release of hormones, maintaining the body's thermoregulation, and having a role in photoperiodism. Extensive work in various organismal systems has identified clock factors as obligatory intermediates that control numerous physiological processes directly relevant to human diseases and behavioral disorders (for review, see Takahashi *et al.*, 2008). For example, a *Bmal1/Mop3* (*Arnt1*)–null mutant mouse exhibits infertility, decreased body weight usually associated with abnormal gluconeogenesis and lipogenesis, premature aging, and sleep fragmentation (Bunger *et al.*, 2000; Rudic *et al.*, 2004; Laposky *et al.*, 2005; Shimba *et al.*, 2005; Kondratov *et al.*, 2006), whereas a *ClockΔ19* (antimorph) mouse mutant is hyperphagic and obese, hypersensitive to chemotherapeutic agents, and exhibits a manic phenotype (Naylor *et al.*, 2000; Rudic *et al.*, 2004; Gorbacheva *et al.*, 2005; Turek *et al.*, 2005). Others, such as the *Cry1* and *Cry2* double-null mutant mouse, exhibit a delay in tissue regeneration as monitored in the liver (Matsuo *et al.*, 2003). *Csnk1e* ($CK1\varepsilon^{tau}$ mutant) mutant animals have an enhanced metabolic but reduced growth rate (Oklejewicz *et al.*, 1997; Lucas *et al.*, 2000), whereas both *Csnk1d* (CK1δ)- and *timeless*-null mutations result in a lethal phenotype (Gotter *et al.*, 2000; Xu *et al.*, 2005). Additional physiological phenotypes, including diminished pupillary light reflex, impaired temporal regulation of metabolism and feeding, age-related autoimmune diseases, and defects in skeletal muscle regeneration, have also been described in mice exhibiting mutations in other clock-related genes, such as *Rora, b,* and *c, Dec 1* and *2, Opn4, Vip, Vipr2,* and *Nocturnin* (for review, see Takahashi *et al.*, 2008). Moreover, deletion and mutations of mouse *Period* genes result in numerous changes in an animal's phenotype, including shortening or loss of the circadian period (in the case of Per1 and Per2 double-null mutant mice), sensitization of animals to drugs, improper alcohol intake, altered glucose metabolism, and abnormal cellular proliferation (Zheng *et al.*, 1999, 2001; Shearman *et al.*, 2000; Bae *et al.*, 2001; Cermakian *et al.*, 2001; Fu *et al.*, 2002). Of interest, neither *Per1*- nor *Per3*-null mutant mice exhibit a phenotype that is reminiscent of that observed in animals in which the expression of checkpoint proteins is compromised (Fu *et al.*, 2002); however, *Per2*-null mutant mice do. Accordingly, *Per2*-null mice show increased hyperplastic growth, tumor development, and severe morbidity, a phenotype that is accompanied by hair graying and hair loss, which is exacerbated in the presence of genotoxic stress (Fu *et al.*, 2002). Although there have been attempts to identify molecular signatures responsible for the *Per2*-null phenotype (Fu *et al.*, 2002), the mechanistic foundation that further supports the observed phenotype is lacking.

Connections between clock molecules and the cellular DNA damage response have been identified. In *Neurospora crassa*, the clock gene *period 4* was identified as an orthologue of the mammalian checkpoint kinase 2 (Chk2) gene (Pregueiro *et al.*, 2006). In colon cancer cell lines, overexpression of Per1 sensitizes cells to DNA damage–induced apoptosis by a yet-unknown mechanism that involves interaction with Chk2 (Gery *et al.*, 2006). However, unlike Per2, Per1 does not seem to act as a tumor suppressor, since homozygous Per1 mutant mice display only a shorter circadian period with reduced precision and stability, and ablation of the *per1* gene does not affect cell proliferation (Zheng *et al.*, 2001). Finally, the human Timeless (hTim) protein seems to be required for the phosphorylation and activation of Chk1 by the ataxia telangiectasia and Rad3-related protein (ATR), whereas Per3 appears to physically bind to both ATM and Chk2. However, the role of hTim in circadian regulation of mammalian cells is controversial (Unsal-Kacmaz *et al.*, 2005), and the *per3* gene product is not necessary to sustain circadian rhythmicity in mice (Shearman *et al.*, 2000). Overall these studies suggest a scenario in which multiple circadian players converge on a multilevel cellular clock that links environmental conditions to the biochemical and genetic machinery of the cell to influence cell cycle progression and the response to genotoxic stress.

More recently, we performed interaction studies using human Period 2 (hPer2) as bait to map and identify protein–protein interactions and endogenous protein partner complexes (Gotoh *et al.*, 2014). The transcription factor and checkpoint-component p53 (human p53 transcription factor [hp53]) is among the novel hPer2 interactors. Association of hPer2 to the C-terminus region of hp53 results in formation of a trimeric complex in which the oncogenic protein murine [human] double minute-2 (Mdm2) is bound to the N-terminus of hp53. As a result, hPer2 promotes hp53 stability by a mechanism that involves inhibition of hp53 ubiquitination by Mdm2 (Gotoh *et al.*, 2014). The end result is the intersection of circadian and checkpoint components at the key hp53 node and the modulation of the hp53 transcriptional response. Our findings are in agreement with the observation that endogenous p53 is largely undetectable in thymocytes from *Per2*-null mice and that de novo accumulation of p53 seems to occur several hours after the insult is applied in *Per2*-null animals (Fu *et al.*, 2002), an observation that goes along with our findings of hPer2 acting as a transcriptional regulator of the *TP53* gene (Gotoh *et al.*, 2014).

A number of additional findings indirectly point toward cross-talk between Per2 function and the p53-mediated DNA damage response; however, it remains unclear how Per2 relates to that process mechanistically. For example, it is known that overexpression of Per2 results in reduced cellular proliferation and increased apoptosis in lung and mammary carcinoma, but not in embryonic fibroblast NIH3T3 cells, by a transcriptional mechanism that involves the up-regulation of proapoptotic components (i.e., *TP53* and *BAX* [encodes the Bcl-2-associated X protein, Bax]) and the simultaneous attenuation of antiapoptotic transcripts, including *MYC*, *BCL2L1*, and *BCL2* (Hua *et al.*, 2006). Sun *et al.* (2010) expanded these findings to leukemia cells by showing that Per2 overexpression promotes p53-dependent G2/M arrest by down-regulation of *CCNB1* and *MYC* expression followed by apoptosis. In line with these observations is the finding that overexpression of Per2 in hematopoietic cancer cell lines results in a phenotype that includes growth inhibition, cell cycle arrest, apoptosis, and loss of clonogenic ability (Gery and Koeffler, 2009). More recently, the known $Ser^{662}Gly$ ($S^{662}G$) mutation in Per2, responsible for familial advanced sleep phase syndrome, has been linked to enhanced resistance to x-ray–induced apoptosis and increased E1A- and RAS-mediated oncogenic transformation (Gu *et al.*, 2012). Accordingly, animals bearing the $Per2^{S662G}$ mutation show accelerated tumorigenesis in a $p53^{R172H/+}$ background. This effect is independent of the length of the circadian cycle but influences the relative phases of expression of p53-regulated, clock-controlled cell cycle genes (i.e., *CDKN1a* [encoding cyclin-dependent kinase inhibitor p21, $p21^{CIP1/WAF1}$] and *CCND1*; Gu *et al.*, 2012). More recently, we showed that hPer2 acts on hp53 by controlling its stability and activity in unstressed conditions (Gotoh *et al.*, 2014) and hypothesized that exposure to genotoxic stress triggers a rapid, hp53-mediated transcriptional checkpoint response by releasing hp53 from a preformed, nucleus-localized, hPer2/hp53 stable endogenous complex. Our findings establish the spatial distribution of

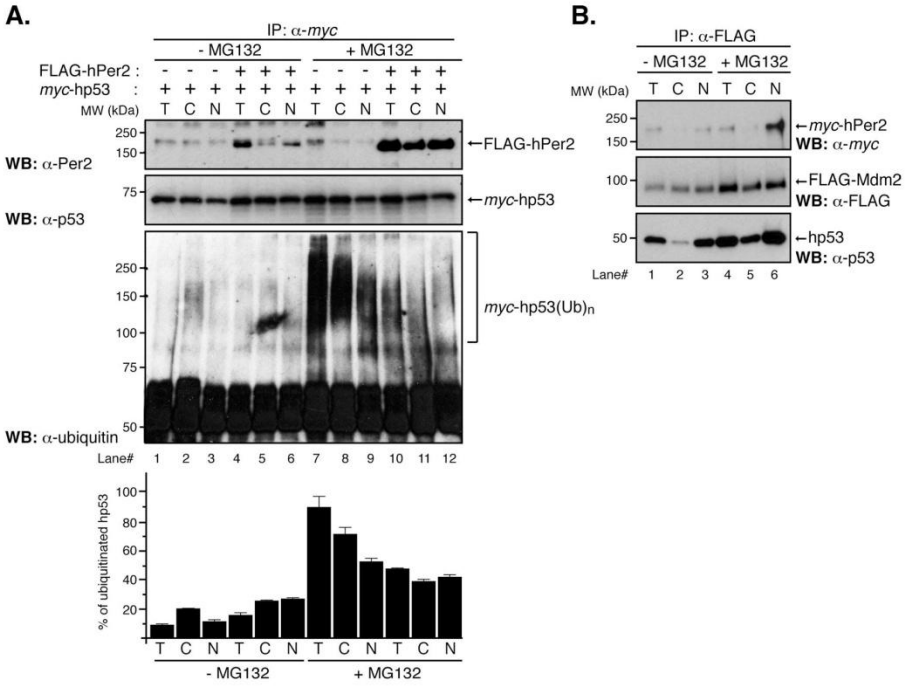

FIGURE 1: Distribution of the hPer2/hp53 complex among cellular compartments. (A) HCT116 cells were transfected with pCS2+*myc*-hp53 and either pCS2+FLAG-hPer2 (+) or empty vector (–) and maintained in complete medium for 20 h before adding or not (control; –MG132) MG132 (50 μM) and ubiquitin aldehyde (5 nM). Cells were maintained an additional 4 h before harvesting. Lysates (6.4×10^5 cells) were used to prepare the cytosolic (C) and total (T) fractions, whereas 32×10^5 cells were used for nuclear (N) preparation. Total, cytosolic, and nuclear extracts were incubated with α-*myc* antibody and protein A beads in NP40 lysis buffer containing MG132 and ubiquitin aldehyde. Washed samples were analyzed by immunoblotting using specific antibodies. Ubiquitinated *myc*-hp53 complexes (*myc*-hp53$(Ub)_n$) are indicated between brackets. Immunoblot data from a single experiment repeated three times with similar results. Quantification of the sample's ubiquitinated signal was performed using ImageJ, version 1.45 (National Institutes of Health software package; Schneider *et al.*, 2012; bar graph). (B) HCT116 lysates (2.8×10^5 cells for T/C; 14×10^5 cells for N) from pCS2+FLAG-Mdm2– and pCS2+*myc*-hPer2– cotransfected cells treated or not (–MG132) with 50 μM MG132 and 5 nM ubiquitin aldehyde were immunoprecipitated using α-FLAG and protein A beads and analyzed by immunoblotting for endogenous hp53 (bottom) and *myc*- and FLAG-expressed proteins (top and middle, respectively).

the various hPer2, hp53, and Mdm2 complexes, the need for hPer2 association with hp53 to maintain basal levels of this protein, and the relevance of hPer2/hp53 dissociation for an effective hp53-mediated DNA damage checkpoint response.

RESULTS

Spatial organization and shuttling of circadian molecules are common themes when it comes to understanding how oscillations are generated and sustained in biological clock systems. They are also common subjects when considering how sensor components segregate signals in response to stress conditions at various points in the cell cycle. In light of our previous findings in which the circadian factor hPer2 directly binds the tumor suppressor and checkpoint component hp53 in unstressed cells, we now ask whether the complex's spatial organization, as well as association, is critical for an effective hp53-mediated transcriptional response under stress conditions.

Subcellular distribution of hPer2/hp53 complexes

To assess whether functional compartmentalization of the hp53/hPer2 complex occurs, we performed cell fractionation experiments and monitored the formation of polyubiquitinated hp53 complexes and hPer2 binding in extracts from cells treated with proteasome inhibitors (Figure 1, A and B). Human colon carcinoma HCT-116 (HCT116) cells ($p53^{+/+}$) were cotransfected with *myc*-hp53 and FLAG-hPer2 or empty vector (–) and treated with MG132 (+MG132) or vehicle (–MG132). Total, cytosolic, and nuclear fractions were analyzed for hp53/hPer2 complex formation and the presence of polyubiquitinated hp53. Input levels of *myc*-hp53 and FLAG-hPer2, as well as of endogenous hp53 and hPer2 levels, were monitored in each fraction (Supplemental Figure S1, A and B) and normalized to those of *myc*-hp53 for the experiment shown in Figure 1A. Unlike nontreated MG132 cells, immunoprecipitation of *myc*-hp53 showed the presence of stable *myc*-hp53$(Ub)_n$ forms in total (T) and cytosolic (C) fractions and, to a lesser extent, in the nuclear (N) fraction of samples treated with MG132 (Figure 1A, bottom, lanes 1–3 vs. lanes 7–9). These results most likely represent the effect of proteasome inhibitors in preserving the *myc*-hp53 ubiquitinated complexes and accumulation in the cytosol as the preferred site for their ubiquitin-mediated degradation.

Significantly, overexpression of FLAG-hPer2 followed by *myc*-hp53 binding abrogated the formation of hp53(Ub)$_n$ in both nuclear and cytosolic fractions (Figure 1A, bottom, lanes 7–9 vs. lanes 10–12), in agreement with the subcellular distribution of hPer2 in those compartments (Figure 1A, top, lanes 10–12, and Supplemental Figure S1B) and the proposed role of hPer2 in modulating hp53 polyubiquitination. These results establish a physical and functional presence of hp53/hPer2 complex in the cytosol and nucleus. Further support comes from results shown in Figure 1A (lanes 1–6), in which studies similar to the ones described earlier were conducted in the absence of MG132 (–MG132), allowing the proteasomal machinery to be fully functional. As a result, hp53(Ub)$_n$ forms were undetected (lanes 1–6), and only trace amounts of hPer2 were associated with *myc*-hp53 in immunoprecipitated nuclear samples (Figure 1A, top and bottom, lane 6) even when input amounts were comparable to those used in the +MG132 experiment (Supplemental Figure S1B, top, lanes 4–6 vs. lanes 10–12). As previously shown, Per2 is degraded by the proteasomal pathway unless associated (Yagita *et al.*, 2002), and thus the level of FLAG-hPer2 was expected to be low in both the cytosolic and nuclear compartments in the absence of MG132 but detectable if associated to a protein counterpart. In sum, our data establish that 1) the hPer2/hp53 complex can be found in both the nuclear and cytosolic subcellular compartments and 2) physical interaction between hp53 and hPer2 might influence hPer2 degradation as well.

Next we asked whether Mdm2 associates with the hPer2/hp53 once in the nucleus. To answer this question, we cotransfected HCT116 cells with FLAG-Mdm2 and *myc*-hPer2 and looked for formation of the trimeric complex with endogenous hp53 (Figure 1B). Transfected cells were incubated in the absence (–) or presence (+) of MG132 and subjected to cellular fractionation. Consistent with their endogenous distribution, input *myc*-hPer2 was found in both cytosolic and nuclear fractions (Supplemental Figure S1C, lanes 2 and 3; Gotoh *et al.*, 2014), and FLAG-Mdm2 preferably distributed in the nuclear fraction (Supplemental Figure S1C, lane 2), although some signal was detected in the cytosol, most likely as a result of MG132 addition and inhibition of self-ubiquitination (Supplemental Figure S1C, lane 5). Consequently, endogenous hp53 levels were also increased in MG132-treated samples (Supplemental Figure S1C, lanes 2 and 3 vs. lanes 5 and 6).

Analysis of α-FLAG–immunoprecipitated samples shows that FLAG-Mdm2 associated with *myc*-hPer2 and hp53 in the nuclear fraction of cells treated with MG132, whereas the trimeric complex was less conspicuous but still detectable in the absence of the proteasome inhibitor (Figure 1B, lane 3 vs. lane 6). Of interest, *myc*-hPer2 did not seem to be associated with the Mdm2/hp53 complex in the cytosolic fraction (Figure 1B, lanes 2 and 5) but likely formed a two-component complex with hp53 in the absence of ubiquitination (Figure 1A, lanes 11 and 12). Because the input levels of *myc*-hPer2 were comparatively similar in –MG132 and +MG132 samples (Supplemental Figure S1C, top), one might speculate that the trace levels of hPer2 associated with the FLAG-Mdm2/hp53 complex within the nuclear fraction in MG132-untreated cells (Figure 1B, lane 3) were the result of either hPer2 being a substrate of Mdm2-mediated ubiquitination once the complex was in place or the action of an additional nuclear E3-ligase for hPer2 (i.e., β-TRCP; Ohsaki *et al.*, 2008). Further experiments need to be done to test both possibilities. As expected, FLAG-Mdm2 was detected in association with hp53 in the cytosolic compartment, in agreement with previous findings (Freedman and Levine, 1998), and relative amounts of FLAG-Mdm2/hp53 complex increased in MG132-treated samples (Figure 1B, lane 2 vs. lane 5). In summary, our data establish that hPer2/hp53/Mdm2 exists only in the nucleus and that the hPer2/hp53 and hp53/Mdm2 complexes can be readily detected in both nuclear and cytosolic fractions.

Functional insights into the hPer2/hp53 complex

We previously identified the hp53/hPer2 complex within the nuclear compartment (Figure 1). Thus we next asked whether hp53 transcriptional activity was compromised when bound to hPer2. To answer this question, we first needed to generate a form of the hp53/hPer2 complex that would be constitutively bound and not dissociate once formed in cells. For this task, we generated a chimera set in which either hPer2 full-length or glutathione *S*-transferase was cloned downstream of hp53 and immediately after a flexible linker (called hp53(ch)hPer2 and hp53(ch)GST hereafter, respectively; Figure 2A). The rationale behind this design is that hPer2 would interact with hp53 by flipping over and forming a stable, covalently bound complex through their domain interactions, which would be nondissociable as seen using biofluorescence complementation assays (unpublished data). As a result, we expect to find the ubiquitination of hp53 compromised without altering its compartmentalization. Therefore hp53(ch)hPer2 would be an adequate tool to evaluate the effect of a nondissociable hp53/hPer2 complex in hp53 downstream gene activation.

To further functionally validate the hp53(ch)hPer2 chimera, we evaluated the ubiquitination status of hp53 in the complex (Figure 2B). In vitro ubiquitination assays were performed using recombinantly expressed proteins (FLAG-hp53, FLAG-hp53(ch)GST, FLAG-hp53(ch)hPer2(356-574/683-872), and FLAG-hp53(ch)hPer2) preincubated, or not (–), with *myc*-hPer2, followed by *myc*-Mdm2 addition. Once the ubiquitination reaction took place, hp53 and its chimera proteins were immunoprecipitated and analyzed for ubiquitin incorporation by immunoblotting (Figure 2B and Supplemental Figure S2). Results show that FLAG-hp53 and FLAG-hp53(ch)GST behave similarly with respect to overall ubiquitination status when prebound to hPer2 and compared with their controls in the absence of hPer2 addition (Figure 2B, bottom, lane 7 vs. lane 8 and lane 2 vs. lane 3). Consistent with its role as a stable complex, ubiquitination of FLAG-hp53(ch)hPer2(356-574/683-872) and FLAG-hp53(ch)hPer2 closely resembled the basal signal obtained with just hp53 (or hp53(ch)GST) when preincubated with hPer2 (Figure 2B, bottom, lane 5 vs. lanes 3 and 8; Supplemental Figure S2, lane 3 vs. lane 5), further validating the chimera as an nondissociable hp53/hPer2 complex mimetic. In all cases, binding components were confirmed by immunoblotting and are shown in Figure 2B (top and middle).

Next we compared the localization of hp53(ch)hPer2 with that of *myc*-tagged hp53 and its chimera form (hp53(ch)GST) in human non–small cell lung carcinoma-1299 (H1299) cells (p53-null). Accordingly, we transfected H1299 cells with the various constructs and monitored their subcellular localization by fluorescence microscopy. Representative pictures are shown in Figure 3 and Supplemental Figure S3. In most normal cells, p53 is cytoplasmic; however, it is primarily located in the nucleus in rapidly growing normal cells, transformed cells, and various tumor cells, including those from breast and colon (Liang and Clarke, 2001). In agreement, *myc*-hp53 and *myc*-hp53(ch)GST were largely detected in the nuclear compartment (Figure 3 and Supplemental Figure S3, i and ii). The hp53(ch)hPer2 chimera was detected in both cytosolic and nuclear compartments (Figure 3 and Supplemental Figure S3, vi), in agreement with hPer2/hp53 distribution as in Figure 1A. Moreover, hp53(ch)hPer2 was recognized by α-p53 and α-Per2 antibodies targeting conformational native epitopes in both proteins, suggesting that the integrity of the folding in the complex was not compromised. Comparable results were also obtained with tagged forms of the chimera complex

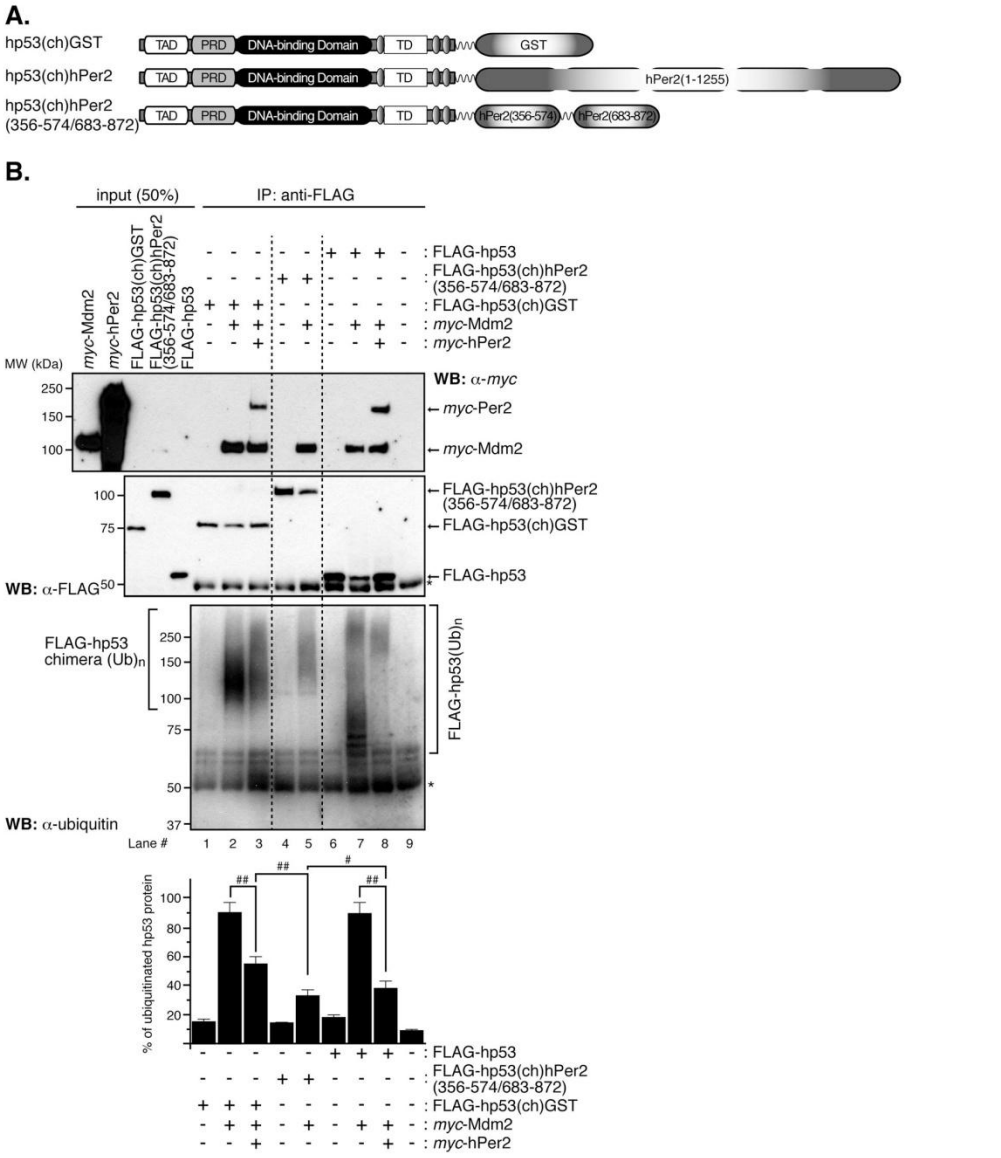

FIGURE 2: In vitro ubiquitination of hp53 is compromised when stably bound to hPer2. (A) Schematic representation of all chimeras designed for this study. Constructs were 5′ FLAG-tagged, *myc*-tagged, or untagged upstream of hp53, followed by downstream cloning of GST, hPer2, or hPer2(356-574/683-872) open reading frames. A linker encoding for six Gly was inserted between both the hp53 and hPer2 genes and the two hPer2-coding fragments. (B) In vitro transcribed and translated FLAG-hp53, FLAG-hp53(ch)hPer2(356-574/683-872), FLAG-hp53(ch)GST, *myc*-Mdm2, and *myc*-hPer2 proteins were used for ubiquitination experiments. When indicated, *myc*-hPer2 and either FLAG-hp53 or FLAG-hp53(ch)GST were preincubated; thus the complex was formed before adding *myc*-Mdm2. For the FLAG-hp53(ch)hPer2(356-574/683-872) chimera, the translated protein and *myc*-Mdm2 were incubated together before the ubiquitination reaction took place. Ubiquitination was carried out as described in *Materials and Methods*. FLAG-tagged proteins were immunoprecipitated with α-FLAG/protein A beads and blotted using α-ubiquitin antibody. Membranes were then stripped and reprobed with α-FLAG and -*myc* antibodies to detect complex bound proteins. Asterisk indicates IgG heavy chain. Immunoblot data from a single experiment repeated three times with similar results. Quantification of the sample's ubiquitinated signal was performed using ImageJ, version 1.45 (bar graph). Statistical comparisons were evaluated by *t* test. $^{\#}p \leq 0.05$; $^{\#\#}p < 0.005$.

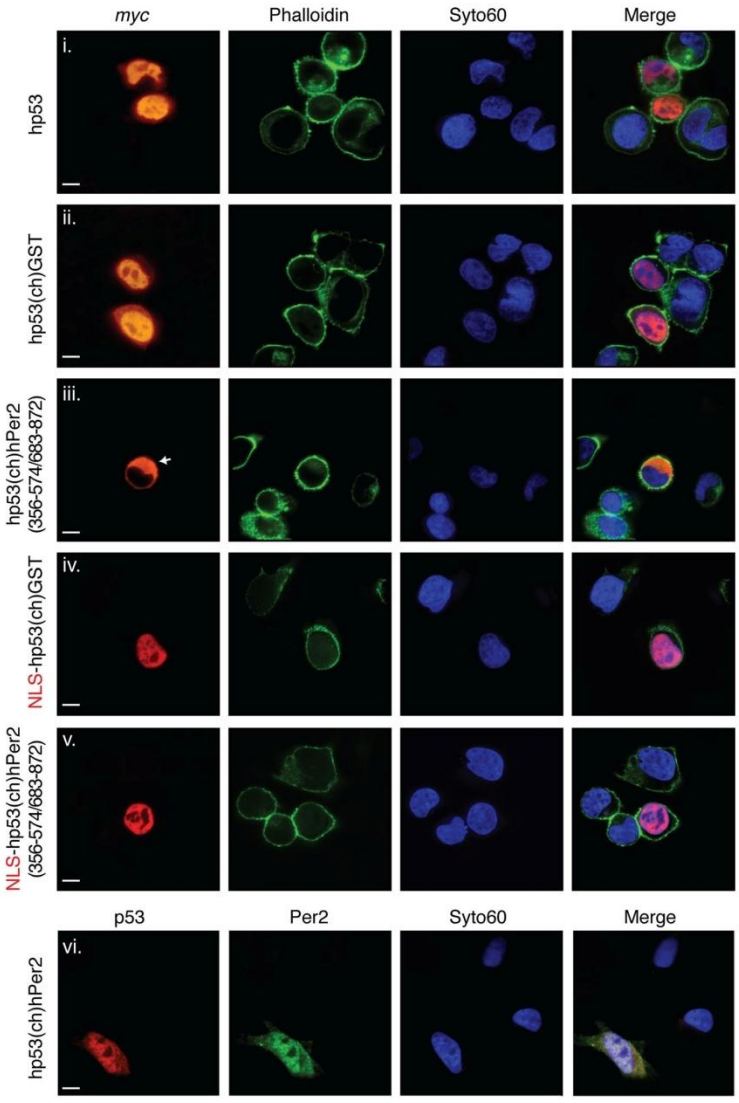

FIGURE 3: Relevance of hPer2-interacting domains for hp53 localization. H1299 cells were transfected with *myc*-tagged forms of hp53, hp53(ch)GST, hp53(ch)hPer2(356-574/683-872), NLS-hp53(ch)GST, and NLS-hp53(ch)hPer2(356-574/683-872) (i–v) or the untagged form of hp53(ch)hPer2 (vi). Proteins were visualized by confocal microscopy using α-*myc*-Cy3–conjugated primary antibody (i–v) or α-p53 and -Per2 primary antibodies and α-mouse Cy3– and α-rabbit Alexa Fluor 488 (Life Technologies)–conjugated secondary antibodies, respectively (vi). Actin fibers and DNA were stained with phalloidin Alexa Fluor 488 and Syto60 (Life Technologies), respectively. Merge images (right) were from protein staining, phalloidin, and DNA (i–v) and protein and DNA (vi). A Nikon ECLIPSE TE2000-E microscope and NIS-Elements AR 3.0 software were used to record images. Scale bars, 10 μm.

(unpublished data). Profile plotting of signal intensity along cross sections of cells transfected with the various constructs unambiguously determined their distribution and levels of expression (Supplemental Figure S3).

Localization of p53 in the nucleus is the result of the presence of three monopartite nuclear localization signals (NLSs) located within the C-terminus of p53, with NLS1 (^{316}PQPKKKP^{322}) being the most active (Shaulsky *et al.*, 1990). Remarkably, it is the C-terminus of hp53 that interacts with hPer2, and, thus, it seems reasonable that hp53 NLSs would be occluded at the interface of the two interacting molecules. Moreover, the strongest NLS described in hPer2 so far is a bipartite sequence located between residues 778 and 794 (Yagita *et al.*, 2002) that in hPer2 directly interacts with hp53 and most likely would not be exposed. Therefore we ask what element(s) actually drive the hp53(ch)hPer2 complex to the nucleus. To answer this question, we generated additional chimeras of hp53 in which the hPer2-interacting fragments 356–574 and 683–872 (which contain the hPer2 NLS) were cloned downstream of hp53 (contains all NLSs) and were separated by flexible linkers (called hp53(ch)hPer2(356-574/683-872) hereafter; Figure 2A). As shown in Figure 3 and Supplemental Figure S3iii, hp53(ch)hPer2(356-574/683-872) failed to localize in the nucleus of H1299 cells and readily accumulated in the cytoplasmic compartment, suggesting that neither NLS was functional and that hp53(ch)hPer2 translocation had most likely been driven by a yet-to-be identified NLS in hPer2 or that there is an additional cargo protein associated with the complex involved in translocation. To evaluate this possibility, we engineered an NLS sequence, in this case from SV40 (Kalderon *et al.*, 1984), inserted it upstream of hp53(ch)hPer2(356-574/683-872), and monitored its localization in H1299 cells. Of interest, the sole addition of this NLS resulted in hp53(ch)hPer2(356-574/683-872) shuttling to the nucleus, supporting the existence of a yet-to-be identified component related to hPer2 that provides a signal for transportation (Figure 3 and Supplemental Figure S3, iii vs. v). Finally, we showed that hCry1 was able to bind hPer2/hp53 when tested in vitro, a result that points to the existence of multiple regulators of diverse biochemical nature. Binding of hCry1 could be explained as the result of its interaction with the C-terminus of hPer2 (Yagita *et al.*, 2002), a region that does not overlap with the binding site mapped for hp53 (Supplemental Figure S4A; Gotoh *et al.*, 2014). Despite this result, this last finding needs to be taken with caution, as we failed to find compelling evidence to prove the existence of an endogenous hPer2/hCry1/hp53 complex in cells, a result that might reflect its transient nature or simply expose the low efficiency of the immunoprecipitating antibodies that were used.

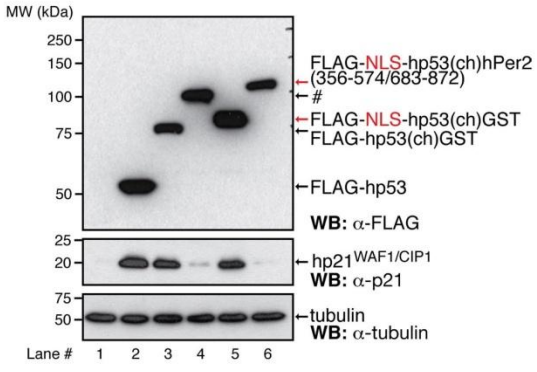

FIGURE 4: Binding of hPer2 to hp53 prevents hp21 from being expressed. H1299 cells were transfected with pCS2+FLAG-hp53, -hp53(ch)GST, -NLS-hp53(ch)GST, -hp53(ch)hPer2(356-574/683-872) (labeled #), or -NLS-hp53(ch)hPer2(356-574/683-872) and harvested 24 h later. Cell lysates (~40 μg) were resolved by SDS–PAGE and recombinant (top left and right) and endogenous proteins (middle and bottom left and right) detected by immunoblotting using α-p21, -FLAG, and -tubulin antibodies.

hp53 transcriptional activity is compromised when bound to hPer2

First, we investigated whether shuttling of the hPer2/hp53 complex from the cytosol to the nucleus was sufficient to trigger hp53-mediated downstream signaling (Figure 4 and Supplemental Figure S4B). Accordingly, we transfected H1299 cells (p53-null) with various chimera constructs, as well as with wild-type hp53, and monitored the expression of the cyclin-dependent inhibitor human $p21^{WAF1/CIP1}$ ($hp21^{WAF1/CIP1}$), a transcriptional target of p53, by immunoblotting. Transfection of cells with hp53, FLAG-hp53(ch)GST, and FLAG-NLS-hp53(ch)GST resulted in localization of all three proteins in the nucleus (Figure 3, i, ii, and iv) and $hp21^{WAF1/CIP1}$ expression (Figure 4, lanes 2, 3, and 5, and Supplemental Figure S4B, lanes 3 and 4). As expected, transfection of H1299 with FLAG-hp53(ch)hPer2(356-574/683-872) did not lead to $hp21^{WAF1/CIP1}$ expression, as the complex remained sequestered in the cytosol (Figures 3iii and 4, lane 4). Of interest, and despite the addition of an NLS to favor shuttling, transfection of cells with either FLAG-NLS-hp53(ch)hPer2(356-574/683-872) (Figure 4, lane 6) or FLAG-hp53(ch)hPer2 (Supplemental Figure S4B, lane 6) did not result in $hp21^{WAF1/CIP1}$ expression. These findings show that other events besides translocation are involved in triggering hPer2-mediated hp53 downstream signaling.

To further investigate the contribution of hPer2 in p53-mediated signaling, we tested the ability of hPer2 to modulate the reporter activity of a p53-responsive promoter *CDKN1a* (called $hp21^{WAF1/CIP1}$-luc hereafter) in the context of H1299 cells cotransfected with various hp53 and hPer2 chimeras when exposed, or not, to genotoxic stimuli (Figure 5, A and B). Chimeric transfections did not alter cell viability (Supplemental Figure S5). Unlike cells transfected with FLAG-hp53(ch)hPer2, H1299 cells show a roughly fourfold increase in $hp21^{WAF1/CIP1}$-luc activity compared with empty vector–transfected cells when expressing comparative levels of either FLAG-hp53 or hp53(ch)GST in the absence of radiation (–γ-IR; Figure 5B and Supplemental Figure S6A). As expected, H1299 cells transfected with either FLAG-hp53 or hp53(ch)GST and exposed to genotoxic stress (+γ-IR) showed a greater enhancement of $hp21^{WAF1/CIP1}$ activity (~50% more than similar untreated cells) that is down-regulated to basal levels when cells were transfected with FLAG-hp53(ch)hPer2 instead (Figure 5B and Supplemental Figure S6A). Moreover, this result seems to be independent of the radiation dose, as shown in Supplemental Figure S7. In accordance, $hp21^{WAF1/CIP1}$ activity remained low in FLAG-hp53(ch)hPer2(356-574/683-872)–transfected cells despite overexpression of the recombinant proteins and relocalization of the FLAG-NLS-hp53(ch)hPer2(356-574/683-872) chimera to the nucleus (Figure 3 and Supplemental Figures S4B, S6B, and S8E). Collectively these results suggest that when bound to hPer2, hp53 is unable to perform its transcriptional function despite the chimera being localized in the same cellular compartment (Figures 3 and 5B).

We then expanded our studies to examine the transcriptional effect of hp53(ch)hPer2 chimera on other hp53 target genes (i.e., *SFN* [encodes 14-3-3σ], *BAX*, *MYC*, *CDKN1a*, *GADD45α* [encodes growth arrest and DNA damage–inducible protein 45α, Gadd45α]) by measuring mRNA levels using quantitative reverse-transcription PCR (qRT-PCR). The rationale behind this experiment is that hp53(ch)hPer2 would counteract the effect of hp53 (or hp53(ch)GST) in gene expression due to its incapability of dissociating hPer2 from hp53, thus acting as a dominant-negative complex. Moreover, we expect that, whereas genotoxic stress (+γ-IR) would exacerbate specific p53-mediated gene expression, hp53(ch)hPer2 would continue to maintain a negative effect despite the stimuli.

As shown in Figure 5C, untreated H1299 cells (–γ-IR) transfected with hp53(ch)hPer2 showed down-regulation of both *SFN* and *CDKN1a* expression relative to the values obtained for hp53 transfection. Conversely, *MYC* exhibited positive regulation, whereas *BAX* and *GADD45α* remained largely unchanged. These results are in agreement with the positive role of hp53 in transcription of *SFN* and *CDKN1a* and its repressor role toward *MYC*. Three independent controls were simultaneously tested for all analyzed genes and incorporated as supplementary material (Supplemental Figure S8, A–C). There were no significant differences in gene expression when 1) empty vector (EV)–transfected cells were exposed, or not, to γ-IR, ruling out off-target effects (Supplemental Figure S8A), 2) cells transfected with either FLAG-hp53(ch)GST or FLAG-hp53 showed comparative levels of expression for all transcripts in the absence of radiation (Supplemental Figure S8B), and 3) under genotoxic stress (Supplemental Figure S8C). In all cases, gene expression levels were relative to those obtained by transfecting FLAG-hp53.

Next H1299 cells were exposed to genotoxic stress (+γ-IR) and transcripts amplified and compared relative to that of FLAG-hp53 (–γ-IR) (Figure 5C). As expected, both *SFN* and *CDKN1a* transcripts increased in response to radiation, confirming activation of the hp53 pathway (Figure 5C, white vs. black bars). The relevance of hPer2 dissociation for hp53 activity was evident when similar transcript levels were measured in extracts from hp53(ch)hPer2-transfected cells and were found significantly down-regulated (Figure 5C, black vs. black dashed bars). In other cases, neither hp53 nor hp53(ch)hPer2 transfections affected the expression of hp53 target genes (i.e., *GADD45α* and *BAX*) independently of whether cells were exposed or not and collected shortly after genotoxic stress (–/+ γ-IR). Finally, *MYC* expression was upregulated, approximately threefold, in hp53(ch)hPer2-transfected H1299 cells relative to FLAG-hp53, opposing its repressor role on *MYC* expression. Similar experiments were performed using FLAG-hp53(ch)hPer2(356-574/683-872), a chimera construct that effectively blocks hp53 ubiquitination (Supplemental Figure S8D) but remains secluded in the cytosolic compartment unless an NLS is added (Figure 3). As expected, transcript analyses of FLAG-hp53(ch)hPer2(356-574/683-872)–H1299 transfected cells showed a pattern

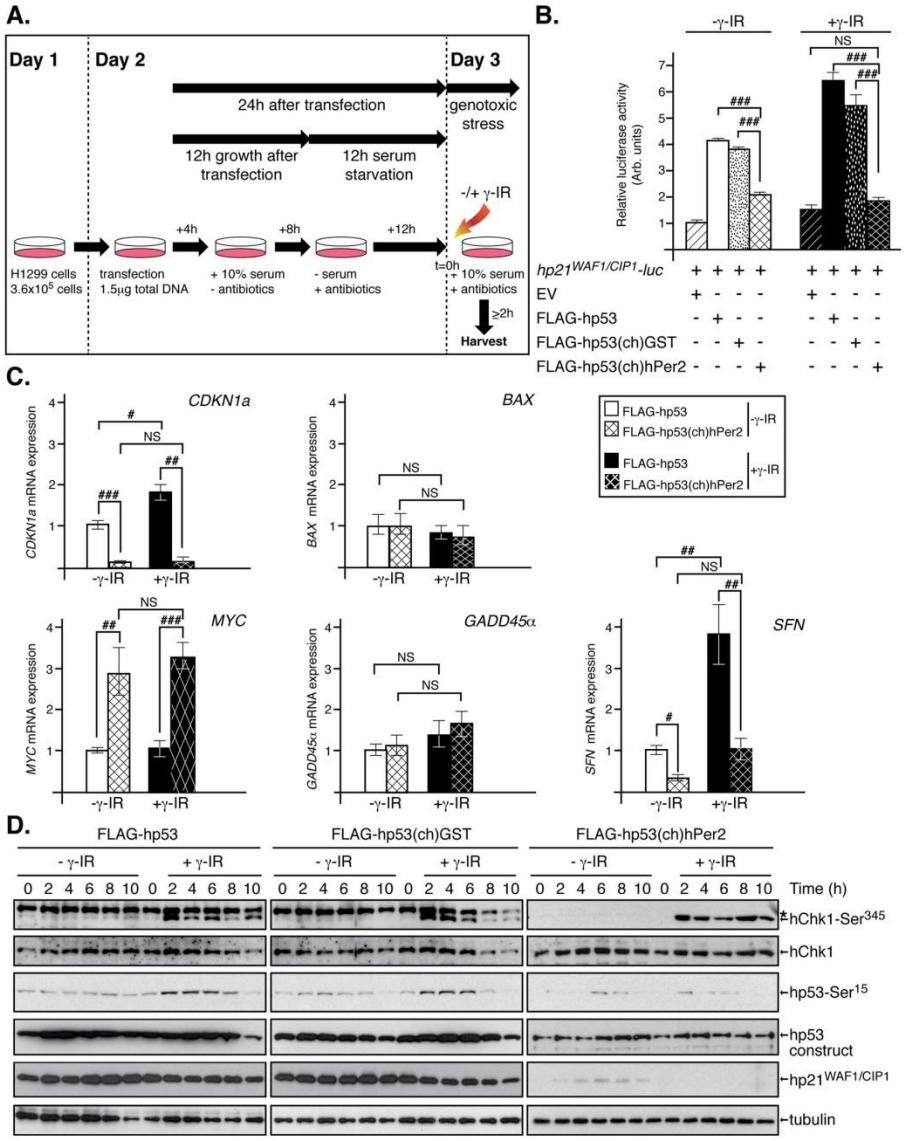

FIGURE 5: The hPer2 protein maintains hp53 transcriptionally inactive when complexed. (A) Schematic representation of the approach followed. In all cases, H1299 cells were harvested after transfection and before irradiation (γ-IR, 5 Gy; $t = 0$). (B, C) Cells harvested 2 h after irradiation. (D) Time points taken at 2-h intervals after irradiation. (B) H1299 cells were cotransfected with the reporter *hp21*$^{WAF1/CIP1}$-luc construct, pCS2+FLAG-hp53, pCS2+FLAG-hp53(ch)GST, pCS2+FLAG-hp53(ch)hPer2, or EV, with pCMV-β-gal as internal control. Extracts from cells treated (+γ-IR) or not (–γ-IR) with radiation were assayed for luciferase and β-galactosidase activities. The experiment was replicated thrice; error bars indicate SEM, and data were evaluated by ANOVA using Bonferroni posthoc test (SPSS). $^{###}p \leq 0.001$. (C) H1299 cells were transfected with either pCS2+FLAG-hp53 or pCS2+FLAG-hp53(ch)hPer2 and treated (+γ-IR) or not (–γ-IR) with radiation. The qRT-PCR data were normalized to the levels of expression in untreated FLAG-hp53–transfected cells (–γ-IR). Data are presented as the mean ± SEM from three independent experiments performed in triplicate. Statistical comparisons were evaluated by ANOVA using Bonferroni or Games-Howell posthoc analyses when needed (SPSS). NS, not significant; $^{#}p \leq 0.05$; $^{##}p \leq 0.01$; $^{###}p \leq 0.001$. (D) H1299 cells were transfected with pCS2+FLAG-hp53, pCS2+FLAG-hp53(ch)GST, or pCS2+FLAG-hp53(ch)hPer2 and treated (+γ-IR) or not (–γ-IR) with radiation as indicated in A and *Materials and Methods*. Aliquots of lysates taken at different times (20 μg) were blotted using specific antibodies

of expression that resembles the one observed when cells were transfected with hp53(ch)hPer2 and opposite to that resulting from hp53 transfection (Supplemental Figure S8D). Taken together, our data support a model in which hp53 binding to hPer2 is required for maintaining basal levels of hp53 in the nucleus in an inactive transcriptional state by forming a stable complex. Moreover, our findings imply that unbound hp53 from hPer2/hp53 is an absolute requirement to signaling downstream in response to DNA damage.

The hPer2 protein directly influences checkpoint signaling

In an attempt to gain better understanding of the role of hPer2 in hp53-mediated checkpoint signaling, we investigated the integrity of the checkpoint pathway upstream of hp53 and for hp21$^{WAF1/CIP1}$ expression in various transfected scenarios in irradiated H1299 cells (Figure 5D and Supplemental Figure S8F). Phosphorylation of downstream ATM/ATR kinase (i.e., Ser^{345} in Chk1) precedes p53 stabilization and is a marker of checkpoint activation (for review, see Meek, 2009). Therefore H1299 cells were transfected with EV, FLAG-hp53, FLAG-hp53(ch)GST, FLAG-hp53(ch)hPer2, or FLAG-hp53(ch) hPer2(356-574/683-872) and exposed, or not, to genotoxic stress. Extracts were analyzed for endogenous active forms of hChk1 and hp53 and levels of hp21$^{WAF/CIP1}$ (Figure 5D and Supplemental Figure S8F). First, we monitored hChk1 protein in all samples to find steady levels of expression throughout the time course analyzed in both exposed and transfected samples (Figure 5D and Supplemental Figure S8F). In addition, activation of Chk1 by phosphorylation in Ser^{345} was detected as early as 2 h postirradiation in exposed samples from transfected cells (+γ-IR), thus confirming both checkpoint activation and the integrity of the p53 upstream signal cascade in all cases (Figure 5D and Supplemental Figure S8F). On the other hand, phosphorylation of Ser^{15} of hp53 was detected exclusively in extracts from FLAG-hp53 and FLAG-hp53(ch)GST cells and in response to radiation (Figure 5D), suggesting that, if present, hp53 would get activated. Of interest, neither FLAG-hp53(ch)hPer2 nor FLAG-hp53(ch)hPer2(356-574/683-872) was phosphorylated on Ser^{15} of the hp53 portion of the chimera, implying that this site might not be accessible when the complex with hPer2 is formed (Figure 5D and Supplemental Figure S8F). Together our present data and previous studies support a model in which binding of hPer2 to hp53 modulates its stability and compromises hp53 function (Figure 6; Gotoh *et al.*, 2014).

DISCUSSION

The connection of circadian components to various aspects of cell division promises a better understanding of how cells sense and respond to changes in environmental conditions. At the transcriptional level, the integration of clock core components to multiple signaling networks is evident from studies carried out using genome-wide RNA interference screening analysis and high-throughput microarray technologies (Duffield *et al.*, 2002; Panda *et al.*, 2002; Mullenders *et al.*, 2009; Zhang *et al.*, 2009). Indeed, these studies have thoroughly identified genes whose knockdown directly modulates the circadian clock and others whose expression is controlled by clock core components (Duffield *et al.*, 2002; Panda *et al.*, 2002; Mullenders *et al.*, 2009; Zhang *et al.*, 2009). Regardless of the analysis platform, it is clear that cell cycle and circadian components are interlocked through genetic, protein interaction, and physiological mechanisms and that perturbation of the circadian system affects cell growth and proliferation (Fu *et al.*, 2002; Matsuo *et al.*, 2003; Miller *et al.*, 2007). Accordingly, circadian-regulated cell cycle genes such as *CCND1*, *WEE1*, *MYC*, *GADD45α*, and *CDKN1a* are known to show periodic patterns of expression in a 24-h cycle, a finding further strengthened by the identification of Per2 and Bmal1 as direct modulators of *WEE1*, *MYC*, and *CDKN1a* expression (Grundschober *et al.*, 2001; Fu *et al.*, 2002; Matsuo *et al.*, 2003; Grechez-Cassiau *et al.*, 2008). Further theoretical analyses of protein interaction networks helped place gene products that are directly or indirectly associated to known clock components, including various cell cycle modulators, in a global interactome map, which has provided clues about the many aspects of cell physiology directly regulated by the clock (for review, see Zhang and Kay, 2010).

An initial question relates to the subcellular localization of hp53, hPer2, and Mdm2 and their respective complexes. Our studies establish the presence of the hp53/hPer2 complex in both cytosolic and nuclear compartments, whereas the presence of the trimeric complex with Mdm2 seems to be restricted to the nucleus (Figure 1 and Supplemental Figure S1). Our chimera experiments provide evidence of distinct roles of hPer2 in both subcellular compartments. We believe that, when in the cytosol, hPer2 provides the signal needed for the hp53/hPer2 complex to translocate to the nucleus, whereas in the nucleus, hPer2 helps to maintain hp53 in a stable, inactive form until a stimulus (either external or internal) is applied to the biological system (Figure 6). This model is largely supported by our previous work (Gotoh *et al.*, 2014) and experiments showing that 1) blockage of the hp53 C-terminus NLSs by binding to hPer2 domains (hp53(ch)hPer2(356-574/683-872)), but not full-length hPer2 (hp53(ch)hPer2), prevents hp53 from nuclear localization (Figure 3, iii and vi, and Supplemental Figure S3), 2) addition of NLS to the same construct relocalizes the chimera protein in the nucleus (Figure 3v and Supplemental Figure S3), 3) only a constitutive hp53/hPer2-bound chimera (hp53(ch)hPer2) localizes in both compartments (Figure 3vi and Supplemental Figure S3), suggesting a role for hPer2 in hp53 translocation, and, finally, 4) constitutive association of hPer2 to hp53 in the form of [hp53(ch)hPer2] prevents hp53 from exerting its transcriptional activity in cells even in the presence of genotoxic stress (Figure 5 and Supplemental Figures S7 and S8). At present, it cannot be formally excluded that hPer2, hCry1, and hp53 or a fraction of these molecules could, a priori, form a trimeric complex in the cell. This is largely due to our finding that in vitro–expressed proteins were able to form multiple stable complexes (Supplemental Figure S4A). In addition, rhythmic hPer2 heterodimerizes with hCry1 through feedback to the nucleus and sustains oscillations. Thus, it is plausible that two pools of hPer2 might exist—one bound to hp53 and a separate pool that associates with its circadian counterpart. Nevertheless, the two pools of hPer2 might not be exclusive and might serve to assign distinct functions to hPer2 in each of these pools.

Once the hp53/hPer2 complex is in the nucleus, Mdm2 binds to the N-terminus domain of hp53, forming a trimeric complex in which hp53 ubiquitination does not take place (Figures 1B and 6;

(α-Chk1 and α-p21 for endogenous Chk1 kinase and hp21$^{WAF1/CIP1}$, respectively; α-FLAG for FLAG-hp53, FLAG-hp53(ch) GST, and hp53(ch)hPer2; α-Chk1-Ser^{345} for phosphorylation in Ser^{345} of endogenous Chk1; and α-p53-Ser^{15} for phosphorylation in Ser^{15} in FLAG-hp53, FLAG-hp53(ch)GST, and hp53(ch)hPer2). Tubulin was used as a loading control (bottom). Asterisk indicates a nonspecific signal.

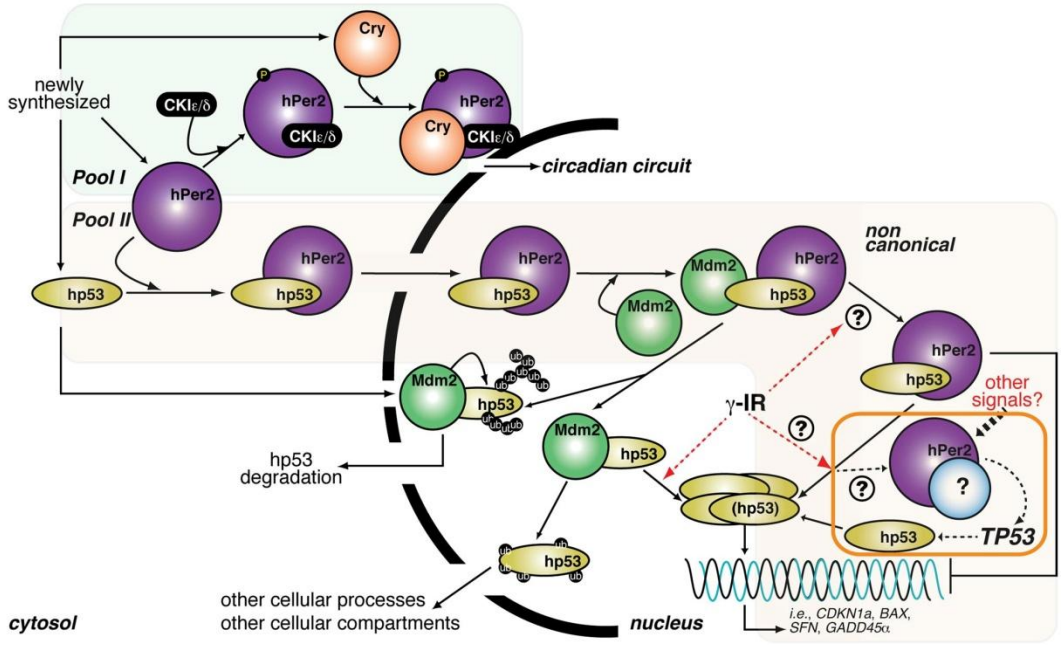

FIGURE 6: Proposed model of hPer2 and hp53 interaction and function. Newly synthesized hp53, hPer2, and Cry localize in the cytosolic compartment where the Cry/hPer2/CKIε/δ (pool I) is formed, and hPer2 is incorporated in one or more complexes that constitutes pool II. Pool I: As extensively reviewed, cytosolic hPer2 is phosphorylated by casein kinase I ε/δ (CKIε/δ) and initially degraded by the ubiquitin proteasome pathway (Ko and Takahashi, 2006). Later, Cry accumulates and associates with hPer2/CKIε/δ, and this complex translocates to the nucleus, where Cry disrupts the Clock/Bmal1-associated transcriptional complex, resulting in inhibition of *CRY*, *PER*, and *REB-ERVα* and derepression of *BMAL1* transcription and modulation of the expression of other clock-controlled genes (shown as "circadian circuit" for simplicity). Pool II: The hPer2 protein associates with cytosolic hp53, forming a stable complex (Gotoh *et al.*, 2014) that translocates to the nuclear compartment and keeps hp53 in a functionally inactive but stable state, ensuring that basal levels of hp53 exist ("priming state"). This heterodimer eventually incorporates Mdm2, forming a trimeric and stable Mdm2/hp53/hPer2 complex. In response to, for example, a genotoxic stress (labeled as γ-IR in the cartoon), the trimeric complex disassembles by a yet-unknown mechanism, which leads to release of hp53 and downstream activation of genes involved in cell cycle arrest and DNA repair. An amplification loop exists in which hPer2, alone or in association with an unidentified partner, transcriptionally activates *TP53*, further sustaining the hp53-mediated response (boxed in orange). Alternatively, cytosolic hp53 enters the nucleus, where it is targeted by Mdm2 and either polyubiquitinylated and degraded back into the cytosol or monoubiquitinated and translocated to a different compartment, as has been described (for review, see Kruse and Gu, 2009).

Gotoh *et al.*, 2014). This is in addition to the already established canonical p53 pathway, in which nuclear trafficking of hp53 is followed by Mdm2 binding and either monoubiquitination and nuclear export or p53 polyubiquitination and proteasomal degradation (incorporated in Figure 6; Honda *et al.*, 1997; Li *et al.*, 2003). We speculate that, under physiological conditions, hp53 remains an inactive component of the hp53/hPer2/Mdm2 and hp53/hPer2 complexes and is therefore unable to modulate the expression of downstream target genes (Figures 5 and 6 and Supplemental Figure S4).

Regulation of stress-mediated p53 activation has largely relied on a well-established model in which p53 stabilization precedes activation. Stabilization is primarily accomplished via the release of p53 from its interaction with Mdm2 by a mechanism that involves checkpoint activation, p53 phosphorylation, and inhibition of p53's interaction with Mdm2 (for review, see Meek, 2009), thus preventing p53 ubiquitination and proteasomal degradation (for review, see Kruse and Gu, 2009). Once stabilized, p53 is further posttranslationally modified, and its tetrameric form binds to DNA at specific high- and low-affinity p53 response elements, which regulates the expression of target genes via the recruitment of coactivators and corepressors. Despite being capable of providing an explanation for the many modes by which p53 controls gene expression, the canonical model is not sufficient to explain more recent genetic studies. Therefore further refinement has been introduced. As a result, the most recently updated model takes into consideration the many stress types that converge in p53, the various posttranslational modifications to which p53 is subjected (i.e., acetylation, sumoylation), and the tissue-specific function of p53. The end result is a model in which regulatory redundancy among posttranslational modifications is a common theme and serves to permit p53 to sense different signals and intensities, which allows for a signaling response that is properly modulated and tissue specific (for review, see Vousden, 2009). As expected, there is also a myriad of p53 binding partners, whose interactions exert selective influences on p53 target genes,

ranging from Mdm2 and MdmX negative regulators to orphan receptors, and for which a wealth of studies already exists (for review, see Vousden, 2009). Thus some common steps exist in the regulation of p53 activity (stabilization, modification, protein interaction, and promoter-specific activation), but many players differentially intervene in each step to influence the outcome of the response.

Questions arise about how free hp53 accumulates in response to radiation and what the role of hPer2 is in this event. Although we cannot provide a definitive mechanism for how the transition from hPer2 bound to hPer2 free leads to hp53 accumulation and transcriptional response (Figure 6, dashed arrow), it does not seem to be globally associated with hPer2 dissociation and shuttling, as is the case for HCT116 cells (Supplemental Figure S10A), but, more likely, to be specific for certain cell types, as is for HEK293 cells (Supplemental Figure S10B). In addition, it also seems linked to posttranslational events, as we found that hPer2 is associated with checkpoint kinases in response to radiation (unpublished data). Finally, we cannot rule out the existence of additional players in this response, including other circadian factors that may act by sequestering hPer2 away from (or "pulling hPer2 out of") the complex with hp53 when cells are exposed to a genotoxic stimulus. As a result, our model stresses the need for the existence of an hp53 tetramer that is free of hPer2 in order for its transcriptional activity to take place (Figures 5 and 6 and Supplemental Figure S4); nonetheless, more in-depth studies need to be performed to uncover the exact mechanism.

An additional component in the model refers to the regulation of *TP53* (encodes p53) transcription by hPer2, a process we propose that acts as a form of amplification loop that helps sustain the initial hPer2/hp53-mediated response (Supplemental Figure S9; Gotoh *et al.*, 2014). The relevance of hPer2-mediated *TP53* transcription is exposed when the expression of hp53 downstream target genes in the context of hPer2 overexpression is analyzed (Supplemental Figure S9A; Gotoh *et al.*, 2014). Based on our proposed model, overexpression of hPer2 should lead to stabilization of hp53 and inactivation of its transcriptional activity as a result of hPer2/hp53 complex formation. However, Gotoh *et al.* (2014) reported that this is not the case and that whereas hp53 is stabilized by hPer2 overexpression, transcription of the hp53 downstream target genes remains largely unaltered. A way to reconcile these data is to monitor *TP53* transcription in the context of hPer2 overexpression (Supplemental Figure S9, A and B; Gotoh *et al.*, 2014). Accordingly, our data show that whereas cells expressing hPer2 (HCT116 cell, $p53^{+/+}$) up-regulate *TP53* (Supplemental Figure S9A), the pool of hp53 complexed to hPer2 is only a fraction of the total level of hp53 in the cell, and thus "free" hp53 still exists and is able to transcriptionally activate downstream target genes (Supplemental Figure S9, A and B). This concept is further validated in H1299 cells (p53-null), in which hPer2 overexpression does not result in *CDKN1a* expression but FLAG-hp53 and -hPer2 cotransfection does when the level of hp53 is greater than that of hPer2 (Supplemental Figure S9C). Finally, an interesting aspect of our work is the level within the checkpoint hierarchy at which hPer2 intersects this pathway, the hp53 node. Because cancer development largely relies on sustained inactivation of the p53 pathway, the existence of factors that respond to environmental signals and influence hp53 stability encourages the search for unconventional drug targets and would certainly provide a new direction as to when and how to treat various cancers.

Our results, which establish a connection between the circadian regulatory system and the DNA-damage response mechanism at the level of hPer2–hp53 interaction, have important implications for our understanding of the etiology of cancer and the development of novel treatment modalities. Because cancer initiation and progression largely rely on a variety of DNA-damage repair mechanisms going awry in normal cells, thus facilitating tumor growth, the identification of hPer2 as a factor that responds to environmental signals and stabilizes hp53 provides a unique opportunity to evaluate the influence of the environment in the development of, for example, sporadic forms of cancers. Furthermore, our findings encourage a search for unconventional drug targets and treatment regimens based on the dynamics of the circadian control system.

MATERIALS AND METHODS

Plasmid constructs

The FLAG-tagged, *myc*-tagged, and untagged chimera constructs of hp53 and hPer2 were generated as follows. The hp53 cDNA clone was amplified by PCR and the stop codon removed before cloning into the LIC site of either pCS2+FLAG or *myc* tag vectors. For the GST chimera construct of hp53, the GST sequence was cloned downstream of hp53 into the *SalI*/*Xho*I sites in either vector. A glycine linker of six residues was introduced between hp53 and GST to favor flexibility. These chimera constructs are called FLAG-hp53(ch)GST and *myc*-hp53(ch)GST throughout the text. For the hPer2 chimera of hp53, the two hPer2-interacting fragments (residues 356–574 and 683–872) were subcloned downstream of hp53 following essentially the approach described except that hPer2(356-574) and hPer2(683-872) fragments were sequentially cloned into the *SalI*/*Xho*I and *SalI*/*SalI* sites, respectively. As was the case with the GST chimera construct, six glycine residues were added between hp53 and hPer2(356-574) and between the hPer2 fragments. These chimera constructs are referred to as FLAG-hp53(ch)hPer2(356-574/683-872) and *myc*-hp53(ch)hPer2(356-574/683-872). Chimeras containing an NLS were generated by cloning the NLS sequence encoding the TPPKKKRKVEDP residues from SV40 (Rexach and Blobel, 1995) upstream of hp53 using the appropriate pCS2+ as the template. The constructs are called FLAG-NLS-hp53(ch)GST, *myc*-NLS-hp53(ch)GST, FLAG-NLS-hp53(ch)hPer2(356-574/683-872), and *myc*-NLS-hp53(ch)hPer2(356-574/683-872). Full-length Per2-containing chimeras were generated as follows. The hPer2 cDNA was cloned downstream of hp53 into the *SalI*/*Xba*I sites. A six-glycine linker was genetically engineered between hp53 and hPer2 sequences to allow for flexible rotations. The full-length chimeras are referred to as FLAG-hp53(ch)hPer2, *myc*-hp53(ch)hPer2, and hp53(ch)hPer2. The $hp21^{WAF1/CIP1}$-Luc reporter plasmid was a kind gift from Daiqing Liao (University of Florida, Gainesville, FL) and is described in Zhao *et al.* (2003).

Cell culture and transfections

The HCT116 and H1299 cell lines were purchased from the American Type Culture Collection and maintained according to the manufacturer's recommendations. For transfection experiments, cells were seeded in six- or 12-well plates until they reached 50–80% confluence. Transfections were optimized using Lipofectamine LTX (Life Technologies, Grand Island, NY) for HCT116 and H1299 following the manufacturer's instructions. Otherwise, transfections in all cell lines were in HyClone HyQ-RS reduced serum medium (Thermo Scientific, Waltham, MA) for 4 h for H1299 and HCT116. Proteins were then allowed to express at 37°C/5% CO_2 in the appropriate medium containing 10% fetal bovine serum without antibiotics, after which they were either collected or further synchronized. Extracts for protein analysis were prepared in NP-40 lysis buffer containing 10 mM Tris-HCl (pH 7.5), 137 mM NaCl, 1 mM EDTA, 10% glycerol,

0.5% NP-40, 80 mM β-glycerophosphate, 1 mM Na_3VO_4, 10 mM NaF, and protease inhibitors (10 μM leupeptin, 1 μM aprotinin A, and 0.4 μM pepstatin).

In vitro binding assays

In vitro transcription and translation of pCS2+*myc*-hPer2, *myc*-Mdm2, *myc*-hCry1, FLAG-hPer2, and FLAG-hp53 were carried out using the SP6 high-yield TNT system (Promega, Madison, WI) following the manufacturer's instructions, although, unlike the standard procedure, the reaction was cold. Aliquots (1–4 μl) of indicated recombinant proteins were preincubated for 20 min at room temperature to allow the complex to form before adding NP40 lysis buffer. Immunoprecipitation of the various complexes was carried out essentially as described.

Immunoprecipitation and immunoblot assays

For (co)immunoprecipitation experiments, transfected cells were harvested in lysis buffer, and extracts (~100 μg) were incubated with either α-FLAG M2 agarose beads (Sigma-Aldrich, St. Louis, MO) or α-*myc* (9E10) beads (Santa Cruz Biotechnology, Dallas, TX) for either 2 h or overnight at 4°C with rotation before washing. Where indicated, immunoprecipitations were carried out in a two-step procedure, with extracts being incubated with the antibody (α-*myc*, α-FLAG, or α-p53) overnight at 4°C before the addition of protein A beads (50% slurry; Sigma-Aldrich). Sample beads were then washed with lysis buffer, resolved by SDS–PAGE, and analyzed by immunoblotting using specific primary antibodies (α-FLAG [Sigma-Aldrich], α-*myc* [Santa Cruz Biotechnology], α-Per2 [Sigma-Aldrich]), α-p53 [Santa Cruz Biotechnology], and α-ubiquitin [Enzo Biomol, Farmingdale, NY]). When indicated, the purity of the various cellular fractions was monitored by immunoblotting using α-tubulin (Sigma-Aldrich) and α-lamin A/C (Santa Cruz Biotechnology) antibodies for the cytosolic and nuclear fractions, respectively. In all cases, horseradish peroxidase–conjugated α-rabbit or α-mouse immunoglobulin G (IgG) secondary antibodies (GE Healthcare Life Sciences, Buckinghamshire, UK; Cell Signaling, Danvers, MA) were used for immunoblotting following standard procedures. Chemiluminescence reactions were performed using the SuperSignal West Pico substrate (Pierce, Rockford, IL).

In other experiments, aliquots of total cell extracts were analyzed for expression of endogenous proteins. Circadian-synchronized HCT116 cells were collected at different times after synchronization and extracts (20–100 μg) analyzed for endogenous expression of hPer2, hp53, Mdm2, hCry1, and tubulin using specific antibodies. In addition, H1299 cells transfected with FLAG-hp53, FLAG-hp53(ch)GST, FLAG-hp53(ch)hPer2(356-574/683-872), FLAG-hp53(ch)hPer2, or EV were treated or not (control; –γ-IR) with ionizing radiation (5 Gy; +γ-IR; Di Leonardo *et al.*, 1994) and collected at different times after irradiation. Extracts (20 μg) were analyzed for expression of endogenous and recombinant proteins as well as posttranslational modifications by immunoblotting using α-FLAG, -Chk1 (Santa Cruz Biotechnology), -Chk1-Ser^{345} (Cell Signaling), -p53-Ser^{15} (Cell Signaling), -p21 (Cell Signaling), and -tubulin (Sigma-Aldrich) antibodies.

Finally, endogenous hp21 expression was monitored in extracts (30–40 μg) from H1299 cells transfected with FLAG-hp53, FLAG-hp53(ch)GST, FLAG-NLS-hp53(ch)GST, FLAG-hp53(ch)hPer2(356-574/683-872), NLS-FLAG-hp53(ch)hPer2(356-574/683-872), FLAG-hp53(ch)hPer2, FLAG-hp53(ch)hPer2, or EV using an α-p21 antibody (Cell Signaling). Fusion proteins were detected using α-FLAG antibody as described. In all cases, tubulin levels were monitored by immunoblotting and used as a loading control.

RNA extraction and qRT-PCR

Cell samples were obtained from cultures and treated or not (control; –γ-IR) with ionizing radiation (5 Gy; +γ-IR) 2 h before collection. In other experiments, cells were transfected and/or circadian synchronized before radiation treatment. Total RNA was extracted from cell pellets using the Trizol Reagent (Life Technologies) following the manufacturer's instructions. RNA was quantified by spectrophotometric reading at 260 nm and analyzed for quality assurance using an Agilent 2100 Bioanalyzer (Agilent Technologies, Santa Clara, CA) at the Virginia Bioinformatics Institute Proteomics Core Facility (Blacksburg, VA). qRT-PCR was conducted essentially as previously described (Yang *et al.*, 2008). Briefly, total RNA was pretreated with DNaseI (Promega) at 37°C for 30 min, and a 1-μg sample was used as a template for first-strand cDNA synthesis using the iScript cDNA Synthesis system (Bio-Rad, Hercules, CA). qRT-PCR assay was performed using IQ SYBR Green Supermix (Bio-Rad) as follows: 10 ng of cDNA (50 ng for the 14-3-3σ gene) was added to a 20-μl reaction volume containing the indicated primers for amplification (see Supplemental Methods and Supplemental Table S1). Real-time assays were performed in triplicate on a MyIQ single-color Real-Time PCR Detection instrument (Bio-Rad). Data were collected and analyzed with Optical System Software, version 1.0. The glyceraldehyde-3-phosphate dehydrogenase and β-actin genes were used as internal controls to compute the relative expression level (ΔC_T) for each sample. The fold change of gene expression in each sample was calculated as $2^{-\Delta\Delta Ct}$.

Immunofluorescence microscopy

H1299 cells were cultured on coverslips for 24 h and then transfected with pCS2+*myc*-hp53, -hp53(ch)GST, -hp53(ch)hPer2(356-574/683-872), -NLS-hp53(ch)GST, or -NLS-hp53(ch)hPer2(356-574/683-872) or untagged hp53(ch)hPer2 using Lipofectamine LTX (Life Technologies). After transfection, cells were fixed (3.7% formaldehyde/phosphate-buffered saline [PBS]/0.5% Triton X-100), washed with PBS/0.5% Triton X-100 and then 0.1% Triton X-100, and blocked with goat serum at room temperature for 30 min. Subcellular localization of *myc* fusion proteins was detected using an anti-*myc*-Cy-3–conjugated antibody (Sigma–Aldrich). Localization of untagged chimera recombinant protein (hp53(ch)hPer2) was visualized using α-p53 (Sigma-Aldrich) and -Per2 antibodies (Santa Cruz Biotechnology). Actin and nuclei were visualized by incubating fixed cells with phalloidin-Alexa 488 (Life Technologies) and SYTO 60 (Life Technologies). Fluorescence was visualized using a Nikon Eclipse TE2000-E microscope equipped with a Cascade II E2V CCD97 camera (Photometrics, Tucson, AZ) at 488, 568, and 647 nm. Images were processed using the NIS-Elements AR 3.0 Nikon software.

Gene reporter activity

H1299 cells were seeded onto 12-well plates and cotransfected with ~200 ng of *hp21*$^{WAF1/CIP1}$-luciferase (Luc) and pCS2+FLAG-hp53, -hp53(ch)GST, -hp53(ch)hPer2, or -hp53(ch)hPer2(356-574/683-872) or empty vector (pCS2+FLAG) each. The pCMV-β-gal (~200 ng) plasmid was included as an internal control. Cells were treated or not (controls; –γ-IR) with ionizing radiation (5 Gy; +γ-IR) and harvested 2 h later. Reporter activity was measured using the Bright-Glo Luciferase Assay System (Promega) according to the manufacturer's instructions. Readings were recorded from a Glomax Luminometer, and results were normalized for expression of β-gal, which was determined separately using the Galacto-Light Plus System (Bio-Rad). Experiments were done in triplicate and repeated at least twice.

Statistical analyses

Data were processed using either a two-tailed unpaired Student's *t* test or an analysis of variance (ANOVA) followed by either Bonferroni or, when necessary, Games-Howell post hoc test (SPSS; IBM, Armonk, NY). Levene's test was used to determine homogeneity of variances, whereas data normality was examined using Shapiro–Wilk *W* test and Box–Cox *Y* transformation (JMP 9; SAS) and applied when necessary. Values of $p \leq 0.05$ were considered statistically significant.

ACKNOWLEDGMENTS

We thank John Tyson, Jill Sible, Daniel Capelluto, and James Maller for critical reading of the manuscript and all members of the Finkielstein laboratory for help and discussions. We also thank J. Webster for comments and editing of the manuscript. We are grateful to Steven L. McKnight (University of Texas Southwestern Medical Center, Dallas, TX) and Daiqing Liao for providing us with the hPer2 cDNA and pWAF1-Luc constructs, respectively. We also acknowledge C. Santos and J. Yang for generating reagents used throughout this research. This work was supported by a National Science Foundation CAREER Award (MCB-0844491), the Avon Foundation (02-2009-033), the Fralin Life Science Institute (F441598), and the Susan G. Komen Foundation (BCTR0706931) to C.V.F.

REFERENCES

Albrecht U, Bordon A, Schmutz I, Ripperger J (2007). The multiple facets of Per2. Cold Spring Harb Symp Quant Biol 72, 95–104.

Bae K, Jin X, Maywood ES, Hastings MH, Reppert SM, Weaver DR (2001). Differential functions of mPer1, mPer2, and mPer3 in the SCN circadian clock. Neuron 30, 525–536.

Bunger MK, Wilsbacher LD, Moran SM, Clendenin C, Radcliffe LA, Hogenesch JB, Simon MC, Takahashi JS, Bradfield CA (2000). Mop3 is an essential component of the master circadian pacemaker in mammals. Cell 103, 1009–1017.

Cermakian N, Monaco L, Pando MP, Dierich A, Sassone-Corsi P (2001). Altered behavioral rhythms and clock gene expression in mice with a targeted mutation in the Period1 gene. EMBO J 20, 3967–3974.

Di Leonardo A, Linke SP, Clarkin K, Wahl GM (1994). DNA damage triggers a prolonged p53-dependent G1 arrest and long-term induction of Cip1 in normal human fibroblasts. Genes Dev 8, 2540–2551.

Duffield GE, Best JD, Meurers BH, Bittner A, Loros JJ, Dunlap JC (2002). Circadian programs of transcriptional activation, signaling, and protein turnover revealed by microarray analysis of mammalian cells. Curr Biol 12, 551–557.

Freedman DA, Levine AJ (1998). Nuclear export is required for degradation of endogenous p53 by MDM2 and human papillomavirus E6. Mol Cell Biol 18, 7288–7293.

Fu L, Pelicano H, Liu J, Huang P, Lee C (2002). The circadian gene Period2 plays an important role in tumor suppression and DNA damage response in vivo. Cell 111, 41–50.

Gery S, Koeffler HP (2009). Per2 is a C/EBP target gene implicated in myeloid leukemia. Integr Cancer Ther 8, 317–320.

Gery S, Komatsu N, Baldjyan L, Yu A, Koo D, Koeffler HP (2006). The circadian gene per1 plays an important role in cell growth and DNA damage control in human cancer cells. Mol Cell 22, 375–382.

Gorbacheva VY, Kondratov RV, Zhang R, Cherukuri S, Gudkov AV, Takahashi JS, Antoch MP (2005). Circadian sensitivity to the chemotherapeutic agent cyclophosphamide depends on the functional status of the CLOCK/BMAL1 transactivation complex. Proc Natl Acad Sci USA 102, 3407–3412.

Gotoh T, Vila-Caballer M, Santos CS, Liu J, Yang J, Finkielstein CV (2014). The circadian factor Period 2 modulates p53 stability and transcriptional activity in unstressed cells. Mol Biol Cell 25, 3081–3093 .

Gotter AL, Manganaro T, Weaver DR, Kolakowski LF Jr, Possidente B, Sriram S, MacLaughlin DT, Reppert SM (2000). A time-less function for mouse timeless. Nat Neurosci 3, 755–756.

Grechez-Cassiau A, Rayet B, Guillaumond F, Teboul M, Delaunay F (2008). The circadian clock component BMAL1 is a critical regulator of p21WAF1/CIP1 expression and hepatocyte proliferation. J Biol Chem 283, 4535–4542.

Grundschober C, Delaunay F, Puhlhofer A, Triqueneaux G, Laudet V, Bartfai T, Nef P (2001). Circadian regulation of diverse gene products revealed by mRNA expression profiling of synchronized fibroblasts. J Biol Chem 276, 46751–46758.

Gu X, Xing L, Shi G, Liu Z, Wang X, Qu Z, Wu X, Dong Z, Gao X, Liu G, *et al*. (2012). The circadian mutation PER2(S662G) is linked to cell cycle progression and tumorigenesis. Cell Death Differ 19, 397–405.

Honda R, Tanaka H, Yasuda H (1997). Oncoprotein MDM2 is a ubiquitin ligase E3 for tumor suppressor p53. FEBS Lett 420, 25–27.

Hua H, Wang Y, Wan C, Liu Y, Zhu B, Yang C, Wang X, Wang Z, Cornelissen-Guillaume G, Halberg F (2006). Circadian gene mPer2 overexpression induces cancer cell apoptosis. Cancer Sci 97, 589–596.

Kalderon D, Richardson WD, Markham AF, Smith AE (1984). Sequence requirements for nuclear location of simian virus 40 large-T antigen. Nature 311, 33–38.

Ko CH, Takahashi JS (2006). Molecular components of the mammalian circadian clock. Hum Mol Genet 15(Spec No 2), R271–R277.

Kondratov RV, Kondratova AA, Gorbacheva VY, Vykhovanets OV, Antoch MP (2006). Early aging and age-related pathologies in mice deficient in BMAL1, the core component of the circadian clock. Genes Dev 20, 1868–1873.

Kruse JP, Gu W (2009). Modes of p53 regulation. Cell 137, 609–622.

Laposky A, Easton A, Dugovic C, Walisser J, Bradfield C, Turek F (2005). Deletion of the mammalian circadian clock gene BMAL1/Mop3 alters baseline sleep architecture and the response to sleep deprivation. Sleep 28, 395–409.

Li M, Brooks CL, Wu-Baer F, Chen D, Baer R, Gu W (2003). Mono- versus polyubiquitination: differential control of p53 fate by Mdm2. Science 302, 1972–1975.

Liang SH, Clarke MF (2001). Regulation of p53 localization. Eur J Biochem 268, 2779–2783.

Lucas RJ, Stirland JA, Mohammad YN, Loudon AS (2000). Postnatal growth rate and gonadal development in circadian tau mutant hamsters reared in constant dim red light. J Reprod Fertil 118, 327–330.

Matsuo T, Yamaguchi S, Mitsui S, Emi A, Shimoda F, Okamura H (2003). Control mechanism of the circadian clock for timing of cell division in vivo. Science 302, 255–259.

Meek DW (2009). Tumour suppression by p53: a role for the DNA damage response? Nat Rev Cancer 9, 714–723.

Miller BH, McDearmon EL, Panda S, Hayes KR, Zhang J, Andrews JL, Antoch MP, Walker JR, Esser KA, Hogenesch JB, Takahashi JS (2007). Circadian and CLOCK-controlled regulation of the mouse transcriptome and cell proliferation. Proc Natl Acad Sci USA 104, 3342–3347.

Mullenders J, Fabius AW, Madiredjo M, Bernards R, Beijersbergen RL (2009). A large scale shRNA barcode screen identifies the circadian clock component ARNTL as putative regulator of the p53 tumor suppressor pathway. PLoS One 4, e4798.

Naylor E, Bergmann BM, Krauski K, Zee PC, Takahashi JS, Vitaterna MH, Turek FW (2000). The circadian clock mutation alters sleep homeostasis in the mouse. J Neurosci 20, 8138–8143.

Ohsaki K, Oishi K, Kozono Y, Nakayama K, Nakayama KI, Ishida N (2008). The role of {beta}-TrCP1 and {beta}-TrCP2 in circadian rhythm generation by mediating degradation of clock protein PER2. J Biochem 144, 609–618.

Oklejewicz M, Hut RA, Daan S, Loudon AS, Stirland AJ (1997). Metabolic rate changes proportionally to circadian frequency in tau mutant Syrian hamsters. J Biol Rhythms 12, 413–422.

Panda S, Antoch MP, Miller BH, Su AI, Schook AB, Straume M, Schultz PG, Kay SA, Takahashi JS, Hogenesch JB (2002). Coordinated transcription of key pathways in the mouse by the circadian clock. Cell 109, 307–320.

Pregueiro AM, Liu Q, Baker CL, Dunlap JC, Loros JJ (2006). The Neurospora checkpoint kinase 2: a regulatory link between the circadian and cell cycles. Science 313, 644–649.

Rexach M, Blobel G (1995). Protein import into nuclei: association and dissociation reactions involving transport substrate, transport factors, and nucleoporins. Cell 83, 683–692.

Rudic RD, McNamara P, Curtis AM, Boston RC, Panda S, Hogenesch JB, Fitzgerald GA (2004). BMAL1 and CLOCK, two essential components of the circadian clock, are involved in glucose homeostasis. PLoS Biol 2, e377.

Schneider CA, Rasband WS, Eliceiri KW (2012). NIH Image to ImageJ: 25 years of image analysis. Nat Methods 9, 671–675.

Shaulsky G, Goldfinger N, Ben-Ze'ev A, Rotter V (1990). Nuclear accumulation of p53 protein is mediated by several nuclear localization signals and plays a role in tumorigenesis. Mol Cell Biol 10, 6565–6577.

Shearman LP, Jin X, Lee C, Reppert SM, Weaver DR (2000). Targeted disruption of the mPer3 gene: subtle effects on circadian clock function. Mol Cell Biol 20, 6269–6275.

Shimba S, Ishii N, Ohta Y, Ohno T, Watabe Y, Hayashi M, Wada T, Aoyagi T, Tezuka M (2005). Brain and muscle Arnt-like protein-1 (BMAL1), a component of the molecular clock, regulates adipogenesis. Proc Natl Acad Sci USA 102, 12071–12076.

Sun CM, Huang SF, Zeng JM, Liu DB, Xiao Q, Tian WJ, Zhu XD, Huang ZG, Feng WL (2010). Per2 inhibits k562 leukemia cell growth in vitro and in vivo through cell cycle arrest and apoptosis induction. Pathol Oncol Res 16, 403–411.

Takahashi JS, Hong HK, Ko CH, McDearmon EL (2008). The genetics of mammalian circadian order and disorder: implications for physiology and disease. Nat Rev Genet 9, 764–775.

Turek FW, Joshu C, Kohsaka A, Lin E, Ivanova G, McDearmon E, Laposky A, Losee-Olson S, Easton A, Jensen DR, *et al.* (2005). Obesity and metabolic syndrome in circadian clock mutant mice. Science 308, 1043–1045.

Unsal-Kacmaz K, Mullen TE, Kaufmann WK, Sancar A (2005). Coupling of human circadian and cell cycles by the timeless protein. Mol Cell Biol 25, 3109–3116.

Vousden KH, Prives C (2009). Blinded by the light: the growing complexity of p53. Cell 137, 413–431.

Xu Y, Padiath QS, Shapiro RE, Jones CR, Wu SC, Saigoh N, Saigoh K, Ptacek LJ, Fu YH (2005). Functional consequences of a CKIdelta mutation causing familial advanced sleep phase syndrome. Nature 434, 640–644.

Yagita K, Tamanini F, Yasuda M, Hoeijmakers JH, van der Horst GT, Okamura H (2002). Nucleocytoplasmic shuttling and mCRY-dependent inhibition of ubiquitylation of the mPER2 clock protein. EMBO J 21, 1301–1314.

Yang J, Kim KD, Lucas A, Drahos KE, Santos CS, Mury SP, Capelluto DG, Finkielstein CV (2008). A novel heme-regulatory motif mediates heme-dependent degradation of the circadian factor period 2. Mol Cell Biol 28, 4697–4711.

Zhang EE, Kay SA (2010). Clocks not winding down: unravelling circadian networks. Nat Rev Mol Cell Biol 11, 764–776.

Zhang EE, Liu AC, Hirota T, Miraglia LJ, Welch G, Pongsawakul PY, Liu X, Atwood A, Huss JW3rd, Janes J, *et al.* (2009). A genome-wide RNAi screen for modifiers of the circadian clock in human cells. Cell 139, 199–210.

Zhao LY, Liu Y, Bertos NR, Yang XJ, Liao D (2003). PCAF is a coactivator for p73-mediated transactivation. Oncogene 22, 8316–8329.

Zheng B, Albrecht U, Kaasik K, Sage M, Lu W, Vaishnav S, Li Q, Sun ZS, Eichele G, Bradley A, Lee CC (2001). Nonredundant roles of the mPer1 and mPer2 genes in the mammalian circadian clock. Cell 105, 683–694.

Zheng B, Larkin DW, Albrecht U, Sun ZS, Sage M, Eichele G, Lee CC, Bradley A (1999). The mPer2 gene encodes a functional component of the mammalian circadian clock. Nature 400, 169–173.

Appendix B:

Drugs (2016) 76:1507–1521
DOI 10.1007/s40265-016-0646-4

CURRENT OPINION

Chronotherapy: Intuitive, Sound, Founded…But Not Broadly Applied

Julia M. Selfridge[1,2] · Tetsuya Gotoh[2] · Samuel Schiffhauer[2] · JingJing Liu[2] · Philip E. Stauffer[2] · Andrew Li[1,2] · Daniel G. S. Capelluto[3,4] · Carla V. Finkielstein[1,2]

Published online: 3 October 2016

Abstract Circadian rhythms are a collection of endogenously driven biochemical, physiological, and behavioral processes that oscillate in a 24-h cycle and can be entrained by external cues. Circadian clock molecules are responsible for the expression of regulatory components that modulate, among others, the cell's metabolism and energy consumption. In clinical practice, the regulation of clock mechanisms is relevant to biotransformation of therapeutics. Accordingly, xenobiotic metabolism and detoxification, the two processes that directly influence drug effectiveness and toxicity, are direct manifestations of the daily oscillations of the cellular and biochemical processes taking place within the gastrointestinal, hepatic/biliary, and renal/urologic systems. Consequently, the impact of circadian timing should be factored in when developing therapeutic regimens aimed at achieving maximum efficacy, minimum toxicity, and decreased adverse effects in a patient. However, and despite a strong mechanistic foundation, only 0.16 % of ongoing clinical trials worldwide exploit the concept of 'time-of-day' administration to develop safer and more effective therapies. In this article, we (1) emphasize points of control at which circadian biology intersects critical processes governing treatment interventions; (2) explore the extent to which chronotherapeutics are incorporated into clinical trials; (3) recognize roadblocks; and (4) recommend approaches to precipitate the integration of chronobiological concepts into clinical practice.

Key Points

Circadian factors influence rhythmic oscillations in biochemical activity that modulate the body's daily changes in physiology and behavior.

Circadian timing is relevant to mechanisms involved in biotransformation of therapeutics influencing drug effectiveness and toxicity; however, its clinical application is poorly exploited.

In this article, emphasis is placed on the current state of knowledge about the use of chronobiological concepts in clinical practice, including strategic approaches to facilitate their integration.

1 Introduction

Circadian rhythms are daily cycles of physiological and behavioral processes endogenously generated by an organism that can be externally modulated by cues such as light, temperature, and food intake (for review see Dibner et al. [1]). Their relevance to human diseases has become evident as perturbation of circadian rhythms is associated with altered insomnia and sleep syndromes, jet-lag,

✉ Carla V. Finkielstein
finkielc@vt.edu

[1] Virginia Tech Carilion School of Medicine and Research Institute, 2 Riverside Circle, Roanoke, VA 24016, USA

[2] Integrated Cellular Responses Laboratory, Department of Biological Sciences, Biocomplexity Institute, 1015 Life Science Circle, Virginia Tech, Blacksburg, VA 24061, USA

[3] Protein Signaling Domains Laboratory, Department of Biological Sciences, Biocomplexity Institute, 1015 Life Science Circle, Virginia Tech, Blacksburg, VA 24061, USA

[4] Center for Soft Matter and Biological Physics, Virginia Tech, Blacksburg, VA 24061, USA

allergies and asthma, cardiovascular diseases, stroke, hypertension, metabolic diseases, neurological and psychiatric disorders, and hormone-dependent cancers (see previous publications [2–9] and references within). As a result, there has been increased interest in deciphering the molecular regulatory systems to which all circadian components connect and, more importantly, in understanding how circadian-triggered output signals maintain the body's physiology in harmony with its evolving environment. These findings have yielded far-reaching advances in many areas of science, health, and medicine, including a much-needed molecular foundation to the ancient field of chronotherapy, in which treatments for diseases are administered at times of the day most likely to yield the greatest efficacy.

2 Clock Core Regulation of Output Signals

Core circadian clock genes are defined as genes whose protein products are necessary components for the generation and regulation of circadian rhythms. As such, clock proteins are interlocked through transcriptional/translational feedback loops that control circadian timing (for review, see Lowrey and Takahashi [10]). The chief mediator of the mammalian circadian clock is the heterodimer complex formed by the *b*rain-*m*uscle-*a*ryl hydrocarbon receptor nuclear translocator-*l*ike protein *1* (BMAL1) and the *c*ircadian *l*ocomotor *o*utput *c*ycles *k*aput protein (CLOCK; or its paralog *n*euronal *PAS* domain protein *2* [NPAS2]) (Fig. 1). Briefly, the positive arm of the feedback loop involves binding of CLOCK/BMAL1 to E-box response elements located in the regulatory region of target genes, of which *PERIOD* (*PER1*, *PER2*, and *PER3*) and *CRYPTOCHROME* (*CRY1* and *CRY2*) genes are essential components [11–13]. The PER and CRY proteins accumulate in the cytosol, heterodimerize (PER/CRY), and translocate to the nucleus where they auto-repress their transcription by binding to and inhibiting CLOCK/BMAL1 [14]. Later, the PER/CRY repressor complex is degraded and CLOCK/BMAL1 is released and reassumes a new transcriptional cycle that generates the 24-h timekeeping system. Additionally, a mechanism that constitutes the negative feedback loop provides robustness to the cycle by controlling *BMAL1* and, to a much lesser degree, *CLOCK* transcription [15]. In this scenario, CLOCK/BMAL1 transcriptionally activates the *r*etinoic acid receptor-related *o*rphan *r*eceptor (*RORα/β/γ*) and *REV-ERB* genes, which in turn bind to the *r*etinoic acid-related *o*rphan *r*eceptor *e*lements (*RORE*s) located in the promoter region of *BMAL1* and either activate or repress its expression, respectively (Fig. 1). The epigenetic regulation of circadian clock gene expression aligns well with diurnal variations in histone modifications, including phosphorylation, acetylation, and methylation, which are usually coupled to changes in cellular metabolism, as these modifications use varying metabolites and are influenced by environmental cues [16]. Selective chromatin remodeling of *clock-controlled genes* (*ccgs*) is maintained by balancing the intrinsic histone acetyltransferace (HAT) activity of CLOCK and the histone deacetylase activity of sirtuin 1 (SIRT1), an oxidized nicotinamide adenine dinucleotide (NAD^+)-dependent enzyme whose activity exhibits robust circadian rhythmicity [17–19]. Interestingly, CLOCK, BMAL1, and SIRT1 transcriptionally regulate the expression of the rate-limiting enzyme in NAD^+ biosynthesis, the nicotinamide phosphoribosyl-transferase (NAMPT), establishing a feedback loop in which SIRT1 regulates the levels of its own co-factor (Fig. 1) [20, 21].

An additional level of regulation relates to the role of post-translational modifications in sustaining circadian periodicity by controlling protein stability. Accordingly, cytosolic phosphorylation of PERs and CRYs is mediated by *c*asein *k*inase *I* ε and δ (CKIε/δ [22–25]), an event that triggers their binding to the E3-ligases *F-b*ox/*W*D repeat-containing protein *1* (Fbw1, also named β-TrCP1) and *F-b*ox/LRR-repeat protein *3* (Fbxl3), respectively, followed by ubiquitin-mediated proteasomal degradation (Fig. 1) [26–28]. It is not surprising to find that the extent of the regulatory kinases involved in controlling the clock mechanism is growing. For example, the α and β isoforms of glycogen synthase kinase-3 (GSK3) are now known to target PER, REV-ERBα, and CRY1/2 proteins and, conversely, GSK3 activity status is itself circadian-regulated in the suprachiasmatic nuclei of the brain [29, 30].

In addition to the aforementioned events, the CLOCK/BMAL1 heterodimer is responsible for coordinating the rhythmic transcriptional expression of *ccgs* in multiple tissues [31–33]. Among rhythmic transcripts are those encoding protein products involved in maintaining tissue homeostasis, cellular metabolism, and the regulation of cell division and death processes [32, 33]. Examples of *ccgs* include (1) the proto-oncogene *c-MYC*, which has a central role in G1 cell growth control, differentiation, and apoptosis; (2) the tumor-suppressor genes *TP53* and *GADD45α*, whose protein products are responsible for most of the antiproliferative responses triggered in response to various forms of stress (endogenous and genotoxic); (3) the E3 ubiquitin–protein ligase mouse double minute 2 homolog (MDM2), a negative regulator of p53; and (4) caspases, G2/M kinases (e.g., *WEE1*), G1/S cyclins, cyclin-dependent kinase inhibitors, transcription factors, and ubiquitin-associated factors that are involved in regulating cell division and death (Fig. 1; Zhang et al. [34] and references within). An additional level of regulation results from unexpected findings that showed that clock components

directly interact with key cell cycle regulators (Hunt and Sassone-Corsi [35] and references within). Specifically, PER1 interacts with the ataxia-telangectasia mutated (ATM) and checkpoint 2 (CHK2) proteins directly involved in the cellular response to ionizing radiation and double-strand DNA breaks. Another clock component, the human timeless homolog TIM, associates with the ATM-related kinase ataxia telangiectasia and Rad3-related protein (ATR) and its substrate ATR-interacting protein (ATRIP). More recent findings show that PER2 directly binds to p53, an association that influences p53 stability in unstressed conditions and activity in response to genotoxic stress (Fig. 1) [36, 37]. Despite emerging findings, we still lack a clear understanding of how molecules from the circadian and cell cycle circuitries are interlocked and operate to make cell proliferation or death decisions.

A multi-level analysis of the whole transcriptome in various clock tissues unveiled that only a small fraction of all clock-controlled transcripts consistently oscillate in all tissues, suggesting the existence of oscillatory patterns of expression that are tissue specific [31–33]. Furthermore, genome-wide studies have shown that only a fraction of cycling messenger RNAs exhibit a robust oscillation and that, more likely, post-transcriptional modifications (i.e., circadian control of poly(A) tail length) is responsible for the rhythmic behavior of most cell messengers [38–44]. Therefore, there is a direct impact in the time-dependent expression level and stability of key regulatory molecules and, consequently, in the various biochemical pathways that maintain tissue function and body's homeostasis. Today, a comprehensive picture of the events that trigger, entrain (by means of Zeitgeber ['time giver'] signals such as light and temperature [45]), and sustain circadian rhythms has been established and is supported by strong molecular data; the challenge lies in how to incorporate and implement this newly gained knowledge into the clinic to make treatment options as effective and safe as possible.

3 Coupling Metabolic Rhythms to the Body's Daily Physiology

In-depth studies spanning decades of prolific work using experimental models, in vitro methods, and human clinical data cemented what once seemed a provocative hypothesis [46]: that the endogenous circadian and metabolic processes were intimately interconnected (for review see Bass and Takahashi [47], Asher and Schibler [48], and Sahar and Sassone-Corsi [49]). At present, examples of their crosstalk are numerous and varied and include a direct role for core clock components in the rhythmic biosynthesis of fatty acids, sterols, bile acids, gluconeogenesis, energy homeostasis, and lipid and glycogen catabolism (Fig. 1; see Bass and Takahashi [47] and references within). Accordingly, homozygous *clock* mutant mice exhibit hepatic steatosis, attenuated energy balance, hyperlipidemia, hyperleptinemia, hypertension, hyperglycemia, and insufficient compensatory insulin production; all indicators of a metabolic syndrome phenotype that, in this model, is also associated with obesity and the development of type 2 diabetes mellitus [50].

As direct molecular outputs of the clock, the rhythmic regulation of metabolic processes (e.g., gluconeogenesis, lipogenesis, oxidative metabolism, and respiration) influence, among others, daily changes in cerebral activity, vascular tone, blood pressure, heart rate, hormone levels (e.g., leptin, growth hormone, and insulin), cytokine secretion, body temperature, and renal activity (Fig. 1) [51]. Thus, not surprisingly, circadian desynchronization in humans (e.g., by shiftwork, high-fat diet intake, prolonged wakefulness) have direct implications in the temporal coordination of metabolic processes and, consequently, in health and disease [52, 53]. Epidemiological, clinical, and population-based statistics show that circadian–metabolism misalignment is emerging as the most common cause of cardiovascular disease, diabetes, inflammation, thrombosis, and even some forms of cancer in western societies [53]. The aforementioned connections stress the concept that the body is more susceptible to challenges (e.g., infections, toxins, injuries) at specific phases of the circadian cycle than at others and that circadian dysregulation is likely to favor a pathological condition. Most of all, it hints to 'times-of-day' at which a given tissue might be metabolically more sensitive to targeted treatment modalities in the clinic. Furthermore, the multiple oscillations in the expression and activity of rate-limiting regulatory enzymes in critical metabolic pathways establish times at which targeted treatments could yield the greatest results.

4 'Time-of-Day' Medicine

Personalized medicine, a milestone that was unthinkable in the pre-human genome project era, is rapidly becoming a reality. Today, this innovative approach to disease prevention arises from the possibility of more precisely predicting a person's risk of disease onset based on each person's unique genetic makeup and clinical information [54]. Adding to this is the possibility of tailoring treatments based on the patient's unique genetic background, lifestyle factors, and environmental exposure—an area of study usually referred to as personalized therapy or, more recently, precision medicine [55]. As a result, customizing an individual patient's treatment weighs the entire spectrum of healthcare and creates important changes in clinical practice.

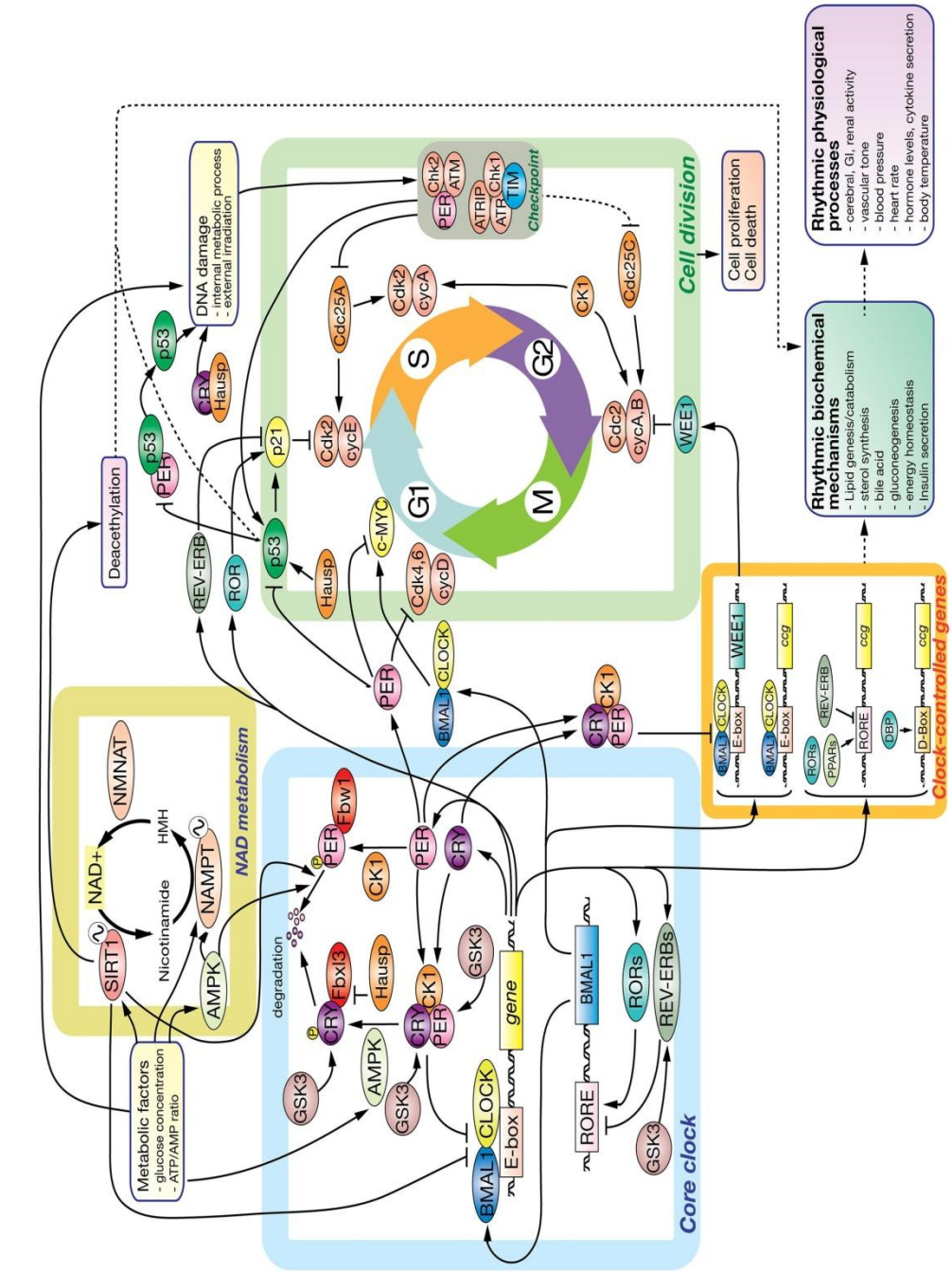
Rhythmic physiological processes
- cerebral, GI, renal activity
- vascular tone
- blood pressure
- heart rate
- hormone levels, cytokine secretion
- body temperature
Rhythmic biochemical mechanisms
- Lipid genesis/catabolism
- sterol synthesis
- bile acid
- gluconeogenesis
- energy homeostasis
- insulin secretion
Cell proliferation
Cell death
Cell division
Checkpoint
DNA damage
- internal metabolic process
- external irradiation
Deacethylation
Metabolic factors
- glucose concentration
- ATP/AMP ratio
NAD metabolism
NAD+
NMNAT
NAMPT
HMH
Nicotinamide
SIRT1
AMPK
Core clock
degradation
gene
E-box
Clock-controlled genes
D-Box
RORE
DBP
RORs
REV-ERBs
PPARs
REV-ERB
WEE1
Cdc25C
Cdc25A
Cdk2
cycA
cycE
cycA,B
cycD
Cdk4,6
c-MYC
p21
p53
Hausp
Chk2
Chk1
ATM
ATR
ATRIP
TIM
PER
CRY
CK1
GSK3
Fbw1
Fbxl3
BMAL1
CLOCK
G1
S
G2
M

◀**Fig. 1** Engaging the mammalian clock regulatory network in signal transduction. Interlocked systems are represented by *independent panels* (i.e., core clock, cell division, nicotinamide adenine dinucleotide [NAD] metabolism, clock-controlled genes, and output metabolic processes) where major players and regulatory relationships are connected by *arrows* (*dashed arrows* indicate that other intermediaries or processes might exist). As summarized in the *center-left panel*, the core components of the mammalian clock consist of casein kinase 1ε/δ (CK1); chryptochrome proteins (CRY); period proteins (PER); circadian locomotor output cycles kaput protein (CLOCK); and brain-muscle-aryl hydrocarbon receptor nuclear translocator-like 1 protein (BMAL1). Briefly, CLOCK/BMAL1 heterodimers selectively bind to E-box enhancers and drive the expression of *PER*, *CRY*, and *REV-ERBα* genes. REV-ERBα proteins then repress *BMAL1* transcription through Rev-Erbα/*r*etinoic acid-related *o*rphan *r*eceptor (ROR) *e*lements (RORE) in its promoter. Thus, *BMAL1* RNA falls while *PER* and *CRY* RNA levels peak. As the day progresses, PER proteins accumulate in the cytoplasm, become phosphorylated by CK1, ubiquitinated by E3-ligases (e.g., F-*b*ox/LRR-repeat protein *3* [Fbxl3] and *F-b*ox/*W*D repeat-containing protein *1* [Fbw1]), and targeted for degradation by the proteasome system. Later in the day, CRY accumulates, associates with PER/CK1, and the trimeric complex translocates to the nucleus where CRY disrupts the CLOCK/BMAL1-associated transcriptional complex, resulting in *CRY*, *PER*, and *REV-ERBα* transcriptional inhibition and de-repression of *BMAL1* transcription. Thus, both transcriptional feedback loops are co-regulated by CLOCK/BMAL1. In addition, core clock components modulate the expression of *clock-controlled genes* (*ccgs*) that encode for intermediaries in processes that relate to cell growth, division, death, and maintenance, cell communication and metabolite transport, redox state, detoxification and stress response, carbohydrate, nucleobase, and amino acid metabolisms, extracellular adhesion and communication, protein turnover, hormone synthesis and secretion, and lipid synthesis and accumulation, among other clock-controlled responses (*lower panels* [34]). Points of intersection between circadian components and the cell division machinery exist and are relevant to the timely progression of the cell cycle (for review see Hunt and Sassone-Corsi [35] and Antoch and Kondratov [95]). For example, PER/CRY modulates *CCND1*, *c-MYC*, and the cyclin-dependent inhibitor p21 expression, therefore influencing G1 initiation and progression. Furthermore, CK1 activity is implicated in progression through the S and G2 phases by targeting cyclin A/Cdk complexes and expression of *WEE1*, a dual-specificity kinase that phosphorylates cyclin B/Cdc2 complex for inhibition and G2 arrest. CRY (through its interaction with Hausp) and PER (by stabilizing p53) influence checkpoint activation in response to genotoxic stress [74, 75]. An additional intersecting loop worth mentioning in the context of clock functioning refers to the role of the adenosine monophosphate-activated protein kinase (AMPK) as a metabolic sensor [76]. When activated, AMPK signals back to the clock core by phosphorylating PER and CRY and promoting their degradation, creating a reciprocal loop between the clock and metabolism. *AMPK* AMP-activated protein kinase, *ATM* ataxia-telangectasia mutated, *ATR* ataxia telangiectasia and Rad3-related protein, *ATRIP* ATR interacting protein, *ccg* clock-controlled gene, *Cdc25A* cell division cycle 25A phosphatase, *Cdk2* cyclin-dependent kinase 2, *Chk1* checkpoint kinase 1, *Chk2* checkpoint kinase 2, *cycA, B* cyclins A and B, *cycD* cyclin D, *cycE* cyclin E, *DBP* D site of albumin promoter (albumin D-box) binding protein, *GI* gastrointestinal, *G2* gap 2 phase, *GSK3* glycogen synthase kinase-3, *Hausp* herpesvirus-associated ubiquitin-specific protease, *M* mitosis phase, *NMNAT* mononucleotide adenylyltransferase 1, *NAMPT* nicotinamide phosphoribosyl-transferase, *P* phosphate, *PPARs* peroxisome proliferator-activated receptors, *REV-ERB (NR1D1)* nuclear receptor subfamily 1, group D, member 1, *S* DNA synthesis phase, *SIRT1* NAD-dependent deacetylase sirtuin-1, *TIM* timeless, *WEE1* Mitosis inhibitor protein kinase

As precision medicine is formulated to achieve the goal of maximizing benefit and efficacy, lowering toxicity and side effects, and favoring the greatest possible quality of life for a patient, it is necessary to recognize that "effectiveness", as broadly considered here, depends on multi-factorial elements (genetics included) that influence the distribution, uptake/efflux, and breakdown of a given therapy, and the elimination of any byproducts. What makes these biological processes worth re-examination in the context of seeking to achieve the greatest personalized therapeutic outcome is that all of them are periodic and most rate-limiting steps are clock-controlled [56]. A clear example comes from studies carried out using human and animal subjects in which the temporal abundance and distribution of plasma proteins, especially albumin and α-1-glycoprotein, was found to be relevant to drug binding and tissue absorption (for review see Musiek and Fitzgerald [57] and references within). In fact, early work showed that peak concentrations of most plasma proteins occurs in the early afternoon, albeit some variation in time exists between young adults and elderly subjects. Furthermore, their oscillations are independent of the proportion of red blood cells in the plasma and more likely reflect the daily variation in protein synthesis that results from liver metabolism [57]. As protein carrier levels oscillate, it is imperative to factor 'time of administration' into the treatment equation to optimize precision medicine and develop safer and more effective treatments.

Chronobiology is a broadly defined field of biology that is concerned with biological phenomena that exhibit cyclical behavior. It is divided into sub-disciplines that place specific emphasis on dynamic oscillatory signatures that either remain normal (chronophysiology) or are altered (chronopathology). Accordingly, chronophysiology focuses on the timely organization of biochemical and behavioral processes that, although tissue specific, need to be globally synchronized to ensure the body's homeostasis. Conversely, chronopathology recognizes alterations in parameters over time that deviate from the mean value and, thus, serve as prognostic factors by helping to recognize a pre-pathological condition. These concepts are the foundation for a more specific field of study known as chronotherapy, in which 'time' becomes a critical variable when it comes to studying the effects of 'when' a given treatment modality needs to be administered. As chronotherapy represents the therapeutic application of chronopharmacology, it embraces several specific principles that relate to the type of disease being treated, the patient's physiology, and the efficacy and tolerability that the patient exhibits to a given formulation considering biological timing and endogenous periodicities. Accordingly, the goal of chronotherapy is to ensure that, in vivo,

the availability of a drug is timed to correspond with the rhythms of the disease and, thus, optimizing the therapeutic outcomes while minimizing adverse effects (for review see Kaur et al. [58]). As expected, many aspects of pharmacology are time-of-day-dependent, including (1) the abundance and activity of molecules involved in drug absorption and metabolism (considered under chronokinetics); (2) the physiological system targeted by the therapeutic (considered under chronodynamics); (3) the controlled-release formulations (considered under chronomodulated delivery and chronoformulation); and (4) the effectiveness of a therapeutic (considered under chronoeffectiveness) [56]. Lastly, as toxicological information is critical to the goals of chronotherapy, chronotoxicology considers the toxic responses and adverse effects of active substances and, thus, helps define optimal times at which medical regimens should be administered to enhance both effectiveness and tolerance [58].

Over the past several decades, circadian biologists have faced the challenge of identifying molecular players, uncovering elusive mechanistic details, and deciphering regulatory networks to explain how 'time' relates to processes relevant to normal physiology, disease onset and progression, and treatment outcome. Acquiring this knowledge helped expose the fundamental difference dividing the practice of clinical medicine versus the application of chronotherapy as most health professionals see the body's physiology as a relatively invariant, rather than dynamic, homeostatic unit. The principles of chronotherapy do not disregard any valid or conventionally accepted approach or method to diagnose and treat diseases, nor do they disregard any new trends in modern medicine; instead, this discipline points to optimizing each aspect of the treatment process to achieve the greatest personalized therapeutic outcome.

5 Pharmacodynamics and the Molecular 'Best Time' to Administer a Therapy

There is a need to consider the many organizational levels, from molecular and cellular to tissue and organ, at which drugs can act when assessing their biochemical and physiological effects on the body. This concept, initially embraced within the basic principles of pharmacodynamics, now considers that different cells from different organs have different periodicities in the activity of their biochemical processes—from transcription/translation to metabolism—and in the temporal organization of their signal transduction cascades. Consequently, the notion of chronopharmacodynamics seems suited to weigh in on how circadian oscillation in a physiological system influences therapeutic outcomes.

Circadian variations in parameters associated with ligand (e.g., drug, hormone, neurotransmitter)–receptor interaction and signaling were among the earliest biological processes to be pharmacodynamically characterized. Findings determined the existence of diurnal variations in potency (related to receptor occupancy), efficacy (related to intracellular signaling system and tissue response), sensitivity (related to receptor binding) [59], and the level and activity of downstream signaling components triggered by ligand–receptor binding including enzymes, metabolites, and even secondary messengers (Musiek and Fitzgerald [57] and references within). Today, knowledge of the chronopharmacodynamic action of cardiovascular drugs, chemotherapeutic agents, analgesic and non-steroidal anti-inflammatory compounds, antidepressant drugs, anxiolytics, and antipsychotic compounds has conferred numerous benefits to patients with various clinical conditions. For example, cardiovascular disorders (e.g., hypertension, arrhythmias, coronary heart disease) are treated with different chemistries (lipophilic vs. hydrophilic) of β-receptor blocking drugs (e.g., atenolol, propranolol, acebutolol) following chronopharmacodynamic and kinetic rationales. This takes into account decades of research that established the rhythm organization of the cardiovascular system and is a reflection of circadian variations in hemodynamic parameters, ventricular stroke volume, heart rate, plasma concentration of hormones (e.g., noradrenaline, renin, angiotensin, aldosterone), and cyclic adenosine monophosphate [cAMP], as well as blood-associated parameters such as viscosity, platelet aggregability, and fibrinolytic activity (for review see Paschos et al. [60] and the classic work summarized in Lemmer et al. [61] and references within). Accordingly, the onset of cardiovascular diseases and early symptomatology have strong temporal dependencies. For example, morbid and mortal events in myocardial infarction and ischemic events peak between 6 a.m. and 12 p.m.; thus, the use of β-blockers such as oral doses of propranolol is recommended early in the morning. In fact, the therapeutic value of propranolol mostly comes from its dose–response relationship, which is dependent on the circadian phase at which it is administered, and less from its chronopharmacokinetics. Thus, ingestion of oral propranolol hours before wakening blocks β-adrenoreceptors in the sympathetic tissue, altering its tone, hemodynamic conditions, and heart rate at hours of early activity in individuals [61]. Compounds such as nitroglycerin and isosorbide mononitrate/dinitrate (ISMN/ISDN) act as vasodilators and are used to treat angina pectoris symptoms to relieve chest pain. The therapeutic action of nitrate derivatives results from activation of the vascular nitric oxide (NO)/cyclic guanosine monophosphate (cGMP) pathway, which, in turn, elicits venodilation and aortic and large elastic artery

distensibility, promoting hemodynamic changes [62]. Interestingly, whereas ISDN exhibits only slight pharmacokinetic changes in relation to the time of drug administration, its therapeutic action is more pronounced when orally administered early in the morning (~2 a.m.), with most angina attacks taking place between 2 and 4 a.m. [61]. These are just a few examples in which time of administration is critical to restoring or eliciting aspects of vascular physiology that are either directly regulated by the master clock or indirectly modulated through slave oscillators. In fact, the release of glucocorticoids, angiotensin II, and catecholamines, as well as the activity of endothelial NO synthase is subject to diurnal variations, affecting vasoactive response and blood pressure. Similarly, processes such as vascular angiogenesis and thrombogenesis rely on signaling events that are clock controlled; thus, targeted therapies need to consider the time-of-day expression/activity of target molecules when developing protocols for administration. More recently, improvements in the therapeutic treatment of hypercholesterolemia with statins, a group of competitive inhibitors of hydroxymethylglutaryl (HMG)-coenzyme A reductase, have benefited from knowledge of the rhythmic activity of the enzyme. Accordingly, the optimal dose administration time for statins such as cerivastatin and simvastatin is in the evening, whereas fluvastatin benefits from a bedtime ingestion, lovastatin should be ingested after meals in the evening, and atorvastatin does not exhibit an optimal time-of-day dosing benefit [63]. As examples accumulate, and chronopharmacodynamic-based applications have been reviewed extensively elsewhere, we direct the reader to excellent disease-specific articles that summarize in great detail the current state of knowledge on time-dependent administration of therapeutics for various diseases and disorders of different type and pathogenesis [63–65].

6 Coordinating Drug Pharmacokinetics with Circadian Physiology

The rhythmic physiology of a specific group of organ systems—intestine, hepatobiliary, and renal—determines the effectiveness of drug absorption, distribution, metabolism, and excretion and, thus, its blood concentrations and bioavailability [56] (Fig. 2). Compelling molecular and biochemical data support the existence of a gut clock that modulates time-dependent gut physiology and, therefore, influences the absorption and distribution of drugs (for review see Dallmann et al. [56] and Musiek and Fitzgerald [57]). Accordingly, genetically modified mouse models carrying specific disruptions in circadian genes, for instance *clock* mutant mice [66], show a severe deregulation in the absorption of nutrients that is accompanied by disruptions in intestinal circadian activity.

Absorption of orally administered therapeutic agents in the gastrointestinal tract depends on key variables, including (1) the chemistry of the drug (i.e., hydrophobicity and degree of ionization as pH changes); (2) the rhythmic physiology of the gastrointestinal tract (i.e., circadian changes in gastric pH [67], gastrointestinal blood flow [68], gastric emptying time and motility [69, 70]); and (3) the expression of unique transporters on epithelial cells of the gut (Fig. 2) [71, 72]. Circadian patterns of absorption for lipophilic drugs and water-soluble compounds are markedly different, as documented in various animal models and human clinical studies in which a myriad of pharmacokinetic parameters were evaluated (e.g., maximum [peak] drug concentration [C_{max}], time to reach C_{max} following drug administration [t_{max}], and area under the plasma concentration–time curve [AUC]) [57, 73]. Accordingly, most lipophilic compounds exhibit more rapid absorption in the morning (active period) than in the evening hours in humans as gut perfusion, gastric pH, and intestinal blood flow are simultaneously favored, a result that translates to higher C_{max} and shorter t_{max} values during morning administration [68, 73]. In contrast, absorption of water-soluble compounds does not exhibit circadian variation and, thus, assimilation remains steady throughout the day [73, 74]. To date, drugs spanning different chemistries and uptake mechanisms have confirmed diurnal variation in absorption, which argues for consideration of this when developing oral therapeutic administration regimens [57, 64]. Studies in healthy volunteers have examined the relevance of the method for delivering lipophilic compounds (e.g., immediate vs. sustained release, intravenous) and administration time in the pharmacokinetics of absorption. As the concept of bioavailability, defined as the extent and rate at which a substance becomes available at the site of action, relates to absorption, formulations of lipophilic drugs with immediate release have shown a circadian phase dependency on their action that has not been observed when using sustained-release formulations or after intravenous inoculation. Consequently, absorption of immediate-release preparations of, for example, nifedipine [75], cyclosporine [76], and non-steroidal anti-inflammatory drugs [77] peak in the early morning (e.g., 8 a.m., 22.5 min t_{max} for nifedipine [peroral administration]; 6 a.m. for acetaminophen [peroral administration]; beginning of the active period for cyclosporine [78], for which drug bioavailability is greater than at night).

Effective drug distribution is largely dependent on its lipophilicity, affinity to, and abundance of carrier proteins in the blood flow (Fig. 2). These considerations impact a drug's efficacy and the magnitude of adverse effects as unbound drug does not distribute within the target site and

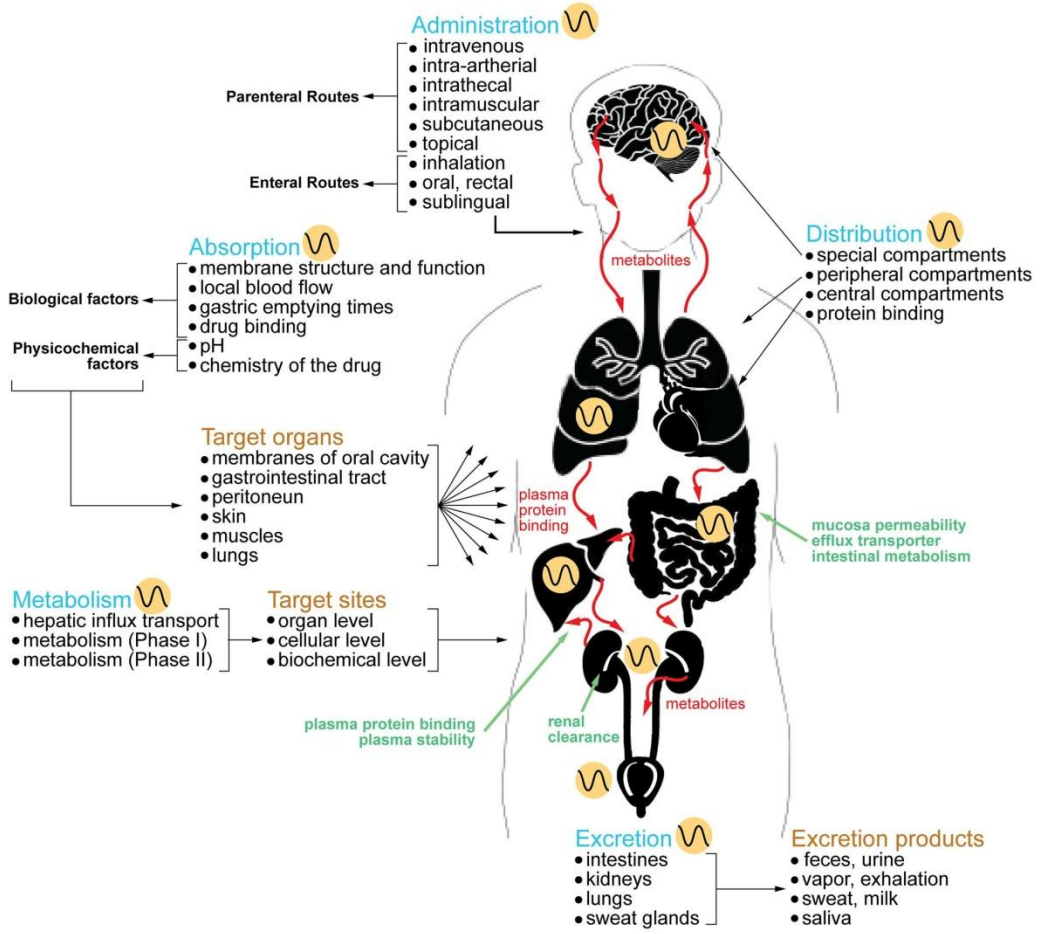

Fig. 2 Circadian timing, a new dimension in the pharmacological landscape of drug therapies: schematic representation of the disposition process of pharmaceutical therapeutics within the human body (absorption, distribution, metabolism, and excretion) and possible routes of drug administration (processes are indicated by *blue text*). Therapy administration strategies focus on attaining a therapeutic drug concentration in plasma within a window of values between the minimal effective concentration and the concentration that causes toxicity. Effective absorption results from a combination of biological and physicochemical factors, with the former being greatly influenced by circadian timing. Drug distribution is accomplished rapidly via circulation and is influenced by local changes in blood flow. Central compartments refer to major organs and tissues such as liver, lung, heart, brain, and kidney; peripheral compartments, on the other hand, refer to tissues where drugs are slowly metabolized and redistributed, such as adipose tissue and skeletal muscle. As many drugs bind to plasma proteins (e.g., albumin), 'protein binding' indicates an additional mode of distribution that also serves the purpose of facilitating elimination when the drug is secreted by renal glomerular filtration. Biotransformation takes place at various levels in the body, although the liver is the primary organ of drug metabolism and the gastrointestinal tract is the most important extrahepatic site. Other secondary organ sites, as indicated in the figure, carry out drug-metabolizing reactions. Cellular metabolism refers to the processes that occur mainly in the smooth endoplasmic reticulum of the cell and that chiefly involve oxidation reactions. The biochemical processes are divided into two phases in which drugs are chemically modified (Phase I) and conjugated (Phase II), if necessary, to facilitate their elimination. Lastly, excretion of drugs and byproducts is largely accomplished by the kidney, although compounds can also be eliminated via bile, sweat, saliva, exhaled air, or milk. The excretion process may involve renal glomerular filtration, renal tubular secretion, renal tubular reabsorption, and biliary excretion; thus, the nature of the mechanism impacts on the rate of elimination and can prolong the effect of the drug in the system. *Yellow circles* with an *inclusive wave symbol* indicate clock-controlled biochemical and physiological processes

accumulates in unwanted tissues. Daily alterations in blood flow—daytime increase and night-time decline—depends on the circadian time-dependent function of the autonomic nervous system [79]. Accordingly, blood flow contributes to the difference in drug distribution observed when dosing takes place at different times [80].

Circadian variation in the level of plasma proteins reflects the great extent of the fluctuations in metabolic activity in the liver. Examples include albumin, globulins, and α-glycoproteins, whose concentrations are elevated during the daytime, peak at noon, and fall to a minimum at night [81]. As a result, it is expected that drug–protein binding varies in a diurnal fashion depending on the concentration of the carrier molecule in the plasma (Fig. 2) [78, 82]. While this premise has been demonstrated to work in clinical settings for various antiepileptic agents, chemotherapeutics, and anti-inflammatory drugs (for review see Erkekoglu and Baydar [83]), other drugs with more specific carriers display peak binding at night (e.g., carbamazepine [peak at ~8 p.m.], as evaluated in patients with epilepsy not responding to conventional dosing schedules [84]) or early afternoon (e.g., 5-fluorouracil [optimal timing varies according to sex and genetic background], as evaluated in patients with metastatic colorectal cancer receiving standard dosage [85]). Unlike the case of hydrophobic molecules, distribution of water-soluble drugs in tissues requires the expression of transporters and channels that allow for transit to occur. In this scenario, drug distribution depends on the circadian expression of specific transporters [71, 72]. Beyond distribution, there is a point at which the dose becomes toxic to consider when the therapeutic treatment takes place at a constant rate over a 24-h period.

Xenobiotic detoxification takes place primarily in the liver, although other extrahepatic detoxification systems exist (e.g., brain, kidney), in a two-phase process in which drugs are chemically modified (Phase I) and then conjugated to facilitate their excretion into bile, feces, sweat, saliva, and urine (Phase II; Fig. 2). Remarkably, genome-wide studies of the liver transcriptome have confirmed early observations that most genes encoding members of the microsomal cytochrome P450 family of enzymes driving Phase I, as well as members of epoxide hydrolases, oxidoreductases and sulfo-, glutathione-S-, UDP-glucuronosyl-, methyl-, and acetyl-transferases relevant to Phase II, show a circadian oscillatory pattern of expression [32, 33, 86] and activity that is reflected in fluctuations in drug metabolites eliminated in urine (for review see previous publications [47, 48, 87]).

Lastly, the process of excretion of metabolized drugs via bile flow and urine depends on the functional capacity of the kidney to reabsorb or secrete drugs across the epithelium (Fig. 2). The rate of elimination and its efficiency depends on two critical renal physiological variables: (1) the volume of blood delivered to the kidney per unit of time—renal blood flow; and (2) the rate of filtered fluid through the kidney per unit of time—the glomerular filtration rate. The renal blood flow is largely responsible for the daily elimination of most ionized drugs into urine with a peak of secretion during the active phase [88]. Unlike renal blood flow, the glomerular filtration rate seems to be a steady process that persists even during the resting phase [88]. The role of clock components in regulating the rhythmic elimination of metabolites by the renal system became evident in *CRY1/CRY2* knockout animals. Accordingly, *CRY* knockout mice exhibit an abnormal renal blood flow that most likely results from a disrupted renin-angiotensin-aldosterone system and, partially, by oscillations in arterial blood pressure and cardiac output [89]. Moreover, the expression of the sodium-proton exchanger 3 system, relevant for the daily variations in urine pH (from 4.5 to 8.0), is abrogated in the proximal tubule of *CRY* knockout animals, indicating the clock's control of drug elimination via urine acidification. Not surprisingly, reabsorption/secretion of water-soluble drugs and small organic ions accompany a robust diurnal expression of membrane transporters (e.g., ABC and Slc) in the proximal tubule of the kidney [90].

In summary, it is evident that clock components act at multiple regulatory levels influencing several aspects of the body's physiology and, consequently, a drug's pharmacokinetics and therapeutic/toxicological outcomes.

7 Circadian Biology in Today's Clinical Trials

The application of circadian timing to patient treatment is an emerging practice in clinical trials that is still in its infancy and is mostly tested with regards to neurological disorders. Today, the US National Institutes of Health provides, through the ClinicalTrials.gov website (https://clinicaltrials.gov), the most compelling global registry of publicly and privately supported clinical trials involving any category of circadian intervention applicable to human subjects. As of June 2016, a total of 217,258 registered studies are ongoing in the USA and 193 countries around the world. Of these, 37 % (81,111 studies) are located only in the USA, 46 % (100,114 studies) are located in non-US countries, and 6 % (12,469 studies) are international multisite clinical trials (Fig. 3a). Registered studies are of various types, comprising interventional (~80 % of cases), observational (~19 %, including drug treatments, behavioral studies, and surgical procedures), and other US Food and Drug Administration (FDA)-regulated studies that meet the criteria of 'expanded access' (http://www.fda.gov/). Therefore, this database provides a comprehensive

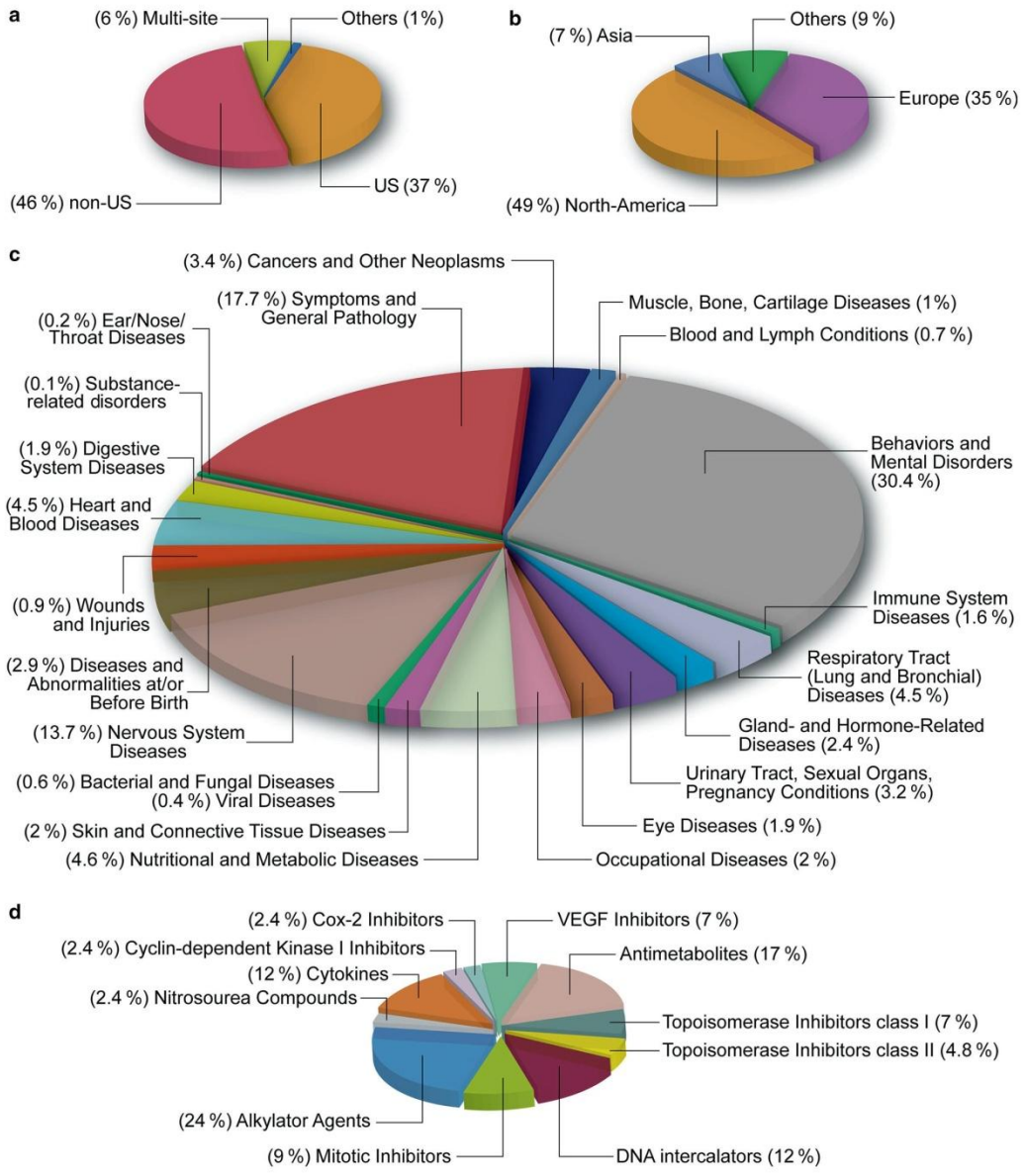

Fig. 3 The impact of chronotherapy in the clinical trial world. **a** Pie chart showing the distribution of currently listed clinical trials based on their geographic locations. **b** Pie chart illustrating clinical trials in which chronotherapy is considered part of the treatment strategy by geographic location. **c** Pie chart divided into sectors proportionate to the distribution of clinical trials involving a form of chronotherapy treatment categorized by disease condition. **d** Pie chart showing the pharmacological categories of anticancer drugs whose pharmacokinetics, pharmacodynamics, tolerability, and/or efficacy are influenced by circadian timing [55]. In all cases, categories are given as a percentage of the whole pie. *Cox-2* cyclo-oxygenase-2, *VEGF* vascular endothelial growth factor

overview of the current status of chronotherapy being considered as part of the design of clinical trials.

Presently, 348 registered clinical studies (~0.16 % of existing clinical trials) worldwide include a form of circadian intervention, of which the majority are in Europe (122 studies), North America (171 studies), and Asia (24 studies) (Fig. 3b). Of note, chronotherapy may not be a variable under consideration when it comes to medical studies in which human volunteers are administered slow and sustained-release pharmacological formulations; however, other chrono-interventions are possible either earlier, to ameliorate the symptoms of the disease, or later, as part of the recovery phase.

Of the 348 chronotherapy studies, 45 % are categorized as related to 'behavior and mental disorders' and 'diseases of the nervous system' (Fig. 3c) and span studies in which aggression, alcohol consumption and related disorders, Alzheimer's disease, anxiety, Asperger's syndrome, attention–deficit disorder with hyperactivity, attention–deficit and disruptive behavior disorders, autism spectrum disorder, various behavioral symptoms, bipolar disorder, bulimia nervosa, child development disorders, compulsive behavior, ataxia, arthralgia, aphasia, amnesia, acromegaly, acute pain, and cognition and communication disorders are among the most noticeable. The remaining ~55 % of trials are divided into various categories, with each representing a proportion from 0.2 % (viral diseases) to 4.6 % (nutritional and metabolic diseases) (Fig. 3c).

Consideration of circadian biology has been given in the treatment of diseases of the immune system, heart and blood, nutrition and metabolism, and cancer and neoplasms in clinical trials; however, the number of ongoing studies in each category is insignificant in the context of all ongoing studies in those specific areas. For example, only 3.4 % of clinical trials involving circadian interventions apply to any form of cancer study (Fig. 3c; 0.15 % when considering all existing cancer trials) despite mounting evidence of the relevance of timing in xenobiotic metabolism and detoxification of drugs and in processes that are critical for tumor initiation and progression [64, 91]. Presently, breast neoplasms of various origins, and to a lesser extent others from bone, brain, and colorectal tissues, are the largest group of proliferative diseases targeted for circadian interventions. However, the majority of those studies are of an observational type and aim to investigate, for example, whether disorders in sleep architecture (1) follow breast cancer surgery (ClinicalTrials.gov identifier NCT01171508); (2) are associated with chemotherapeutic treatment in patients with specific clock polymorphisms (e.g., NCT01887925); (3) act as a prognostic factor in the progression of metastatic breast cancer (e.g., NCT00519168); or (4) can be corrected using behavioral (e.g., NCT02002533) or bright light (e.g., NCT02658708) therapies in patients undergoing chemotherapy. In addition, a few interventional clinical trials seek to (1) determine the optimal circadian time for administering chemotherapeutic combinations in women with metastatic breast cancer (e.g., NCT00003730); and (2) monitor circadian biometrics using wearable devices as an attempt to develop supplemental screening technologies to mammography and ultrasound for the purpose of diagnosis (e.g., NCT02511301). Lastly, a limited number of interventional studies evaluate approaches for chemoprevention of breast and prostate cancer using dietary supplements (e.g., NCT01611038) and behavioral strategies (e.g., NCT00342407 and NCT02609373) in individuals experiencing shift-work schedules. Overall, the gold standard for treatment of cancer patients is the conventional 24-h schedule, with constant-rate infusion, of chemotherapeutics; a protocol that leaves no room for chronotherapeutic administration. Remarkably, this conventional approach has remained largely invariable despite the fact that 40 or more anticancer drugs have already been tested in animal models for their tolerability, pharmacokinetics, and/or tumor efficacy and have been shown to be influenced by circadian timing (Fig. 3d; for review see Levi et al. [64]).

Another example that exposes the limited application of circadian biology in clinical trials is its occurrence in studies involving nutritional and metabolic diseases (Fig. 3c; 4.6 % of all studies involving circadian interventions). When evaluated in this category, circadian interventions are repeatedly represented in studies of diabetes, glucose metabolism disorders, insulin resistance, metabolic diseases, and obesity. Accordingly, most clinical trials are directed at evaluating the effect of circadian misalignment on insulin sensitivity (e.g., NCT02580513), risk of diabetes (e.g., NCT01786564 and NCT00989534), daily oscillations in glucose values (e.g., NCT00848822), and variations in skeletal muscle energy metabolism (e.g., NCT02261168). In addition, studies explore alterations in the function of the circadian clockwork in subjects who are healthy, obese, and have type 2 diabetes (e.g., NCT02384148), the use of chronotherapeutic interventions for prevention of cardiovascular events (e.g., NCT00725127), the time-dependent safety and tolerability of drugs for the treatment of diabetes (e.g., NCT00377676), the relevance of time-restricted feeding for the control of blood sugar (e.g., NCT01895179), and whether circadian phase adjustments can improve metabolic conditions in night-shift workers (e.g., NCT02108353). A small number of additional trials tangentially explore a relationship between circadian biology and disorders in iron metabolism (e.g., NCT01810965), dyslipidemias (e.g., NCT00770445), and calcium metabolism (e.g., NCT00004358). Thus, whereas data from molecular, biochemical, and engineered animal models have bolstered our appreciation of the oscillatory behavior of metabolic processes in health and disease, the translation of

this fundamental knowledge to the clinic has been limited. Yet most circadian studies remain in the domain of diseases and disorders of the nervous system (Fig. 3c, 44.1 % of all registered clinical studies using a form of chronotherapy), a proportion that becomes insignificant (0.07 %) in the context of the total number of ongoing clinical trials.

8 Filling the Research Translational Gap One Step at a Time

Circadian biology long ago moved from defining the genetic components and anatomical structures responsible for the generation of rhythms to, more recently, molecularly identifying clock-driven processes governing the body's physiology and behavior (for review see Golombek and Rosenstein [45]). Thus, it seems reasonable to assume that concepts and processes associated with circadian biology would have been translated broadly into more effective treatment interventions. However, the initial success that followed the use of chronotherapy to alleviate symptoms associated with bronchial asthma, hypertension, rheumatoid arthritis, and gastric ulcers, and improved tolerability and efficacy of chemotherapeutic treatment regimens (e.g., cyclophosphamide, cisplatin, 5-fluorouracil [92, 93]) have not been enough of a catalyst to integrate chronotherapy widely in clinical trials. Among the top-100 best-selling branded drugs on the market (IMS Health, based on 2015 US data) and another 119 components named on the World Health Organization essential medicines list were drugs that directly target products of genes with rhythmic expression (e.g., Nexium® for esophagitis/gastritis [AstraZeneca], Advair Diskus® for asthma [GlaxoSmithKline], Ritalin® for attention–deficit hyperactivity disorder [Novartis], Tamiflu® for influenza [Genentech], Viagra® for erectile dysfunction [Pfizer] [34]). Furthermore, the majority of these drugs have a half-life shorter than 6 h; thus, patients would greatly benefit from a timed dosage. Consequently, there is a need for a multi-level strategy to be launched that would facilitate the translational transition and incorporation of circadian timing into practice. To accomplish this goal, we (1) urge health professionals to consider including newly gained knowledge in circadian biology, its relationship to health and disease, and its relevance to the clinical practice, longitudinally in the medical school curricula (as outlined by Selfridge et al. [94]); (2) recommend that clinical pharmacists and pharmacy practitioners emphasize, whenever possible (e.g., via use of standard of care sheets), the importance of 'time of administration' as a variable to augment treatment efficacy and avoid variations associated with drug pharmacokinetics; (3) emphasize the need for circadian biologists to weigh the relevance of other multi-components such as sex, age, ethnicity, body mass index, activity–rest schedule, and eating times (and the meal's composition) in their studies to better address the likely impact of those variables on treatment strategies and to understand inter-individual differences; and, more importantly, (4) support an inclusive 'team science' approach, in which the summation of each individual's expertise provides a more holistic and comprehensive understanding of a biomedical challenge, which would include circadian biologists to help accelerate scientific transitions and progress. Today, the numerous advances in molecular circadian biology, chronopharmacology, and the evolving landscape in translational research that has resulted from various strategic initiatives sponsored by the National Institutes of Health favor a scenario where all these recommendations can find fertile ground.

9 Conclusions

As in many aspects of life, there is a great deal of truth in the proclamation that 'timing is everything'; thus, it should not come as a surprise that this saying also applies to the administration of medical treatments. Largely disregarded in the standard medical practice because it lacked a strong mechanistic foundation, circadian biology has waited decades to emerge as a complementary and inclusive scientific discipline capable of bridging molecular genetics, biochemistry, physiology, pharmacology, pathology, and clinical research. Given the possibilities that this field of research opens to clinicians today, it could impact the quality of life of patients and the effectiveness of disease therapies. The clinical translation of chronotherapy to diseases such as hypertension, arthritis, asthma, and peptic ulcers resulted in such significant benefits for patients that it is now standard practice [73]. Therefore, health professionals and regulatory agencies have a sense of urgency regarding the implementation of chronotherapy when designing clinical studies and evaluating trial results.

Acknowledgments The authors would like to thank all members of the Finkielstein Laboratory for their help and discussions. We would also like to thank Dr J. Webster for comments and manuscript edition. JMS and CVF conceived the manuscript. CVF wrote the manuscript. The authors apologize to the many outstanding colleagues in the specific fields whose work has not been cited due to space limitations.

Compliance with Ethical Standards

Conflict of interest The authors have declared that no conflicting interest exists.

Funding This work was supported by grants from the National Science Foundation (MCB-1517298) and the Fralin Life Science Institute to CVF.

References

1. Dibner C, Schibler U, Albrecht U. The mammalian circadian timing system: organization and coordination of central and peripheral clocks. Annu Rev Physiol. 2010;72:517–49.
2. Huang W, Ramsey KM, Marcheva B, Bass J. Circadian rhythms, sleep, and metabolism. J Clin Invest. 2011;121(6):2133–41.
3. Waterhouse J, Reilly T, Atkinson G, Edwards B. Jet lag: trends and coping strategies. Lancet. 2007;369(9567):1117–29.
4. Portaluppi F, Tiseo R, Smolensky MH, Hermida RC, Ayala DE, Fabbian F. Circadian rhythms and cardiovascular health. Sleep Med Rev. 2012;16(2):151–66.
5. Shea SA, Hilton MF, Hu K, Scheer FA. Existence of an endogenous circadian blood pressure rhythm in humans that peaks in the evening. Circ Res. 2011;108(8):980–4.
6. Masri S, Sassone-Corsi P. The circadian clock: a framework linking metabolism, epigenetics and neuronal function. Nat Rev Neurosci. 2013;14(1):69–75.
7. Kronfeld-Schor N, Einat H. Circadian rhythms and depression: human psychopathology and animal models. Neuropharmacology. 2012;62(1):101–14.
8. Markt SC, Valdimarsdottir UA, Shui IM, Sigurdardottir LG, Rider JR, Tamimi RM, et al. Circadian clock genes and risk of fatal prostate cancer. Cancer Causes Control. 2015;26(1):25–33.
9. Monsees GM, Kraft P, Hankinson SE, Hunter DJ, Schernhammer ES. Circadian genes and breast cancer susceptibility in rotating shift workers. Int J Cancer. 2012;131(11):2547–52.
10. Lowrey PL, Takahashi JS. Genetics of circadian rhythms in Mammalian model organisms. Adv Genet. 2011;74:175–230.
11. Gekakis N, Staknis D, Nguyen HB, Davis FC, Wilsbacher LD, King DP, et al. Role of the CLOCK protein in the mammalian circadian mechanism. Science. 1998;280(5369):1564–9.
12. Hogenesch JB, Gu YZ, Jain S, Bradfield CA. The basic-helix-loop-helix-PAS orphan MOP3 forms transcriptionally active complexes with circadian and hypoxia factors. Proc Natl Acad Sci USA. 1998;95(10):5474–9.
13. Kume K, Zylka MJ, Sriram S, Shearman LP, Weaver DR, Jin X, et al. mCRY1 and mCRY2 are essential components of the negative limb of the circadian clock feedback loop. Cell. 1999;98(2):193–205.
14. Lee C, Etchegaray JP, Cagampang FR, Loudon AS, Reppert SM. Posttranslational mechanisms regulate the mammalian circadian clock. Cell. 2001;107(7):855–67.
15. Preitner N, Damiola F, Lopez-Molina L, Zakany J, Duboule D, Albrecht U, et al. The orphan nuclear receptor REV-ERBalpha controls circadian transcription within the positive limb of the mammalian circadian oscillator. Cell. 2002;110(2):251–60.
16. Sahar S, Sassone-Corsi P. Metabolism and cancer: the circadian clock connection. Nat Rev Cancer. 2009;9(12):886–96.
17. Doi M, Hirayama J, Sassone-Corsi P. Circadian regulator CLOCK is a histone acetyltransferase. Cell. 2006;125(3):497–508.
18. Nakahata Y, Kaluzova M, Grimaldi B, Sahar S, Hirayama J, Chen D, et al. The NAD+-dependent deacetylase SIRT1 modulates CLOCK-mediated chromatin remodeling and circadian control. Cell. 2008;134(2):329–40.
19. Imai S, Armstrong CM, Kaeberlein M, Guarente L. Transcriptional silencing and longevity protein Sir2 is an NAD-dependent histone deacetylase. Nature. 2000;403(6771):795–800.
20. Nakahata Y, Sahar S, Astarita G, Kaluzova M, Sassone-Corsi P. Circadian control of the NAD+ salvage pathway by CLOCK-SIRT1. Science. 2009;324(5927):654–7.
21. Ramsey KM, Yoshino J, Brace CS, Abrassart D, Kobayashi Y, Marcheva B, et al. Circadian clock feedback cycle through NAMPT-mediated NAD + biosynthesis. Science. 2009;324(5927):651–4.
22. Eide EJ, Woolf MF, Kang H, Woolf P, Hurst W, Camacho F, et al. Control of mammalian circadian rhythm by CKIepsilon-regulated proteasome-mediated PER2 degradation. Mol Cell Biol. 2005;25(7):2795–807.
23. Kurabayashi N, Hirota T, Harada Y, Sakai M, Fukada Y. Phosphorylation of mCRY2 at Ser557 in the hypothalamic suprachiasmatic nucleus of the mouse. Chronobiol Int. 2006;23(1–2):129–34.
24. Lee C, Weaver DR, Reppert SM. Direct association between mouse PERIOD and CKIepsilon is critical for a functioning circadian clock. Mol Cell Biol. 2004;24(2):584–94.
25. Yin L, Wang J, Klein PS, Lazar MA. Nuclear receptor Rev-erbalpha is a critical lithium-sensitive component of the circadian clock. Science. 2006;311(5763):1002–5.
26. Busino L, Bassermann F, Maiolica A, Lee C, Nolan PM, Godinho SI, et al. SCFFbxl3 controls the oscillation of the circadian clock by directing the degradation of cryptochrome proteins. Science. 2007;316(5826):900–4.
27. Ohsaki K, Oishi K, Kozono Y, Nakayama K, Nakayama KI, Ishida N. The role of {beta}-TrCP1 and {beta}-TrCP2 in circadian rhythm generation by mediating degradation of clock protein PER2. J Biochem. 2008;144(5):609–18.
28. Siepka SM, Yoo SH, Park J, Song W, Kumar V, Hu Y, et al. Circadian mutant Overtime reveals F-box protein FBXL3 regulation of cryptochrome and period gene expression. Cell. 2007;129(5):1011–23.
29. Gallego M, Virshup DM. Post-translational modifications regulate the ticking of the circadian clock. Nat Rev Mol Cell Biol. 2007;8(2):139–48.
30. Besing RC, Paul JR, Hablitz LM, Rogers CO, Johnson RL, Young ME, et al. Circadian rhythmicity of active GSK3 isoforms modulates molecular clock gene rhythms in the suprachiasmatic nucleus. J Biol Rhythms. 2015;30(2):155–60.
31. Miller BH, McDearmon EL, Panda S, Hayes KR, Zhang J, Andrews JL, et al. Circadian and CLOCK-controlled regulation of the mouse transcriptome and cell proliferation. Proc Natl Acad Sci USA. 2007;104(9):3342–7.
32. Panda S, Antoch MP, Miller BH, Su AI, Schook AB, Straume M, et al. Coordinated transcription of key pathways in the mouse by the circadian clock. Cell. 2002;109(3):307–20.
33. Storch KF, Lipan O, Leykin I, Viswanathan N, Davis FC, Wong WH, et al. Extensive and divergent circadian gene expression in liver and heart. Nature. 2002;417(6884):78–83.
34. Zhang R, Lahens NF, Ballance HI, Hughes ME, Hogenesch JB. A circadian gene expression atlas in mammals: implications for biology and medicine. Proc Natl Acad Sci USA. 2014;111(45):16219–24.
35. Hunt T, Sassone-Corsi P. Riding tandem: circadian clocks and the cell cycle. Cell. 2007;129(3):461–4.
36. Gotoh T, Vila-Caballer M, Liu J, Schiffhauer S, Finkielstein CV. Association of the circadian factor Period 2 to p53 influences p53′s function in DNA-damage signaling. Mol Biol Cell. 2015;26(2):359–72.
37. Gotoh T, Vila-Caballer M, Santos CS, Liu J, Yang J, Finkielstein CV. The circadian factor Period 2 modulates p53 stability and

transcriptional activity in unstressed cells. Mol Biol Cell. 2014;25(19):3081–93.
38. Feng D, Liu T, Sun Z, Bugge A, Mullican SE, Alenghat T, et al. A circadian rhythm orchestrated by histone deacetylase 3 controls hepatic lipid metabolism. Science. 2011;331(6022):1315–9.
39. Hatanaka F, Matsubara C, Myung J, Yoritaka T, Kamimura N, Tsutsumi S, et al. Genome-wide profiling of the core clock protein BMAL1 targets reveals a strict relationship with metabolism. Mol Cell Biol. 2010;30(24):5636–48.
40. Koike N, Yoo SH, Huang HC, Kumar V, Lee C, Kim TK, et al. Transcriptional architecture and chromatin landscape of the core circadian clock in mammals. Science. 2012;338(6105):349–54.
41. Kojima S, Sher-Chen EL, Green CB. Circadian control of mRNA polyadenylation dynamics regulates rhythmic protein expression. Genes Dev. 2012;26(24):2724–36.
42. Le Martelot G, Canella D, Symul L, Migliavacca E, Gilardi F, Liechti R, et al. Genome-wide RNA polymerase II profiles and RNA accumulation reveal kinetics of transcription and associated epigenetic changes during diurnal cycles. PLoS Biol. 2012;10(11):e1001442.
43. Menet JS, Rodriguez J, Abruzzi KC, Rosbash M. Nascent-Seq reveals novel features of mouse circadian transcriptional regulation. eLife. 2012;1:e00011.
44. Rey G, Cesbron F, Rougemont J, Reinke H, Brunner M, Naef F. Genome-wide and phase-specific DNA-binding rhythms of BMAL1 control circadian output functions in mouse liver. PLoS Biol. 2011;9(2):e1000595.
45. Golombek DA, Rosenstein RE. Physiology of circadian entrainment. Physiol Rev. 2010;90(3):1063–102.
46. Rutter J, Reick M, McKnight SL. Metabolism and the control of circadian rhythms. Annu Rev Biochem. 2002;71:307–31.
47. Bass J, Takahashi JS. Circadian integration of metabolism and energetics. Science. 2010;330(6009):1349–54.
48. Asher G, Schibler U. Crosstalk between components of circadian and metabolic cycles in mammals. Cell Metab. 2011;13(2):125–37.
49. Sahar S, Sassone-Corsi P. Circadian rhythms and memory formation: regulation by chromatin remodeling. Front Mol Neurosci. 2012;5:37.
50. Turek FW, Joshu C, Kohsaka A, Lin E, Ivanova G, McDearmon E, et al. Obesity and metabolic syndrome in circadian Clock mutant mice. Science. 2005;308(5724):1043–5.
51. Feng D, Lazar MA. Clocks, metabolism, and the epigenome. Mol Cell. 2012;47(2):158–67.
52. Dibner C, Schibler U. Circadian timing of metabolism in animal models and humans. J Intern Med. 2015;277(5):513–27.
53. Roenneberg T, Merrow M. The circadian clock and human health. Curr Biol. 2016;26(10):R432–43.
54. Goldberger JJ, Buxton AE. Personalized medicine vs guideline-based medicine. JAMA. 2013;309(24):2559–60.
55. Ashley EA. The precision medicine initiative: a new national effort. JAMA. 2015;313(21):2119–20.
56. Dallmann R, Brown SA, Gachon F. Chronopharmacology: new insights and therapeutic implications. Annu Rev Pharmacol Toxicol. 2014;54:339–61.
57. Musiek ES, Fitzgerald GA. Molecular clocks in pharmacology. Handb Exp Pharmacol. 2013;217:243–60.
58. Kaur G, Phillips C, Wong K, Saini B. Timing is important in medication administration: a timely review of chronotherapy research. Int J Clin Pharm. 2013;35(3):344–58.
59. Reinberg AE. Concepts in chronopharmacology. Annu Rev Pharmacol Toxicol. 1992;32:51–66.
60. Paschos GK, Baggs JE, Hogenesch JB, FitzGerald GA. The role of clock genes in pharmacology. Annu Rev Pharmacol Toxicol. 2010;50:187–214.
61. Lemmer B, Scheidel B, Behne S. Chronopharmacokinetics and chronopharmacodynamics of cardiovascular active drugs. Propranolol, organic nitrates, nifedipine. Ann N Y Acad Sci. 1991;618:166–81.
62. Bode-Boger SM, Kojda G. Organic nitrates in cardiovascular disease. Cell Mol Biol (Noisy-le-grand). 2005;51(3):307–20.
63. Schachter M. Chemical, pharmacokinetic and pharmacodynamic properties of statins: an update. Fundam Clin Pharmacol. 2005;19(1):117–25.
64. Levi F, Okyar A, Dulong S, Innominato PF, Clairambault J. Circadian timing in cancer treatments. Annu Rev Pharmacol Toxicol. 2010;50:377–421.
65. Dallmann R, Okyar A, Levi F. Dosing-time makes the poison: circadian regulation and pharmacotherapy. Trends Mol Med. 2016;22(5):430–45.
66. Pan X, Hussain MM. Clock is important for food and circadian regulation of macronutrient absorption in mice. J Lipid Res. 2009;50(9):1800–13.
67. Bron R, Furness JB. Rhythm of digestion: keeping time in the gastrointestinal tract. Clin Exp Pharmacol Physiol. 2009;36(10):1041–8.
68. Lemmer B, Nold G. Circadian changes in estimated hepatic blood flow in healthy subjects. Br J Clin Pharmacol. 1991;32(5):627–9.
69. Goo RH, Moore JG, Greenberg E, Alazraki NP. Circadian variation in gastric emptying of meals in humans. Gastroenterology. 1987;93(3):515–8.
70. Kumar D, Wingate D, Ruckebusch Y. Circadian variation in the propagation velocity of the migrating motor complex. Gastroenterology. 1986;91(4):926–30.
71. Ando H, Yanagihara H, Sugimoto K, Hayashi Y, Tsuruoka S, Takamura T, et al. Daily rhythms of P-glycoprotein expression in mice. Chronobiol Int. 2005;22(4):655–65.
72. Stearns AT, Balakrishnan A, Rhoads DB, Ashley SW, Tavakkolizadeh A. Diurnal rhythmicity in the transcription of jejunal drug transporters. J Pharmacol Sci. 2008;108(1):144–8.
73. Baraldo M. The influence of circadian rhythms on the kinetics of drugs in humans. Expert Opin Drug Metab Toxicol. 2008;4(2):175–92.
74. Sukumaran S, Almon RR, DuBois DC, Jusko WJ. Circadian rhythms in gene expression: Relationship to physiology, disease, drug disposition and drug action. Adv Drug Deliv Rev. 2010;62(9–10):904–17.
75. Lemmer B, Nold G, Behne S, Kaiser R. Chronopharmacokinetics and cardiovascular effects of nifedipine. Chronobiol Int. 1991;8(6):485–94.
76. Baraldo M, Risaliti A, Bresadola F, Chiarandini P, Dalla Rocca G, Furlanut M. Circadian variations in cyclosporine C2 concentrations during the first 2 weeks after liver transplantation. Transplant Proc. 2003;35(4):1449–51.
77. Levi F, Schibler U. Circadian rhythms: mechanisms and therapeutic implications. Annu Rev Pharmacol Toxicol. 2007;47:593–628.
78. Ritschel WA, Forusz H. Chronopharmacology: a review of drugs studied. Methods Find Exp Clin Pharmacol. 1994;16(1):57–75.
79. Anderson NH, Devlin AM, Graham D, Morton JJ, Hamilton CA, Reid JL, et al. Telemetry for cardiovascular monitoring in a pharmacological study: new approaches to data analysis. Hypertension. 1999;33(1 Pt 2):248–55.
80. Innominato PF, Levi FA, Bjarnason GA. Chronotherapy and the molecular clock: clinical implications in oncology. Adv Drug Deliv Rev. 2010;62(9–10):979–1001.
81. Scheving LE, Pauly JE, Tsai TH. Circadian fluctuation in plasma proteins of the rat. Am J Physiol. 1968;215(5):1096–101.
82. Lemmer B, Bruguerolle B. Chronopharmacokinetics: are they clinically relevant? Clin Pharmacokinet. 1994;26(6):419–27.

83. Erkekoglu P, Baydar T. Chronopharmacokinetics of drugs in toxicological aspects: a short review for pharmacy practitioners. J Res Pharm Pract. 2012;1(1):3–9.
84. Yegnanarayan R, Mahesh SD, Sangle S. Chronotherapeutic dose schedule of phenytoin and carbamazepine in epileptic patients. Chronobiol Int. 2006;23(5):1035–46.
85. Ortiz-Tudela E, Innominato PF, Rol MA, Levi F, Madrid JA. Relevance of internal time and circadian robustness for cancer patients. BMC Cancer. 2016;16:285.
86. Akhtar RA, Reddy AB, Maywood ES, Clayton JD, King VM, Smith AG, et al. Circadian cycling of the mouse liver transcriptome, as revealed by cDNA microarray, is driven by the suprachiasmatic nucleus. Curr Biol. 2002;12(7):540–50.
87. Bellet MM, Sassone-Corsi P. Mammalian circadian clock and metabolism—the epigenetic link. J Cell Sci. 2010;123(Pt 22):3837–48.
88. Koopman MG, Koomen GC, Krediet RT, de Moor EA, Hoek FJ, Arisz L. Circadian rhythm of glomerular filtration rate in normal individuals. Clin Sci (Lond). 1989;77(1):105–11.
89. Doi M, Takahashi Y, Komatsu R, Yamazaki F, Yamada H, Haraguchi S, et al. Salt-sensitive hypertension in circadian clock-deficient Cry-null mice involves dysregulated adrenal Hsd3b6. Nat Med. 2010;16(1):67–74.
90. Zuber AM, Centeno G, Pradervand S, Nikolaeva S, Maquelin L, Cardinaux L, et al. Molecular clock is involved in predictive circadian adjustment of renal function. Proc Natl Acad Sci USA. 2009;106(38):16523–8.
91. Hanahan D, Weinberg RA. Hallmarks of cancer: the next generation. Cell. 2011;144(5):646–74.
92. Gorbacheva VY, Kondratov RV, Zhang R, Cherukuri S, Gudkov AV, Takahashi JS, et al. Circadian sensitivity to the chemotherapeutic agent cyclophosphamide depends on the functional status of the CLOCK/BMAL1 transactivation complex. Proc Natl Acad Sci USA. 2005;102(9):3407–12.
93. Zhang X, Diasio RB. Regulation of human dihydropyrimidine dehydrogenase: implications in the pharmacogenetics of 5-FU-based chemotherapy. Pharmacogenomics. 2007;8(3):257–65.
94. Selfridge JM, Moyer K, Capelluto DG, Finkielstein CV. Opening the debate: how to fulfill the need for physicians' training in circadian-related topics in a full medical school curriculum. J Circadian Rhythms. 2015;13:7.
95. Antoch MP, Kondratov RV. Circadian proteins and genotoxic stress response. Circ Res. 2010;106(1):68–78.

Appendix C:

Interplay between E3 ligases modulate Period 2's accumulation and influences circadian oscillation

JingJing Liu[1,2], Samuel Schiffhauer[1], Xianlin Zhou[1], Liang Jiang[1], Tetsuya Gotoh[1] & Carla V. Finkielstein[1,*]

[1] Integrated Cellular Responses Laboratory, Department of Biological Sciences, Virginia Polytechnic Institute and State University, Blacksburg, VA, United States

[2] Present address: Molecular and Cellular Oncogenesis, The Winstar Institute, Philadelphia, PA 19104, United States

[*]Correspondence and request for materials should be addressed to C.V.F. (email: finkielc@vt.edu)

Abstract

The circadian clock relies on post-translational modifications that set the timing for the degradation of core regulatory components and the pace of clock progression. Despite their importance, identification of the E3-ligases involved in ubiquitin-mediated degradation of clock components in mammalian models remains a daunting task. In fact, β-transducin repeat containing proteins (β-TrCPs) remain the major recognition subunits of phosphorylated substrates for most clock proteins, including the circadian factor PERIOD 2 (PER2) and mediate ubiquitination and proteasomal degradation. Previously, we established a role for PER2 in modulating the stability and function of the tumor suppressor p53 through its ability to prevent mouse double minute 2 homolog (MDM2)-mediated p53's ubiquitination and turnover. In this study, we *i*) identify the endogenous PER2:MDM2 complex, *ii*) map its interaction sites, *iii*) establish PER2 and β-TrCP1 as target substrates for MDM2, *iv*) reveal a phosphorylation-independent mechanism for PER2 ubiquitination and degradation, *v*) determine the existence of an MDM2:β-TrCP1 regulatory loop that modulates PER2 turnover, and *vi*) demonstrate the relevance of the loop for determining circadian period length. Therefore, we propose the existence of a new regulatory node in the clock network that can receive, connect, and distribute a diverse set of signals acting on cellular homeostasis.

Introduction

From vertebrates to bacteria, the molecular circadian clock is formed by a transcriptional-translational feedback loop where the expression of its core components drives the different phases of the daily cycle and whose protein products influence the cell's biochemistry {Bell-Pedersen, 2005 #13}. In mammalian cells, the positive limb of the clock is driven by the heterodimer formed by the *c*ircadian *l*ocomotor *o*utput *c*ycles *k*aput (CLOCK) and the *b*rain and *m*uscle *A*rnt-*l*ike protein-*1* (BMAL1) complex, which initiates the transcription of *PERIOD* and *CRYTOCHROME* genes (*PER 1,2,3* and *CRY 1,2*) and other *c*lock-*c*ontrolled *g*enes (*ccgs*). Dimerization of PER and CRY is relevant to the negative limb of the feedback loop as the nuclear translocation of the complex further inhibits CLOCK/BMAL1 transcriptional activity [for review see {Buhr, 2013 #315}]. Remarkably, this process also involves the rhythmic remodeling of chromatin through the recruitment of methytransferases, histone deacetylase, and the intrinsic histone acetyl transferase activity of CLOCK {Buhr, 2013 #315}. The stability of PER and CRY proteins is relevant to the termination of the repression phase and the initiation of a new round of transcription, a process that is mediated by distinct phosphorylation events in PER and CRY that precede E3-ligase-mediated ubiquitination and proteasomal degradation [for review see {Buhr, 2013 #315} and references within].

At the core of the mammalian clock mechanism is PER2, a large protein with a well-defined N-terminus HLH-PAS (*H*elix-*L*oop-*H*elix *P*er-*A*rnt-*S*ingle minded) domain responsible for multiple protein-protein interactions including homo- and hetero-dimerization among PER proteins {Yagita, 2000 #185}. In addition, PER2 exhibits a number of motifs and short domains that play critical functional roles in its cellular localization (nuclear localization and export signal motifs), stability (binding domain for E3 ligase), and post-translational-targeted modifications (including *c*asein *k*inase *1* ε/δ, CK1 ε/δ and *g*lycogen *s*ynthase *k*inase 3β, GSK3β, phosphorylation sites), the result of which, influences the periodic accumulation and distribution of PER2 in the cell [for review see {Ripperger, 2012 #317}]. Furthermore, the stability of PER2, which seems to increase or decrease based on its phosphorylation status, is influenced by environmental stimuli and homeostatic cellular conditions {Gallego, 2007 #55; Zhou, 2015 #218; Kaasik, 2013 #318}. As a result, PER2 acts as a cellular rheostat that integrates signals and helps to robustly compensate profound changes in environmental conditions that would otherwise affect the circadian clock.

Phosphorylation of PER2 by CK1 ε/δ can either stabilize or destabilize the circadian factor depending on which cluster site in PER2 the modification takes place in. Accordingly, $PER2^{S662G}$, a PER2 variant linked to familial advanced sleep phase syndrome {Lowrey, 2000 #321}, contains a missense mutation that prevents priming-dependent phosphorylation of flanking sites by CK1 ε/δ stabilizing PER2 independent of its location {Shanware, 2011 #319}. Conversely, a priming-independent cluster located in the C-terminus of PER2's PAS domain is targeted by CK1 ε/δ and is required for ubiquitin ligase-mediated degradation of PER2 {Eide, 2005 #323}. At present, our understanding of the molecular players involved in PER2 degradation is reduced to the sole role of β-TrCP, an F-box/WD40 repeat-containing substrate recognition subunit of the ubiquitin ligase complex SCF (*S*kp1-*C*ul1-*F*-box) that channels phosphorylation-dependent degradation of proteins {Eide, 2005 #323; Ohsaki, 2008 #282}. The mammalian β-TrCP E3 ligase subfamily includes β-TrCP1 and β-TrCP2, both of which are closely related in sequence, indistinguishable in function, but encoded by different genes {Fuchs, 2004 #325}. In addition, other multiple F-box/WD40-containing isoforms exist and result from alternative splicing of the *BTRCP* gene {Fuchs, 2004 #325}. Biochemical evidence points to direct interactions between β-TrCP1/2

and PER1, whereas β-TrCP1, seems to be the sole form implicated in the binding of PER2 *in vitro* {Shirogane, 2005 #327; Eide, 2005 #323}. Despite these findings, there has been not a clear answer on whether β-TrCP-targeted selectivity actually happens *in vivo* besides the fact that β-TrCP-mediated degradation contributes to generating cyclic levels of PER proteins relevant to the function of the clock {Ohsaki, 2008 #282}. As has been noted, endogenous β-TrCPs' activities depend on their localization and abundance in cells with β-TrCP1 predominantly located in the nucleus and β-TrCP2, the most unstable form of both E3-ligases, in the cytoplasmic compartment {Fuchs, 2004 #325}. Interestingly, findings show that overexpression of both dominant-negative forms of β-TrCP in cells neither increased PER2 stability nor accumulated phosphorylated PER2; instead, it resulted in rapid degradation of PER2 by, yet, an unknown mechanism {Ohsaki, 2008 #282}.

We previously reported that PER2 forms a stable complex with p53 that undergoes time-of-the-day-dependent nuclear-cytoplasmic shuttling, thus, generating an asymmetric distribution of each protein in different cellular compartments {Gotoh, 2016 #332}. In unstressed cells, PER2 mediates p53's stability by binding p53's C-terminus and preventing p53's ubiquitination of targeted sites by the RING finger-containing E3 ligase *m*ouse *d*ouble *m*inute *2* homolog (MDM2) {Gotoh, 2014 #63}. Remarkably, PER2:p53:MDM2 co-exist as a trimeric and stable complex in the nuclear compartment, although, p53 is released from the complex to become transcriptionally active once cells experience a genotoxic stimuli {Gotoh, 2015 #206}. As a result, we asked whether PER2 could also act as a bona fide substrate for the E3 ligase activity of MDM2 in the absence of p53. Unlike β-TrCP, MDM2 acts as a scaffold protein to facilitate catalysis by bringing the E2 ubiquitin-conjugating enzyme and substrate together in a phosphorylation-independent manner. Our findings show that PER2 binds near the N-terminus of MDM2 in a region located downstream of the p53-binding site mapped in MDM2. Furthermore, our results show that PER2:MDM2's interaction does not abrogate MDM2's E3 ligase activity and, thus, PER2 is efficiently poly-ubiquitinated both *in vitro* and in cells. Accordingly, PER2's half-life is critically modulated by MDM2's expression and its enzymatic activity as shown in cells where MDM2 levels were either enhanced or silenced and its catalytic activity specifically inhibited. Moreover, and besides the regulatory role of CK1ε/δ/β-TrCP in MDM2 turnover {Inuzuka, 2010 #329}, our data show that a feedback loop exists and that MDM2 can also target β-TrCP1 for degradation in a phosphorylation-independent fashion. As a result, fine-tuning the levels of active MDM2 directly influences period length, thus, advocating for tight control of PER2 turnover in the cells that expand the phosphorylation-centric view of its degradation. Consequently, PER2 targeting by MDM2 not only expands MDM2's suite of specific substrates beyond the cell cycle to include circadian components but also uncovers novel regulatory players that likely impact our view of how other mechanisms crosstalk and modulate the clock itself.

Results

In vertebrates, phosphorylation-dependent β-TrCP-mediated ubiquitination and proteasomal degradation provides a means of regulating endogenous levels of PER2 in the cell and, thus, its daily accumulation [for review see {Gallego, 2007 #55}]. As a large body of evidence supports a more central role of PER2 as the integrator of intracellular signals and as a sensor of environmental conditions, much of the effort has been devoted to understanding how various phosphorylation events determine PER2's degradation rate {Gallego, 2007 #55;Vanselow, 2006 #328;Vanselow, 2007 #271;Zhou, 2015 #218;Kaasik, 2013 #318} whereas other phosphorylation-independent mechanisms of degradation have remained largely unexplored. Building on our previous finding that PER2 forms a stable complex with p53 and MDM2 {Gotoh, 2015 #206;Gotoh, 2014 #63}, we evaluated whether the RING E3 ligase can provide an alternative route of degradation for PER2 that is independent of post-translational events and, at the same time, influence the circadian period.

The oncogenic E3 ligase MDM2 interacts with PER2 in the absence of p53. We previously reported the identification of protein interactors of PER2 by subsequent screening of a human cDNA liver library using a bacterial two-hybrid system {Gotoh, 2014 #63}. Target clones were isolated from a dual selective media using a PER2 bait, identified by sequencing, and categorized based on gene ontology {Gotoh, 2014 #63}. Among those clones were various length cDNA fragments encoding regions of the circadian factor *cry*tochrome (CRY), a known direct interactor of PER2, and the tumor suppressor p53 whose stability and function we have proven to be directly modulated by PER2 {Gotoh, 2015 #206;Gotoh, 2014 #63}. Here, we report the identification of the human MDM2 homolog as a direct interactor of PER2 suggesting that, in addition to the already identified PER2:p53:MDM2 nuclear complex, PER2:MDM2 might exist as its own entity and their association might be independent of p53 binding (Fig. 1A).

We first evaluated the presence of the PER2:MDM2 complex in cells lacking endogenous expression of p53. Initial experiments were carried out using colorectal HCT116 cells [*TP53*(+/+), *PER2*(+/+); named $HCT116^{p53+/+}$ hereafter] and, to avoid confounding variables, its null-isogenic HCT116 cell variant lacking p53 expression [*TP53*(-/-), *PER2*(+/+); named $HCT116^{p53-/-}$ hereafter] {Bunz, 1998 #211}. As p53 and MDM2 form a regulatory feedback loop in which p53 transcriptionally up-regulates *MDM2* expression, cells lacking p53 protein usually exhibit constitutive low levels of MDM2 expression, an event enhanced by MDM2's self-ubiquitination activity and increased turnover [for review see {Iwakuma, 2003 #330}]. To circumvent this problem, $HCT116^{p53-/-}$ cells were transfected with *myc*-tagged *MDM2* and PER2:MDM2 association was detected by immunoprecipitation of endogenous PER2. As shown in Fig. 1B, α-PER2, but not control IgG, antibody brings down PER2-associated MDM2 in both $HCT116^{p53+/+}$ and $HCT116^{p53-/-}$ further supporting their p53-independent interaction. Similar results were obtained using a human non-small cell lung carcinoma line (H1299) that possesses a homozygous partial deletion of the *TP53* gene and lacks p53 expression. In this case, complexes were detected in cells co-transfected with *myc-PER2* and either FLAG-*MDM2* or its ubiquitin ligase activity-deficient mutant FLAG-*MDM2(*C^{470}*A)* {Honda, 2000 #331}, and with the E3 ligase β-TrCP1 as well (Fig. S1A).

Next, we asked whether modification in the critical PER Ser^{662} site plays a role in PER2-binding to MDM2 and β-TrCP1 ligases. Accordingly, *in vitro* transcribed and translated proteins were incubated and complexes were allowed to form before immunoprecipitation. As shown in Fig. 1C, MDM2 binding to PER2 is independent of post-translational modification in Ser^{662} as both of the PER2 forms, wild-type and $S^{662}A$ mutant, bound MDM2 to the same extent *in vitro* (Fig. 1C, lanes 1 and 2) and in transfected cells (Fig. S1B). Conversely, as modification in this site is relevant to PER2:β-TrCP1 priming (REF), their

binding seemed compromised in the case of PER2($S^{662}A$) as decreased levels of β-TrCP1 were detected compared to PER2 wild-type (Fig. 1C, lanes 3 and 4). Lastly, we evaluated whether PER2 binding and $S^{662}A$ modification played a role in preventing MDM2:β-TrCP1 association, as it is known that phosphorylated MDM2 acts as a β-TrCP1 substrate {Inuzuka, 2010 #329}. A two-step binding assay was performed in which either form of PER2 was pre-incubated with FLAG-MDM2 and the complex was purified by affinity chromatography before adding recombinant β-TrCP1. Unexpectedly, our *in vitro* binding results showed that either form of PER2 is able to associate in a stable complex with MDM2:β-TrCP1 (Fig. 1C, lanes 5-7), a result that prompted us to map the region of binding between PER2 and MDM2 to better understand the interplay among these molecules. Accordingly, recombinant FLAG-MDM2($C^{470}A$) was pre-incubated with various epitope-specific antibodies that recognize native conformations in MDM2 [{Chen, 1993 #333}, 4B2: residues 19 to 59; SMP14: residues 154 to 167; 4B11: residues 383 to 491 (comprises the RING domain)] before adding recombinant *myc*-PER2 (Fig. S1C). As shown in Fig. 1D, pre-incubation with α-MDM2 clone SMP14 completely abolished PER2 binding suggesting that the epitope comprising residues 154-167 in MDM2 is critical for the stability of the PER2:MDM2 interaction. Furthermore, pull-down experiments using various recombinant GST-expressed fragments of PER2 [named GST-PER2 (1-172), GST-PER2 (173-355), GST-PER2 (356-574), GST-PER2 (575-682), GST-PER2 (683-872), GST-PER2 (873-1,120), GST-PER2 (1,121-1,255)] and [^{35}S]-MDM2 showed that association primarily occurs in the C-terminus of the PAS domain, residues 356 to 574, and in a further inward region that is heavily post-translationally modified comprising residues 683 to 872 (Fig. 1E and S1D). Remarkably, both MDM2 interacting regions in PER2 are targeted for priming-independent (the former) and priming-dependent (the latter), CK1 phosphorylation and are reportedly involved in β-TrCP1-dependent turnover of PER2 {Gallego, 2007 #55}. Overall, our findings establish the existence of a PER2:MDM2 complex whose association is independent of the presence of p53, thus, suggesting that alternative E3 ligases may be acting on PER2.

Period 2 is a bona fide substrate of MDM2. The E3 ligase MDM2 catalyzes the direct transfer of ubiquitin molecules from the E2 enzyme to the substrate in a RING-finger-dependent manner through a mechanism that involves direct recognition and simultaneous binding of both the E2-conjugated ubiquitin and the substrate {Berndsen, 2014 #334}. Furthermore, unlike β-TrCPs, for which specific substrate phosphorylation appears to be a requirement for binding, MDM2's substrate recognition does not require an *a priori* modification {Fuchs, 2004 #325}. As PER2 binds MDM2 opposite its RING domain, we next asked whether MDM2's catalytic activity could result in PER2 ubiquitination. To test this possibility, we evaluated PER2 ubiquitination in four different scenarios including *i*) an *in vitro* assay where recombinant purified E1 and E2 enzymes (Ubch5a, b, c), *myc*-MDM2 or *myc*-MDM2($C^{470}A$), and FLAG-PER2 were added stepwise to the reaction (Fig. 2A), *ii*) a cell-free system enriched in E1 and E2 enzymes (HeLa S100 fraction) also containing *in vitro* transcribed and translated *myc*-MDM2, or *myc*-MDM2($C^{470}A$), and FLAG-PER2 (Fig. 2B), *iii*) a dose-dependent *in vitro* assay in which PER2 ubiquitination was monitored in the presence of increasing amounts of MDM2 (Fig. 2C) and *iv*) in $HCT116^{p53-/-}$ cells co-transfected with FLAG-PER2 and either *myc*-MDM2 or *myc*-MDM2($C^{470}A$) in the presence of MG132, a cell-permeable proteasome inhibitor (Fig. 2D) {Gotoh, 2016 #332;Gotoh, 2014 #63}. To rule out the contribution of phosphorylation events in substrate recognition, we incorporated lambda phosphatase, a dual specificity enzyme with activity towards phosphorylated Ser/Thr/Tyr residues, in assay *ii*. In all cases, the PER2:MDM2 complex was immunoprecipitated and either PER2 levels or its ubiquitin intermediates (PER2-$[Ub]_n$) were detected by immunoblotting.

Results showed that under the most reductionist experimental conditions, FLAG-PER2 is specifically poly-ubiquitinated by *myc*-MDM2, a result that is further supported by the converse result obtained when using the catalytically inactive form of MDM2 (Fig. 2A, lanes XXX and XXX). Furthermore, MDM2-mediated ubiquitination is independent of substrate phosphorylation as PER2-$[Ub]_n$ intermediates were detected even when pre-treated with lambda phosphatase (Fig. 2A, lanes XXX and XXX). Interestingly, some level of mono-ubiquitination was detected in PER2 when a similar *in vitro* assay was performed using methyl-ubiquitin as substrate, opening the possibility that, as is the case with p53 {Li, 2003 #103}, MDM2 could be responsible for both modifications in PER2 (Fig. S2).

As is the case with p53, in which the extent of MDM2-mediated substrate poly-ubiquitination depends on MDM2 levels {Li, 2003 #103}, accumulation of PER2-$[Ub]_n$ intermediates also increased along with the levels of MDM2 when monitored in immunoprecipitated samples from *in vitro* reactions in which FLAG-PER2 was constant and *myc*-MDM2 was augmented (Fig. 2C).

Lastly, co-transfected $HCT116^{p53-/-}$ cells expressing recombinant FLAG-PER2 and either *myc*-MDM2 or *myc*-MDM2($C^{470}A$) proteins were treated with MG132 to facilitate the accumulation of PER2-$[Ub]_n$ intermediates (Fig. 2D). As shown in Fig. 2D, PER2-$[Ub]_n$ conspicuously accumulated only in MG132-treated samples overexpressing *myc*-MDM2 while remaining close to basal levels in those expressing the inactive form of the enzyme (Fig. 2D, lanes 1-3) despite the level of expression of the latter, which was greatly enhanced (Fig. 2C, *lower panel*). As expected, $HCT116^{p53-/-}$ cells exhibited largely undetectable levels of endogenous MDM2 (Fig. 2C, lane 1 in *lower panel*) and, thus, the basal levels of PER2-$[Ub]_n$ detected in control samples (Fig. 2C, lane 1) might reflect the endogenous activity of either β-TrCP1 or that o, a yet unknown E3 ligase of the PER2 substrate.

We then asked whether MDM2-mediated polyubiquitination of PER2 impacts PER2's half-life. $HCT116^{p53+/+}$ cells were transfected with FLAG-*MDM2* and harvested at different times after being treated with cycloheximide (CHX), an inhibitor of protein biosynthesis previously used to estimate the half-life of other core clock proteins {Gotoh, 2016 #332;Yoo, 2005 #192}. Analysis of cell lysates showed endogenous levels of PER2 that were remarkably reduced shortly after CHX addition in samples overexpressing MDM2 (Fig. 2E, *upper panel*); thus, PER2's half-life was shortened 2-fold ($t_{1/2}$ mock *vs.* MDM2-trasfected was 1.45 h *vs.* 2.95 h; Fig. 2E, *bar graph*). Overall, our results support a model in which MDM2 directly targets PER2 for polyubiquitination in a phosphorylation-independent manner that favors proteasome-mediated degradation of PER2.

Period 2 turnover is at the crossroad of the MDM2-β-TrCP1 regulatory loop. We next evaluated the half-life of PER2 in unstressed cells under conditions in which the endogenous levels of either MDM2 or β-TrCP1 were downregulated. Based on our findings, we hypothesized that a decrease in endogenous MDM2 levels would favor PER2 stability and a prolonged half-life. Conversely, downregulation of β-TrCP1 should have a much more modest effect on PER2 half-life and, therefore, closely mimic that of mock-treated samples as substrate phosphorylation is an absolute requirement for β-TrCP1 targeted activity. $HCT116^{p53+/+}$ cells, which express both MDM2 and β-TrCP1 and form a stable endogenous complex (Fig. S3), were transfected with siRNA targeting either MDM2 or β-TrCP1 and lysates were collected at various times after CHX addition and examined for the expression of endogenous levels of PER2, MDM2, and β-TrCP1 (Fig. 3A). Results unmasked two distinct, yet related, features associated with PER2 levels as siRNA treatment seemed to influence both PER2's accumulation and its stability and half-life (Fig. 3A, *upper panel*). As shown, the endogenous levels of PER2 increased, albeit at different levels, as a result of knocking down either E3 ligase even before CHX addition with a 4- *vs.* 2-fold

increase detected in *siMDM2 vs. siβ-TrCP1* samples compared to mock samples (Fig. 3A, lanes 1, 7, and 13 and *bar graph*). When analyzing PER2's half-life, both siRNA-treated samples stabilize PER2 to largely the same extent and with similar half-life ($t_{1/2}$ siMDM2: 2.3 h, $t_{1/2}$ siβ-TrCP1: 2.4 h) in notable contrast to that of mock samples ($t_{1/2}$ mock: 1.7 h; Fig. 3A, *upper panel*). To understand the meaning of these results from a signaling standpoint, we turned our attention to two additional findings that emerged from the analysis of the endogenous levels of MDM2 and β-TrCP1 that resulted from knocking down either ligase in each independent experiment (Fig. 3A, lanes 7-12 and 13-18, *middle panels*). Unexpectedly, *siMDM2* treatment resulted in increased amounts of endogenous β-TrCP1 to much greater levels than those detected in mock-treated samples suggesting that β-TrCP1 might itself be a target of MDM2 (Fig. 3A, lanes 1-6 and 7-12, *middle panels*). Whereas the converse result was, to some extent, expected as previous evidences shows that β-TrCP1 targets casein kinase 1 ε/δ (CK1δ)-mediated phosphorylated MDM2 in response to DNA damage and during the G1-S phase of unstressed cells {Inuzuka, 2010 #329}. That is, the amount of MDM2 accumulated in *siβ-TrCP1*-treated samples, although greater than that identified in *siMDM2* lysates (Fig. 3A, lanes 7-12 *vs.* 13-18), remained lower than those detected in mock lysates for which a basal level of expression of β-TrCP1 expression exists (Fig. 3A, lanes 13-18 *vs.* 1-6). In summary, these results further support the role of MDM2 in PER2 stability and unveils an additional regulatory feedback loop that might exist between MDM2 and β-TrCP1 and provides an alternative path for controlling PER2 cellular levels (Fig. 3B).

The MDM2 E3 ligase targets β-TrCP1 for ubiquitination. To investigate whether β-TrCP1 might also be a direct substrate of MDM2, we generated a dominant negative form of β-TrCP1 [named β-TrCP1ΔF hereafter, {Fuchs, 2004 #325}] that cannot interact with the ubiquitin E3 component Skp1 and is, therefore, functionally inactive. Initially, *in vitro* reactions were performed using recombinant FLAG-β-TrCP1ΔF as a substrate and either *myc*-MDM2 or its catalytically inactive form *myc*-MDM2($C^{470}A$) proteins (Fig. 4A). Protein complexes were allowed to form and enzymatic reactions took place in the presence (+, Fig. 4A, lanes 5-12), or absence (-, Fig. 4A, lanes 1-4) of ubiquitin-containing mixture as described in the Methods section. The p53:MDM2 and p53:MDM2($C^{470}A$) complexes were used as control reactions in the assay (Fig. 4A, lanes 3-4 *vs.* 11-12). In all cases, complexes were immunoprecipitated and their components and modifications identified by immunoblotting. Results show that FLAG-β-TrCP1ΔF was able to form a stable complex with both *myc*-MDM2 and *myc*-MDM2($C^{470}A$) (Fig. 4A, lanes 1-2 and 9-10, *upper and middle panels*) and that addition of ubiquitin promoted the formation of FLAG-β-TrCP1ΔF-$[Ub]_n$ intermediates in *myc*-MDM2-containing samples as detected using α-ubiquitin antibody (Fig. 4A, lane 9, *lower panels*). In the context of previously reported findings showing that phosphorylated MDM2 is targeted by β-TrCP1, our data support a model in which the converse reaction is possible; thus, MDM2 could also target β-TrCP1 for polyubiquitination generating a regulatory feedback loop.

To further explore this possibility, we monitored the endogenous levels of β-TrCP1 in $HCT116^{p53+/+}$ cells overexpressing either FLAG-MDM2 or FLAG-MDM2($C^{470}A$) and following CHX treatment (Fig. 4B). In agreement with the proposed role of MDM2 in modulating β-TrCP1 stability, threshold expression of FLAG-MDM2 led to a reduction in endogenous levels of β-TrCP1 compared to mock samples (Fig. 4B, lanes 7-12 vs. 1-6, *upper panel*) whereas overexpression of the MDM2's dominant negative form favors both accumulation and stability of β-TrCP1 (Fig. 4B, lanes 13-18 vs. 1-6, *upper panel*). Altogether, our data suggest that the interplay between MDM2 and β-TrCP1 might represent a unique feedback node for

modulating PER2 stability. Hence, we examined whether the combined effect of altering the activity of MDM2-β-TrCP1 components and availability of phosphorylated substrates impact the half-life of PER2. To test this possibility, we took advantage of two selective compounds, sempervirine nitrate [named SN hereafter, {Sasiela, 2008 #339}] and PF-670462 [named PF670 hereafter, {Badura, 2007 #341}], shown to specifically inhibit the ubiquitin ligase activity of MDM2 and the kinase activity of CK1δ, respectively {Clement, 2008 #342;Zhou, 2015 #218;Kim, 2013 #219}. Accordingly, HCT116p53$^{+/+}$ cells were incubated with SN, PF670, or a combination of both shortly before CHX addition as described in the Methods section. Lysates from cells collected at different times after CHX treatment were analyzed for the levels of PER2 by immunoblotting (Fig. 5A). In agreement with our previous results using *siMDM2* (Fig. 3A), inhibition of MDM2 activity by SN resulted in enhanced stability and greater half-life of PER2 compared with control samples (Fig. 5, lanes 7-12 *vs.* 1-6). Interestingly, whereas the accumulation of PER2 was expected in the context of PF670 treatment, its effect in lengthening PER2's half-life was unanticipated (Fig. 5, lanes 13-18 *vs.* 1-6, *upper panel*) but in agreement with our proposed model (Fig. 3B). Accordingly, as PF670 treatment also favors accumulation of endogenous MDM2 (Fig. 5, lanes 13-18 *vs.* 1-6, *middle panel*) by inhibiting the kinase responsible for MDM2 phosphorylation and β-TrCP1-mediated turnover {Inuzuka, 2010 #329}; thus, a pool of active MDM2 is available for feedback to target β-TrCP1 for degradation, a hypothesis that justifies the reduction in β-TrCP1 levels observed between control and PF670-treated samples (Fig. 5, lanes 13-18 *vs.* 1-6, *middle panel*). Lastly, we hypothesized that PER2's accumulation and half-life would be greatest when CK1δ and MDM2 activities were simultaneously inhibited, as PER2 is phosphorylated and targeted by β-TrCP1 and MDM2 is active and can target PER2 for degradation, a prediction further supported by the data shown in Fig. 5 (lanes 19-24). Overall, our data supports a model in which the stability of PER2 is compromised by altering either the levels or activity of MDM2 and β-TrCP1 and by blocking CK1δ-mediated substrate phosphorylation (Fig. 5B).

The MDM2's regulatory loop modulates the period length of the circadian oscillator. Maintenance of the transcriptionally negative feedback loop of the mammalian clock relies on the expression of its rate-limiting component PER2 for the formation of a functional PER2:CRY inhibitory complex {Chen, 2009 #345}. Thus, parameters such as timing, subcellular localization, post-translational modifications, and the level of PER2's expression are critical for determining the phase and length of the circadian clock {Chen, 2009 #345;Lee, 2001 #101;Lee, 2011 #343;Lee, 2011 #344}. Consequently, we hypothesized that alteration in PER2 levels as a result of tuning the MDM2's regulatory loop should affect the circadian oscillator. Furthermore, we expect that this phenotype would be enhanced when alteration in MDM2's activity is combined with inhibition of CK1δ. To test these hypotheses, we measured real-time bioluminescent rhythms in mouse embryonic fibroblast (MEF) cells in which the mouse *PER2* gene (*mPer2*) was *knocked-in* and the luciferase gene inserted downstream; thus, mPER2 is expressed as a chimera protein with luciferase being fused *in-frame* to the C-terminus of mPer2 [named MEF$^{mPer2::LUC}$ hereafter, {Yoo, 2004 #351}]. Further studies confirmed that MEF$^{mPer2::LUC}$ cells maintain robust rhythms in luciferase activity for several days and the mPer2::LUC fusion protein show rhythms of accumulation and posttranslational modifications that mirror those described *in vivo* {Yoo, 2004 #351;Chen, 2009 #345}. Thus, MEF$^{mPer2::LUC}$ provides an *in vitro* model to study transcriptional and post-transcriptional events regulating circadian oscillations *in vivo* {Welsh, 2004 #350;Chen, 2009 #345;Lee, 2011 #343;Lee, 2011 #344}.

Our initial studies focused on measuring the period length of the circadian oscillator in MEF$^{mPer2::LUC}$ cells in which MDM2's level was either augmented by its overexpression or silenced by siRNA targeting (Figs. 6A-B and Fig. S5A-C). In all scenarios, transfected cells were synchronized by dexamethasone before luciferase rhythms were recorded as indicated in the Methods section. Results show that whereas mock MEF$^{mPer2::LUC}$-transfected cells were able to maintain robust and regular oscillatory cycles, MEF$^{mPer2::LUC}$ cells overexpressing MDM2 exhibited a shorter period length (24.00 ± 0.101 h *vs.* 23.38 ± 0.024 h, $p<0.01$), a result that is in agreement with the predicted reduction in PER2 levels (Fig. 6A and Fig. S5A) and likely impacts the amount of PER2:CRY complex available in the negative arm of the circadian feedback loop. Furthermore, transfections of MEF$^{mPer2::LUC}$ with increasing amounts of *myc*-MDM2 resulted in a dose-dependent shortening of the circadian period length by up to ~1.5h (Fig. S5B) that resulted significant even at low levels of *myc*-MDM2 transfection, suggesting that a tight regulation of MDM2 needs to be maintained under physiological conditions to ensure proper oscillation.

Next, we challenged the model by hypothesizing that knockdown expression of MDM2 by siRNA transfection (named *siMDM2*) of MEF$^{mPer2::LUC}$ cells should result in the converse phenotype and, thus, a lengthened period (Fig. 6B and Fig. S5C). Accordingly, siMDM2-transfected cells maintained seemingly undetectable levels of MDM2 even 96h after circadian synchronization and during kinetic luminescence imaging recording (Fig. S5C). In this context, our data show that downregulation of MDM2 expression resulted in significant lengthening of the circadian period (24.00 ± 0.252 h *vs.* 25.05 ± 0.398 h, $p<0.05$), confirming that MDM2 is required for normal circadian oscillations. Later, MEF$^{mPer2::LUC}$ cells were treated with the cell permeable MDM2 inhibitor SN at a dose that *i*) prevented MDM2 auto-ubiquitination and degradation, and *ii*) did not affect cell viability (Fig. S5D-E). Synchronized MEF$^{mPer2::LUC}$ cells were maintained in the presence of the inhibitor throughout the time course during bioluminescence recording (Fig. 6C). Average bioluminescence rhythms of SN-treated cells show a dramatic lengthening of the circadian period of ~2 h (24.00 ± 0.158 h *vs.* 26.05 ± 0.259 h, $p<1x10^{-5}$), which closely resembles the result obtained when transfecting MEF$^{mPer2::LUC}$ cells with siMDM2 (Fig. 6B-C), suggesting that control over MDM2's activity remains a major point of regulation. Therefore, despite the fact that changes in MDM2 levels influence circadian oscillations, MDM2's E3 ligase activity is actually the chief contributor to the observed phenotype.

Lastly, we evaluated whether the combined effect of PF670 and SN on PER2 stability (Fig. 5A) results in a synergistic change in circadian lengthening (Fig. 6D). In this scenario, synchronized MEF$^{mPer2::LUC}$ cells were maintained with either inhibitor, PF670 or SN or a combination of both (PF670+SN) and the long-term effect in bioluminescence rhythms were simultaneously recorded throughout the time course analyzed. In agreement with Fig. 6C and {Zhou, 2015 #218} for PF670, treatment of MEF$^{mPer2::LUC}$ cells with either inhibitor resulted in an increased circadian period length, although their combined effect was not additive and did not result in a non-significant difference when compared to PF-670 treatment alone.

Overall, our findings support a model in which the interplay between E3 ligases, MDM2, and β-TrCP1, with different substrate recognition specificities becomes relevant to the stability of a core regulator, PER2, of the negative feedback loop of the circadian cycle. Furthermore, our data show that CK1δ and MDM2 activities play a relevant role in fine tuning the self-regulatory MDM2-β-TrCP1 loop and, consequently, the length of the circadian oscillation.

Discussion

Timely degradation of regulatory proteins is essential for most aspects of cellular homeostasis and relevant to signaling processes involved in cell growth, proliferation, and survival. It is, therefore not surprising that malfunctioning of any aspect of the protein degradation process results in a wide spectrum of diseases and disorders [for review see {Schwartz, 2009 #354}]. Because the mammalian circadian rhythm also relies on the continuous cycle of protein synthesis and degradation for functioning, it is not exempted from problems associated with protein turnover dysregulation. Indeed, mice bearing loss-of-function mutations or knock-down expression in genes encoding ubiquitin-modifying enzymes involved in regulating the clock (*e.g.*, *FBXL3*, *FBXL21*, *FBW1A*, *HUWE1*, *PAM*, *UBE3A*, *SIAH2*) exhibit a phenotype where the free-running period of locomotor activity is longer, shorter, or dampened [for review see {Stojkovic, 2014 #352}]. As clock components control the expression of an array of genes involved in multiple cellular mechanisms, it is not surprising to find that alteration in their expression and accumulation is linked to various human diseases XXREFXXXX. This brings into consideration the relevance of PER2, a circadian component whose function lies at the intersection of the cellular response to DNA-damage {Gotoh, 2015 #206}, and whose turnover depends on its phosphorylation by CK1δ and β-TrCP1 binding, followed by ubiquitination and proteasomal degradation [see {Gallego, 2007 #55} and references within]. Whereas substantive research has made a compelling case for how PER2 accumulates and how its level modulates the function of the clock, it poses the question of whether PER2 turnover remains exclusively a β-TrCP1 matter. And, whereas the answer could have certainly been affirmative, a seemingly unnoticed observation suggested to us that alternative scenarios should exist, as shown by the counterintuitive finding that PER2's half-life was shorter in culture cells co-expressing the dominant negative forms of β-TrCP1 and 2 (β-TrCP1ΔF and 2 ΔF) {Ohsaki, 2008 #126}. As a result, we turn to our findings that established that PER2 is able to form a trimeric complex with MDM2 and p53 {Gotoh, 2014 #63} and asked whether MDM2 might play a role in PER2 stability.

Our results show that PER2 binds MDM2 (PER2:MDM2) in a p53-independent manner *in vitro* and exists as a readily detectable endogenous complex in various cell settings (Fig. 1 and S1). Furthermore, binding of PER2 to MDM2 occurs in a region distinct from those identified for p53 binding and E3 ligase activity (Fig. 1), a result in agreement with the existence of the PER2:MDM2:p53 complex {Gotoh, 2014 #63}. Next, we established PER2 as a novel substrate of MDM2 and, conversely, MDM2 resulted in a previously uncharacterized E3 ligase responsible for PER2 ubiquitination (Fig. 2). The relevance of these initial findings lay in the existence of an alternative mechanism to recognize and target PER2 for degradation that is independent of post-translational modifications. This is a non-trivial finding as, to the best our knowledge, all well-established E3 ubiquitin ligases acting on clock components only recognize phosphorylated substrates. This include, in addition to β-TrCPs, the E3 ligases FBXL3 and FBXL21, which act on AMPK-mediated phosphorylated CRY1/2 {Lamia, 2009 #355}, HUWE1 and PAM, which act on GSK3β-mediated phosphorylated REV-ERBα {Yin, 2010 #356}, and UBE3A, which acts on GSK3β-mediated phosphorylated BMAL1 {Sahar, 2010 #358}. The challenge of identifying novel E3 ubiquitin ligases targeting clock components have led to the development of screenings that revolve around identifying enzyme-substrate binding or functional interactions {Ruffner, 2007 #360; DeBruyne, 2015 #359}. Of these, the recent identification of the ubiquitin ligase Siah2, which regulates REV-ERVα turnover, has been the most promising finding, yet, it remains to the domain of ligases that recognize phosphorylated substrates {DeBruyne, 2015 #359}.

We found that the accumulation and half-life of endogenous PER2 varied in scenarios in which MDM2 levels or activity were modulated, which also altered the cell's circadian period length (Figs. 2, 3, and 6). These findings raise the question of what the role of MDM2 would be, if any, in clock signaling. A glimpse of the possibilities emerged from previous findings showing that β-TrCP1 targets MDM2 for degradation in a CK1-dependent fashion {Inuzuka, 2010 #329}. Furthermore, our data establish the existence of a feedback loop in which MDM2 targets β-TrCP1 in a phosphorylation-independent fashion (Fig. XXX), and thus, two components of the core clock mechanism (β-TrCP1 and CK1) were found at the crossroad of MDM2 regulation and a third one, PER2, was found to be a substrate. Consequently, it is reasonable to expect that the interplay among these proteins would likely provide a tight and fine-tuned regulation of PER2 levels and circadian rhythms (Figs. 5 and 6).

We then asked, how would MDM2's primary role as a PER2 regulator fit in the functioning of the actual mammalian clock mechanism when acting under normal physiological conditions. This is certainly a difficult question to address, especially considering that MDM2 distribution in normal cells is largely nuclear, that MDM2 could promote either mono- or poly-ubiquitination of substrates depending on its endogenous levels, and that rhythmic levels of MDM2 protein and transcripts are largely absent in unstressed cells [for review see {Marine, 2010 #367} and {Gotoh, 2016 #332}]. Whereas these well-established premises create constraints around the possible function of MDM2 within the clock molecular mechanism, we propose a few scenarios for further consideration. For example, it is possible that, under physiological conditions, translocation of PER2 to the nucleus would initially result in mono-ubiquitination events due to the low levels of endogenous MDM2 present in normal cells. In this model, mono-ubiquitination and time-of-day accumulation of CK1δ-dependent phosphorylation events in PER2 may serve to prime the substrate for β-TrCP1-mediated degradation. Indeed, it is not uncommon to find that the generation of polyubiquitination substrates targeted for proteasomal degradation require both priming of mono-ubiquitinated substrates and intrinsic E3 ligase activity of more than one enzyme as has been shown, for example, in the case of p53 {Grossman, 2003 #368;Lai, 2001 #369}. In a different scenario, our findings open the possibility of PER2's stability being modulated by signals that converge in MDM2, for example those that respond to genotoxic and cytotoxic cellular stress, and for which a change in period length might provide a fitness advantage. Indeed, MDM2's activity can be modulated by post-translational modifications, stability, localization, or binding and be exquisitely tuned by, for example, alteration in oxygen levels, exposure to low-dose radiation, and even slight changes in growth factor concentrations {Marine, 2010 #367}. Indeed, phase resetting of the mammalian circadian clock has been shown to occur in response to DNA-damage and metabolic stress in both cell cultures and animal models, a phenotype that is increasingly associated with the existence of crosstalk mechanisms between clock proteins and checkpoint components {Gotoh, 2015 #206;Oklejewicz, 2008 #127;Papp, 2015 #371;Gaddameedhi, 2012 #372}.

At this point, the role of MDM2:PER2 interaction in the mammalian system and within any of the scenarios described above remains largely within the domain of speculation and represents an area of active research in our laboratory. We expect that mounting biochemical, molecular, and genetic evidence will provide a conceptual framework within which we can understand how cells relate and respond to environmental perturbations, no longer in isolation, but in the context of multicellular systems.

Methods

Bacterial two-hybrid screening. The two-hybrid interaction screening was performed using the BacterioMatch II system (Stratagene) following manufacturer's instructions. A specific bait (pBT-*PER2*) and target plasmid pair from a liver library (pTRG cDNA library) were co-transformed with the bait vector plus the pTRG target vector. Selection was performed as indicated in {Gotoh, 2014 #63} and positive colonies were transferred from selective screening medium onto a dual selective screening medium plate containing 3-amino-1,2,4-triazole (3-AT) and streptomycin. The pBT-*LFG2*/pTRG-*Gal11*^{P} co-transformant was used as a positive control whereas co-transformation of pBT-*PER2* with either empty pTRG or pTRG-*Gal11*^{P} vectors were used as negative controls. All positive cDNA clones were isolated, sequenced, with some of them already having been reported, and their interaction functionally verified {Gotoh, 2014 #63}.

Cell culture, transient transfections, and treatments. Human colorectal carcinoma HCT116 [*TP53*(+/+), *PER2*(+/+)] and human non-small cell lung carcinoma H1299 cell lines were purchased from the American Type Culture Collection (ATCC) and propagated according to manufacturer's recommendations. The H1299 cells contain a homozygous partial deletion of the *TP53* gene that results in the absence of p53 expression. The HCT116 null-isogenic clone [*TP53*(-/-), *PER2*(+/+)] was obtained from XXXXXXXXXXX and maintained in McCoy's 5a modified medium containing 50 U/ml of penicillin and 50 μg/ml of streptomycin. The MEF$^{mPer2::LUC}$ cells (kind gift of S. Kojima, Virginia Tech) were cultured in Dulbecco's Modified Eagle's Medium (DMEM) supplemented with 10% fetal bovine serum (FBS), 50 U/ml of penicillin, and 50 μg/ml of streptomycin, and maintained at 37°C and 5% CO_2.

Plasmid transfections were performed at 50-80% cell confluency and optimized using Lipofectamine LTX (Invitrogen) and HyClone HyQ-RS reduced serum medium (ThermoFisher) following the manufacturer's instructions. Vectors encoding for PER2, MDM2, MDM2(C470A), β-TrCP1, or p53 had their corresponding cDNA cloned downstream of the indicated tag in pCS2+. Proteins were allowed to express for several hours before cells were either harvested or circadian synchronized. Synchoronization was by either serum shock {Balsalobre, 1998 #9} or dexamethasone treatment {Balsalobre, 2000 #269}. Lysates were from cells collected at the indicated times, with t=0 occurring just prior to cycloheximide (CHX, 100 μg/ml) addition.

For siRNA transfections, HCT116 cells were grown in McCoy'5A media containing 10% FBS and penicillin (50 U/ml) until reaching 60-80% confluency. Knockdown was optimized using Dharmafect 2 reagent (GE Dharmacon) to deliver siRNAs targeting either MDM2 (5'-GAGATTTGTTTGGCGTGCCAAGCTT-3') or β-TrCP1 (5'-CGGAAACTCTCAGCAAGCTATGAAA-3') following the manufacturer's instructions. A scramble siRNA sequence with no homology to any known mammalian gene, served as control. Forty-eight hours after transfection, cells were serum shocked for 2 h after which the media was replaced with a serum-free version and cycloheximide was added. Samples were collected at different times after treatment and extracts were prepared in NP-40 lysis buffer containing 10 mM Tris-HCl (pH 7.5), 137 mM NaCl, 1mM EDTA, 10% glycerol, 0.5% NP-40, 80 mM β-glycerophosphate, 1mM Na_3VO_4, 10 mM NaF, and 1xprotease inhibitor cocktail (ThermoFisher).

Lastly, endogenous levels of PER2 were monitored in HCT116 treated with CHX and incubated with sempervirine (named SN, 1μg/ml, ChromaDex Inc.), PF670462 (named PF670, 1 μM, Cayman Chemical

Co.), or a combination of both inhibitors throughout the time course analyzed. The vehicle (DMSO) was used as control.

Immunoprecipitation and immunoblot assays. Immunoprecipitation of protein complexes were from either transfected cell extracts or *in vitro* binding reactions. Unless indicated, proteins were in NP-40 lysis buffer, and extracts (0.5-1 mg) were incubated by rotation for either α-FLAG M2 agarose beads (Sigma-Aldrich) or α-*myc* (9E10) beads (Santa Cruz Biotechnology) for either 2 h or overnight at 4^{o}C, respectively. In other cases, immunoprecipitations were carried out in a two-step procedure with extracts first being incubated with an uncoupled antibody (α-FLAG, α-*myc*, or α-PER2) overnight at 4^{o}C before the addition of protein A beads (50% slurry; Sigma-Aldrich). Bound beads were washed four times with NP-40 lysis buffer before the addition of Laemmli buffer. Complexes were resolved by SDS-PAGE and immunoblotting using the specific antibodies indicated in each case. Primary antibodies were α-FLAG (Sigma-Aldrich), α-*myc* (Santa Cruz Biotechnology), α-PER2 (Sigma-Aldrich), α-MDM2 (Santa Cruz Biotechnology), α-β-TrCP1 (Cell Signaling Technology), and α-ubiquitin (Enzo Biomol). Secondary antibodies were horseradish peroxidase-conjugated α-rabbit or α-mouse IgGs (GE Healthcare and Cell Signaling, respectively) and chemiluminescence reactions were performed using the SuperSignal West Pico Substrate (Pierce).

In vitro binding and epitope blocking assays. *In vitro* transcription and translation of either pCS2+*myc*- or –FLAG *PER2*, *β-TrCP1*, *β-TrCP1ΔF*, *MDM2*, *MDM2(C470A)*, and p53 were carried out using the SP6 high-yield TNT system (Promega) following manufacturer's instructions. As indicated in each case, aliquots (1-4μl) of the indicated recombinant proteins were pre-incubated for 15 min at room temperature to allow complex formation before adding NP-40 lysis buffer. Epitope blocking was performed by pre-incubating *in vitro* the transcribed and translated FLAG-MDM2(C470A) with XXXXX μg/ml of α-4B11, -4B2, or –SMP14 antibody for 2 h at 4^{o}C before adding recombinant *myc*-PER2. Binding reactions were allowed to proceed overnight at 4^{o}C with rotation. In all cases, immunoprecipitation was carried out as described in the previous section.

Protein pull-down assay. Various cDNA clones encoding fragments of PER2 (residues 1-172, 173-355, 356-574, 575-682, 683-872, 873-1,120, 1,121-1,255) were cloned in pGEX-4T, expressed as recombinant GST-tagged proteins in *E. coli* strain *Rosetta* (Novagen), and purified using glutathione sepharose affinity chromatography following manufacturer's instructions (GE Healthcare). Pull-down experiments were carried out using 5 μg of each recombinant GST-tagged protein-bound beads, or an equivalent amount of GST bound glutathione beads as control, and 4 μl of *in vitro* transcribed and translated [^{35}S]-FLAG-MDM2 in binding buffer containing 20 mM Tris-HCl (pH 7.4), 100 mM NaCl, 5 mM EDTA, and 0.1% Triton X-100. Reactions were incubated for 1 h at 4^{o}C with rotation; after which, bead-bound complexes were washed with binding buffer containing either low (100 mM) or high (1M) salt concentration. Bound proteins were analyzed by SDS-PAGE and autoradiography.

Ubiquitination and degradation assays. Aliquots (1-4 μl) of *in vitro* transcribed and translated tagged-proteins, or a combination of them, were allowed to bind before adding 1x ubiquitination buffer (Enzo Biomol), 2 mM dithiothreitol, 20 μg/ml ubiquitin-aldehyde, 100 μg/ml ubiquitin, 1x ATP-energy regeneration system (5 mM ATP/Mg^{2+}; Enzo Biomol), 40 μM MG132 (Cayman Chemical Co.), and 1 mg/ml of HeLa S100 lysate fraction (Enzo Biomol) to a final volume of 10 μl. Reactions were then incubated for 30 min at 37°C in a water bath; after which, NP-40 lysis buffer was added and ubiquitinated proteins were immunoprecipitated following the two-step protocol described in the section above.

Detection of ubiquitinatinated forms of PER2 in cells was carried out by co-transfecting HCT116 [*TP53*(+/+), *PER2*(+/+)] cells with pCS2+FLAG-PER2 and either pCS2+*myc*-MDM2 or pCS2+*myc*-MDM2(C470A) plasmids. Cells were maintained in complete media for 24h to allow for the recombinant proteins' expression before adding 50 μM MG132 and ubiquitin aldehyde (5 nM). Cells were harvested 4 h later and lysates were immunoprecipitated using α-FLAG antibody as described. Proteins were resolved by SDS–PAGE and ubiquitinated forms of PER2 were detected by immunoblotting using an α-ubiquitin antibody.

To monitor protein degradation, *in vitro* transcribed and translated recombinant proteins were incubated in a reaction mixture containing ubiquitin and ATP-energy regenerating system but lacking MG132 and ubiquitin aldehyde. In addition, the HeLa S100 lysate fraction was replaced by a similar concentration of total cell extract enriched in 26S proteasome. Reactions were allowed to proceed for 30 min at 37°C before adding Laemmli buffer. Samples were resolved by SDS-PAGE and immunoblotting.

Analysis of protein half-life. Accumulation and half-life of endogenous proteins in HCT116 cells extracts (20-80 μg) was monitored by immunoblotting samples collected at different times after CHX addition as indicated elsewhere in the Methods section. Protein bands were quantified by immunoblot analysis using Bio-Rad ImageLab 5.1 software/Gel Doc XR+ system and values were normalized to tubulin levels. Unless indicated, the percentage of remaining protein was normalized to t=0 and the data fitted using Microsoft Excel.

Real-time bioluminescence assay. Cells, $MEF^{mPer2::LUC}$, were seeded in 35 mm dishes and circadian synchronized by dexamethasone treatment (100 ng/ml, 2 h). Following, the media was replaced by phenol-red-free DMEM containing 50 μM luciferin and cells were allowed to stabilize in a LumiCycle 32-channel automated luminometer (Actimetrics) placed in a 37°C incubator for 24 h before sempervirine (1μg/ml), PF670462 (1 μM), or both inhibitors were added. In these assays, bioluminescence was continuously recorded for at least 5 additional days and data were analyzed using the LumiCycle analysis software (Actimetrics).

In other experiments, $MEF^{mPer2::LUC}$ cells were transiently transfected with either pCS2+*myc-MDM2* or *siRNA MDM2* for 24 or 48 h, respectively before dexamethasone synchronization. Following media exchange, bioluminiscence was recorded at least 5 additional days. In each case, raw data was collected after dexamethasone synchronization (t=0) and for the remaining of the experiment. Raw data beginning t=24 h after synchronization was considered when calculating the circadian period length and phase using JMP Statistical Software (SAS Institute Inc). The fitted model was based on a nonlinear sine wave regression with additional linear and quadratic terms added to the trend and dampening as indicated in {Oklejewicz, 2008 #127}.

References

Acknowledgements

The authors thank Dr. D. G. S. Capelluto and Dr. J. K. Kim for critical reading of the manuscript and all members of the Finkielstein laboratory for help and discussions. We would also like to thank Dr. J. Webster for comments and manuscript editing. This work was supported by the National Science Foundation MCB division (MCB-1517298) and the Fralin Life Science Institute to C.V.F.

Author Contributions

J.L. performed all experiments and statistical analyses discussed in this article except those specifically mentioned below. S.S. contributed with Figs. XXXXXXX, X.Z. contributed with Fig. XX, and T.G. performed the experiments shown in Figures XXXXX. C.V.F. and J.L conceived this project, analyzed the overall data, refined the hypothesis, and proposed the model. C.V.F. supervised and coordinated all investigators for the project and wrote the manuscript.

Figure Legends

Figure 1. The circadian factor Period 2 directly interacts with Mdm2. A. A bacterial two-hybrid screening was developed to identify protein interactors of PER2 *in vivo* based on transcriptional activation. Positive clones encoding putative interacting proteins were maintained on LB Tet/Cam media (*upper panel*), and patched in His-dropout selective media containing either 3-amino-1,2,4-triazole (3-AT, *middle panel*) or 3-AT and streptomycin (*lower panel*). Patches of co-transformants served as positive (pBT-*LFG2* and pTRG-*Gal11*^{P}) and negative (pBT-*PER2* and pTRG empty vector) controls. **B.** Extracts from isogenic HCT116 cells were analyzed for the presence of endogenous PER2:MDM2 (*left panels*) or PER2:*myc*-MDM2 (*right panels*) complexes by immunoprecipitation using α-PER2 antibody and blotting using the indicated antibodies. **C.** *In vitro* transcribed and translated tagged proteins (lanes 1 to 7) were incubated and complexes were immunoprecipitated using α-FLAG antibody. Complex components were identified by immunoblotting. **D.** Competition experiments were carried out by pre-incubating FLAG-MDM2(C470A) with each of the indicated α-MDM2 antibodies (α-4B11, -4B2, -SMP14) before adding recombinant *myc*-PER2. Protein binding was monitored in FLAG-bound beads by immunoblotting. **E.** Pull-down assay was carried out using recombinant GST-tagged PER2 protein fragments comprising various lengths of PER2 [GST-PER2(1-172), GST-PER2(173-355), GST-PER2(356-574), GST-PER2(575-682), GST-PER2(683-872), GST-PER2(873-1,120), GST-PER2(1,121-1,255)] and radiolabeled [^{35}S]-MDM2. The GST protein was used as negative control.

Figure 2. The E3-ligase MDM2 targets PER2 for ubiquitination and modulates PER2's stability. A. XXXXXXXXXXXXXXXX. **B.** XXXXXXXXXXXXXXXX. **C.** *In vitro* transcribed and translated FLAG-PER2 was incubated with increasing amounts of recombinant *myc*-MDM2 [ratio of PER2:MDM2 was of 1:0 to 1:5] in the presence of ubiquitin as indicated in the Methods section. The FLAG-PER2 protein was immunoprecipitated and its ubiquitin-conjugated forms were detected by immunoblotting using α-ubiquitin antibody. **D.** Cells, HCT116, were co-transfected with FLAG-*PER2*, *myc-MDM2*, *myc-MDM2(C470A)*, or empty vector (control, -) and maintained in the presence (+) or absence (-) of MG132. Cells were harvested and PER ubiquitination detected by immunoprecipitation using α-FLAG antibody and immunoblotting with α-ubiquitin (*upper panel*), α-PER2 (*middle panel*), or α-*myc* (*lower panel*)

antibodies. **E.** HCT116 cells were transfected with either empty vector (mock) or FLAG-*MDM2* and proteins were allowed to express for 24h before adding cycloheximide (CHX, 100 μg/ml, t=0h). Cells were harvested at different times after CHX addition and extracts analyzed for endogenous PER2 and MDM2, and FLAG-MDM2 levels by immunoblotting using specific antibodies. Tubulin was a loading control (*lower panel*). Protein levels of PER2 were quantified using ImageJ Software v1.45 and values normalized to tubulin levels. Graphs indicate the amount of PER2 remaining (in a.u.) plotted as a function of time (*right graph panel*). The curve was fitted using Microsoft Excel. Data are presented as mean ± SEM from three independent experiments performed in triplicate. Bar graph indicates PER2 and MDM2 protein levels at t=0 in lanes 1 and 7.

Figure 3. The interplay between MDM2 and β-TrCP1 modulates PER2 turnover. A. HCT116 cells were transfected with si-*MDM2* (25 nM), si-*β-TrCP1* (25 nM), or a scrambled siRNA sequence (mock) for 48 h before CHX addition (t=0) as described in the Methods section. Cells were harvested at different times after CHX addition and extracts were analyzed for the expression of PER2, MDM2, and β-TrCP1 by immunoblotting using specific antibodies. Tubulin was a loading control (*lower panel*). Protein levels of PER2 were quantified and plotted as indicated in Figure 2E (*right graph panel*). Data are presented as mean ± SEM from three independent experiments performed in triplicate. Bar graph indicates PER2, MDM2, and β-TrCP1 protein levels at t=0 in lanes 1, 7, and 13. **B.** Schematic representation of the regulatory MDM2:β-TrCP1 loop. C. Cells, HCT116, were transfected with FLAG-*MDM2*, FLAG-*MDM2(C470A)*, or empty vector (mock) and the levels of b-TrCP1 and MDM2 proteins were monitored in extracts collected at different times after CHX addition. Tubulin was a loading control (*lower panel*). The level of β-TrCP1 was determined for each experimental condition and graphs generated as described in Figure 2E. Data are presented as mean ± SEM from three independent experiments performed in triplicate.

Figure 4. The E3-ligase β-TrCP1 is a *bona fide* substrate of MDM2. A. *In vitro* ubiquitination reactions (lanes 5 to 12) were carried out using recombinant tagged proteins MDM2, MDM2(C470A), Δ-β-TrCP1, and p53 as described in the Methods sections. Controls (lanes 1 to 4) were carried out in the presence of the indicated proteins (+), although the ubiquitination mixture was replaced by buffer (named – ubiquitination). Complexes were immunoprecipitated using an α-FLAG antibody and samples resolved by SDS-PAGE and immunoblotting. Binding was detected using α-*myc* and –FLAG antibodies (*upper and middle panels*) and ubiquitinated intermediates identified using an α-ubiquitin antibody (*lower panel*). **B.** Schematic representation of the proposed network that modulates PER2 levels through the MDM2:β-TrCP1 regulatory loop.

Figure 5. The stability of PER2 increases as result of modulating the activity of the MDM2:β-TrCP1 loop. HCT116 cells were incubated with sempervirine nitrate (SN, 1 μg/ml), PF-670462 (PF-670, 1 μM), a combination of both inhibitors, or DMSO (control) throughout the time course analyzed. Lysates were prepared from cells collected at t=0 and after CHX addition and proteins were resolved by SDS-PAGE and immunoblotting using α-PER2, -MDM2, and -β-TrCP1 antibodies. Tubulin was a loading control (*lower panel*). The level of PER2 was determined for each experimental condition and graphs generated as described in Figure 2E. Data are presented as mean ± SEM from three independent experiments performed in triplicate.

Figure 6. The function of the E3 ligase MDM2 influences the circadian period length. A. $MEF^{mPer2::LUC}$ cells were transfected with either pCS2+-*myc* (mock) or pCS2+-*myc*-MDM2 and proteins

were allowed to express before cells were circadian synchronized with dexamethasone and placed in a lumicycle instrument. The abundance of PER2::LUC was evaluated by monitoring luminescence intensity throughout 7 days (*left panel*). In other scenarios, $MEF^{mPer2::LUC}$ cells were transfected with si*MDM2* (**B**) or treated with sempervirine (SN, 1μg/ml, **C**) before synchronization with dexamethasone and bioluminescence recording. **D.** Synchronized $MEF^{mPer2::LUC}$ cells were incubated with sempervirine (SN, 1μg/ml), PF670462 (PF670, 1 μM), or a combination of both inhibitors throughout the time course analyzed. For **A**, **B**, and **C**, bar graphs indicate the length of the circadian period calculated using JMP Statistical Software (*right panel*). For **D**, the circadian period length was calculated using the LumiCycle analysis software (Actimetrics). The vehicle (DMSO) was used as control. Values are the mean ± SEM from three independent experiments. Statistical significance was determined by t-test. ***$p \leq 0.001$, *$p \leq 0.05$.

Supplementary Figure Legends

Figure S1. *In vitro* binding studies of MDM2 and β-TrCP1. A. H1299 cells were co-transfected with pCS2+*myc-PER2*, FLAG-*MDM2*, FLAG-*MDM2(C470A)*, or FLAG-*β-TrCP1* and extracts were immunopricipitated and bound proteins analyzed by immunoblotting using specific antibodies. **B.** Schematic representation of MDM2 constructs [MDM2(1-117), MDM2(1-230), MDM2(1-434), MDM2(117-497), MDM2(230-497), MDM2(434-497)] used in binding mapping experiments. An N-terminus FLAG-tag is encoded in all MDM2 constructs. Structural and functional domains in MDM2 are indicated as boxes in the full-length representation. NES, nuclear export signal; NLS, nuclear localization signal. Epitope mapping of specific MDM2 antibodies are indicated as: 4B2, comprises residues 19-50; SMP14, comprises residues 154-167; and 4B11, comprises residues 383-491. **C.** HCT116 $p53^{-/-}$ cells were co-transfected with pCS2+*myc-PER2*, *myc-PER2*(S662A), pCS2+3xFLAG-MDM2, or 3xFLAG-MDM2(C470A). Cell extracts were incubated with α-FLAG antibody and protein A beads (50% slurry) and bound proteins were identified by immunoblotting using α-tag antibodies. **D.** *In vitro* transcribed and translated FLAG-MDM2 fragments were incubated with *myc*-PER2 and the complex was allowed to form before samples were immunoprecipitated using α-FLAG antibody and protein A beads as indicated in the Methods section. The complex was then washed with increasing concentration of NaCl (100 mM, 250 mM, and 500 mM) and bound PER2 was detected using α-*myc* antibody.

Figure S2. MDM2 promotes polyubiquitination of PER2 *in vitro*. *In vitro* transcribed and translated FLAG-PER2 and FLAG-p53 were incubated with *myc*-MDM2 in the presence of a reaction mixture containing ubiquitin, ATP-regenerating system, MG132, and an enriched fraction of E1 and E2 enzymes. FLAG-tagged proteins were immunoprecipitated and components were resolved by SDS-PAGE and identified by immunoblotting using specific antibodies. Ubiquitin-modified intermediates of PER2 and p53 were detected using an α-ubiquitin antibody.

Figure S3. Endogenous MDM2 interacts with β-TrCP1 *in cells*. Lysates from HCT116 cells were incubated with either α-MDM2 or IgG antibodies and endogenous complexes were immunoprecipitated and proteins detected using specific antibodies.

Figure S4. MDM2's level and activity influence circadian period length. A. In a parallel set of dishes, *myc-MDM2* transfected $MEF^{mPer2::LUC}$ cells were monitored for either PER2::LUC luminescence activity (Figure 6) or MDM2 protein expression (**A**). MDM2 was detected in lysates (40 μg) 24 h after

transfection (t=-2), 2h after dexamethasone treatment (t=0), and at other times after synchronization (t=24, 40, 40.5, and 52 h) by immunoblotting using an α-*myc* antibody. Mock indicates transfection with empty plasmid. **B.** $MEF^{mPer2::LUC}$ cells were transfected with various amounts of pCS2+-*myc-MDM2*, synchronized with dexamethasone, and monitored for luminescence activity over time (*left panel*). The circadian period length for each treatment was determined using JMP Statistical Software (*right panel*). **C.** Knockdown expression of MDM2 in $MEF^{mPer2::LUC}$ cells was confirmed by immunoblotting of lysates collected 24 and 48 h after *siMDM2* transfection (25 nM), following dexamethasone addition (t=0), and at different times after synchronization (t=72 and 96 h). **D.** Cell viability was assayed in $MEF^{mPer2::LUC}$ cells incubated with different concentrations of sempervirine (SN) for up to 7 days using an MTT cell viability kit following the manufacturer's instruction (ThermoFisher). Values are the mean ± SEM from three independent experiments repeated in triplicate. **E.** Inhibition of MDM2's degradation by sempervirine was tested *in vitro* using recombinant *myc*-MDM2 and *myc*-MDM2(C470A) and increasing concentrations of the inhibitor (0.5-4 μg/ml) in a reaction mixture supplemented with ubiquitin as indicated in the Methods section. Samples were analyzed by immunoblotting and bands quantified using Image J software (*bar graph*). **F.** Summary of the circadian period length data obtained from the various treatment modalities included in Figure 6.

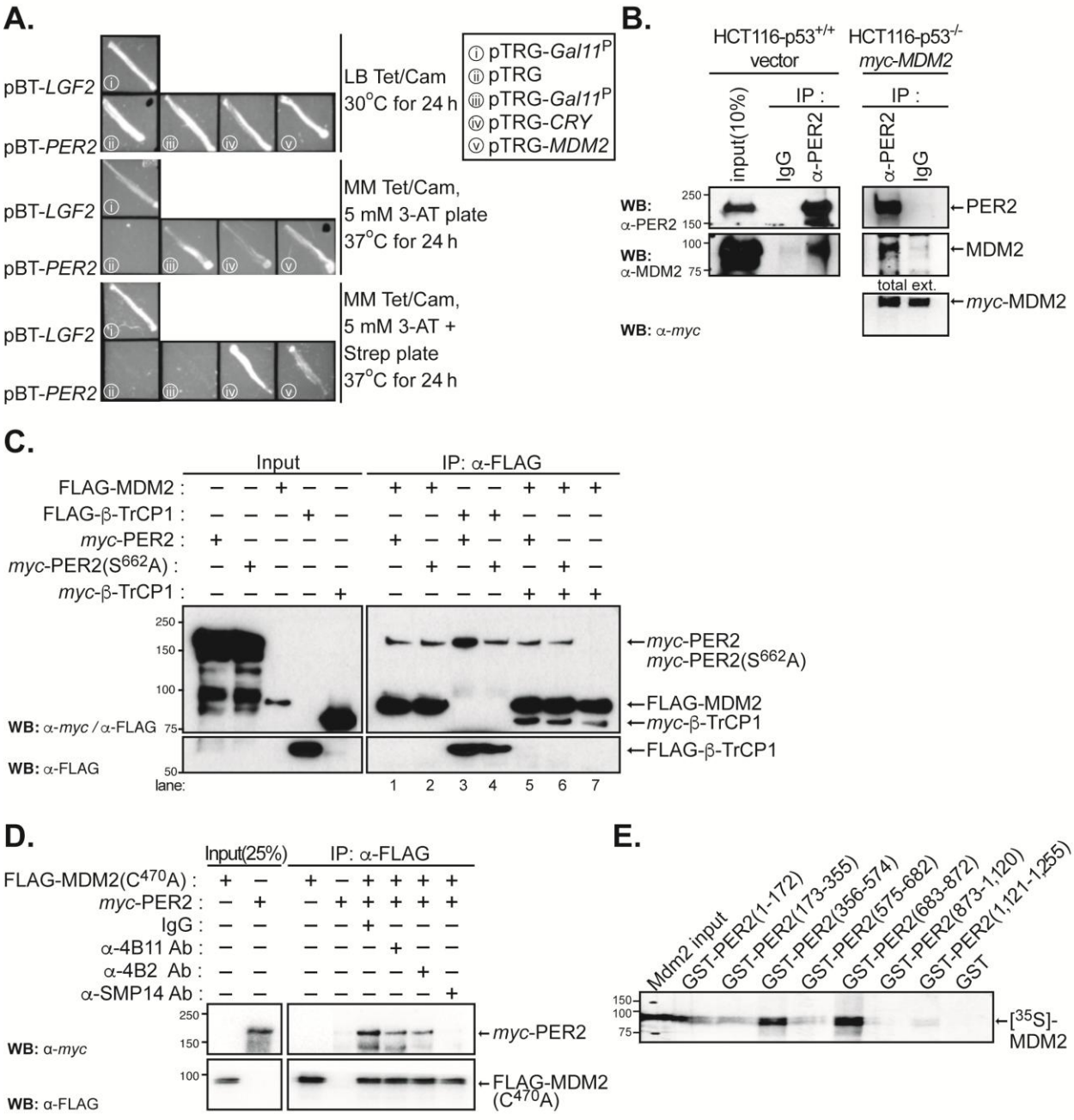
A.
pBT-LGF2
pBT-PER2
LB Tet/Cam
30°C for 24 h
MM Tet/Cam,
5 mM 3-AT plate
37°C for 24 h
MM Tet/Cam,
5 mM 3-AT +
Strep plate
37°C for 24 h
ⓘ pTRG-Gal11P
ⓘⓘ pTRG
ⓘⓘⓘ pTRG-Gal11P
ⓘⓥ pTRG-CRY
ⓥ pTRG-MDM2
B.
HCT116-p53+/+
vector
HCT116-p53-/-
myc-MDM2
input(10%)
IP :
IgG
α-PER2
WB:
α-PER2
WB:
α-MDM2
WB: α-myc
PER2
MDM2
total ext.
myc-MDM2
C.
Input
IP: α-FLAG
FLAG-MDM2 :
FLAG-β-TrCP1 :
myc-PER2 :
myc-PER2(S662A) :
myc-β-TrCP1 :
WB: α-myc / α-FLAG
WB: α-FLAG
lane:
myc-PER2
myc-PER2(S662A)
FLAG-MDM2
myc-β-TrCP1
FLAG-β-TrCP1
D.
Input(25%)
IP: α-FLAG
FLAG-MDM2(C470A) :
myc-PER2 :
IgG :
α-4B11 Ab :
α-4B2 Ab :
α-SMP14 Ab :
WB: α-myc
WB: α-FLAG
myc-PER2
FLAG-MDM2
(C470A)
E.
Mdm2 input
GST-PER2(1-172)
GST-PER2(173-355)
GST-PER2(356-574)
GST-PER2(575-682)
GST-PER2(683-872)
GST-PER2(873-1,120)
GST-PER2(1,121-1,255)
GST
[35S]-
MDM2

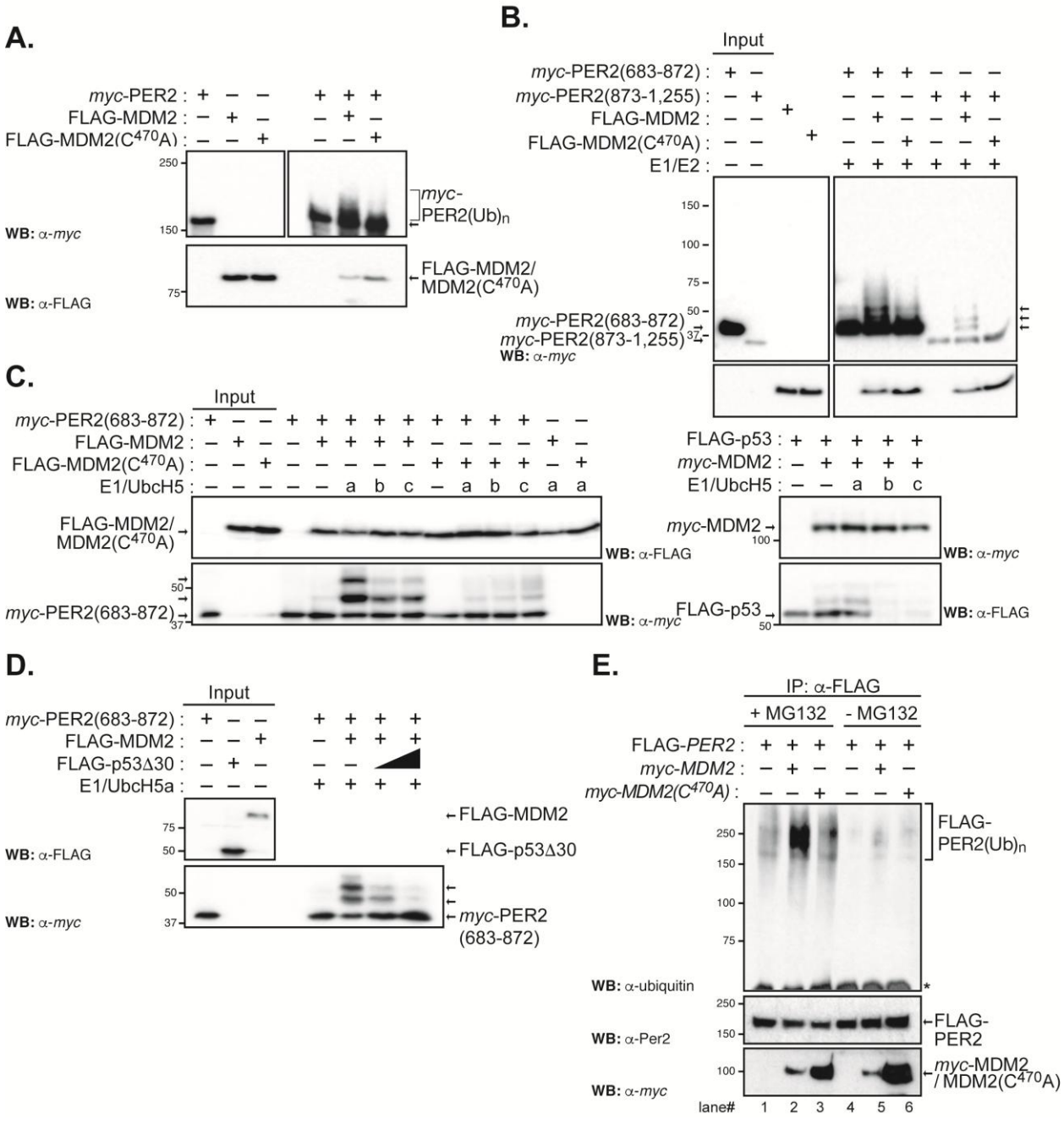
A.
myc-PER2
FLAG-MDM2
FLAG-MDM2(C470A)
myc-PER2(Ub)n
FLAG-MDM2/ MDM2(C470A)
WB: α-myc
WB: α-FLAG
B.
Input
myc-PER2(683-872)
myc-PER2(873-1,255)
FLAG-MDM2
FLAG-MDM2(C470A)
E1/E2
myc-PER2(683-872)
myc-PER2(873-1,255)
WB: α-myc
C.
Input
myc-PER2(683-872)
FLAG-MDM2
FLAG-MDM2(C470A)
E1/UbcH5
FLAG-MDM2/ MDM2(C470A)
WB: α-FLAG
myc-PER2(683-872)
WB: α-myc
FLAG-p53
myc-MDM2
E1/UbcH5
myc-MDM2
WB: α-myc
FLAG-p53
WB: α-FLAG
D.
Input
myc-PER2(683-872)
FLAG-MDM2
FLAG-p53Δ30
E1/UbcH5a
WB: α-FLAG
WB: α-myc
FLAG-MDM2
FLAG-p53Δ30
myc-PER2 (683-872)
E.
IP: α-FLAG
+ MG132
- MG132
FLAG-PER2
myc-MDM2
myc-MDM2(C470A)
FLAG-PER2(Ub)n
WB: α-ubiquitin
WB: α-Per2
WB: α-myc
FLAG-PER2
myc-MDM2 / MDM2(C470A)
lane#
1 2 3 4 5 6

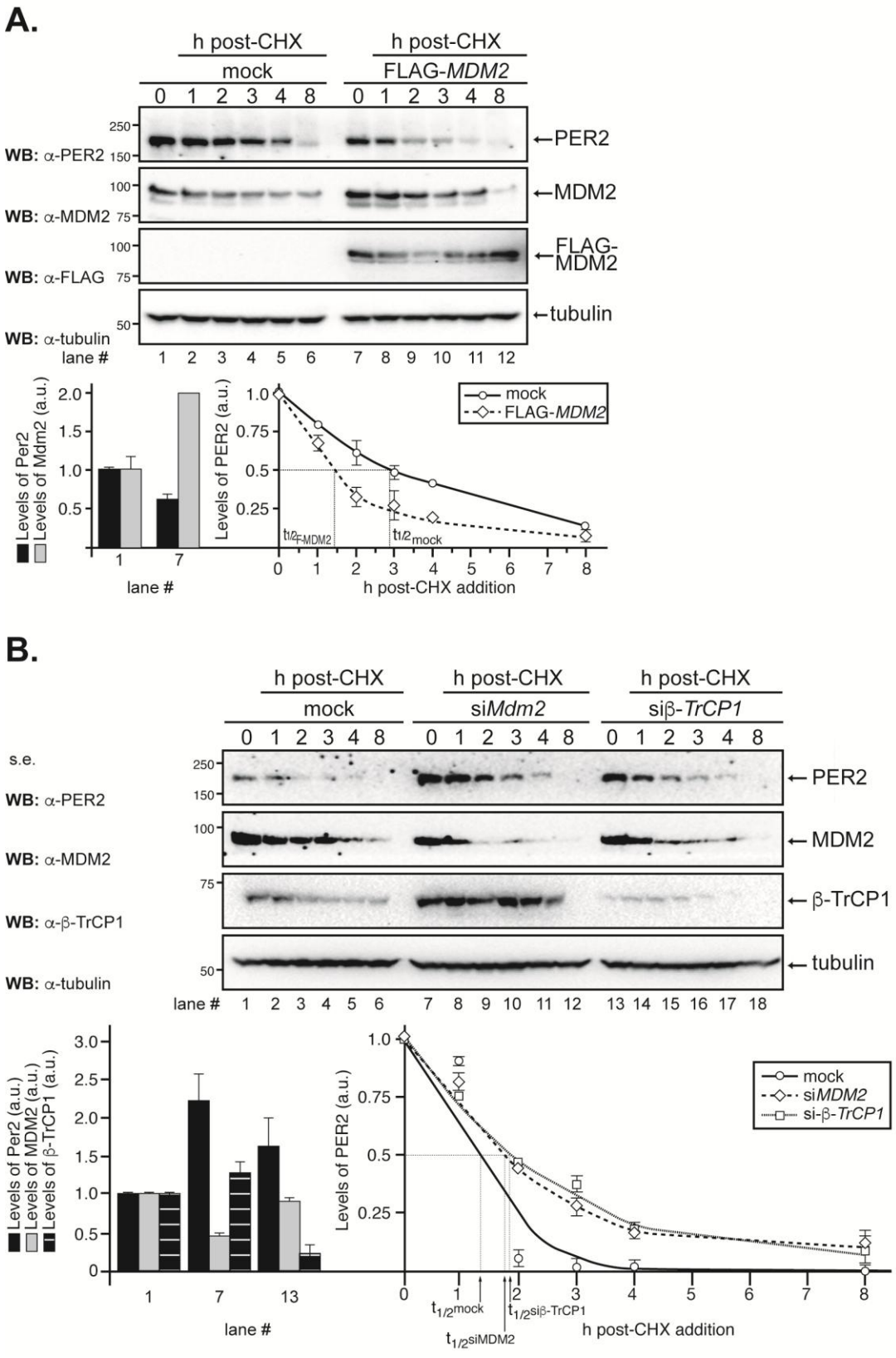
A.
h post-CHX
mock
FLAG-MDM2
0 1 2 3 4 8
WB: α-PER2
WB: α-MDM2
WB: α-FLAG
WB: α-tubulin
PER2
MDM2
FLAG-MDM2
tubulin
lane #
Levels of Per2
Levels of Mdm2 (a.u.)
Levels of PER2 (a.u.)
mock
FLAG-MDM2
h post-CHX addition
B.
h post-CHX
mock
siMdm2
siβ-TrCP1
s.e.
WB: α-β-TrCP1
β-TrCP1
Levels of MDM2 (a.u.)
Levels of β-TrCP1 (a.u.)
siMDM2
si-β-TrCP1

Figure_4_Liu *et al.*

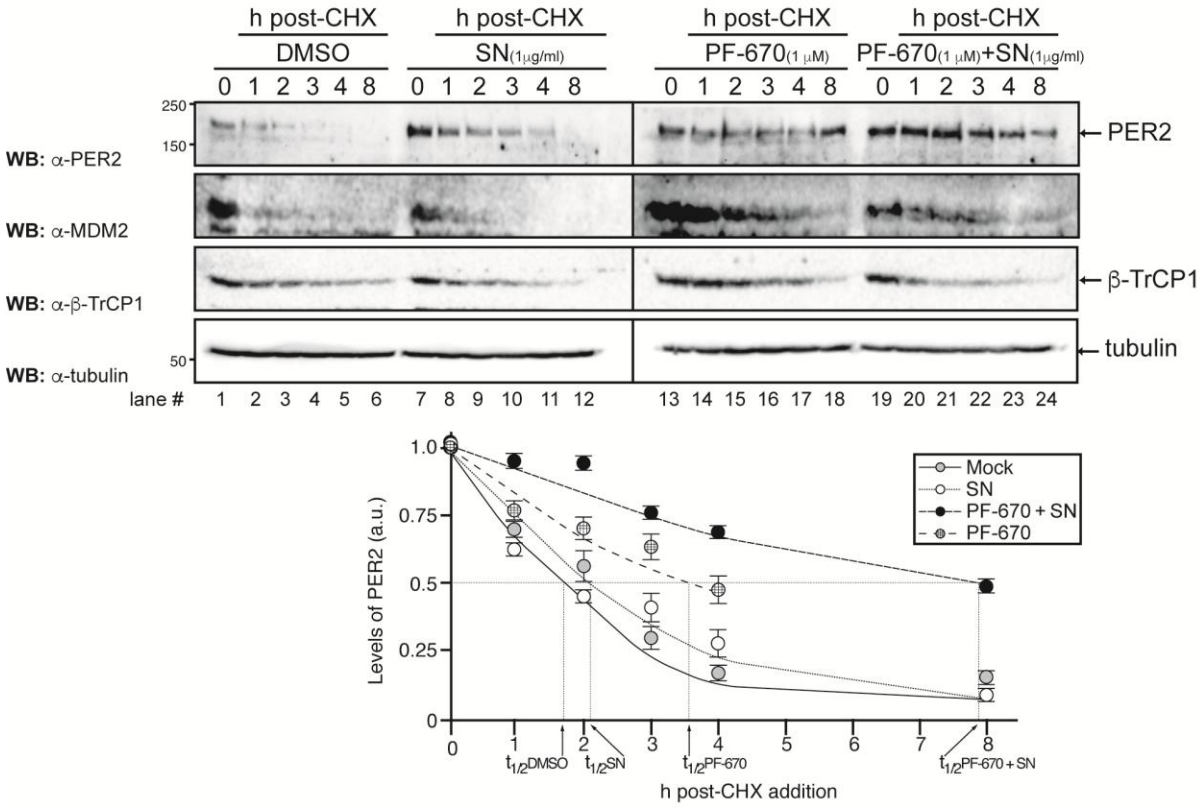

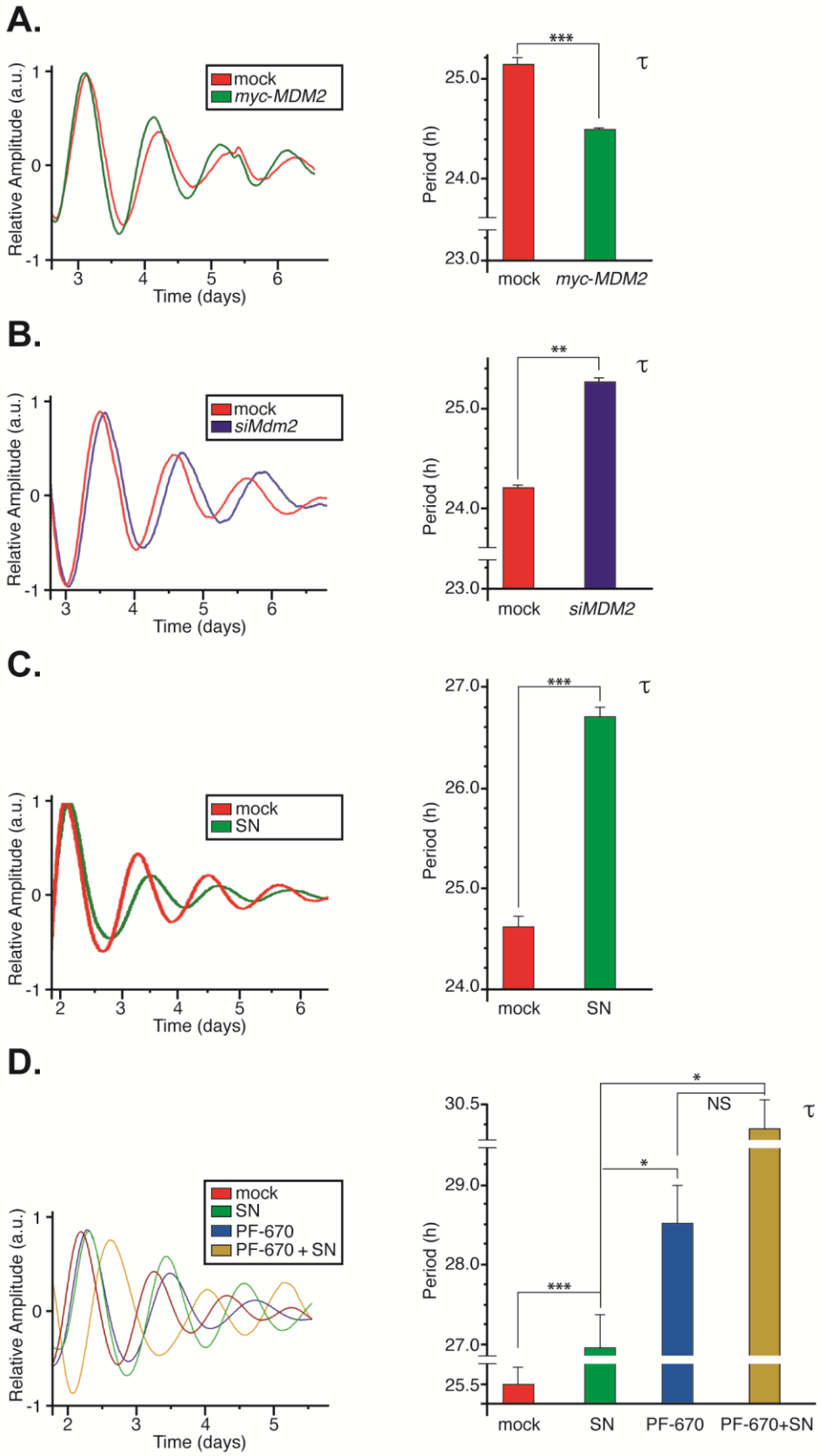
A.
mock
myc-MDM2
Relative Amplitude (a.u.)
Time (days)
***
τ
Period (h)
mock
myc-MDM2
B.
mock
siMdm2
Relative Amplitude (a.u.)
Time (days)
**
τ
Period (h)
mock
siMDM2
C.
mock
SN
Relative Amplitude (a.u.)
Time (days)
***
τ
Period (h)
mock
SN
D.
mock
SN
PF-670
PF-670 + SN
Relative Amplitude (a.u.)
Time (days)
*
NS
*
***
τ
Period (h)
mock
SN
PF-670
PF-670+SN

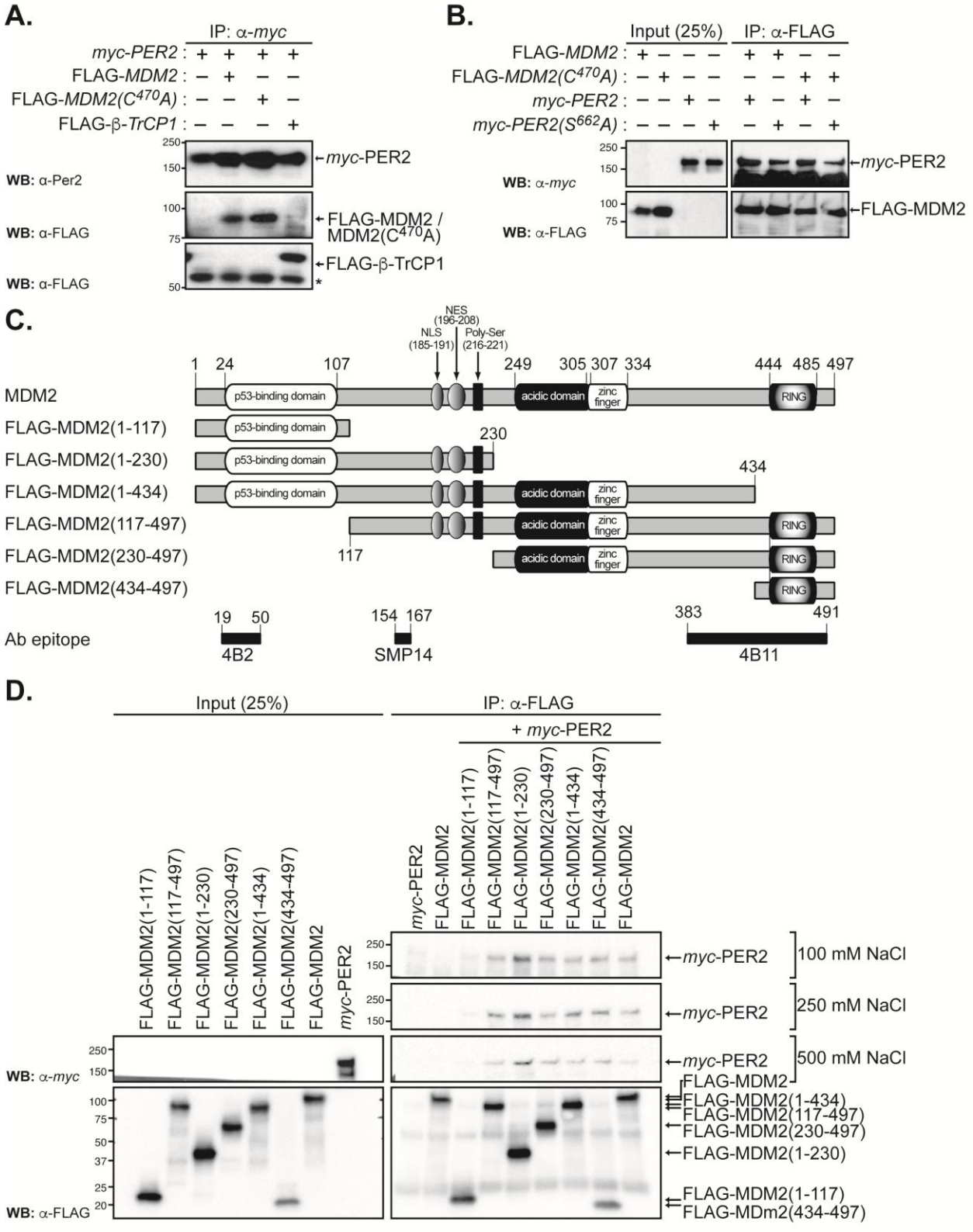
A.
IP: α-myc
myc-PER2 : + + + +
FLAG-MDM2 : – + – –
FLAG-MDM2(C470A) : – – + –
FLAG-β-TrCP1 : – – – +
250
150
←myc-PER2
WB: α-Per2
100
75
←FLAG-MDM2 / MDM2(C470A)
WB: α-FLAG
50
←FLAG-β-TrCP1
WB: α-FLAG
*
B.
Input (25%)
IP: α-FLAG
FLAG-MDM2 : + – – – + + – –
FLAG-MDM2(C470A) : – + – – – – + +
myc-PER2 : – – + – + – + –
myc-PER2(S662A) : – – – + – + – +
250
150
←myc-PER2
WB: α-myc
100
75
←FLAG-MDM2
WB: α-FLAG
C.
NES (196-208)
NLS (185-191)
Poly-Ser (216-221)
1 24 107 249 305 307 334 444 485 497
MDM2
p53-binding domain
acidic domain
zinc finger
RING
FLAG-MDM2(1-117)
FLAG-MDM2(1-230)
230
FLAG-MDM2(1-434)
434
FLAG-MDM2(117-497)
117
FLAG-MDM2(230-497)
FLAG-MDM2(434-497)
Ab epitope
19 50
4B2
154 167
SMP14
383 491
4B11
D.
Input (25%)
IP: α-FLAG
+ myc-PER2
FLAG-MDM2(1-117)
FLAG-MDM2(117-497)
FLAG-MDM2(1-230)
FLAG-MDM2(230-497)
FLAG-MDM2(1-434)
FLAG-MDM2(434-497)
FLAG-MDM2
myc-PER2
250
150
←myc-PER2
100 mM NaCl
250 mM NaCl
500 mM NaCl
WB: α-myc
100
75
50
37
25
20
WB: α-FLAG
←FLAG-MDM2
←FLAG-MDM2(1-434)
←FLAG-MDM2(117-497)
←FLAG-MDM2(230-497)
←FLAG-MDM2(1-230)
←FLAG-MDM2(1-117)
←FLAG-MDm2(434-497)

Figure_S2_Liu *et al.*

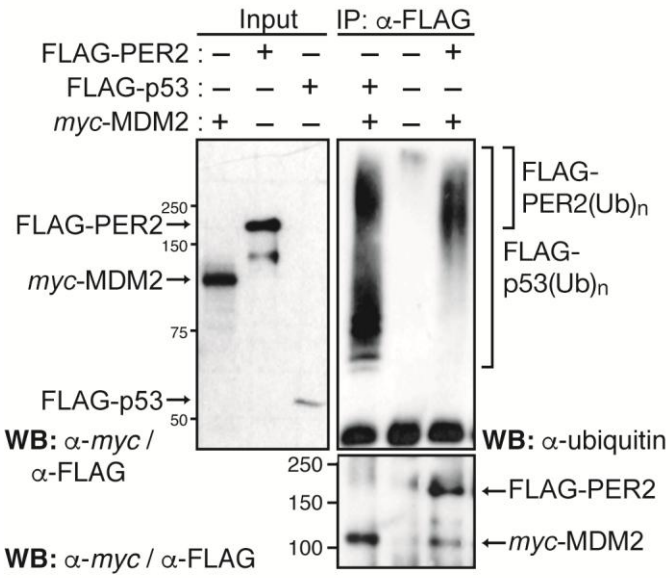

Figure_S3_Liu *et al.*

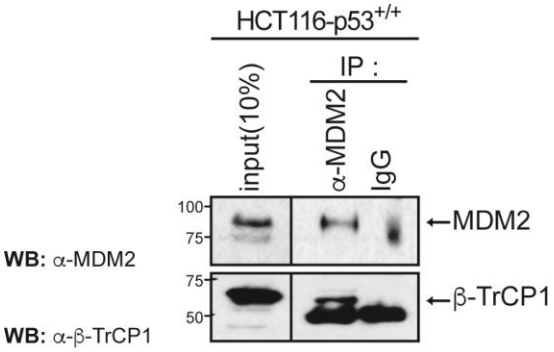

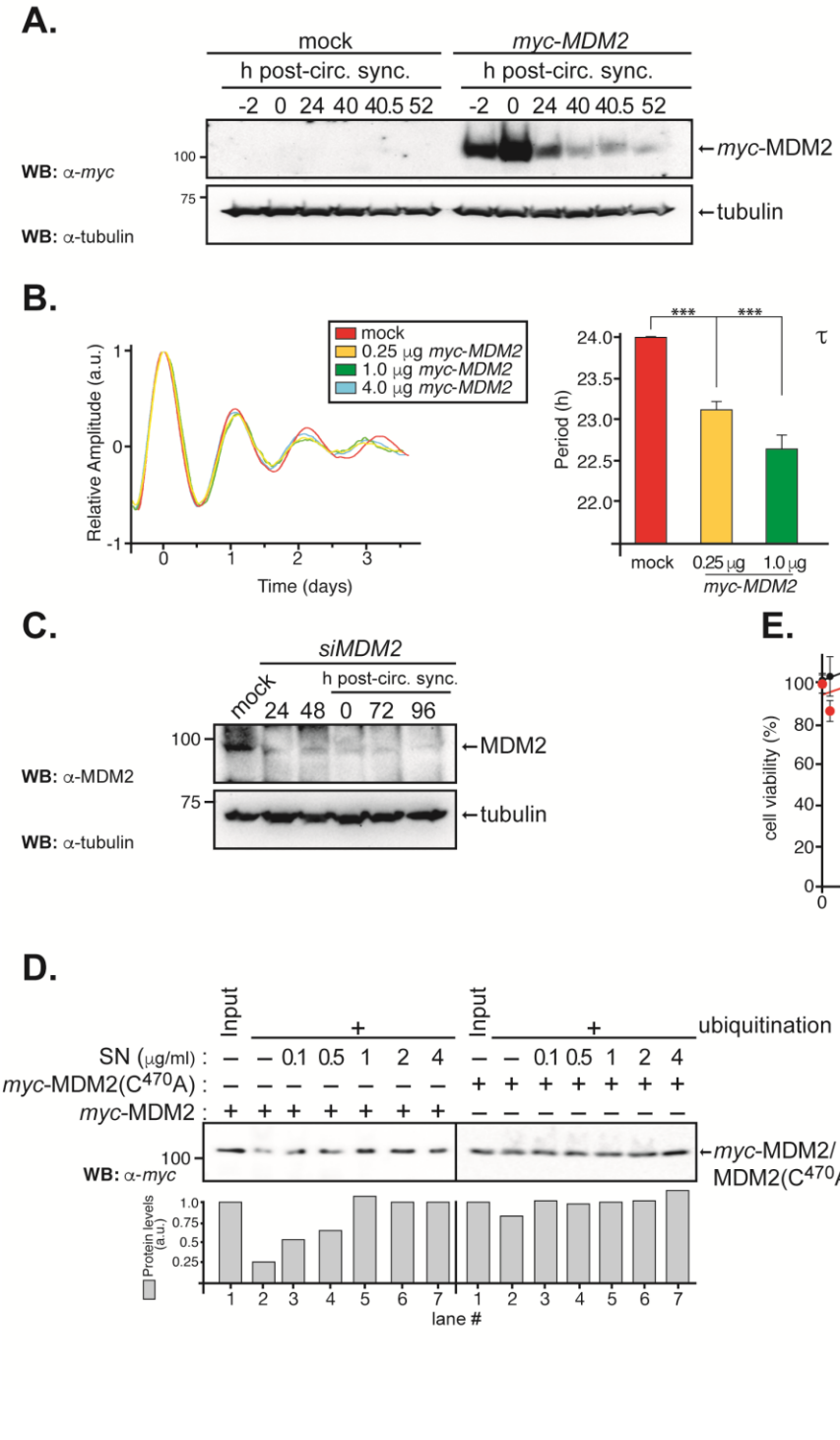

F.

Fig.	Treatment	Period (h)	p value
6A	mock	25.17 ± 0.004	<0.001
	myc-Mdm2	24.53 ± 0.001	
6B	mock	24.20 ± 0.011	<0.01
	siMdm2	25.25 ± 0.017	
6C	mock	24.62 ± 0.007	<0.001
	SN	26.72 ± 0.011	
6D	mock	25.50 ± 0.603	
	SN	26.87 ± 0.566	<0.05
	PF-670	28.50 ± 0.493	NS
	PF-670+SN	29.67 ± 0.917	